UNIVERSIDAD AUTÓNOMA DE MADRID
Facultad de Ciencias
Departamento de Química-Física Aplicada

BIO-HYBRID MATERIALS BASED ON ZEIN: SYNTHETIC APPROACHES, CHARACTERIZATION, AND EXPLORATION OF PROPERTIES

Doctoral Thesis

Ana Clécia Santos de Alcântara

Supervisors:

Dr. Pilar Aranda
Dr. Margarita Darder

CSIC
Consejo Superior de Investigaciones Científicas

Instituto de Ciencia de Materiales de Madrid (ICMM), CSIC.
Departamento de Nuevas Arquitecturas en Química de Materiales

June 2013

CONTENTS

CHAPTER 1

GENERAL INTRODUCTION

This Thesis deals with the preparation and characterization of a class of materials that is commonly referred to as bio-hybrid and bionanocomposite materials. This introductory chapter intends to review some of the key concepts that constitute the basis of the work reported in this dissertation. Firstly, general concepts of hybrid, nanocomposite and more specific concepts of bio-hybrid and bionanocomposite materials are disclosed. Secondly, protein derived bio-hybrids are reviewed, together with a more detailed bibliographic analysis of zein, a particular protein extracted from corn. Third, a brief review of the more used inorganic hosts in the preparation of bio-hybrids is addressed, and finally, the main objectives of this Thesis are disclosed.

1.1 BIO-HYBRID AND BIONANOCOMPOSITE MATERIALS

Since the past two decades, the development of organic-inorganic hybrid materials represents one of the most dynamic research areas in Materials Science and Technology, as this is one of the most creative alternatives to achieve the production and applications of highly versatile materials with many opportunities in view to commercial applications (Gómez-Romero and Sanchez, 2011; Sanchez et al., 2011). Organic-inorganic *hybrid* materials are not simply physical mixtures of various components, but their interaction determines synergistic effects driving to new features and properties (Ruiz-Hitzky, 2004). Within the hybrid materials are included the so-called *nanocomposite* materials, which are formed by two phases, a continuous and a dispersed phase, showing this last one at least one dimension at the nanometer scale. In this context, there are many examples of combination of polymers and inorganic hosts of different chemical nature and topologies, as continuous and dispersed phases, respectively (Ruiz-Hitzky et al., 2008). In this type of hybrid materials, the organic and inorganic counterparts are combined in order to take advantage of synergistic effects between the two components to generate new structural (mechanical) and functional properties (electrical and electronic, optical, magnetic), which may be useful for their potential application in different areas, for example in the development of new biomaterials, catalysts, fibers, films, membranes, sensors or adsorbents among others (Ruiz-Hitzky et al., 2009). Chronologically, the first organic-inorganic material described in the literature was an intercalation compound, resulting from the insertion of alkylammonium species between the layers of lamellar solids, such as smectite clays (montmorillonite) (Gieseking, 1939; and Hendricks, 1941).

Particularly, biological species can be also employed in the preparation of these hybrid materials, giving rise to *bio-hybrid* materials (Ruiz-Hitzky et al., 2008). This class of materials shows interesting properties, which depend not only on the characteristics of the biological species, but also on the type of the interaction mechanisms with the inorganic counterpart. As occurs in common organic-inorganic hybrids, electrostatic interactions, van der Waals forces, hydrogen bonds and water bridges, ion-dipole and coordination, and proton or electron transfer may be involved between both components (Ruiz-Hitzty et al., 2004; Ruiz-Hitzky et al., 2008). Various methods have been employed in order to obtain these bio-hybrid materials, such as intercalation of polysaccharides or proteins in layered host materials or the entrapment of living cells

or enzymes in various inorganic solids as for instance mesoporous silica or sol-gel derived matrices (Ruiz-Hitzky et al., 2008; Ruiz-Hitzky et al., 2009; Ruiz-Hitzky et al., 2010; Ruiz-Hitzky et al., 2011). Thus, representative examples of these bio-hybrid materials are the preparation of bioactive solids through the immobilization of enzymes for biosensors (Avnir et al., 2006), as well as bio-catalysis (Forano and Prevot, 2008), or the development of bio-hybrids based on the incorporation of DNA molecules in layered double hydroxides as nonviral vectors for gene therapy studies (Choy et al., 1999; Choy et al., 2000).

Within this large family of bio-hybrid materials, one of the new fields of great interest refers to the development of *bionanocomposites* (also known as nano-biocomposites), which are nanocomposites based on the assembly of polymers of natural origin (biopolymers) with the most diverse inorganic solids (Ruiz-Hitzky et al., 2008). Similarly to the conventional nanocomposites, bionanocomposites may also exhibit improved structural and functional properties, while offer biocompatible and biodegradable character associated with the biopolymer, which is of great interest for applications in the field of biomedicine and environmental remediation (Ruiz-Hitzky et al,. 2008; Darder et al., 2007; Mittal, 2011; Averous and Pollet, 2012; Ruiz-Hitzky et. al., 2013). Hence, the study of bionanocomposites represents an interdisciplinary area placed at the frontier of Materials Science, Biosciences, and Nanotechnology (Ruiz-Hitzky et al., 2005; Ruiz-Hitzky et al., 2008).

The group of bionanocomposites comprises materials of both natural and synthetic origin. Amazing bionanocomposites can be found in Nature, and illustrative examples are bones, nacre, teeth, crustacean carapaces and mollusk shells. Among them, nacre and bone, which are essentially constituted of calcium carbonate/lustrine A and collagen/hydroxyapatite, respectively, are the most studied natural bionanocomposites, not only due to their potential applications but also because of the opportunity to mimic their hierarchical complexity together with their spectacular structural and/or functional properties (Tang et al., 2003; Ruiz-Hitzky et al., 2008). Thus, an intriguing feature in natural bionanocomposites is the presence of an optimal balance between mechanical properties, durability and other functions, such as density, permeability, color, hydrophobicity, etc. In this sense, certain synthetic bionanocomposites result from the understanding of the lessons from Nature in materials design, for instance artificial nacre. However, in contrast to natural bionanocomposites, which are in general restricted to a few polysaccharides and

proteins (Dunlop and Fratzl, 2010; Swiegers, 2013), synthetic bionanocomposites can be produced with a great variety of biopolymers combined with varied inorganic solids, giving rise to a wide range of possible combinations. Together with the most diverse natural biopolymers (polysaccharides, polypeptides and proteins, nucleic acids,), inorganic solids like carbon particles, metal oxides and hydroxides, carbonates, phosphates, silica and silicates, especially including clay minerals, are employed commonly in the preparation of bionanocomposites (Ruiz-Hitzky et al., 2005; Ruiz-Hitzky et al., 2008). Given the diversity of both organic and inorganic components, assorted strategies such as ion-exchange reactions, supramolecular chemistry, self-assembly, Layer-by-Layer (LbL) deposition, biomimetics, and biomineralization were already reported for the synthesis of artificial bionanocomposites using the same or similar components as those found in Nature (Sanchez et al., 2005; Ruiz-Hitzky et al., 2008; Swiegers, 2013). These synthetic materials can show the most extended applications. For instance, focusing on the bionanocomposite materials derived from the association of polysaccharides and clay minerals, it is worth mentioning the combination of the chitosan polysaccharide with montmorillonite for application in electrochemical sensors (Darder et al., 2003; Darder et al., 2005) or as artificial nacre (Yao et al., 2010), the preparation of xanthan assembled to sepiolite fibrous clays that could mimic the mucous membrane to develop new flu vaccines (Ruiz-Hitzky et al., 2009) or bionanocomposite films with enhanced mechanical properties resulting from the association of thermoplastic starch with montmorillonite or hectorite (Chen and Evans, 2005).

Among bionanocomposites, other interesting examples refer to those derived from proteins, which will be addressed in more detail in Section 1.2. These biomacromolecules become very attractive due to the variety of functional groups present in their peptide chains, which may result in interaction points with the inorganic solids, providing the resulting bionanocomposite materials with structural and functional diversified features.

1.2 BIO-HYBRIDS AND BIONANOCOMPOSITES BASED ON PROTEINS

Although less studied than polysaccharides, proteins have been long and traditionally used as raw materials in a wide range of non-food applications such as adhesive, glues,

paints, textile fibers, paper coatings and various molded plastic items. The term *protein* comes from the Greek "*protop*" (the first, the main, most important), and its presence is essential in living organisms for the development of multiple vital processes (Nelson et al., 2008). Proteins are biopolymers constituted of linear chains built from a series of up to 20 different amino acids, where the combined effect of all these amino acid chains determines the final 3D structure and the chemical reactivity. The organization of a protein is defined by four structural levels (Figure 1.1) (Nelson et al., 2008):

a) *primary structure*: it is referred to the amino acid sequence;

b) *secondary structure:* it is the disposition of the amino acid sequence in space. The most common examples are the alpha helix, beta sheet and turns, which are stabilized by hydrogen bonds;

c) *tertiary structure:* this structure informs on the spatial relationship among secondary structures, and generally it is stabilized by nonlocal interactions, such as hydrophobic core, hydrogen bonds or disulfide bonds. Tertiary structure controls the basic function of the protein, as water solubility or transport and enzymatic functions;

d) *quaternary structure:* reports the union, by weak bonds (non-covalent) of several polypeptide chains with tertiary structure to form a protein complex.

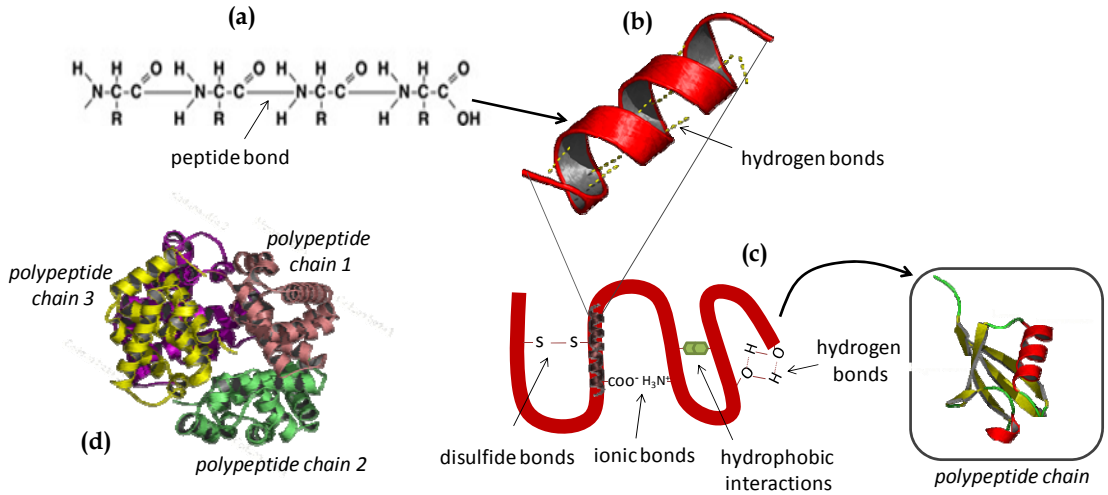

Figure 1.1 Various aspects of a protein structure: (a) primary, (b) secondary, (c) tertiary and (d) quaternary structures.

Proteins can be classified according to the shape and solubility as fibrous, globular or membrane proteins, and among their possible source are included plants (soy, zein,

gluten), animals (collagen, gelatin, casein, keratin) or bacteria (lactate dehydrogenase, chymotrypsin) (Averous and Pollet, 2012). Due to their renewable and biodegradable properties, together with their good film-forming ability, proteins are attractive biopolymers in the synthesis of bio-hybrid materials. However, its high water sensitivity and low mechanical properties are often disadvantages in the resulting protein-based materials. In the case of bionanocomposites, unmodified clays which are naturally hydrophilic can be assembled to diverse proteins as they show good compatibility with this type of biomacromolecules (Averous and Pollet, 2012). In this sense, various advanced bionanocomposite materials based on proteins have been prepared in order to enhance mechanical, as well as barrier and thermal properties, and at the same time possible interactions between the matrix protein and the involved clay are explored. Generally, there are two main processes used to prepare protein-clay bionanocomposites (Angellier-Coussy and Gastaldi, 2012):

i) *wet processes*, where a clay dispersion is added to a protein solution previously prepared, forming a single batch. The resulting protein-clay dispersion is dried by casting or by freezing-drying, forming a bionanocomposite film or foam, respectively;

ii) *dry processes*, which are based on the thermoplastic behavior of certain proteins and employ thermo-mechanical processing routes in the synthesis of protein-clay materials (e.g. extrusion).

The presence of positive and negative sites in a protein structure allows to have neutral, positive and even negative charges depending on the pH value. Thus, it provides the possibility of preparing more diversified bio-hybrids with different type of inorganic solids, including clay minerals. In this sense, it is worth mentioning the pioneering work on protein–clay interactions, which was based on the adsorption of gelatin, a structural protein derived from collagen, in the interlayer region of smectites (Talibudeen, 1950). Here, the pH control below the isoelectric point is crucial to have protonated amino groups belonging to the amino acids of the protein, promoting in this way its adsorption as a positively charged species by replacing the interlayer cations of the clay mineral. The association of gelatin with smectites and fibrous clays was most recently reported by Fernandes et al., where self-supported films of these bionanocomposites show improved mechanical properties and could be modified for application in pH sensing (Fernandes et al., 2009). In relation to this type of structural protein, interesting results were obtained in the combination of collagen and sepiolite fibrous-clay for bone tissue repair (Olmo et al. 1987). In vivo evaluations of the

resulting collagen-sepiolite bionanocomposites cross-linked with glutaraldehyde showed biocompatibility and good mechanical properties, demonstrating a persistence of 100% after several months of subcutaneous implants in rats (Olmo et al., 1996).

In addition to structural proteins, functional proteins, such as enzymes, have been also assembled to smectites. Here again, the pH control is crucial not only in view to achieve its electrostatic interaction with the silicate, by interaction with the protonated amino groups of the enzyme, but also for avoiding protein or enzyme denaturation and maintaining its biological activity (Ruiz-Hitzky et al., 2008).

Among the milk proteins, whey and casein proteins are known for their ability to produce transparent and flexible edible films, which show oxygen and oil barrier properties at low relative humidity, but poor moisture barrier due to their high hydrophilicity and water solubility. To overcome this problem, for instance whey protein has been associated with unmodified and organomodified smectite clays. The resulting bionanocomposite materials showed a significant enhancement of the water vapor barrier properties, but it was accompanied by a decrease of the mechanical behavior for clay loadings higher than 5 wt% (Sothornvit et al., 2010). Similar behavior was reported for soy protein based bionanocomposites. In this case, the introduction of the smectite clay led to a noteworthy reduction of the water vapor permeability, with a decrease of about a factor of 2 at filler contents higher than 10 wt% (Kumar et al., 2010; Kumar et al., 2010). Wheat gluten (WG) is a multicomponent agroproduct comprised of storage proteins, which confer viscoelasticity, selective permeability, and biodegradability. Homogeneous and transparent thermo-pressed WG films can be processed using palygorskite fibrous clay as nanofiller, which can reach a good dispersion and high compatibility within the biopolymer matrix. These bionanocomposites show an increase of the biodegradability with disaggregation and dwindling of WG/palygorskite films after 15 days of burial (Yuan et al., 2010).

Synthetic polypeptides are also able to be assembled to smectite clays following cation exchange mechanisms. Within this perspective, poly-L-lysine has been intercalated into homoionic montmorillonite, giving rise to very stable bionanocomposite materials with improved thermo-mechanical and barrier properties, which are the result of strong host–guest electrostatic interactions (Gougeon et al., 2003).

In a general way, most of the above cited examples of protein-clay bionanocomposites are systems in which water can be used as the main solvent in their preparation, because of the high hydrophilicity of both components. However, when a protein

presents a hydrophobic character, mainly due to the non polar amino acids residues in the structure, the solvent may play a key role in the preparation of these bionanocomposites by using wet processes of synthesis. This is the case of zein, a storage protein extracted from corn, which shows a relatively high hydrophobic character. Corn zein protein has been used as a good renewable and biodegradable material for package film forming, coatings, and plastics applications (Shukla and Cheryan, 2001). As this peculiar protein has been chosen as the principal organic counterpart of the bio-hybrids developed in this Thesis, more detailed information on the characteristics and properties of this protein, as well as on other relevant aspects, are considered in the next section of this Chapter.

1.3 CORN PROTEIN: ZEIN

Corn or maize (*Zea mays* L.) is the only cereal crop indigenous of the Americas and one of the most important food industrial crops in the world (Shukla and Cheryan, 2001). In corn, the proteins content is approximately 10% of the dry weight of the grain, while starch, soluble sugars and oil content range between 70-80%, 1-4% and 3-6%, respectively (Bicudo et al., 2006). The corn proteins are constituted of about 20% of globulins and albumins (water soluble proteins or salt solutions), 40% prolamins (water insoluble proteins and 70% v/v alcohol soluble) and 40% of gluteins (water and alcohol insoluble proteins) (Shukla and Cheryan, 2001). The proteins of these two latter groups are also known as storage protein, and in corn, the class of proteins belonging to the prolamins group is called as *zein*. Prolamin proteins occur specifically in cereals, and, in the corn, they are found exclusively in the endosperm (Shukla and Cheryan, 2001; Anderson and Lamsal, 2011). Zein is used as nitrogen source during germination and early seedling growth and as nitrogen sink during seed development (Mohammad and Esen, 1990). Thus, zein is considered the major storage protein of corn and an important source of protein in the human diet, since it is present in human food due to direct consumption or by consumption of animals whose diet is based on corn, such as poultry or swines (Bicudo et al., 2006). Although zein is known since its first isolation in 1821 by the scientist John Gorham (Lawton, 2002; Anderson and Lamsal, 2011) it is remarkable the recent interest in the study of this protein, not only because of its nutritional value, but also due their potential technological use.

Zein is rich in non-polar amino acid residues such as valine, leucine, proline, isoleucine, alanine, and phenylalanine, which confer a hydrophobic character to the protein and thus, zein is insoluble in water but soluble in aqueous ethanol (60-95%(v/v)), and some organic polar solvents such as propylene glycol and acetic acid (Shukla and Cheryan, 2001; Li et al., 2012). Zein is also soluble in aqueous solutions at pH above 11, in the presence of sodium dodecyl sulfate (SDS) and in water solutions that contain urea at high concentrations (Shukla and Cheryan, 2001). Such features of zein are determined by its structure, and vary widely depending on the protein fraction, processing, chemical modifications and other factors. Thus, a good knowledge of structural and solubility properties of zein becomes essential for the preparation of materials based on this protein.

1.3.1 Structure of zein

Naturally occurring zein is present in whole corn as aggregates linked by disulfide bonds. However, some of those bonds may be broken by the alcohol reducing agents during its extraction (Padua and Wang, 2002). Thus, zein is found as a mixture of protein complexes whose molecular size, solubility and charge depend on the corn variety and the separation method used for extraction. In this sense, zein can be separated into four protein fractions according to the Esen's system (Esen, 1987; Esen, 1990): α-zein (75-85% of the total zein, 21-25kDa), β- zein (10-15% of the total zein, 17-18kDa), γ-zein (5-10% of the total zein, 27kDa), and δ-zein (10kDa). α-Zein is the most abundant fraction and it presents a unique amino acid sequence which is responsible for its high hydrophobic properties, nearly 50 times higher than that of albumin, γ-globulin, and fibrinogen of bovine blood (Wang et al., 2004). Commercial preparations contain primarily α-zein, mainly composed of two sub-fractions, Z19 and Z22, consisting of 210 amino acids for Z19 and 245 amino acids for the Z22 fraction, whose molecular weight range determined by electrophoresis is between 23 to 24 kDa and 26 to 27 kDa, respectively (Shewry and Tatham, 1990). Both Z19 and Z22 peptide chains shared similar amino acid sequences: N-terminals that contain 35 to 36 amino acids, C-terminals that are composed of about 10 amino acids, and the central domain consisting of 9 (for Z19) or 10 (for Z22) repetitive domains comprised each one of about 20 residuals (Figure 1.2) (Shewry and Tatham, 1990).

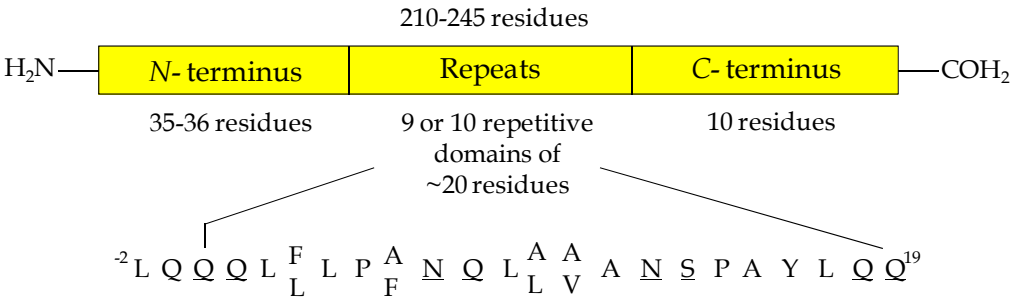

Figure 1.2 Amino acid sequences of Z19 and Z22 subfractions of α-zein (Adapted from Shewry and Tatham, 1990).

Based on the high content in α-helices, the repeating domain was proposed to be composed of flanked hydrophobic helices and linked by polar glutamine-rich turn regions (Figure 1.3). Argos and co-workers (Argos et al., 1982), investigated the secondary and tertiary structure of zein, and reported a possible structure that contains 9 or 10 α-helix segments. Most recently, based on small-angle X-ray scattering measurements (SAXS), Matsushima et al. (Matsushima et al.,1997) proposed that the helical segments were aligned forming a compact rectangular prism with dimensions of 16 x 4.6 x 1.2 nm^3 (Figure 1.3). In this arrangement, the top and bottom surfaces of the molecule (i.e. the bases of the prism) are composed of glutamine-rich loops that show a hydrophilic character, while the side surfaces containing the α-helix (i.e. the faces of the prism) show hydrophobic properties. These and other data have given rise to several possible models for the tertiary structure, although there is not yet a definitive structural model of zein (Padua and Wang, 2002; Bugs et al., 2004).

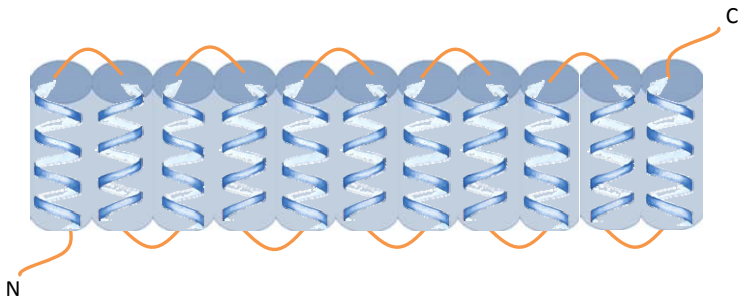

Figure 1.3 The modelic structure of the zein proposed by Matsushima and co-workers (Adapted from Matsushima et al., 1997).

1.3.2 Solubility of zein

Zein is soluble in various primary, binary and ternary solvent systems, mainly determined by the balance between the polar/nonpolar groups in those systems. Because of the large proportion of hydrophobic residues in zein, this protein is not soluble in pure water. It has been proposed that zein exhibits two regions, a hydrophobic-one rich in isoleucine, proline and alanine, located at the final part of the molecule, and another of slightly high polarity that is rich in glutamic acid and tyrosine. Therefore, zein becomes soluble in water at pH above 11, likely due to the ionization of the phenolic groups from the tyrosine and because of the presence of glutamic acid residues. Zein is also soluble in organic solvents with hydroxyl, carboxyl, amino, and other polar groups in proper ratio to non polar groups (Pomes, 1971). Solubilization of zein was studied in binary solvents by Manley and Evans (Manley and Evans, 1943), who tested aqueous systems incorporating ketone, small aliphatic alcohols or dioxane. Among them, aqueous alcohol solutions are the most common solvents for zein. The solubility behavior of zein in ethanol/water mixtures is shown in the form of a ternary phase diagram in Figure 1.4. According to this Figure 1.4, at constant temperature, zein is soluble when its content is below 60% (w/w) (Shukla and Cheryan, 2001). In these conditions, a complete zein solubilization is achieved only when the ethanol concentration ranges between 50% and 90%, with coacervation and precipitation phenomena taking place both above and below this range (Shukla and Cheryan, 2001).

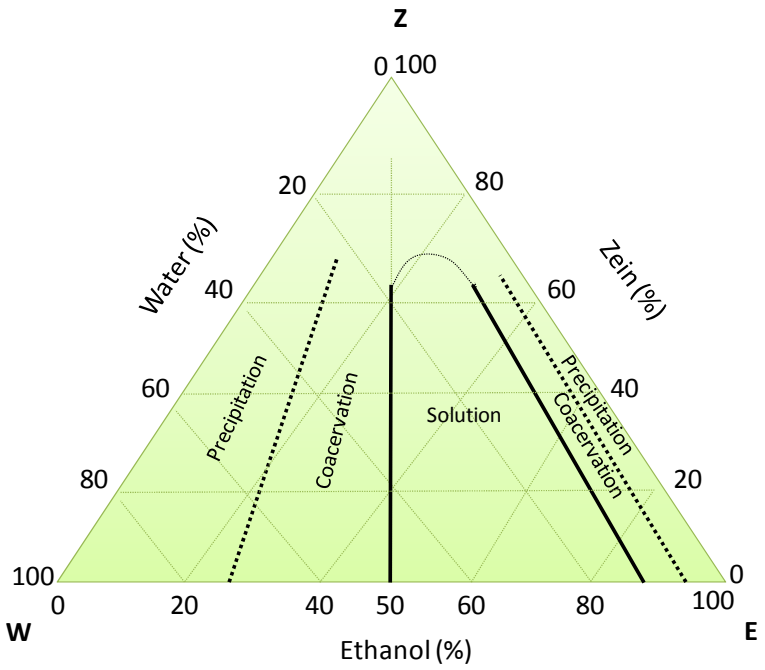

Figure 1.4 Ternary phase diagram for the solubility of zein in ethanol and water. (Adapted from Shukla and Cheryan, 2001).

1.3.3 Zein-based bionanocomposite materials

As indicated above, nowadays there is an increasing technological interest in corn storage proteins, as biodegradable and renewable raw materials from biological origin, which may contribute to decrease the environmental impact of petroleum-derived plastics. Since 1985, zein received the name of substance "generally recognized as safe" (GRAS) by the Food Drug Administration (FDA), (http://www.gpo.gov/fdsys/pkg/CFR-2011-title21-vol3/pdf/CFR-2011-title21-vol3-art184.pdf. Accessed on May 11, 2013. Thenceforth, the interest in this protein is considerably increasing as it may allow for instance the production of edible films or drug coatings. In addition to the GRAS certificate, zein shows some interesting properties that differ from other common proteins, such as its high hydrophobicity, which could be relevant in the preparation of materials in which zein can act as a barrier to moisture and oxygen (Wasa and Takahsahi, 1998; Bicudo et al., 2006). Zein also shows thermoplastic properties which can be profited to achieve an excellent film formation, being widely used in the food and pharmaceutical industries due to its biodegradability and non-toxicity (Lawton, 2002; Yang et al., 2013). In this way, zein is

also employed commonly as a component of a widespread range of products, which include adhesives, biodegradable plastics, gum, fibers, cosmetic powders (Shukla and Cheryan, 2001), microencapsulation systems for drug release (Wang et al., 2005) and pesticides carriers (McArdle, 1998), scaffolds for tissue engineering (Jiang et al., 2010), or even in the fabrication of microfluidic devices (Luecha et al., 2011).

Although it has been reported the use of zein in diverse fields, either as pure zein or in combination with other compounds (e.g. polysaccharides), the association of this protein with inorganic solids is still very recent. In fact, the first work reported in the literature on the preparation of bionanocomposites based on zein was just five years ago (Qu et al., 2008). This pioneering work showed that hydroxyapatite combined with zein protein could have a potential use as scaffolds in tissue engineering due to its good biocompatibility and enhanced mechanical properties compared to scaffolds based on pure zein (Qu et al., 2008). The combination of zein with different clay minerals and organoclays in view to produce new bio-hybrid materials has been recently investigated and patented in our Group at the ICMM (Alcântara et al., 2008; Ruiz Hitzky et al., 2010). These studies introduced results on the main interactions that can take place during zein adsorption from ethanol/water mixtures on organo-smectites, as well as on neat sepiolite and palygorskite microfibrous clays (Alcântara et al., 2008). More recently, it has been reported that these latter bio-hybrids can be used as nanofillers of alginate polysaccharide matrices, showing good water resistance and mechanical properties, as well as enhanced barrier properties toward water vapor and UV-light compared to the pristine polysaccharide, being promising materials for food packaging applications (Alcântara et al., 2011; Alcântara et al., 2012).

With the aim to improve the properties of zein-based films, Luecha and co-authors developed bionanocomposites based on the addition of organomodified montmorillonites in a zein matrix via blown extrusion processing (Luecha et al., 2010.). The introduction of the organoclay did not affect the translucency and yellow color of the resulting films, while the thermal stability was significantly improved. In these materials, the mechanical and barrier properties did not improve linearly with clay content, showing optimal values for 5 wt% in clay content. Bio-hybrids based on zein and organomodified montmorillonite were also used as coating of propylene (PP) films, improving the oxygen and water vapor barrier properties in the resulting films (Ozcalik and Tihminlioglu, 2013).

Due to their biocompatibility and null toxicity, bionanocomposites based on zein and conformed as beads were also investigated as slow-release systems of bioactive molecules, such as drugs. An example of this application is a system in which the ibuprofen drug was intercalated into a MgAl layered double hydroxide (LDH) and then incorporated in a blend consisting of zein and alginate (Alcântara et al., 2010). The synergistic properties afforded by the components in the bionanocomposite result in a system resistant to pH changes, making possible a gradual release of the drug. The presence of zein limited the absorption of water, contributing to a more controlled release in comparison to bionanocomposites based only on alginate or LDH-ibuprofen.

1.4 INORGANIC HOST MATERIALS

Clay minerals are one of the most studied host substrates in the preparation of hybrid materials (Ruiz-Hitzty et al., 2004). They are also interesting for the development of bio-hybrids, because they are constituents of the natural environment, and show in general a nonhazardous nature and biocompatibility, as well as re-usable properties as they can be returned to the Earth after use (Ruiz-Hitzky et al., 2010; Sanchez et al., 2011). In this Thesis, various natural clay minerals of diverse nature, charge and dimension at the nanometer scale were used. One of them was a montmorillonite belonging to the smectite family, and the other two were the fibrous clays, sepiolite and palygorskite. In addition to these clay minerals, two synthetic layered hydroxides, a layered double hydroxide (LDH) and a layered single hydroxide (LSH), were also employed as host materials in this work. Each of the following subsections includes a brief description of these inorganic solids used in this Thesis as host substrates in the development of zein bio-hybrids.

1.4.1 Smectite clays

Montmorillonite, is a phyllosilicate of the smectite clay family, characterized by a colloidal particle size, high specific surface area and large cation exchange capacity (CEC). It is a 2:1 charged layered silicate in which each layer is formed by the repetition of octahedral alumina sheet sandwiched by two tetrahedral silica sheets (Figure 1.5) (Brigatti et al., 2006). In the tetrahedral positions, the Si^{4+} ions may suffer isomorphic substitutions by Al^{3+} or Fe^{3+}, and in the octahedral positions the Al^{3+} ions can be also

replaced by Mg^{2+}or Fe^{2+} generating a negative charge in the layers that is compensated by cations located in the interlayer region of the silicate (Brigatti et al., 2006). The interlayer cations are usually hydrated and can suffer ion-exchange reactions.

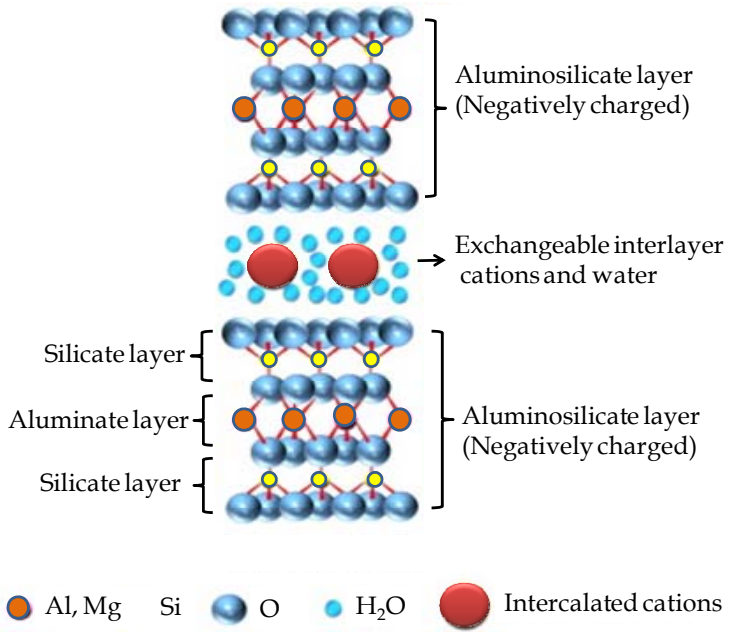

Figure 1.5 Schematic representation of the crystal structure of a montmorillonite.

Montmorillonite clay is one of most common inorganic solids used in the preparation of hybrid materials of the intercalation compound type. Its high aspect ratio (100-1000), large swelling and cation exchange capacities (70 – 100 meq / 100 g of clay) favor its combination with water-soluble molecular and macromolecular species in the preparation of the most diverse hybrid materials, resulting in nanostructured systems that include the bionanocomposite materials. In this context, organic-inorganic hybrids based on montmorillonite have been prepared by ion exchange processes in which the interlayer cations located between the sheets are displaced by various organic cations such as alkylammonium species, dyes, polymers, etc., adopting different geometrical arrangements (Ruiz-Hitzty et al., 2004; Ruiz-Hitzky, 2004). Besides intercalation, it is possible to achieve exfoliated structures when polymers or biopolymers are used in the preparation of the hybrid materials. Intercalation of organic species in laminar solids, generally accompanied by an increase in the interlayer distance of the inorganic host solid, allows the organic compounds to be perfectly accommodated in the intracrystalline space (Figure 1.6a), while exfoliation leads to a total disaggregation of the layers, preserving few units of stacked layers (Figure 1.6b) (Ruiz-Hitzky and Van

Meerbeeck, 2006; Bergaya et al., 2012). The intercalated compound can be a neutral or a positively charged species, and it may also have various functionalities such as alcohols or amino groups among others (Ruiz-Hitzty et al., 2004). Among these molecules, it has been demonstrated that large biopolymers, such as polysaccharides (Darder et al., 2003) and proteins (De Cristofaro and Violante, 2001; Chen and Zhang, 2006) can be intercalated in the interlamellar space of montmorillonites to achieve the formation of bionanocomposites of interest in diverse applications (Ruiz-Hitzky et al., 2005).

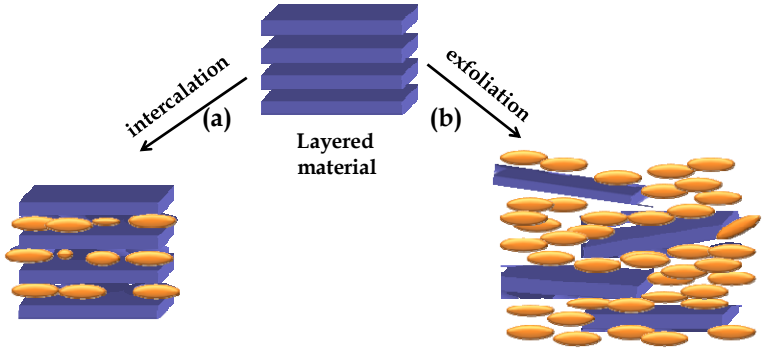

Figure 1.6 Different structures that can be obtained by the incorporation of (bio)polymers into layered clays when preparing (bio)nanocomposite materials: (a) intercalated and (b) exfoliated structures.

1.4.2 Fibrous clays

Sepiolite is a hydrated magnesium silicate of ideal formula ($Si_{12}O_{30}Mg_8(OH)_4(H_2O)_4{\cdot}8H_2O$) and microfibrous morphology that displays a crystalline structure alternating blocks and tunnels of nanometer sections, which are accessible to water and other small molecules (Ruiz-Hitzky, 2001). The presence of pores of different size makes this mineral an excellent adsorbent material. *Palygorskite*, also known as attapulgite, is structurally related to sepiolite, showing a higher aluminum content with respect to magnesium and channels of smaller sections (Galán, 2011). These two fibrous clays are composed of ribbons of a 2:1 phyllosilicate structure, but in opposition to the previously mentioned layered montmorillonite clays, which have continuous tetrahedral and octahedral sheets, these fibrous clays have a discontinuity in the octahedral sheets, due to the regular inversions of the silicon

tetrahedron orientation. The formation of channels in the structure determines the presence of ≡Si-OH groups at the external surface of the silicate fibers (Figure 1.7) (Ruiz-Hitzky, 2001; Galán, 2011). Isomorphic substitution of Si for Al in the tetrahedra is very limited in both minerals. In sepiolite, the octahedral positions are filled by Mg, but recent studies have proposed that some substitutions of Mg by Al or Fe can take place in the octahedral sites (García-Romero, and Suárez, M, 2010). Fe and, to a lesser extent, Mg tend to occupy edge positions in palygorskite whereas the interior positions are occupied predominantly by the smaller Al ion (Galán, E. (1996). These isomorphic substitutions are responsible for a relatively low cation exchange capacity in these silicates (15meq/100 g for sepiolite, for example). Since connections in the direction perpendicular to the layers are assured in part by covalent bonds (Si-O-Si), fibrous minerals cannot present the phenomenon of swelling. Sepiolite and palygorskite differ in their unit cell dimensions, larger for sepiolite than for palygorskite, showing dimensions of the cross-section of the tunnels of 1.06 x 0.37 nm^2 and 0.64 x 0.37 nm^2 for sepiolite and palygorskite, respectively (Ruiz-Hitzky, 2013.). Fiber sizes vary widely, but generally range from approximately 10 nm to 4-5 µm in length, 10 nm to 30 nm in width, and 5 nm to 10 nm in thickness (Cornejo and Hermosin, 1988; Galán, 1996). The presence of micropores and channels in these minerals together with the fine particle size and fibrous morphology, define their high surface area (around 320 and 150 m^2/g for sepiolite and palygorskite, respectively) (Galán, 2011).

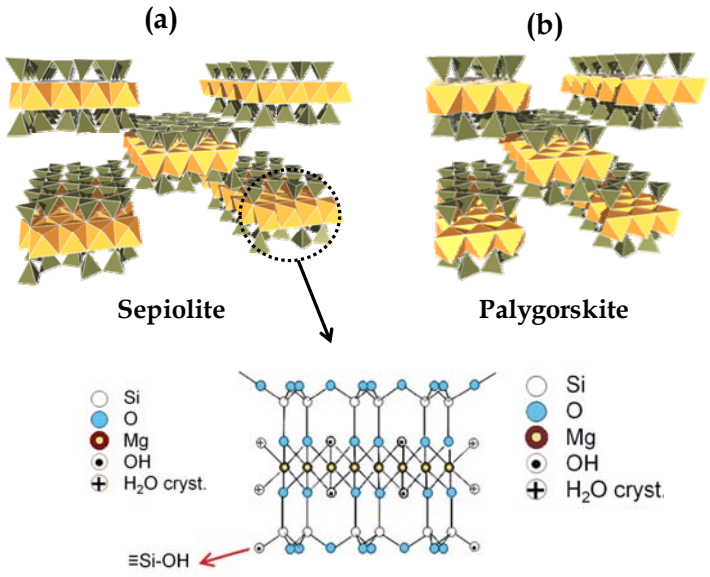

Figure 1.7 Schematic representation of the crystal structure of sepiolite and palygorskite.

Although these clays do not present intercalation properties like smectite clays, sepiolite and palygorskite offer other interesting characteristics: a large specific surface area and microporosity (Ruiz-Hitzky et al., 2011), as already mentioned, and the presence of Si-OH groups at their external surface, which make possible the functionalization of these clays in order to introduce new properties (Ruiz-Hitzky et al., 2011). Thus, as indicated above, the surface properties of these fibrous silicates are the reason of their special ability to interact with many different compounds, including polymers and macromolecules of biological origin, forming hybrid and bio-hybrid materials with implication in many diverse uses and industrial applications. The presence of Si-OH groups is also of special relevance in the formation of hybrid compounds. These free Si-OH silanol groups along the rims of the channels and at the end of the tunnels are directly accessible to diverse organic species including coupling agents and polymers, allowing the preparation of a wide variety of organo-inorganic materials (Galán, 1996; Alvarez et al., 2011; Ruiz-Hitzky et al., 2011).

Bionanocomposites based on sepiolite and palygorskite involving different types of water soluble polysaccharides (starch, agarose, guar gum, locust bean gum, chitosan, alginate, xanthan, carrageenan…), proteins (gelatine, collagen, wheat gluten) and other biomolecules have been reported (Ruiz-Hitzky et al., 2013), as well as the development of biomimetic interfaces in the preparation of bio-hybrids based on phospholipids as immobilization hosts for biological species (Wicklein et al., 2010; Wicklein et al., 2011). These bionanocomposites were usually processed as films (Darder et al., 2006; Fernandes et al., 2009; Yuan et al., 2010), or as hierarchical porous structures (cellular structures) by means of solvent casting or freeze-drying processes (Ruiz-Hitzky et al., 2010). In certain cases, these materials can exhibit enhanced mechanical properties compared to analogous materials based on layered silicates, which could be relevant in numerous applications as for instance thermal and acoustical insulation, as well as in the packaging industry.

Sepiolite has been also used as support of nanoparticles of different origin, such as metals, metal oxides, hydroxides and oxyhydroxides (Ruiz-Hitzky et al, 2011). In fact, the assembly of *magnetic nanoparticles* (NP) on sepiolite and palygorskite via the use of ferrofluids has been recently developed (Ruiz-Hitzky et al., 2011). The resulting materials exhibit good stability and the presence of NP provide the modified fibrous clays with new functionalities, like superparamagnetic behavior in the present case.

These materials have a huge potential in a large variety of applications such as magnetic carriers for drugs targeting, adsorbents, magnetic and magnetooptical sensors or catalysis. (González-Alfaro et al., 2011).

1.4.3 Layered hydroxides

Layered double hydroxides (LDHs) and layered single hydroxides (LSHs), also known as anionic clays, are versatile inorganic host materials showing a layered structure. They have been extensively used in the preparation of hybrid materials due to their remarkable anion-exchange properties, useful in the preparation of diverse intercalation compounds. This type of solids offers a variety of industrial and environmental applications such as anion-exchangers, catalysts, drug delivery systems, anticorrosive additives and others.

- **Layered double hydroxide (LDH)**

Layered double hydroxides (LDHs), also known as hydrotalcite-like compounds or anionic clays, are widely used as catalysts or catalyst precursors, adsorbents, intermediates in the synthesis of advanced ceramic materials, in the preparation of modified electrodes, in medical and environmental applications as inorganic host matrices for drug or herbicide release, or as protective anti-corrosive additives and as nanofillers of polymers (O`Hare, 2002; Cardoso et al., 2006; Centi and Perathoner, 2008; O`Hare and Wang, 2012; Leroux, 2012). Although there are LDHs of natural origin like hydrotalcite, usually these materials are easily synthesized in the laboratory, for both research and applications purposes. The most common synthetic procedures are simple and low cost, allowing the isolation of high purity solids corresponding to the general formula $[M^{2+}_{(1-x)}M^{3+}_{x}(OH)_2](An^-)_{x/n}\cdot zH_2O$, where M is a metal ion, and An^- is an interlayer anion (Bergaya et al., 2006; Forano and Prevot, 2007). LDHs present a similar structure to that of brucite, the mineral of formula $Mg(OH)_2$, where Mg ions are located in the center of the octahedra, defined by OH^- anions occupying their vertices. Isomorphic substitution of divalent cations by trivalent cations in the brucite structure, results in structural layers with a net positive charge. This deficit of charge in the layers is compensated by anions located in the interlayer region. In the natural hydrotalcite

mineral, where Mg^{2+} ions are replaced by Al^{3+} ions and the interlayer region is occupied by CO_3^{2-} together with water molecules, the layer stacking results in a LDH structure of composition $[Mg_6Al_2(OH)_{16}](CO_3)\cdot H_2O$ (Figure 1.8) (Cavani et al., 1991; Rives and Ulibarri, 1999).

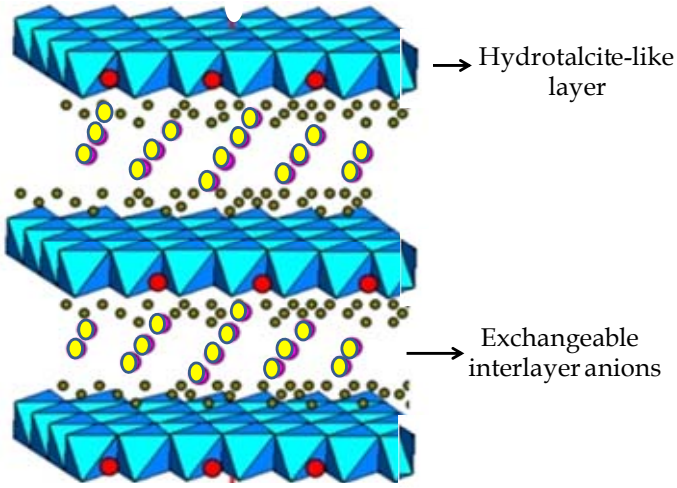

Figure 1.8 Schematic representation of the crystalline structure of a hydrotalcite-like solid, showing the polyhedrons in octahedral coordination in which metal atoms are located in the center and OH groups in the vertices.

The versatility of the LDH is related to both the wide variety of anions that can be intercalated (typically CO_3^{2-}, NO^{3-} , Cl^-, or OH^-) and to the diverse nature and M^{2+}/M^{3+} ratio of cations that can be combined in the synthesis (e.g. M^{2+}: Mg^{2+}, Zn^{2+}, Fe^{2+}, Cu^{2+}…; M^{3+}: Al^{3+}, Cr^{3+}, Mn^{3+}, Fe^{3+}…). The presence of anions in the interlayer space confers anionic exchange properties that have been explored in the preparation of numerous intercalation compounds based on negatively charged organic species, such as carboxylates, sulfonates and diverse type of polymeric species (Trujillano et al., 2002; Leroux and Taviot-Gueho, 2005; Herrero et al., 2009). Likewise, it has been also reported the possibility of assembling biopolymers provided with negatively charged sites, such as alginate or carrageenan polysaccharides (Darder et al., 2005) or DNA (Choy et al., 2004). In these materials, the inorganic counterpart confers good chemical and thermal stability to the resulting bio-hybrid materials.

Different routes of synthesis can be applied in order to obtain hybrid or bio-hybrid materials based on LDH by incorporation of the guest species in the interlayer region of the solid (Nalawde et al., 2009):

a) *ion-exchange reaction*: intercalation of anionic organic compounds provided with negative charges, e.g. $-COO^-$ groups, into the lamellar LDH galleries by anion exchange of the LDH interlayer anions;
b) *co-precipitation method*: also known as *in situ* intercalation, consists on the synthesis of the LDH in the presence of the organic compound. The guest organic species becomes trapped between the sheets of HDL that are being formed during the synthesis;
c) *reconstruction methodology*: In this case, a previously formed LDH is transformed in the corresponding layered double oxide (LDO) by thermal treatment, and then the LDH is reconstructed in an aqueous medium where the organic compound is also present. Here again, the negative sites of the organic compounds compensates the positive charge of the reconstructed LDH.

Although it is well known the intercalation of biopolymers in LDH, examples of the incorporation of other biomacromolecules, such as proteins and related biomolecules, are still very few. In this sense, it is remarkable the work by Nakayama and co-authors (Nakayama et al., 2004), reporting the intercalation of amino acids and various peptides into a MgAl-LDH, by reconstruction from the layered MgAl oxide precursor. This same procedure was employed to achieve the intercalation of amino acids into ZnAl-LDH (Aisawa et al., 2004). In this study, it was found that the intercalation behavior of diverse amino acids was greatly influenced by the type of side-chains, structure and physicochemical properties of the involved amino acid. Other LDHs such as those based on MnAl, NiAl, and ZnCr have been also used as host of phenylalanine (Phe) amino acid being the intercalation compound prepared by the co-precipitation method (Aisawa et al., 2001).

On the other hand, LDH have been widely used as suitable immobilization matrices for entrapment of enzymes for application in electrochemical biosensing, but in these cases a composite material is usually formed without intercalation of the biomolecule in the interlayer space of the LDH (Mousty, 2004; Mousty, 2010; Mousty and Prevot, 2013). An example of these composites was prepared by alternative assembly of hemoglobin (Hb) and horseradish peroxidase (HRP) molecules with LDH nanosheets *via* Layer-by-

Layer (LbL) deposition technique has been used to fabricate a bi-proteinic biosensor. In this case, a stable direct electrochemical redox behavior was observed for an electrode modified with a film comprising two layers of (LDH/Hb/LDH/HRP),owing to the favorable microenvironment imposed by the LDH nanosheets (Kong et al., 2010). Hb was also immobilized recently in a MgAl-LDH by co-precipitation of the LDH at pH 9.0 (Charradi et al., 2010), and the interactions between Hb and LDH particles were investigated by diverse physicochemical techniques. The resulting bio-hybrid was tested as a bioelectrode showing a low detection limit and a very high sensitivity in the amperometric detection of H_2O_2.

- **Layered simple hydroxide (LDH)**

A related family of layered hydroxides is that encompassing the so-called *layered simple hydroxides* (LSH), whose structure is identical to LDH, only that in this case the inorganic layers are composed of only one type of metal cation, such as Mg^{2+}, Cu^{2+}, Zn^{2+} and Ni^{2+} and can be represented by the general formula, $[M^{II}_2(OH)_{4-x}(A^{m-})_{x/m}]\cdot nH_2O$ (Figure 1.9) (Hussein et al., 2012; Si et al., 2012). In this structure, the A^{m-} anions are coordinated to the in-plane metal ions and the inorganic layers are essentially neutral (Rogez et al., 2011). In spite of this, as occurs in LDH solids, LSH can also undergo anion-exchange reactions, by substituting the exchangeable interlayer anions in the LSH lattice with negatively charged organic molecules, leading to the formation of layered bio-hybrids. It should be noted that in these cases, the metal–anion bond results in a strong interaction between molecules intercalated between the layers and the metal inorganic network (Si et al., 2012).

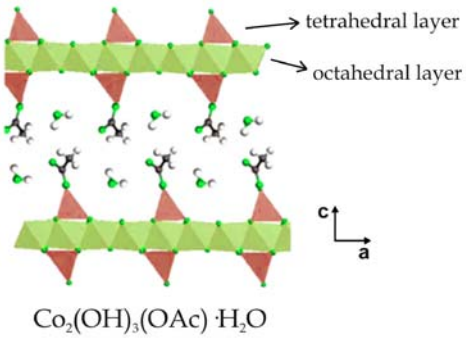

Figure 1.9 Schematic representation of the crystal structure of a typical LSH, cobalt acetate hydroxide in this case. (Si et al., 2012).

Analogously to LDH, LSH show the intrinsic features of layered hydroxides, such as low cost and easy synthesis, good compatibility with diverse anionic guest species, as well as enhanced stability and protection of the intercalated molecule, making them suitable hosts for the development of materials of interest in biomedicine and environmental fields (Hussein et al, 2012; Rogez et al., 2011). Also similarly to the LDH, the co-precipitation method and ion-exchange reaction are procedures of synthesis commonly employed in the preparation of bio-hybrids based on LSH. In addition to these areas, LSH are highly promising matrices for the development of new magnetic and optically active hybrids (Forster et al., 2004; Delahaye et al., 2010). In this sense, an interesting example of new functional bio-hybrid compounds is based on the intercalation of a series of ten peptides in the intracrystalline space of Cu(II) and Co(II) LSH (Si et al., 2012). Studies on the luminescence *vs.* pH of the synthesis medium in these bio-hybrids indicate that the deprotonation of the tyrosine fractions to tyrosinate occurring at high pH is accompanied by the onset of luminescence. This effect increases with increasing OH^- concentration, suggesting that these bio-hybrids may have potential application as chemical sensors. Moreover, their magnetic properties are strongly influenced by the presence of the peptides in the bio-hybrid, showing the copper- and cobalt-based hybrids antiferromagnetic and ferromagnetic behavior, respectively (Si et al., 2012).

1.5 OBJECTIVES OF THIS DISSERTATION

Bio-hybrid materials are a thematic of great relevance in many research fields, being many of them based on polysaccharides and some proteins, but few studies are focused on the corn protein, zein. Thus, this Thesis addresses as main objective the development of new bio-hybrid materials based on zein combined with various inorganic solids, such as clays minerals and layered hydroxides, employing several strategies of synthesis.

Firstly, the fundamental characteristics of zein are addressed. Although the main solvents used for dissolving zein have been reported in the literature (Shukla and Cheryan, 2001), the main physico-chemical characteristics of zein in different solvents such as alkaline media or pure alcohol are still unknown. Since knowledge of these

properties is of outstanding importance for the understanding of the assembly of zein to different inorganic solids, an extensive study of the transformations experienced by zein in different solvents, will be considered as a first step know the nature of the protein species in each medium in view to in the design of hybrid materials based on this protein.

On the basis of this knowledge, a first objective will be addressed to the study of the assembly of zein to layered clays. In this study, montmorillonite containing sodium or alkylammonium cations in the interlayer region of clay will be employed as inorganic substrate. The influence of the interlayer of cation, as well as the choice of the suitable solvent is a crucial issue to reach the function of these zein-montmorillonite bio-hybrids with the protein intercalated. Thus, a systematic study controlling the synthesis conditions in order achieve the intercalation of protein and to understand of formation of the bio-hybrids, the nature of interactions between both components and the main properties of the resulting bio-hybrids will be explored.

The third aim is related to the assembly of the zein protein to natural fibrous silicates. A detailed study of the kind of interactions that take place between the zein and sepiolite and palygorskite fibrous clays, the influence of the zein assembly on the hydrophilic/hydrophobic characteristics on these clays and the most diverse properties of the resulting bio-hybrids will be investigated. Additionally, the preparation of bio-hybrids based on zein and sepiolite modified with magnetic nanoparticles will be also evaluated. Special attention will be given to the physico-chemical characterization and the processing of these zein-fibrous clays bio-hybrids in view of their possible applications.

The fourth aim of this work will be addressed to a preliminary exploration of the development of new bio-hybrids based on zein and other organic solids, in this case, two layered hydroxides a MgAl-layered double hydroxide and a Co-layered simple hydroxides. The physico-chemical characterization of the resulting materials will give information on the different possible interactions between the protein and the positively charged layers of these host solids, as well as on the possible arrangement of zein in these bio-hybrids.

Finally, various types of processing of the zein bio-hybrids will be also evaluated in view of potential applications. Thus, zein-sepiolite bio-hybrids processed as particulate materials will be tested as filler in the development of bionanocomposite materials based on different biopolymer matrices. In this sense, an insight on the reinforcing capacity of zein-based bio-hybrids in biopolymer matrices will be addressed, in view of application as bioplastics provided with water vapor or gas barrier properties or as membranes for gas separation. On the other hand, zein-clay materials will be processed as foams using a new methodology that profits from the solubility of the protein in different solvents. The properties of zein bionanocomposite foams as potential biosorbent for herbicide retention will be evaluated.

CHAPTER 2

MATERIALS AND METHODS

2.1 STARTING MATERIALS

Diverse types of bionanocomposite materials based on the zein protein were prepared in this Thesis using as inorganic counterpart various clays of different nature, fibrous or layered, such as sepiolite and palygorskite or montmorillonite, respectively. Besides them, layered double hydroxide and magnetic nanoparticles were also employed in the preparation of various zein-based bionanocomposites.

2.1.1 Zein

Zein protein (Z) from corn used in this study was furnished by Sigma-Aldrich. This protein is presented as a yellow powder and was reported to be approximately 35% α-zein, which includes two sub-units of average molecular weight of 22 and 24 kDa (Sigma-Aldrich product information).

2.1.2 Sepiolite

Microfibrous sepiolite (SEP) from Vallecas, Madrid – Spain, of >95% purity and commercialized as Pangel® S9 was generously supplied by Tolsa S.A. (Spain). The chemical composition of sepiolite is indicated in Table 2.1. The clay presents a total specific surface area, determined from BET measurements, of 320 m^2/g, of which 150 m^2/g corresponds to the external surface area, and a cation exchange capacity (CEC) value of approximately 15 meq/100g.

Table 2.1. Chemical composition of the sepiolite Pangel® S9 employed in this work.

	SiO_2	Al_2O_3	MgO	Na_2O	MnO_3	CaO	K_2O	F^-
Sepiolite	62.5%	1.20%	25.2%	0.09%	0.50%	0.4%	0.3%	~1%

2.1.3 Palygorskite

Palygorskite (PALY) fibrous clay from State of Piauí – Brazil - was kindly provided by Prof. L. S. Barreto (Universidade Federal de Sergipe, Brazil). BET measurements afforded a total specific surface area of approximately 150 m^2/g, where 120 m^2/g is related to its external surface.

2.1.4 Montmorillonite

A natural Wyoming montmorillonite clay was employed in this Thesis, exchanged with two types of interlayer cations: Na^+ and quaternary ammonium cations. Commercial montmorillonite were purchased from Southern Clay Products (USA) and correspond to the commercial products Cloisite®Na^+ (CloisNa) and Cloisite®30B (Clois30B), respectively (Table 2.2). The cation exchange capacity of this clay is 90 meq/100g. The interlayer cation in Cloisite®30B is known to be bis-(2-hydroxy ethylmethyl hydrogenated tallowalkyl) quaternary ammonium.

Table 2.2 Specifications of the montmorillonite clays used in this work.

Montmorillonite	Interlayer cation	Gallery d-spacing d_{001} (nm)	Organic content (% mass)
CloisNa	Na^+	1.18	-
Clois30B	$CH_3-N^+(CH_2CH_2OH)(CH_2CH_2OH)-T^*$	1.80	28%

* Tallow consists in ~ 65% C_{18}, ~ 30% C_{16} and ~ 5% C_{14}, and a chloride anion.

2.2 OTHER STARTING MATERIALS AND REAGENTS

Table 2.3 presents other reagents used in this work, including its formula, provenance and purity. Deionized water (resistivity of 18.2 MΩ cm) was obtained from a Maxima Ultrapure Water system from Elga.

Table 2.3. Reagents used in this work with their corresponding formula, supplier and purity.

Reagent	Formula	Supplier	Purity (%)
Ethanol	C_2H_5OH	Panreac	A.C.S.
n-Heptane	C_7H_{16}	Sigma-Aldrich	A.C.S.
Acetone	CH_3COCH_3	Cor Química	≥ 99.5%
Hydrochloric acid 37%	HCl	Carlo Erba	A.C.S.
Aluminum chloride hexahydrate	$AlCl_3{\cdot}6H_2O$	Fluka	≥ 99%
Magnesium nitrate hexahydrate	$Mg(NO_3)_2{\cdot}6H_2O$	Fluka	≥ 99%
Sodium carbonate anhydrous	Na_2CO_3	Fluka	≥ 99%
Sodium hydroxide anhydrous	NaOH	Fluka	≥ 98%
Aluminum nitrate nonahydrate	$Al(NO_3)_3{\cdot}9H_2O$	Merck	≥ 99%
Magnesium chloride hexahydrate	$MgCl_2{\cdot}6H_2O$	Panreac	≥ 99%
Cobalt acetate tetrahydrate	$Co(CH_3COO)_2{\cdot}4H_2O$	Sigma-Aldrich	≥ 99%
Ninhydrin spray solution	$C_9H_6O_4$	Merck	≥ 98%
Calcium chloride	$CaCl_2$	Fluka	≥ 99%
2-Methyl-4-chlorophenoxyacetic acid	$C_9H_9ClO_3$	Sigma-Aldrich	≥ 95%

In this Thesis, the alginate and starch from maize polysaccharides (Figure 2.1)were also used as biopolymer matrices in the preparation of bionanocomposites, both obtained from Sigma-Aldrich.

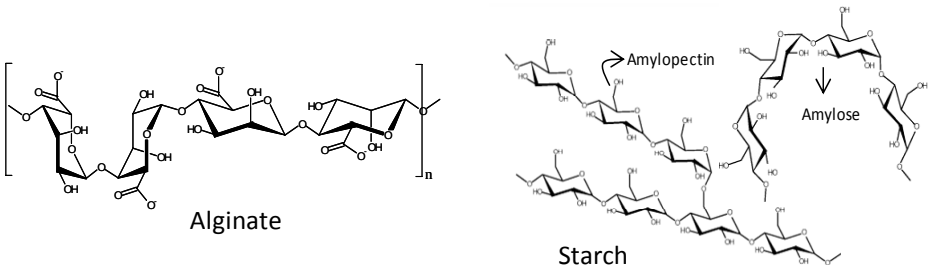

Figure 2.1 Representation of the molecular structure of the alginate and starch polysaccharides.

2.3 SYNTHESIS AND PREPARATION METHODS

2.3.1 Zein-layered clays bio-hybrids

(a) Preparation of zein-CloisiteNa bio-hybrid

For the preparation of zein-CloisiteNa bio-hybrids (Z-CloisNa) three synthesis routes were explored, which differ in the main solvent used to disperse the clay and protein, and in the order of mixing of both components.

- *Synthesis 1*

For the preparation of zein-CloisNa bio-hybrids by this first method, 50 mL of an 80%v/v ethanol solution in water is added to 300 mg of CloisNa, being vigorously stirred by means of a mixer (G2 model, Lomi) in order to properly disperse the clay. On the other hand, solutions of zein (80%v/v ethanol/water) with different content in protein (30, 60, 120, 200, 300, 500, 1000 and 1500 mg) were prepared in 50 mL, in order to achieve different weight proportions of zein to the CloisNa in the bio-hybrid materials (0.1:1, 0.2:1, 0.4, 0.67:1, 1:1, 1.6:1, 3.3:1 and 5:1, respectively). Each zein solution was added to 50 mL of the CloisNa dispersion and the resulting mixture was stirred for 48 h at room temperature (approx. 23ºC). Then, the solid product was isolated by centrifugation (40 minutes, 8000 rpm) and dried overnight at 40 ºC. The bio-hybrid materials prepared from CloisNa through this method were denoted as Z-CloisNa_S1.

- *Synthesis 2*

In this second synthetic method, 300 mg of CloisiteNa were firstly swollen in 20 mL of water. On the other hand, different amounts of zein (30-1500 mg) are added in 80 mL of ethanol. Both volume ethanol and water was calculated to reach a 80:20 final ratio of ethanol: water, after mixing both zein and clay suspensions. It was observed that in pure ethanol, zein was not completely solved, but a separation process of different components of the protein took place (Figure 2.2), showing the presence of an extracted phase (soluble in alcohol) and another solid phase (insoluble in alcohol). The aqueous clay suspension was then added to these two phases system of zein in absolute ethanol. The solid phase of the protein began to solubilize as the liquid phase reached a 80:20

ethanol:water ratio, forming at this point a homogeneous Z-CloisNa suspension. The system was maintained under magnetic stirring for 48 hours at room temperature, and then the solid was separated by centrifugation and dried similarly than in synthesis 1. The bio-hybrids resulting from this synthetic method were denoted as Z-CloisNa_S2.

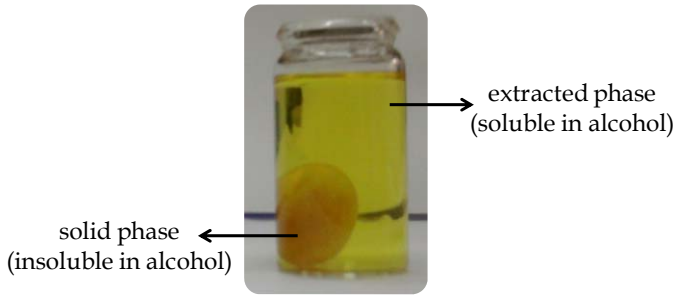

Figure 2.2 Picture showing the separation phenomena observed when zein protein is dispersed in absolute ethanol.

- *Synthesis 3*

The third strategy used for the preparation of Z-CloisNa bio-hybrids is based on the fact that zein can be dissolved in strongly alkaline media. Thereby, different amounts of zein (30-1500 mg) were dissolved in 35 mL of NaOH 0.1 M (pH 13), while 300 mg of CloisNa were swollen in 65 mL of water, both at room temperature. After complete dissolution of the protein, this was added to the suspension of the swollen clay, forming a single batch that was kept under magnetic stirring for 48 h at room temperature. The solid product was separated by centrifugation and washed several times with distilled water for removal of residual NaOH until neutral pH, and then dried overnight at 40 ºC. The bio-hybrid materials resulting from this synthetic procedure were denoted as Z- CloisNa_S3.

(b) Preparation of Zein- Cloisite 30B bio-hybrids

The preparation of the bio-hybrids based on zein protein and Cloisite30B was carried out in the same way followed to prepare Z-CloisNa materials according to method 1, (§2.3.1.(a)- synthesis 1), using 80%v/v ethanol/water as solvent, but substituting

CloisNa by the Cloisite30B organomontmorillonite as inorganic counterpart. The resulting bio-hybrid materials prepared with Clois30B were denoted Z-Clois30B.

(c) Use of zein-layered clays as compatibilisers in biopolymer films preparation

The zein-layered clays bio-hybrids synthesized in this Thesis were employed as compatibilisers in the preparation of biopolymer films. Thus, Z-CloisNa_S3 and Z-Clois30B bio-hybrids of different compositions were used in the preparation of zein and starch films with different bio-hybrid content (0, 1.25 and 3.5% with respect to the biopolymer weight). In the case of zein films loaded with zein-layered clays, 2.5 g of zein were solubilized in 45 mL of aqueous ethanol solution (80% v/v), under vigorous magnetic stirring and kept at 80 ^{o}C. Then, 5 mL of zein-layered clay dispersion in water were added to the zein solution at 80 ^{o}C forming a single batch that was kept under stirring for approximately 30 min to reach room temperature. After total homogenization, the resulting dispersion was placed in a methacrylate box, and dried at room temperature. The starch films based on zein-layered clays bio-hybrids were prepared similarly to the zein films discussed above, except that in this case, the solvent used for the solubilization of the starch polysaccharide was pure water heated at 80^{o}C.

For comparison, zein and starch films containing CloisNa and Clois30B were also prepared in the same conditions than those used for the preparation of the bionanocomposite films filled with bio-hybrids. Blank films of zein and starch (i.e. without clay or bio-hybrid material) were prepared by dissolving 2.5 g of zein or starch in 50 mL of ethanol solution at 80% (v/v) or pure water, respectively. In both systems it was necessary to add 0.5 g of glycerol as plasticizer, keeping the mixtures under magnetic stirring at 80 ^{o}C until complete homogenization of the components.

2.3.2 Zein-fibrous clays bio-hybrids

(a) Preparation of zein-sepiolite and zein-palygorskite bio-hybrids

The method employed in this synthesis was analogous to synthesis 1 used for the preparation of zein-CloisNa bio-hybrids (§2.3.1 (a)). Thus, suspensions of sepiolite or palygorskite (6% g L^{-1}) were prepared in ethanol/water (80%, v/v), being vigorously stirred by means of a mixer (G2 model, Lomi) in order to properly disperse the clay.

Different amounts of zein were dissolved in 50 mL of ethanol/water (80%, v/v) in order to prepare a set of alcoholic solutions with zein concentration ranging between 0.6 and 30 g L^{-1}. Each zein solution was then added to the sepiolite or palygorskite dispersion, forming a single batch that was stirred for 48 h at room temperature (approximately 23 ^{o}C). After that period of time, the solid product was isolated by centrifugation (40 minutes, 8000 rpm) and subsequently dried overnight at 40 ^{o}C. The resulting zein-sepiolite and zein-palygorskite bio-hybrid materials were denoted as Z-SEP and Z-PALY, respectively.

(b) Bionanocomposite membranes using zein-fibrous clays as filler

Zein-sepiolite or zein-palygorskite bio-hybrids were used as fillers of alginate polysaccharide in the preparation of bionanocomposite membranes. Thus, alginate films loaded with different amounts of zein-fibrous clays were produced employing the solution blending method (Cong et al., 2007), where a necessary amount of bio-hybrid was dispersed in deionized water by vigorous stirring for 24 h at room temperature, in order to achieve alginate:bio-hybrid weight ratios of 1:1 , 1:2 and 1:3. The bio-hybrid suspension was gradually added to the previously prepared alginate dispersion in water (2%w/v), forming a single batch that is kept under constant stirring overnight. Finally, the resulting bionanocomposites were placed onto a glass plate and allowed to dry at room temperature. The films prepared from alginate incorporating zein-sepiolite or zein-palygorskite bio-hybrid filler were denoted as ALG/Z-SEP and ALG/Z-PALY, respectively.

For comparison, pure alginate membranes were produced in the same way from a 2% sodium alginate aqueous solution. After casting onto a glass plate, the resulting dried membranes were in some cases immersed in 5% $CaCl_2$ for 15 min to procure a cross-linking of the alginate chains. After the cross-linking process, the membranes were washed with doubly distilled water to remove residual Ca^{2+} ions and allowed to dry at room temperature.

2.3.3 Zein-sepiolite bionanocomposite foams

Tridimensional macroporous zein-sepiolite foams were prepared profiting from the different solubility of zein components in water and ethanol.

(a) Zein-sepiolite foams

Zein-sepiolite bionanocomposite foams were prepared using the following general procedure (Figure 2.3): i) an amount of zein is mechanically mixed with different amounts of pure sepiolite (SEP) (0, 3.5 and 7% with respect to the protein weight); ii) after homogenization, the resulting material was conformed as pellets of 12 mm in diameter, applying a pressure of 1 Ton; iii) the pellets were immersed in 200 mL of absolute ethanol during 24h, provoking the extraction of the soluble fraction of zein; iv) the hybrid materials were removed from the ethanol system and immediately immersed in 200 mL of water, where they were maintained for 24 h more; v) the pellets then were frozen at -20 ^{o}C and subsequently lyophilized in a freeze-drier (Cryodos, Telstar). The zein-sepiolite foams prepared from this method were denoted as Z-Sep.

(b) Zein-sepiolite magnetic foams

- *Incorporation of magnetite-sepiolite heterostructure*

The preparation of the zein-sepiolite magnetic bionanocomposite foams were carried out following the same protocol adopted in the synthesis of zein-sepiolite bionanocomposite foams (Figure 2.3), but in this case the sepiolite employed was previously modified with magnetic nanoparticles (SepNp). The composition of this heterostructure was 50% of sepiolite and 50% of oleic acid-capped magnetite nanoparticles. The resulting magnetic bionanocomposite foams were denoted as Z-SepNp. Magnetic blank foams were also prepared following the same experimental procedure, except that in this case the heterostructure was substituted by pure magnetite nanoparticles (Np), being denoted as Z-Np.

Magnetic nanoparticles (Fe_3O_4) provided with superparamagnetic behavior were prepared in the presence of oleic acid following the methodology reported by Zheng and co-authors (Zheng et al., 2005). These nanoparticles were used to prepare

ferrofluids that were then employed to prepare superparamagnetic sepiolite according to the procedure patented by our research group (Ruiz-Hitzky et al., 2011.). This superparamagnetic sepiolite was applied as adsorbent and also to prepare other multifunctional materials (González-Alfaro et al., 2011; Ruiz-Hitzky et al., 2011.), and it was used in the preparation of various zein-based magnetic foams in this work.

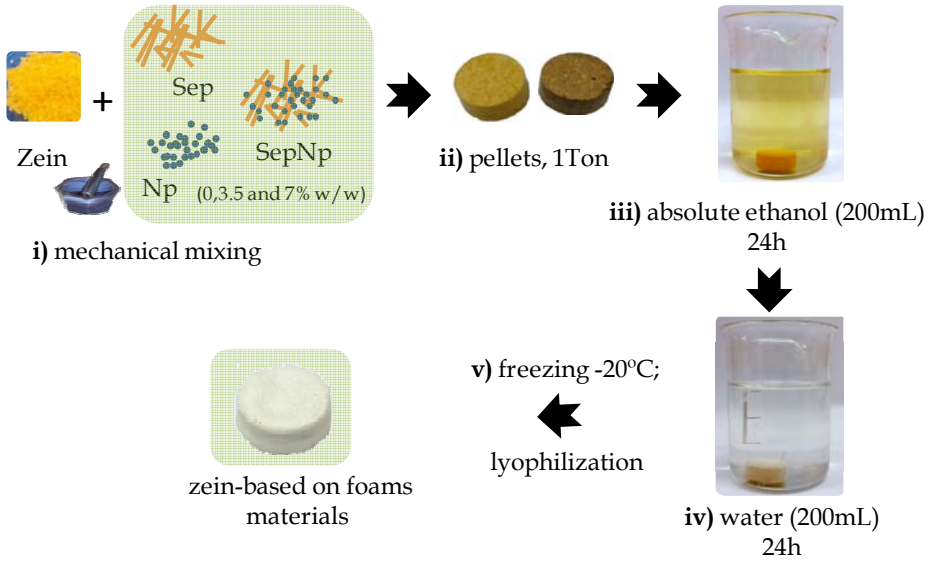

Figure 2.3 Scheme of the general procedure employed for the preparation of the zein–based bionanocomposite foams.

2.3.4 Zein-layered hydroxide bio-hybrids

Diverse approaches were explored using single layered hydroxide (LSH) and layered double hydroxides (LDH) containing different inorganic anions in the interlayer region in order to obtain zein-layered hydroxide bio-hybrid materials. The syntheses of these materials are described below.

(a) Zein-layered double hydroxide bio-hybrids

- *Synthesis of $Mg^{2+}Al^{3+}$- LDH with different inorganic anions in the interlayer region*

For the synthesis of layered double hydroxides (LDH) of Mg and Al in the 2:1 ratio, containing Cl^- (Mg_2Al-Cl), NO_3^- (Mg_2Al-Nit) and CO_3^{2-} (Mg_2Al-Carb) anions, the

coprecipitation reaction was followed at pH constant, according to the procedure described by Constantino and Pinnavaia (Constantino and Pinnavaia, 1995). For the preparation of the Mg_2Al-Cl LDH, a mixture of $MgCl_2 \cdot 6H_2O$ (17.5 mmol) and $AlCl_3 \cdot 6H_2O$ (8.74 mmol) was dissolved in 250 mL of decarbonated bidistilled water. This aqueous solution was added dropwise with a peristaltic pump to 100 mL deionized water kept under a nitrogen flow for removing CO_2. Simultaneously, a solution of 1 M NaOH was also added dropwise to the aqueous system through an automatic dispenser (Dosimat 765 with an 806 Exchange Unit, from Metrohm) controlled by a 781 pH/Ion Meter (Metrohm) to keep a constant pH of 11 during the synthesis. The resulting suspension was vigorously magnetically stirred for 24 h under a nitrogen flow. The solid product was isolated by centrifugation, washed three times with bidistilled and degassed water, and dried overnight at 60 ^oC. The $[Mg_{0.67}Al_{0.33}(OH)_2]Cl_{0.33} \cdot nH_2O]$ LDH was denoted as MgAl-Cl LDH.

The 2:1 Mg:Al LDH containing CO_3^{2-} ions (Mg_2Al-Carb) was prepared analogously to the Mg_2Al-Cl LDH described above, including the same salts and their respective concentration, except that in the different stages of synthesis the nitrogen flow was not employed and the precipitation pH was 9.0 ± 0.1, adjusted with 0.2 M Na_2CO_3 aqueous solution. Once formed, the Mg_2Al-Carb LDH was recovered, washed and dried in an oven at 60 °C. The $[Mg_{0.67}Al_{0.33}(OH)_2]\ CO_{3\ 0.33} \cdot nH_2O]$ was denoted as MgAl-Carb LDH.

The Mg_2Al-NO_3 LDH nitrate was also prepared by a method analogous to the LDH chloride described above, except that $Mg(NO_3)_2 \cdot 6H_2O$ (17.5 mmol) and $Al(NO_3)_3 \cdot 9H_2O$ (8.74 mmol) were used as the source of magnesium and aluminum. The pH of the solution was maintained at 11.0 by adding 1 M NaOH solution. The resulting white precipitate was aged for 24 hours under nitrogen flow, filtered, washed several times with large amounts of deionized and degassed water and finally dried at 60 ^oC in an oven. The $[Mg_{0.69}Al_{0.34}(OH)_2]\ NO_{3\ 0.34} \cdot nH_2O]$ was denoted as MgAl-Nit LDH.

- *Zein-LDH intercalation compound preparation*

-Ion exchange method

For the preparation of bio-hybrids by the ion exchange method, briefly, 0.5 g of zein was dissolved in 50 mL of 0.1 M NaOH through magnetic stirring or by means of an ultrasound tip (VC750 Sonics Vibra-Cell, operating 20KHz), using a tip of 13 mm and applying intermittent pulses of 10 s followed by a standby step of 10 s up to a total applied energy of 60 kJ/0.5 g of zein. The pH of the protein solution was adjusted to 11 by controlled addition of 0.1 M HCl. This solution was slowly added to a suspension containing 2 g of MgAl-Cl or MgAl-Nit LDH freshly prepared in 50 mL of degassed bidistilled water. The pH of the system was reset back to 11 and then maintained under magnetic stirring at 50 ^{o}C under nitrogen flow for 4 days. Afterwards, the solid product was isolated by centrifugation, washed with distilled water and dried at 40 ^{o}C. The resulting hybrid materials derived from MgAl-Cl and MgAl-Nit LDH were denoted as Z-LDH-Cl_ie and Z-LDH-Nit_ie, respectively.

- Co-precipitation method

Intercalation of zein into the MgAl-Cl or MgAl-NO_3 LDH by co-precipitation method was carried out by adding slowly 250 mL of an aqueous solution containing the Mg and Al salts to 100 mL of a zein protein solution (0.5 g of protein/100 mL of 0.1 M NaOH), previously prepared by magnetic stirring or ultrasonication, similarly as described for the ion-exchange method. The metal ions and the protein solutions were constantly purged with N_2 and the pH of the system was controlled at 11.0 using the Metrohm 765 Dosimat. The resultant suspension was stirred for 24 h at room temperature under nitrogen flow. The solid fraction was separated by centrifugation (4500 rpm, 15 min), washed with bidistilled water, and dried overnight at 40 ^{o}C. The bio-hybrid materials synthesized by the co-precipitation method derived from MgAl-Cl and MgAl-Nit LDH were denoted as Z-LDH-Cl_cppt and Z-LDH-NO_3_cppt, respectively.

- Reconstruction method

The synthesis of Z-LDH bio-hybrid materials by the reconstruction method was performed by means of calcination-rehydration reaction. Thus, 1 g of LDH MgAl containing carbonate ions in the interlaminar space (MgAl-CO_3 LDH) was calcined in a muffle furnace (Horbesal, Spain) at 500^{o}C at 10 ^{o}C min^{-1} rate and kept at this

temperature for 5 h in order to form the corresponding dehydrated MgAl layered double oxide (MgAl LDO). On the other hand, zein (0.5 g) was dissolved in 50 mL of 0.1 M NaOH through magnetic stirring or by ultrasonication, similarly to that described for the ion-exchange reaction. After dispersion, the pH of the protein solution was adjusted to 11. The MgAl LDO (0.6 g) was added to 50 mL of the zein solution, while the system was kept under nitrogen atmosphere to prevent the formation of the carbonate-LDH. The solid product was separated by centrifugation, washed and dried of analogous manner as described for the synthesis methods mentioned above. The hybrid material obtained from this synthesis was denoted as Z-LDH_rec.

(b) Zein-Layered single hydroxide bio-hybrids

- *Synthesis of Co-LSH starting material*

The $Co_2(OH)_3(CH_3COO)\cdot H_2O$ LSH was synthesized following the procedure described by Si et al. (Si et al., 2012). Thus, 0.02 mol of $Co(CH_3COO)_2\cdot 4H_2O$ was dissolved in 100 ml of water, maintaining the reaction medium at 70 ^oC under stirring and nitrogen flow. A volume of 30 mL of 0.1 M NaOH mixed with 60 mL of ethanol–water (50%v/v) was added slowly to the previous solution under vigorous stirring. The resultant mixture was kept under stirring for another 30 min before separation. Finally, the resultant suspension was centrifuged and washed with water and ethanol to remove the unreacted reagents, and finally dried at 40 ^oC. The obtained layered material was denoted as Co-LSH.

- *Zein-LSH bio-hybrid preparation*

-Ion exchange method

For the preparation of zein-LDH compound by ion exchange reaction, 0.5 g of zein was solubilized in 15 mL of 0.1 M NaOH under an ultrasound tip, applying an energy of 60 kJ/0.5 g of zein. Then, a water–ethanol mixture (50% v/v) was added to the previously prepared zein solution and the pH was adjusted around 8.2. Next, 0.5 mmol of Co-LSH

solid hydroxide starting material were added to this zein solution under vigorous stirring. The resulting mixture was stirred at 70 ºC for 24 h under constant N_2 flow. Then, the resulting solid was centrifuged, washed with sufficient amounts of water and ethanol, and dried at 40 ºC. The zein-LSH hybrid material obtained by the ion exchange method was denoted as Z-LSH_ie.

-Co-precipitation method

The procedure followed in this case is similar to that described for the preparation of the Co-LSH material, except that in this case were used 30 mL of 0.1 M NaOH in the solubilization of 0.25g of zein. This alkaline zein solution was ultrasonicated by means of an ultrasound tip (total energy applied 60 kJ). Then, 60 ml of ethanol–water (50% v/v) were added to previously alkaline zein solution. The resulting zein solution was added slowly to the aqueous cobalt solution and the reaction was kept under magnetic stirring and nitrogen flow for 30 min. The resulting solid was filtered, washed several times with water and ethanol, and dried at 40ºC. The hybrid material obtained by this procedure was denoted as Z-LSH_cppt.

2.3 CHARACTERIZATION METHODS

Several physico-chemical techniques of characterization were employed in order to obtain information on the composition and stability, as well as on the structural and functional properties of the diverse zein-based bio-hybrid and bionanocomposite materials prepared in this Thesis. In this section, a brief description regarding the instrumental methods and physico-chemical techniques used along this work is detailed.

2.3.1 Elemental analysis

The adsorbed amount of zein in the bio-hybrids was calculated from elemental chemical analysis. This technique provides the total content of C, H, N and S present in an organic-inorganic or organic sample by combustion under pure oxygen atmosphere

at approximately 1000ºC. The samples were analyzed in duplicate in a Perkin Elmer 2400 Series II CHNS/O analyzer.

2.3.2 Powder X-ray diffraction

Structural information of diverse materials was provided from powder X-ray diffraction (XDR) which was obtained using a D8-ADVANCE equipment from BRUKER with SOLX or scintillation detectors, and using copper K_α radiation. The voltage and current source were set at 40 kV and 30 mA, respectively. Diffraction patterns were recorded with a goniometer speed of 2º/min between 2 and 70 degrees (2θ). This technique is especially useful to study materials based on montmorillonite and layered double hydroxides, where changes in the basal distances can be afforded by data from (*00l*) reflection, indicating possible intercalation and/or delamination of the involved layered solids.

2.3.3 Infrared spectroscopy

Fourier transform infrared spectroscopy (FTIR) is a useful tool employed for the identification of chemical species, and it can also provide structural information. FTIR spectra were recorded with two spectrophotometers BRUKER IFS 66v/S and NICOLET - 20SXC, which were employed to analyze different samples. In general, samples were diluted in KBr (~2%) and conformed as pellets under a pressure of 10 Ton. Samples based on sepiolite were prepared as self-standing film (2% w/v) due to higher sensitivity of Si-OH stretching vibrations. The materials were placed in the sample holder and scanned from 4000 to 250 cm^{-1} with 2 cm^{-1} resolution.

2.3.4 Thermal analysis

Thermal analysis is an analytical technique which allows the study of both mass and thermal variations provoked when a sample is heated in a controlled atmosphere. The thermal behaviour of the different prepared materials was analyzed from the simultaneously recorded thermogravimetric (TG) and differential thermal analysis (DTA) curves in a SEIKO SSC/5200 equipment, in experiments carried out under air atmosphere (flux of 100 ml/min) from room temperature to 1000 ºC at 10 ºC/min heating rate.

2.3.5 Nuclear magnetic resonance

Molecular interactions between zein and some of the inorganic solids were investigated by solid-state ^{13}C CP MAS NMR spectra, which were obtained in a Bruker Avance 400 spectrometer, using a standard cross-polarization pulse sequence. In this method, the sample was rotated around the magic angle (54º44') at 12 kHz while a frequency of 100.6 MHz was applied for ^{13}C NMR measurements. A contact time of 2 ms and a period between successive accumulations of 5 s-10 s were used. The number of scans was 800. Chemical shift values were referred to carbon atoms of tetramethylsilane (TMS).

2.3.6 Specific surface area

Specific surface area determinations offer valuable information concerning the microporous structure of the obtained solids. Texture properties of the bio-hybrids and starting clays were determined by applying the BET (Brunauer-Emmett-Teller) method to the adsorption-desorption isotherms. The analyzed samples were degassed overnight at 150 ºC prior to the analysis. The isotherms of adsorption of N_2 at 77 K were obtained by using a Micromeritics ASAP 2010 analyzer.

2.3.7 UV- visible spectroscopy

Ultraviolet-visible spectroscopy (UV-Vis) is a useful technique employed for the qualitative and quantitative determination of diverse analytes. On the one hand, UV-Vis instrumentation (Shimadzu, UV- 1201 spectrophotometer) was employed in this Thesis for the qualitative analysis of zein protein fractions (λ = 600-250 nm) and for quantification of the MCPA herbicide in ethanol solution (λ = 278 nm), applying the Lambert-Beer law. On the other hand, UV-Vis spectroscopy was also used for determination of the light barrier properties of the alginate, zein and starch-based bionanocomposite films. In this case, film samples were cut into rectangles (2 cm x 4 cm) and placed in a special spectrophotometer cell holder for direct evaluation of transmittance, measuring the UV-Vis spectra at wavelengths between 200 and 800 nm.

2.3.8 Gel Electrophoresis

The sodium dodecyl sulfate polyacrylamide gel electrophoresis (SDS-PAGE) technique allows to characterize the zein fractions obtained from pure ethanol, 0.1 M NaOH and 80%(v/v) ethanol aqueous solutions. For this purpose, aliquots of 7.5 µL containing approximately 30 µg of zein were resuspended in equal volumes of deionized water and buffer (0.125 M Tris-Cl, 4% SDS, 20% Glycerol, 10% 2-mercaptoethanol (BME), and bromphenol blue 0.01%, pH 6.4). SDS-PAGE was performed according to Cabra et al. (Cabra et al., 2005). Gels were silver-stained for band visualization.

2.3.9 Electron microscopy

(a) Field Emission Scanning Electron Microscopy

Scanning electron microscopy is an important technique that allows to investigate the morphology and texture of different materials. By this technique, it is possible to examine both the surface and the cross-section of a sample (e.g. film sample), determining its topographic characteristics, presence of pores (e.g. foams), particles agglomeration and homogeneity in the material. A Field Emission Scanning Electron Microscopy (FE-SEM) equipment from FEI Company (FEI-NOVA NanoSEM 230), equipped with an EDAX-Ametek detector that allowed semi-quantitative analysis of elements, was used to characterize diverse materials. Sample preparation was performed by adhering powdered or a small piece of film or foam sample on a carbon tap for direct observation without requirement of any conductive coating on the surface.

(b) Transmission Electron Microscopy

Transmission Electron Microscopy (TEM) technique allows the study of the structure and morphology of a material, on a very small scale with nanometric resolution. The samples are embedded in epoxy resin and then were cut in very thin sections (typically 60 to 100 nanometers) using an ultramicrotome (LEICA EM UC6) equipped with a diamond blade or glass. In some cases, sample as powders was dispersed in bidestilled water and submitted to ultrasonic agitation for 15 min. A drop of the resulting

dispersion was deposited onto a copper grid covered with a carbon conductive coating and was allowed to dry at ambient temperature. The electron micrographs of the samples were obtained Philips Tecnai 20 or LEO-910 STEM equipments, operating at an accelerating voltage of 200 and 80 kV, respectively.

2.3.10 Water sorption

Water sorption is a method that allows the study of the water adsorption capacity of a material at controlled moisture atmosphere. Moisture sorption isotherms display the relationship between water content in a sample at determined equilibrium humidity and then it is possible to investigate the wettability of a material. Moisture sorption isotherms were measured by means of a Dynamic Water Vapor Sorption equipment, Aquadyne DVS from Quantachrome Instruments. Around 10 mg of sample to analyze were purged at 80 ^{o}C until the sample weight remained constant. Mass changes due to water adsorption or desorption were recorded at 25 ^{o}C in the range of relative humidity from 0 to 95%. From these data, the adsorption isotherm of water sorption is obtained.

2.3.11 Mercury porosimetry

Mercury porosimetry provides information on the pore size distribution in the range of the macro- and meso-porosity. Determinations of pore distribution in the bionanocomposite foams were performed using a Poremaster Series equipment from Quantachrome Instruments, which permits to analyze the pore size from 1000 microns to 0.003 microns by mercury intrusion. The study implies first the evacuation of gas from the foam sample, and then Hg is intruded in the sample by increase of Hg pressure from 0.2 up to 50 psi for low pressure measurements and from 20 up to $5.8x10^{4}$ psi for high pressure measurements, which allow to determine pore diameters ranging from 1000 to 4 μm and from 10 to $3x10^{-3}$ μm, respectively. The mercury volume intruded as a function of pressure is monitored in order to determine the pore size distributions from the Washburn equation:

$$D = (-4\gamma \cos \theta)/P \quad \text{(eqn 2.1)}$$

where P is the applied pressure, D is the pore diameter, γ is the surface tension of the mercury (480 dyne cm-1) and θ is the contact angle between mercury and the pore wall, usually taken as 140º (http://www.quantachrome.com/pdf_brochures/07128 28.pdf, Accessed June, 10st, 2013)

2.3.12 Helium pycnometry

Helium pycnometry employs Archimedes' principle of fluid displacement to estimate the density of a solid sample. The total and the closed percentage porosities, the real and apparent densities of the bionanocomposite foams were determined with the help of a helium pycnometer using the Ultrafoam 1200e equipment (Quantachrome). Foam samples shaped as cylinders were introduced in a small cell (7.0699 cm^3 in volume) and the samples were purged under He flow for 1 min before each analysis. The target pressure was 19 psi and the equilibrium time of temperature was 10 s. Measurements were performed by duplicate.

2.3.13 Magnetic Properties

Vibrating Sample Magnetometer (VSM) allows to measure the magnetic properties of the foams containing magnetic particles. VSM measurements were performed at room temperature applying a variable magnetic field from –18000 to 18000 Oe in a vibrating sample magnetometer with an ADE magnetic system (model EV7).

2.3.14 Mechanical properties

Mechanical properties, such as tensile modulus and percentage of elongation at break, of the bionanocomposite film samples were evaluated in a Model 3345 Instron Universal Testing Machine (Instron Engineering Corporation Canton, MA, USA) applying the D 882-88ASTM standard method. Sample cuts with a rectangular shape (ca. 60 mm x 15 mm) were mounted between the grips (Figure 2.4 a), with an initial separation of 50 mm, and the cross-head speed was set to 5 mm min^{-1}.

Mechanical properties from compression tests of the bionanocomposites conformed as foams were evaluated using the same Universal Testing Machine utilized for the film samples. However, in this case, two flat plates (Figure 2.4 b) of 29 mm in diameter were adapted between the grips of the machine, for accommodating the foam samples

(approx. 20 mm in diameter). Then, a compression speed of 1 mm min^{-1} was applied. Three replicates were run for each film or foam sample.

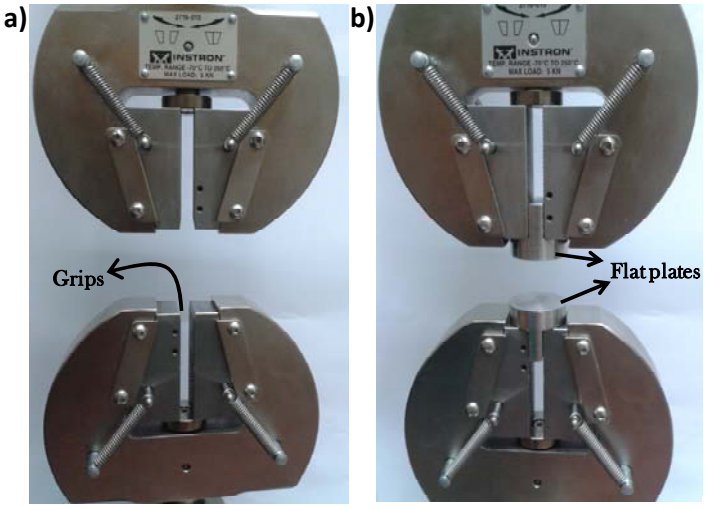

Figure 2.4 Picture of the universal machine employed for tensile (a) and compression (b) tests carried out in zein bionanocomposites conformed as films and foams, respectively.

2.4 Protocols and Applications

2.4.1 Water uptake determination

The water uptake properties of the bionanocomposite materials obtained as films and foams were determined following the standard procedure described by Deng and co-authors, by immersing the samples in distilled water at room ambient for 24 h (Deng et al., 2009). Afterwards, the samples were withdrawn, removing the excess of water, and then weighed on an analytical balance. The swelling ratio of the sample is calculated from equation 2.2 and can be defined as g of water incorporated per g of dry sample.

$$(g/g)\ \text{water content} = (W_t - W_0 / W_0) \qquad \text{(eqn. 2.2)}$$

where W_0 and W_t are the weights of dry and hydrated sample, respectively.

2.4.2 Water vapor transmission rate

Water vapor transmission rate (WVTR) properties of the bionanocomposite film samples were measured gravimetrically using the modified E 96-80 ASTM method (ASTM E96/E96M–12). Circular test cups made from PVC and having a diameter of 45 mm (test area: 15.9 cm^2) were used to place the film samples at the top of the open circular scheme (Figure 2.5). The cups containing 14 g of a desiccant (silica gel) and sealed with the membrane on the top were placed in a closed chamber containing a saturated aqueous NaCl solution (75% R.H., 22ºC). The moisture transmitted through the composite films and adsorbed by the silica gel was determined gravimetrically by weighing the cups initially and after a time period of 2, 8, 12, 24, 48 and 72 h. The rate of the water vapor transmission was obtained from the slope of the line resulting from plotting the weight of transmitted water vapor *vs.* time.

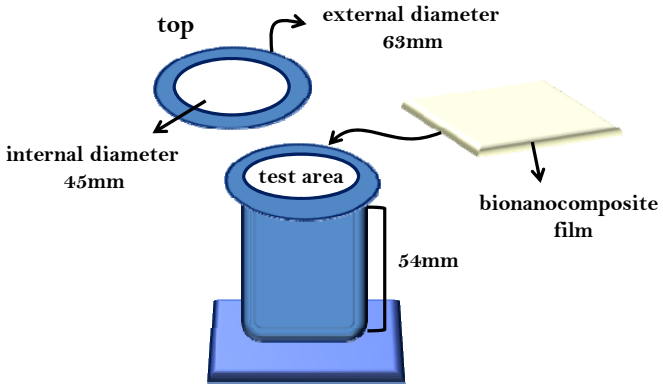

Figure 2.5 Scheme of the test cups used in the water vapor transmission measurements.

2.4.3 Gas Permeation

The permeation of gases is an important measure to evaluate the barrier properties of a membrane, which is associated with passage of a gas through the material in the presence of a pressure differential. Commonly, bionanocomposite membranes based on polymer compounds can show very low permeability, due to the enhancement of their barrier properties. However, the gas barrier properties of these materials can undergo drastic changes depending on the humidity conditions to which they are subjected. Due to this, often the water swollen method is employed in gas permeation processes, in order to evaluate the barrier properties of a membrane in wet conditions.

This methodology is very useful in characterization of membranes which can have application in food packaging at high humidity conditions.

In this sense, gas permeation properties of bionanocomposite membranes of alginate filled with the zein-sepiolite bio-hybrid were evaluated using the water swollen method. For this purpose, membranes were hydrated in water overnight to form a hydrogel. After, the water excess was removed and the membrane was quickly mounted on a flat permeation support, and the permeability of pure gases through the water-swollen hydrogel membranes was determined at different pressures using the constant volume method (Figure 2.6). In order to avoid any disintegration of the membrane in these conditions, these materials were previously subjected to a cross-linking process using calcium chloride as cross-linking agent (5% w/v, 15 min). The gas permeability through the membrane was calculated from the following equation (2.3):

$$P = \frac{Q}{A\,\Delta p}\, l \qquad \text{(eqn.2.3)}$$

where P is the permeability coefficient of the gas expressed in mol s^{-1} Pa^{-1} m^{-1}, Q the permeate gas flow rate, A the effective membrane area for permeation (17cm^2), l the membrane thickness and Δp is the pressure difference across the membrane. The thicknesses of the used membranes were between 0.065 to 0.085 mm.

These measurements were conducted at the laboratory of Prof. A. Ayral (Institut Européen des Membranes, Montpellier-France).

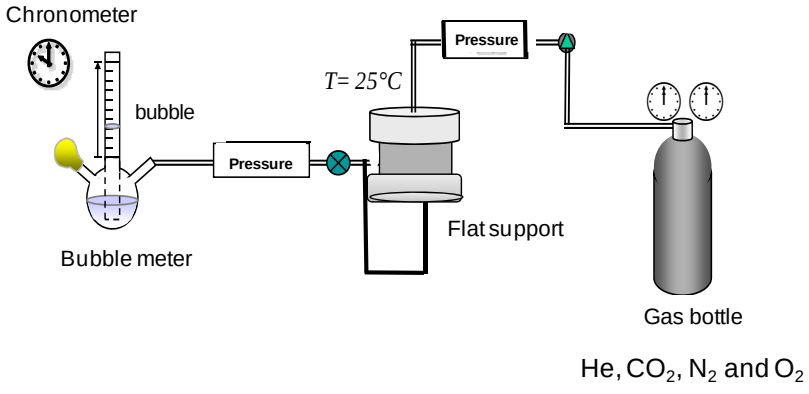

Figure 2.6 Experimental set-up for gas permeation testing.

2.3.4 Adsorption-desorption of the MCPA herbicide

Properties of adsorption-desorption of the 2-methyl-4-chlorophenoxyacetic acid (MCPA) on magnetic bionanocomposite foams were evaluated from batch experiments. Pieces of about 50 mg of the foams were immersed as adsorbent in reaction flasks containing 20 mL of MCPA initial solutions with herbicide concentration ranging from 0.05 to 1 mM and then left to equilibrate for 72 h at 30 ± 2 ^{o}C in an incubator shaker at 100 rpm. Once the equilibrium was reached, approximately 3 mL were taken from the supernatant solutions, and their absorbance was determined at 278 nm by UV-Vis spectroscopy. A calibration curve was obtained, from the absorbance values at 278 nm of solutions of known concentration, by fitting these data to the Lambert-Beer equation. With this calibration curve, it was possible to determine the herbicide equilibrium concentration in the recovered supernatant solutions. The amount of adsorbed MCPA, Q (μmol/g), was determined from the difference between the initial and final amount of herbicide in each tested solution. A kinetic experiment was also conducted at 24, 48, 72 and 144 h, and revealed that 72 h was sufficient to reach the adsorption equilibrium of the MCPA herbicide.

Desorption experiments were conducted in the samples after adsorption from 0.1 mM MCPA solution. The supernatant solutions removed for the adsorption analysis were replaced by 10 mL of either pure water or 70/30 (v/v) water/acetone solution. The system was shaken at 30 ± 2^{o}C for 0.5, 3, 8, 24 and 72 h, and then an aliquot of 3 mL was removed from the supernatant, and re-analyzed spectrophotometrically. All the adsorption–desorption experiments were conducted in duplicate.

CHAPTER 3

ZEIN-LAYERED CLAYS BIO-HYBRIDS

The present Chapter introduces results on the intercalation of zein protein in layered clays, in the present case montmorillonite. Commercial Cloisite®Na and Cloisite®30B containing a type of exchangeable cation, Na^+ and a quaternary alkylammonium ion, respectively, were used. By a systematic control of the synthesis conditions and the use of several spectroscopic methods, it was possible to investigate the zein intercalation mechanism into both types of homoionic clays, as well as to elucidate the structure and properties of the resulting zein–montmorillonite bio-hybrids. It was deduced that zein adsorption processes are strongly influenced by the kind of interlayer cation, the solvent used for the dispersion of the protein, and the order of mixing of both components. The obtained bio-hybrids were evaluated as bio-organoclays for incorporation in biopolymer films.

3.1 INITIAL CONSIDERATIONS

Smectite clays, such as montmorillonites, are often the main choice for designing bionanocomposites due to their low cost and rich intercalation chemistry. Many studies have demonstrated that even large species, such as polypeptides and proteins, can be intercalated in the interlamellar space of montmorillonite, forming a protein-clay bio-hybrid material. In this sense, the intercalation of gelatin, a structural protein derived from partial denaturation of collagen, into montmorillonite was the object of the study carried out in 1950 by Talibudeen (Talibudeen, 1950). This preliminary study was the basis for other bio-hybrids also based on proteins, and currently, the interaction of polypeptide chains (e.g. poly(L-lysine)) and other proteins, such as bovine serum albumin, gelatin, casein or soy, with smectite clays have been vastly studied (De Cristofaro and Violante, 2001; Ruiz-Hitzky et al., 2005; Chen and Zhang, 2006; Lin et al., 2007; Tran and James, 2012). In many citations in the literature, bovine serum albumin (BSA) appears as a model protein in order to study the protein-clay interactions (Lin et al., 2007; Tran and James, 2012). However, apart from the particular characteristics of each protein, the structural size and proportions of hydrophobic residues may be a key factor in order to achieve their intercalation in montmorillonite (Weiss, 1969; De Cristofaro and Violante, 2001). Thus, depending on the type of protein involved, it is possible to obtain different interactions between the clay and the protein, generating the need to investigate possible interactions that can occur in less-studied proteins.

Recently, the possible association of zein protein with both sodium montmorillonite and organoclays was accounted in the development of composite materials for diverse applications, using the thermo-plasticization and blown extrusion techniques (Luecha et al., 2010; Nedi et al., 2012). Nevertheless, a systematic study on the process of formation of zein-montmorillonite bio-hybrid materials and the possible mechanism that leads to such intercalation compounds have not yet been reported. At this respect, the complex structure of zein and the role of the amino acids in its composition have to be considered, as well as the specific conformation of this protein, in order to reach understanding on the mechanism of the bio-hybrid formation.

In the present Chapter, a systematic study on the synthesis and characterization of zein nanocomposites, involving protein intercalation into montmorillonite, is proposed. To reach this purpose, two montmorillonites with exchangeable Na^+ ions as well as with

alkylammonium organocation were used, systematically controlling the synthesis conditions in order to achieve the protein intercalation. To investigate the underlying mechanism of zein intercalation on these homoionic clays, the resulting structure and features were also analyzed. Finally, zein–montmorillonite bio-hybrids were tested as nanofiller in the preparation of bionanocomposite films with the aim to show their potential application as bio-organoclays.

3.2 SYNTHESIS AND CHARACTERIZATION OF ZEIN-LAYERED CLAY BIO-HYBRIDS

Zein-layered clay bio-hybrid materials were prepared by direct adsorption of zein protein in solution on a natural montmorillonite exchanged with two type of cations, the commercial products Cloisite® Na (CloisNa) and the organically modified Cloisite® 30B (Clois30B), which contain Na^+ ions and quaternary alkylammonium cations (2-ethyl hexylhydrogenated tallow alkylammonium cation) in the interlayer region, respectively. In the case of Clois30B systems, zein adsorption was easily achieved from zein water/ethanol solutions. However, regarding the adsorption of zein on CloisNa, other strategies of synthesis, such as the use of alkaline medium, were employed in addition to the hydroalcoholic media to reach protein intercalation. Taking into account that ethanol/water mixtures are the most usual solvent for dissolving zein, a protocol that uses 80%(v/v) ethanol as solvent was firstly tried for the preparation of the bio-hybrids based on Clois30B and CloisNa. In contrast, other approaches for zein adsorption were carried out to reach the goal when using CloisNa, for instance, by using either the protein extracted by phase separation in pure ethanol or that solubilized in alkaline medium (both described in the experimental section, § 2.3.1a, synthesis 2 and 3, respectively).

3.2.1 Zein-montmorillonite bio-hybrids from zein in aqueous ethanol solution (80% v/v)

- *Characterization of the zein ethanol solution*

Given that the inorganic counterpart used in the preparation of these bio-hybrids is a lamellar clay that shows cation exchange properties, it was firstly intended to verify the pH of the starting zein solution in 80% (v/v) ethanol in order to know the global charge of the protein. This hydroalcoholic zein solution shows a pH value of 5.3. Since the isoelectric point of the protein is around 6.2 (Shukla and Cheryan, 2001), the protein will present predominantly protonated groups in its structure at the pH of this synthesis process, thus it will be susceptible to accomplish ion exchange reactions with montmorillonite clays. On the other hand, the molecular weight of the protein was investigated by electrophoresis (SDS-PAGE) (Figure 3.1), indicating the presence of α-zein conformation with two typical bands of approximately 23 and 25 kDa, which correspond to Z19 and Z22 proteins (Cabra et al., 2005), respectively. In this SDS-PAGE gel, it is possible to even observe the presence of α-zein dimers, which are characterized by the presence of bands around 50kDa (Esen, 1987; Sessa et al., 2003). In these conditions, zein chains are quite disaggregated, being thus susceptible for intercalation.

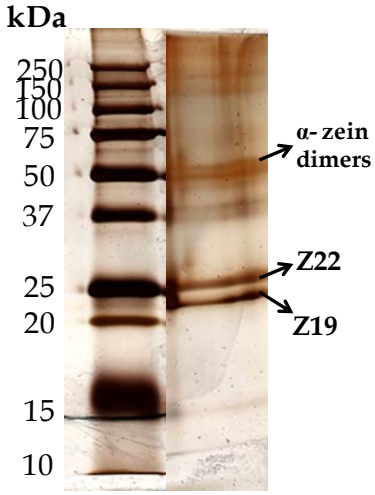

Figure 3.1 SDS-PAGE in acrylamide 20% of zein 80% (v/v) ethanol/water solution. The gel was silver stained.

Solid state NMR and FTIR spectroscopy were also used in order to characterize the protein before and after solubilization in 80% (v/v) EtOH/water, and the results are shown in Figure 3.2. The FTIR spectrum of zein (Figure 3.2a) presents the characteristic bands of proteins at 3308, 1658, and 1538 cm^{-1}, which are assigned to the NH stretching vibration modes of the so-called amide A groups, to the ν_{CO} vibrations of C=O of

amide I, and to the ν_{CN} vibrations of C-N-H bonds of amide II from the peptide groups, respectively. The observation of these bands is associated with the presence of zein predominantly in the α-helix conformation (Forato et al., 2003). In the same spectrum, the stretching vibration bands appearing in the 2950-2850 cm^{-1} range are assigned to CH groups. It is noteworthy that zein dissolved in 80% (v/v) ethanol/water solution shows a similar IR spectrum, confirming that this solvent does not affect the main characteristics of zein (Figure 3.2b), appearing only a broad band at 3341 cm^{-1} that can be associated with the OH groups from the remaining solvent. The ^{13}C NMR spectrum of zein (Figure 3.3) shows the typical signals of the protein at 174 ppm assigned to carbonyl carbons. There are also signals in the 140 to 100 ppm range corresponding to amino acid aromatic side chains residues, in the 70 to 45 ppm range due to α-carbons linked to amino groups, and also signals from 45 to 15 ppm assigned to carbon of the aminoacid aliphatic side chains (Forato et al., 2003; Bicudo et al., 2005). The observed chemical shift of carbonyl groups at 174 ppm, which is sensitive to the secondary structure, could indicate high content in α-helix, corroborating the results from the FTIR studies (Forato et al., 2003).

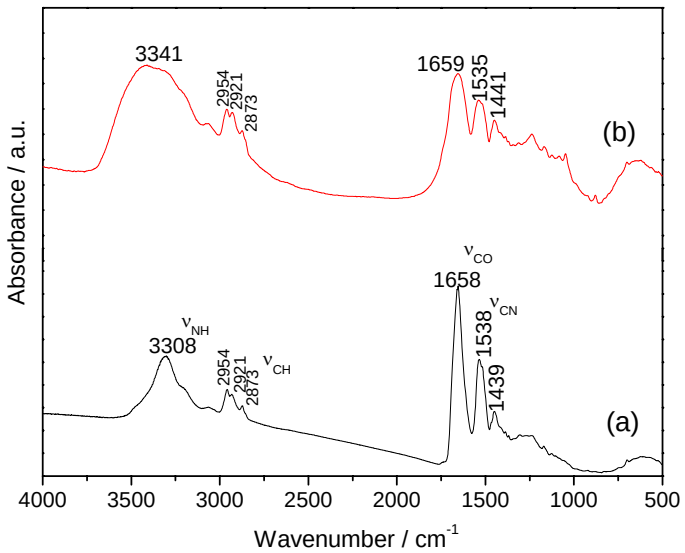

Figure 3.2 FTIR spectra in the 4000-550 cm^{-1} region of (a) starting zein and (b) zein dissolved in 80%(v/v) ethanol/water .

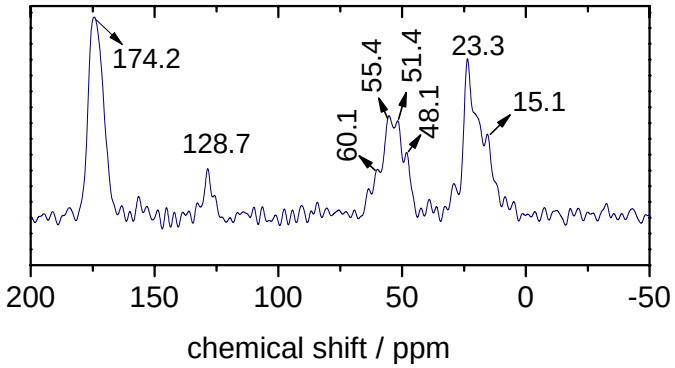

Figure 3.3 ^{13}C NMR spectra of starting zein protein.

The morphology of zein before and after dissolution in 80% (v/v) ethanol/water was investigated by FE-SEM (Figure 3.4). The commercial zein powder used in this work shows a compact and smooth texture formed by thick sheets (Figure 3.4 a and b). However, once the aqueous ethanol solution of zein was left to dry, the morphology of this sample was observed again by FE-SEM. Such images (Figure 3.4 b and c) show the presence of globular aggregates, which may occur from aggregates of small size of around 176 nm up to few microns (approx. 4.0 μm). This morphology may result from the rearrangement of zein molecules during the drying process. The fast evaporation of ethanol may lead to a solution with an increasing content in water that contributes to enhance the zein-zein interactions, minimizing the number of hydrophobic chains exposed to water and, thus, reducing their undesirable interaction with the water molecules after ethanol evaporation. The formation of zein aggregates during the drying process was also reported by Wang et al. in studies focused on the microphases formed from zein in ethanol-water solution (Wang and Padua, 2010).

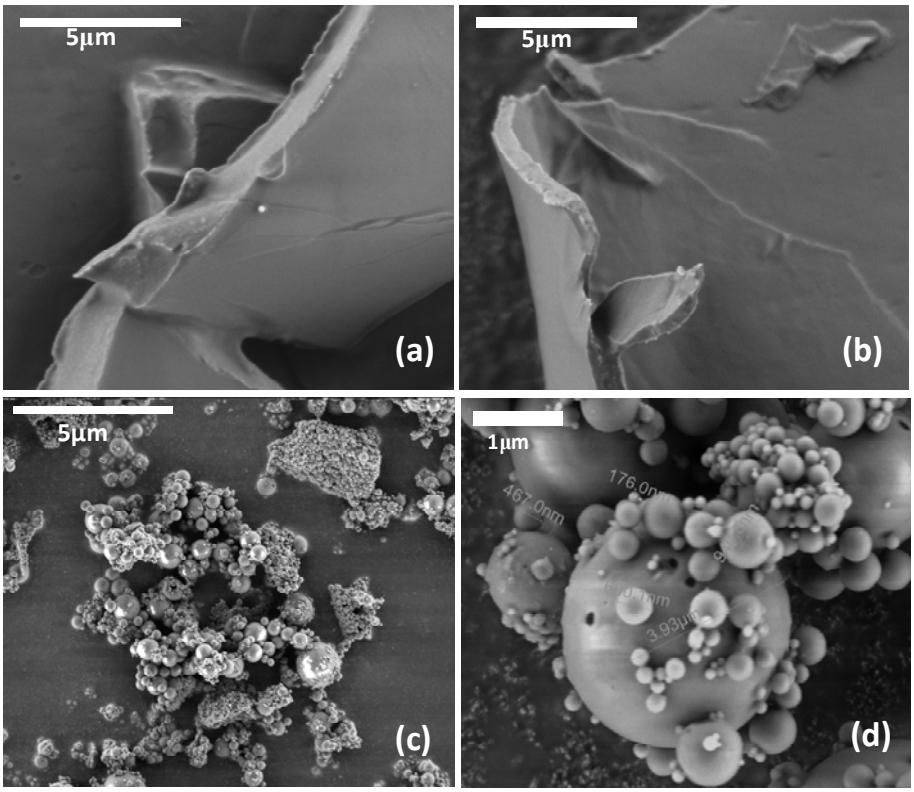

Figure 3.4 FE-SEM images of pristine zein (a and b) and after (c and d) drying a protein solution in 80%(v/v) ethanol/water.

- *Zein-Cloisite Na and Zein-Cloisite 30B bio-hybrids prepared from 80%(v/v) ethanol/water solution*

As commented in the experimental section (§2.3.1a), suspensions of CloisNa and Clois30B layered clays in 80%(v/v) ethanol/water were incorporated to solutions of increasing concentration of protein, resulting in a series of bio-hybrids denoted as Z-CloisNa_S1 and Z-Clois30B, respectively (Scheme 3.1).

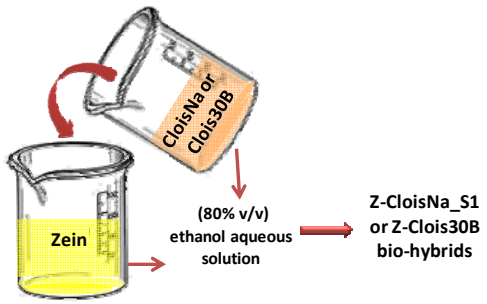

Scheme 3.1 Synthesis of Z-CloisNa_S1 and Z-Clois30B prepared from 80%(v/v) ethanol/water.

The adsorption isotherms of zein on CloisNa and organomodified Clois30B montmorillonites from 80%(v/v) ethanol/water are presented in Figure 3.5. From this graphic, it is clearly observed that the amount of protein adsorbed on Clois30B is higher than on CloisNa. Such differences in the adsorption may be related to a stronger affinity of the zein adsorbate toward the organophilic clay, where the presence of organophilic cations promote the compatibility between the protein and the clay, and thus enlarge the amount of incorporated zein. Thereby, the great disparity observed in the present case in zein adsorption on the two layered clays, suggests that a different adsorption mechanism is taking place in each case. According to the Giles classification (Giles et al., 1960), the adsorption isotherm of zein on CloisNa (Figure 3.5 a) resembles to an H-type isotherm, a special case of the Langmuir isotherm, where the adsorption increases rapidly at low equilibrium protein concentration, reaching a plateau at around 0.9 gL^{-1} with a maximum of adsorbed protein of 10.8 g of zein/100 g of CloisNa. From this equilibrium concentration, the amount of adsorbed zein increases rapidly (see Table 3.1), probably due to the formation of zein aggregates in solution at high zein concentrations, similarly as observed in the study of zein-fibrous clays (Alcântara et al., 2012). In contrast, zein adsorption on Clois30B (Figure 3.5 b) fits to the typical L-type curve (Langmuir isotherm) of Giles classification (Giles et al., 1960), where the adsorbed zein increases gradually with the increase in the starting protein concentrations, reaching a maximum adsorbed protein of 80g of zein/100 g of organoclay at equilibrium concentrations values around 12.6 gL^{-1}. It is evident that the values of zein adsorption in Clois30B are almost three times higher than those in CloisNa, which could indicate that the protein has a better affinity toward the organoclay substrate, and that the mechanism of adsorption of zein in both clays is different.

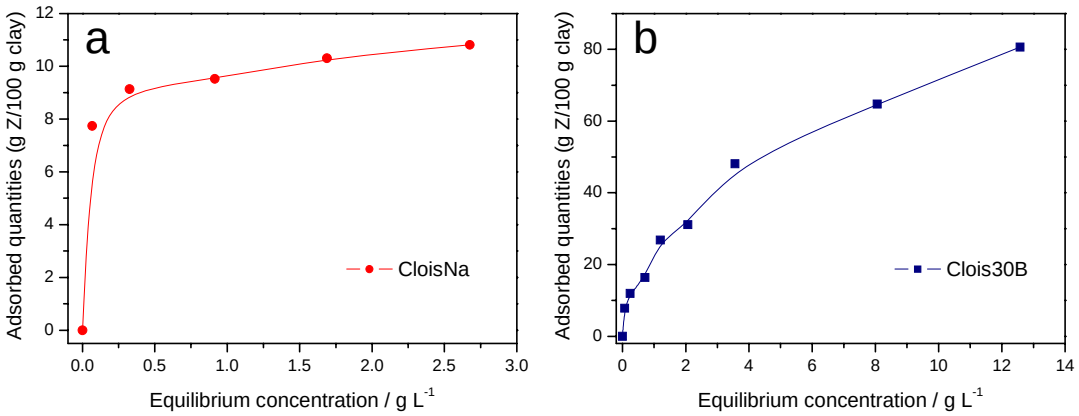

Figure 3.5 Adsorption isotherms at 23°C of zein from 80%(v/v) ethanol/water solution on (a) CloisNa and (b) Clois30B layered clays. Adsorption amounts were deduced from CHNS chemical analyses.

Table 3.1 Bio-hybrids of the Z-CloisNa_S1 and Z-Clois30B, prepared by adsorption of zein from 80%(v/v) ethanol/water solutions containing different initial amounts of zein, and their protein content determined by chemical analysis.

starting amounts (g zein /100 g clay)	zein-cloisiteNa bio-hybrids code	adsorbed zein (g zein /100 g CloisNa)	zein-cloisite30B bio-hybrids code	adsorbed zein (g of zein /100g Clois30B)
10.0	Z-CloisNa_S1-7	7.74	Z-Clois30B-7	7.54
20.0	Z-CloisNa_S1-9	9.13	Z-Clois30B-12	11.9
40.0	Z-CloisNa_S1-9.5	9.52	Z-Clois30B-16	16.7
66.6	Z-CloisNa_S1-10	10.3	Z-Clois30B-26	26.1
100.0	Z-CloisNa_S1-11	10.8	Z-Clois30B-31	31.7
166.0	Z-CloisNa_S1-14	14.6	Z-Clois30B-50	49.4
333.3	Z-CloisNa_S1-20	20.8	Z-Clois30B-64	64.3
500.0	Z-CloisNa_S1-27	27.4	Z-Clois30B-80	80.1

Samples were characterized by XRD with the aim to investigate whether the adsorbed protein was intercalated or not into the homoionic montmorillonites (Figure 3.6). The basal spacing (d_{001}) of the pristine Clois30B (Figure 3.6a) was calculated to be 1.80 nm

from the diffraction peak at 2θ = 4.9º, assigned to the *001* reflection, using the Bragg equation. In the diffractograms of Z-Clois30B bio-hybrid materials (Figure 3.6a), it is observed that this first diffraction peak is displaced towards lower 2θ values, which suggests that the protein is incorporated in the interlayer region of the organoclay. The basal spacing increases with the content of zein adsorbed in the Clois30B clay, reaching for instance a value of 2.52 nm for the Z-Clois30B-50 bio-hybrid. Taking into account the thickness of the silicate layer is 0.96 nm (Aranda et al., 1994), the interlayer distance (Δd_L) in the Z-Clois30B bio-hybrids can be calculated, varying from 0.96 to 1.56 nm for the samples from the lowest to the highest content in zein. It has to be considered that the protein can be accommodated together with the organocations, as it is difficult that zein could replace them. Considering that the α-helix monomer of zein shows a thickness of approximately 1.2 nm (see Chapter 1, Fig.1.3), (Wang et al., 2003), it could be proposed that the protein is intercalated in Clois30B favored by the presence of glutamine groups that can exchange interlayer cations. Besides, those hydrophobic interactions with remaining alkylammonium chains of the organocations located inside the galleries could also favor the intercalation of the protein molecules.

Bio-hybrid materials based on CloisNa at low adsorbed protein content show XRD patterns (Figure 3.6b) in which the *001* reflection peak appears at the same 2θ value than in pristine CloisNa. The XRD pattern of Z-CloisNa_S1-27 with high zein content shows two reflections at low 2θ angles. One of them corresponds to a Δd_L value of 1.18 nm, similar to that of CloisNa, and the second broad peak centered at 1.55 nm, which can be related to the presence of an intercalated phase. In this case, the calculated interlayer spacing gives a value of 0.59 nm, which is lower than the dimensions of the zein monomer. A possible explanation could be related to a partial intercalation on the edges of the clay particles via ion-exchange reaction of Na^+ by protonated glutamine group on the loops of α-helix zein molecules. Anyway, the presence of these two *001* reflections in the diffractograms suggests the formation of a mixed phase under these synthesis conditions. The resulting bio-hybrids are formed with most of the protein molecules situated at the external surface of the sodium montmorillonite. The difficulty to achieve zein intercalation in sodium montmorillonite has been also reported by Park and co-authors in studies on zein/montmorillonite bio-hybrids processed by electrospining (Park et al., 2012). Nedi and co-authors proposed a previous modification of the clay with poly(ethylene glycol) (PEG) as plasticizer of zein-montmorillonite system (Nedi et al., 2012). However, there are not conclusive

evidences of zein intercalation in that work since the reported basal spacing corresponds to the PEG intercalation compound, and it is known the high affinity of this polymer for remaining intercalated (Aranda and Ruiz-Hitzky, 1999).

From these results, it is possible to conclude that zein cannot be intercalated in CloisNa by this method. However, it was possible to achieve the incorporation of the protein in Clois30B and, for this reason, a more detailed characterization of these bio-hybrids was carried out.

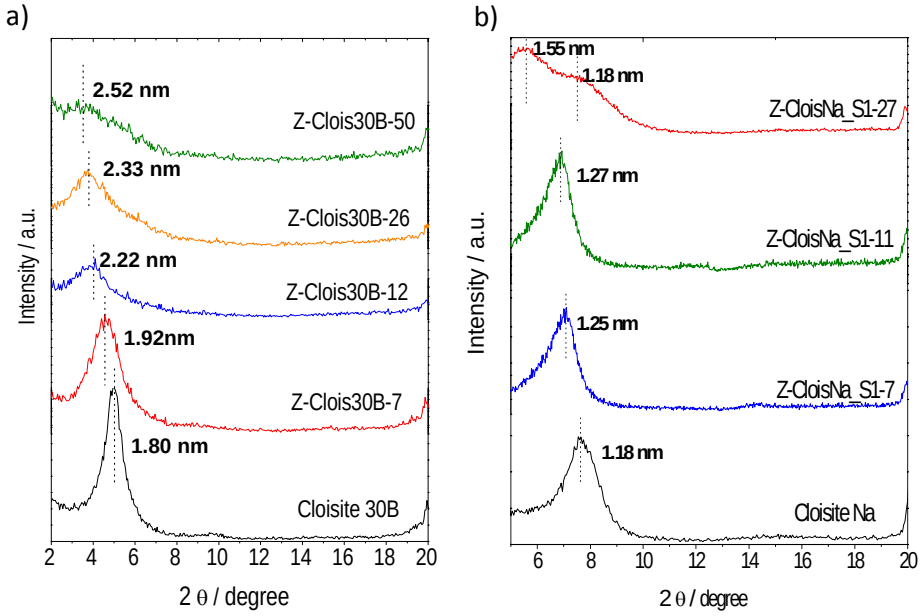

Figure3.6 XRD patterns of (a) Z-Clois30B and (b) Z-CloisNa_S1 bio-hybrids prepared from zein solutions in 80%(v/v) ethanol/water .

In this way, FTIR spectroscopy was used to investigate the possible interactions and structural changes that occurred during the adsorption process of zein on Clois30B (Figure 3.7). The spectrum of Clois30B shows the characteristic vibration modes of the 2:1 layered silicate, where the OH stretching vibration band appears at 3633 cm^{-1}, the Si–O stretching bands are observed around 1100–1050 cm^{-1} range, and the deformation bands assigned to (Al_2OH) and (MgAlOH) appear between 930 and 840 cm^{-1} region (Belver et al., 2012). In addition, the typical bands associated with the quaternary alkylammonium cations can be also evidenced in the pristine organoclay spectrum, showing the stretching vibrations of CH_2 groups at 2928 and 2853 cm^{-1} and the bending of CH_3 and CH_2 at about 1472 cm^{-1}. On the other hand, significant bands of the intercalated protein can be easily identified in the bio-hybrids, such as amide I ($\nu_{C=O}$)

and amide II (ν_{CN}), which were displaced toward higher wavenumber appearing the amide II at 1540 and 1544 cm^{-1} in Z-Clois30B12 and Z-Clois30B64, respectively, while the amide I band appears at 1663 cm^{-1} in both bio-hybrids spectra (Figure 3.7). These shifts could be related to the interactions between such groups of the protein and the silicate. Focusing on the 4000-2500 cm^{-1} region, the stretching band at 3341 cm^{-1} assigned to amide A groups (ν_{NH}) is also observed in the bio-hybrids in addition to that of C-H bonds characteristic of organic compounds in the starting organoclay and the protein. However, in the bio-hybrids spectra, the band at 3341 cm^{-1} of starting zein appears as a broad band at higher wavenumber values, 3387 cm^{-1}. These results could suggest the existence of hydrogen bonding interactions between the protein and the organoclay, similarly to that reported for zein-alginate/layered double hydroxide (Alcântara et al., 2010).

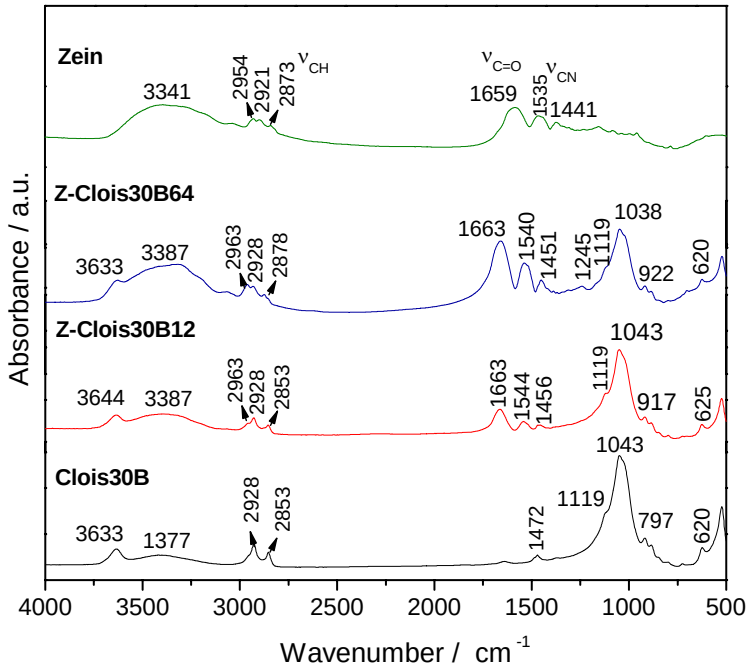

Figure 3.7 FTIR spectra (4000 to 500 cm^{-1}) of neat Cloisite30B, starting zein, and their derived Z-Clois30B-12 and Z-Clois30B-64 bio-hybrids.

The morphology of the Z-Clois30B bio-hybrid samples dried at 40°C in oven was investigated in comparison with pristine Clois30B by FE-SEM. The images of the corresponding bio-hybrids based on Clois30B, containing different zein content, are shown in Figure 3.8 together with the starting Clois30B. Z-Clois30B (Figure 3.8 c and 4.7d) shows a morphology more similar to the pristine silicate than to the protein. The

preservation of the layered arrangement of the pristine silicate in the bio-hybrid suggests that the protein is in close interaction with the clay, either intercalated or on the external surface, avoiding the formation of the previously observed zein aggregates.

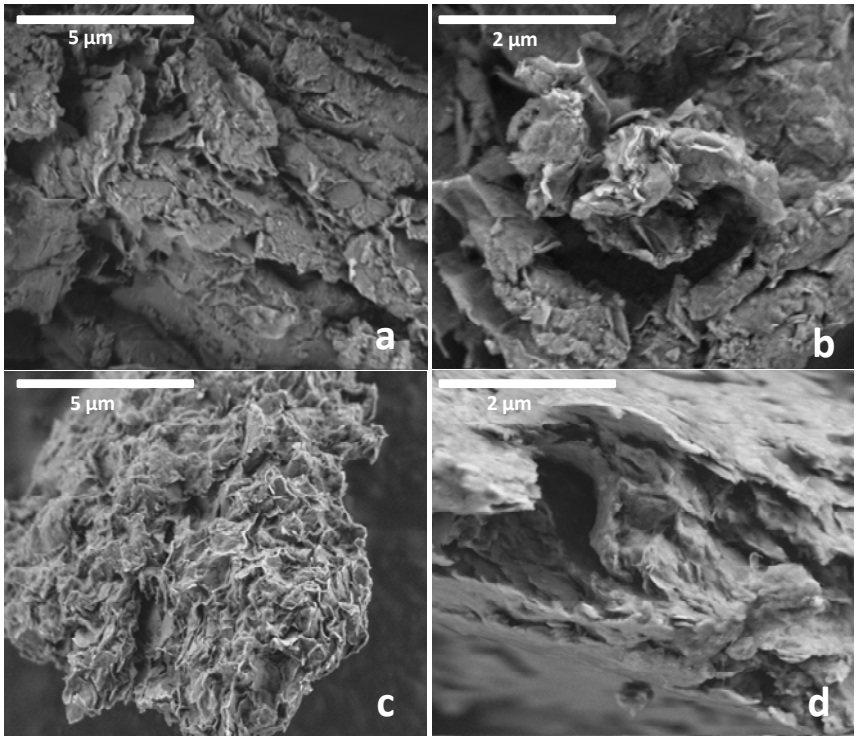

Figure 3.8 FE-SEM images of neat Clois30B (a, b) and Z-Clois30B-80 (c, d) bio-hybrids

Thermal stability of these bio-hybrids was investigated from TG curves recorded in the 25-800ºC range, under air flow conditions (Figure 3.9). In all the samples, a weight loss between room temperature and about 250 ºC, related to the adsorbed water molecules, is evidenced. The weight loss in this step is lower in Clois30B (Figure 3.9 a) and zein (Figure 3.9 b) than in the bio-hybrids (Figure 3.9 c and d), most probably due to the remaining solvent from the synthesis. When heating at temperatures between 270 and 345 ºC, various mass losses are observed, which are mainly related with the combustion of organic matter associated with the neat clay (around 15% of weight loss evidenced by the TG curve of Clois30B, (Cervantes-Uc et al., 2007), and partial decomposition of the biopolymer, which is associated with an exothermic peak of low intensity about 300 ºC. At temperatures above 345 ºC, the observed weight losses are related to the total decomposition of the protein by combustion, which are evidenced by exothermic peaks around 500 ºC, followed of elimination of the structural hydroxyls

of the clay. The thermal behavior of the bio-hybrids with low zein content (Figure 3.9 c) resembles that of Clois30B, while at high zein content (Figure 3.9 c) the thermal profile is more similar to that of neat zein. In addition, an improvement of the thermal stability is observed in the bio-hybrids compared to the pristine protein, which suggests the establishment of interactions between the zein and the organoclay.

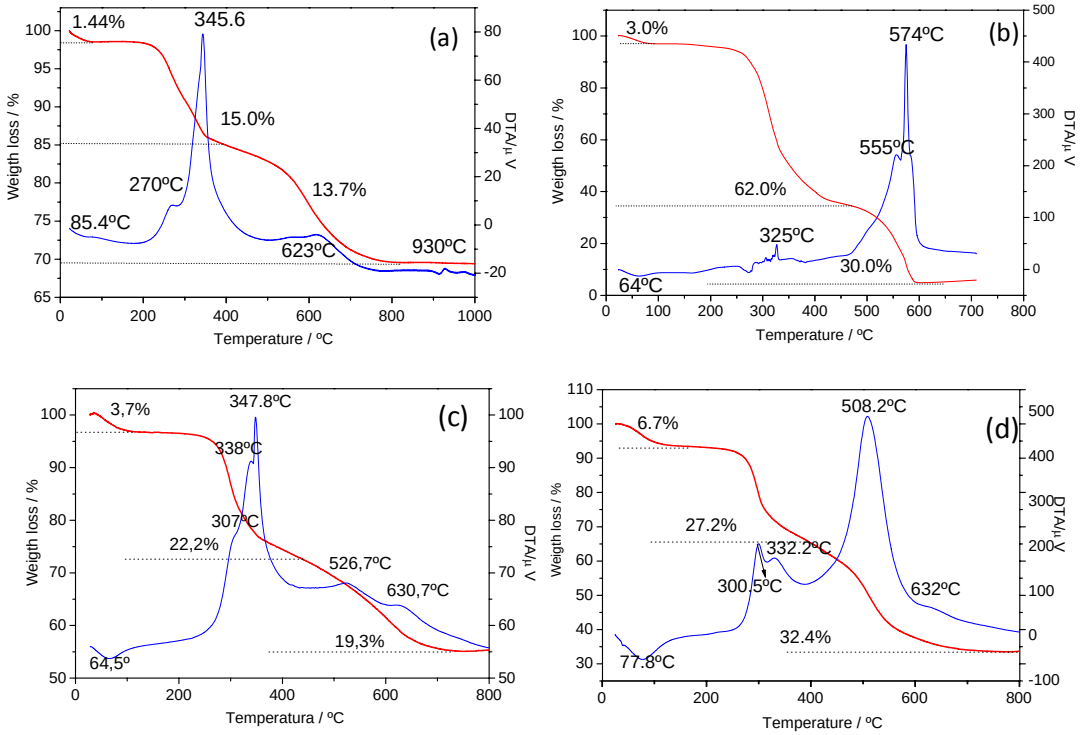

Figure 3.9 TG/DTA curves recorded in air flow obtained for neat Clois30B (a), pure zein (b), Z-Clois30B-12 (c) and Z-Clois30B-80 (d) bio-hybrids.

3.2.2 Zein-CloisiteNa bio-hybrids prepared from absolute ethanol

- *Characterization of the zein fractions formed in absolute ethanol*

It is well-known that zein is not soluble in water or pure alcohol. However, it was observed in this study that, although zein cannot be dissolved in pure ethanol, a separation process of different components of the protein in a soluble phase and a precipitate occurs in these conditions (Figure 2.2, Chapter 2, Experimental section). The two phases correspond to the soluble and insoluble zein fractions in alcohol, being

henceforth denominated as extracted (EXT) and precipitate (PCT), respectively. Colorimetric tests, using a ninhydrin spray solution as revealing agent, were carried out in order to detect the presence of protein in the extracted liquid phase. In fact, the presence of the protein in the ethanol phase was indicated by the purplish color resulting from reaction between ninhydrin and free amino groups from amino acids of solubilized zein (Figure 3.10).

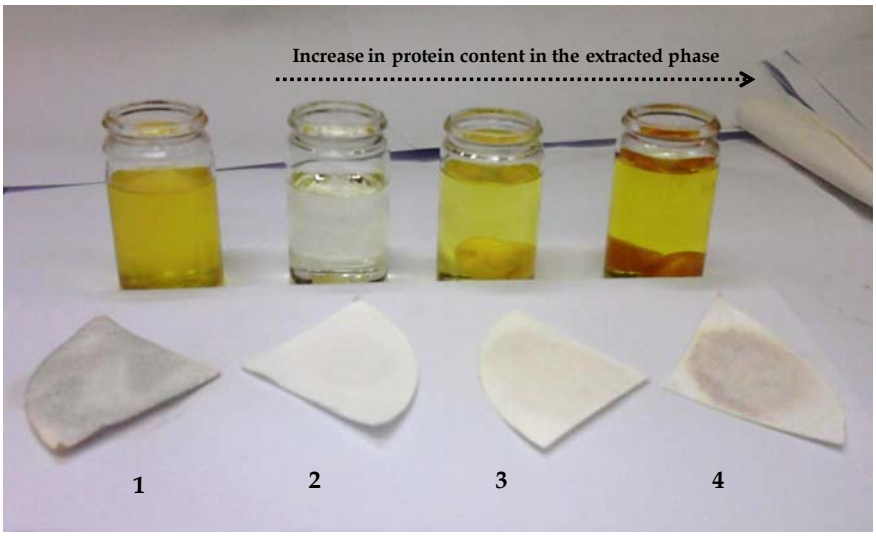

Figure 3.10 Colorimetric assay using ninhydrin spray solution as protein revealing agent in different zein preparations: (1) 0.3%(w/v) zein solution in 80%(v/v) ethanol/water as reference, and (2-4) zein incorporated in pure ethanol in 0.018, 0.15 and 0.3%(w/v) concentration.

Electrophoresis measurements (SDS-PAGE) were also conducted in these two phases and are displayed in Figure 3.11 A. The protein patterns of the PCT phase, after dissolving it in 80%(v/v) ethanol/water, are very similar to those of neat zein also dissolved in the aqueous ethanol solution introduced in the present Chapter (Figure 3.1). The characteristic bands of α-zein and its dimers are observed at approximately 21-25 kDa and 50 kDa, respectively. In this PCT gel, a band set between 150 kDa and 250 kDa is also observed, which could correspond to the presence of other protein aggregates, such as trimers, tetramers and/or oligomers. Together with the bands corresponding to α-zein, SDS-PAGE of the EXT phase presents a band at around 10 kDa. An analogous band was reported by Sessa and co-authors, who extracted zein pigments using ethanol in a Sephadex LH-60 chromatographic column (Sessa et al., 2003). These pigments are yellow-orange colored oxygenated carotenoids known as

xanthophylls, such as lutein and zeaxanthin, which show a molecular weight of around 565 Da (Kale and Cheryan, 2009). It has been also reported that these zein pigments, which are responsible of its yellow color, are located in the core of the triple-helical segments, being strongly linked to the Z19 monomer (Momany et al., 2006). Hence, the 10 kDa band could be related to ethanol-soluble protein components associated with the xanthophyll pigments as reported by Sessa and co-workers (Sessa et al., 2003).

In this sense, UV-Vis spectrophotometry was used to corroborate the presence of these protein components in the extracted liquid phase. For comparison, the spectra of pristine zein and the precipitate phase were also recorded (Figure 3.11 B). The spectrum of the pristine zein solution (Figure 3.11 B - a) presents a band at wavelength 280 nm related to the intrinsic band of protein aromatic residues, and another band at 325 nm assigned to the pigment. The spectrum of the EXT phase in ethanol (Figure 3.11 B- b), shows bands around 280 and 320 nm as in the spectrum of zein, which suggests that ethanol was able to leach some fraction of protein and pigment from the pristine zein. This interpretation is supported by the spectrum of the PCT dissolved in 80%(v/v) ethanol/water (Figure 4.11 B-c), where the intensity of the band at 325 nm is significantly decreased, while the band at 280 nm remains unaltered, confirming the pigment extraction by ethanol to the EXT phase. Focusing on the 300-550 nm region of the spectra of both the zein solution in 80%(v/v) ethanol/water and the EXT phase in ethanol (inset in Figure 3.11B), it is possible to ascertain a maximum absorbance at 442 nm and other maximum values at 419 and 469 nm. These set of bands show the characteristic shape and wavelengths of the carotenoid chromophores (Sessa et al., 2003). In contrast, the spectrum of the PCT fraction in 80%(v/v) ethanol/water does not show these bands, which suggests that most part of the carotenoids have been solubilized by ethanol during the extraction process, being now present in the EXT phase.

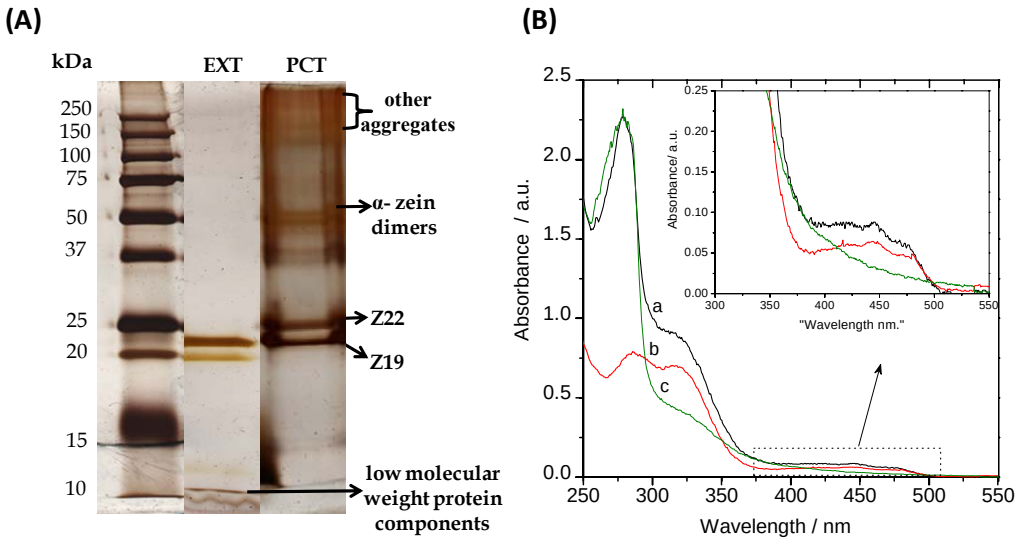

Figure 3.11 (A) SDS-PAGE in 20% acrylamide of the zein fractions separated in absolute ethanol. The PCT was dissolved in 80%(v/v) ethanol/water for the analysis. The electrophoretic gel was silver stained. (B) UV-Visible spectra in the 250-550 nm wavelength region of (a) neat zein and (c) the PCT solubilized in 80%(v/v) ethanol/water, and (b) the EXT phase in absolute ethanol.

Solid state NMR and FTIR spectroscopy were also used to investigate the composition of these zein fractions and the corresponding spectra are presented in Figure 3.12. Unfortunately, there is not a significant difference between the spectra of both phases. The FTIR spectra in the 4000-500 cm^{-1} region (Figure 3.12 A) of zein, EXT and PCT show the bands of amide A (3600-3100 cm^{-1}), amide I (3600-3100 cm^{-1}), and amide II (3600-3100 cm^{-1}) of the protein. The spectrum of the PCT (Figure 3.12 A – c) is very similar to that of the EXT phase (Figure 3.12 A - b), except that the latter shows the presence of a shoulder at 1742 cm^{-1}, which can be attributed to the $\nu_{C=O}$ of free fatty acids (Forato et al., 2003).

^{13}C CP-MAS NMR (Figure 3.12 B) spectra of zein and the two fractions separated from ethanol are complex and very similar, presenting signals between 173-175 ppm due to carbonyls from the peptide groups and the protein side chains. The signals at 128 ppm, those from 45 to 70 and those from 15 to 45 ppm are assigned to aromatic side chains, α-carbons and carbons from the amino acid aliphatic side chains, respectively (Forato et al., 2000).

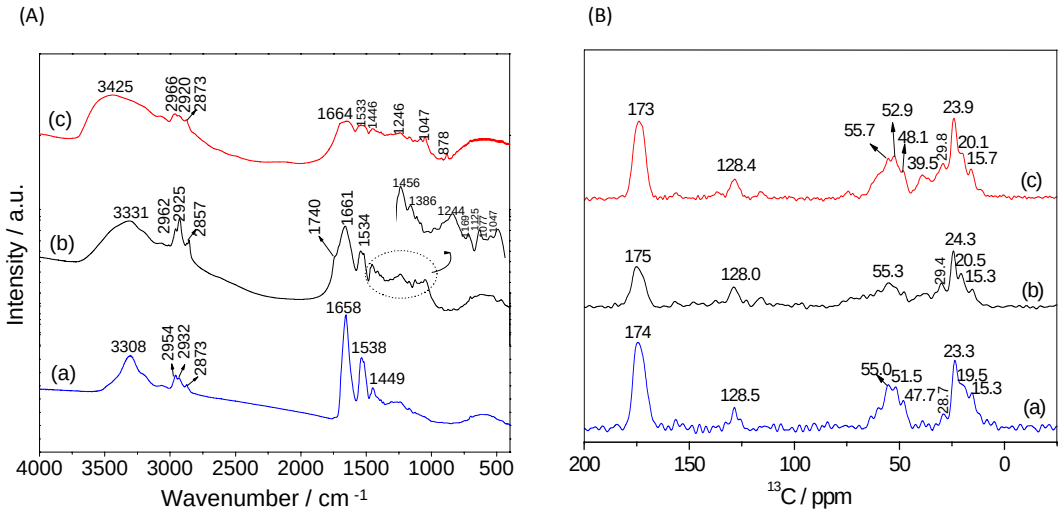

Figure 3.12 (A) FTIR spectra in the 4000-550 cm^{-1} region and (B) ^{13}C NMR spectra of (a) zein protein, and those of the (b) extracted phase and (c) precipitate fraction of zein after treatment in pure ethanol.

The morphology of these zein fractions was also investigated by FE-SEM (Figure 3.13). It is observed that the EXT phase (Figure 3.13 a and b) consists in distorted molecular aggregates, presenting also some plate-like shape agglomerates (indicated by white arrows in Figure 3.13 b). In contrast to the typical zein morphology, the PCT fraction does not show agglomerates (Figure 3.13 c and d), being characterized by the presence of a continuous and homogeneous film of compact texture very similar to the commercial zein morphology (Figure 3.4 a and b). These different morphologies in zein can be associated with the amount of protein in each one of the separated phases. The effect of zein concentration in the texture of zein was reported by Padua and co-authors for zein samples dried from ethanol-water systems (Wang and Padua, 2010). Thus, diluted zein solutions showed the formation of free microspheres occasioned by hydrophobic associations, which is the case of the EXT phase. In contrast, zein in higher concentration has a tendency to form narrow packed aggregates that subsequently fused into a film during the drying process, which may be a similar situation to that of the PCT in the current study.

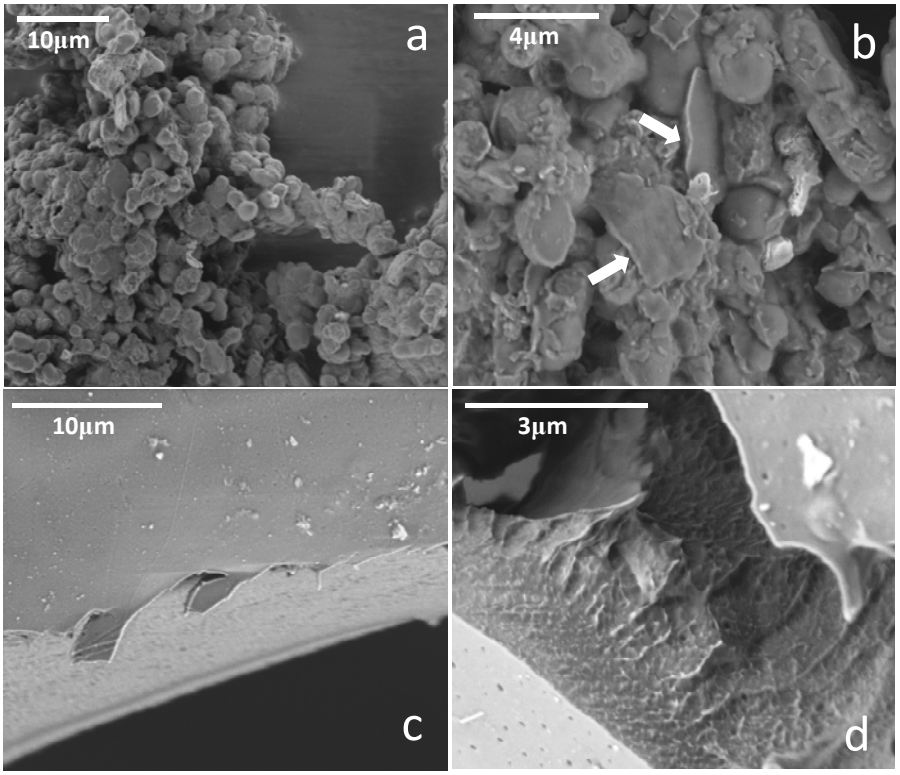

Figure 3.13 FE-SEM images of (a, b) the EXT and (c, d) the PCT fractions separated from 18.7 mg/mL zein incorporated in pure ethanol.

- *Zein- CloisiteNa bio-hybrids formed from zein segregated phases in absolute ethanol*

The second attempt to assembly zein and sodium montmorillonite was carried out by the addition of an aqueous suspension of CloisNa to zein in absolute ethanol (see Experimental section, § 2.3.1 (a), synthesis 2), till reaching a volume ratio in 80:20 of ethanol:water in the mixture, as shown in the Scheme 3.2. The idea is to have the clay swollen in water, in which the soluble parts of zein (EXT phase) can begin to intercalate, and then the insoluble zein (PCT) can be also intercalated as it gets dissolved in the ethanol/water medium.

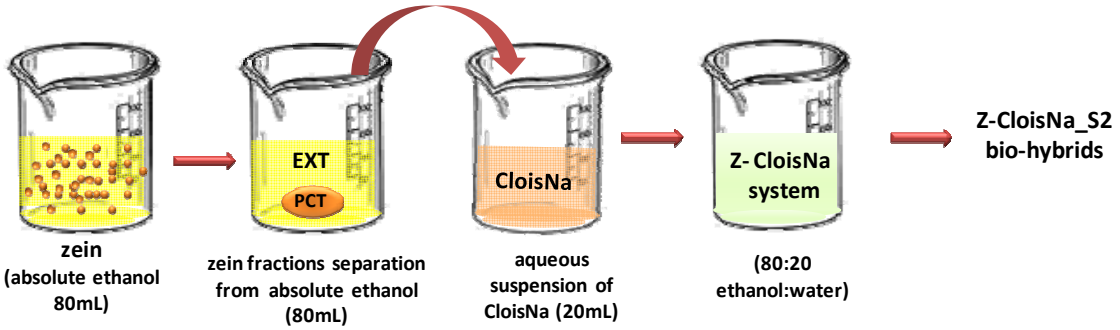

Scheme 3.2 Synthesis of Z-CloisNa_S2 bio-hybrids prepared from zein in absolute ethanol after mixture with a CloisNa aqueous suspension.

The affinity between the protein and CloisNa via this second method was also investigated by analyzing the "pseudo-isotherms" of this adsorption process at 23 °C represented in Figure 3.14. In contrast to the synthesis route 1 (§ 3.2.1), the shape of this "isotherm" indicates that zein present in the system was almost completely adsorbed at low initial concentration, which resembles to the classical H-type isotherm (Giles et al., 1960). This "pseudo isotherm" shows a plateau region at zein equilibrium concentration above 2.0 gL^{-1}, corresponding to approximately 40 g of zein adsorbed per 100g of montmorillonite. At these values, a monolayer-type conformation of the zein molecules in CloisNa is expected. The total amounts of zein adsorbed in the silicate and their respective codes are presented in Table 3.3.

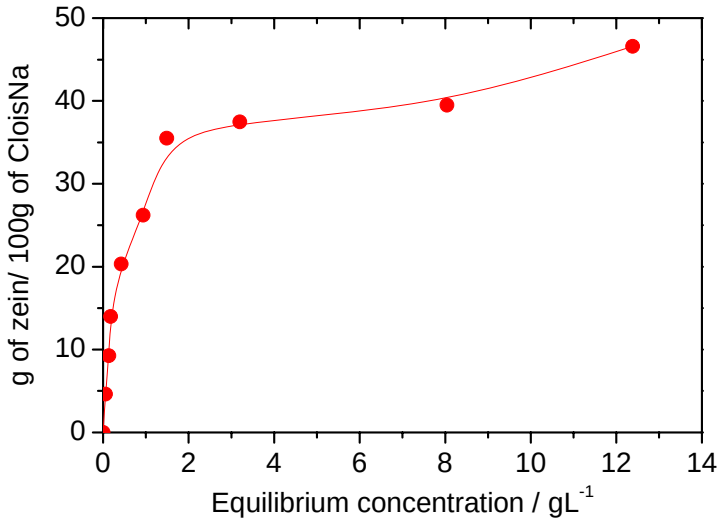

Figure 3.14 Adsorption "pseudo isotherm" of zein in pure ethanol at 23°C after mixture with CloisNa water suspension to reach an 80%(v/v) ethanol/water concentration. Adsorption amounts were deduced from CHNS chemical analyses

Table 3.3 Zein-CloisiteNa bio-hybrids prepared by adsorption of zein in ethanol at different initial amounts of zein and CloisNa in water in order to reach an 80%(v/v) ethanol/water concentration.

Starting amounts (g zein /100 g clay)	Zein-cloisiteNa bio-hybrids code	adsorbed zein (g zein /100 g CloisNa)
10.0	Z-CloisNa_S2-9	9.25
20.0	Z-CloisNa_S2-14	14.0
40.0	Z-CloisNa_S2-20	20.3
66.6	Z-CloisNa_S2-26	26.2
100.0	Z-CloisNa_S2-35	35.5
166.0	Z-CloisNa_S2-37	37.5
333.3	Z-CloisNa_S2-40	39.5
500.0	Z-CloisNa_S2-46	46.6

Figure 3.15 shows the XRD patterns of Z-CloisNa-S2 bio-hybrids. The intercalation of zein in the interlayer space of the clay is confirmed by the shift of the *001* peak at lower 2θ values. Although the XRD pattern of Z-CloisNa_S2-9 shows a broad peak, it is possible to evidence two phases at 1.61 and 1.29 nm, which suggests mixed phases with and without intercalated protein, respectively. The d_{001} increases with zein content and can reach a value of around 1.88 nm for zein content higher than 25 g of protein per 100 g of CloisNa. Considering a thickness of the silicate layer of 0.96 nm, the increment of the interlayer distance can be estimated in about 0.92 nm for Z-Clois_S2-37 and Z-Clois_S2-46 bio-hybrids, this latter having the highest content in zein. In this case, it is clear the intercalation of the protein is probably distorting its structure to be accommodated in the interlayer region. Similar results were reported for other proteins intercalated in sodium montmorillonite, such as bovine serum albumin (BSA) (De Cristofaro and Violante, 2001). Anyway, comparing the experimental methods employed in the synthesis 1 (section 3.2.1) and the present route 2 in order to obtain Z-CloisNa bio-hybrids, it is clear that this last one seems to be more effective to achieve

the incorporation of zein molecules in the intracrystalline space of sodium montmorillonite.

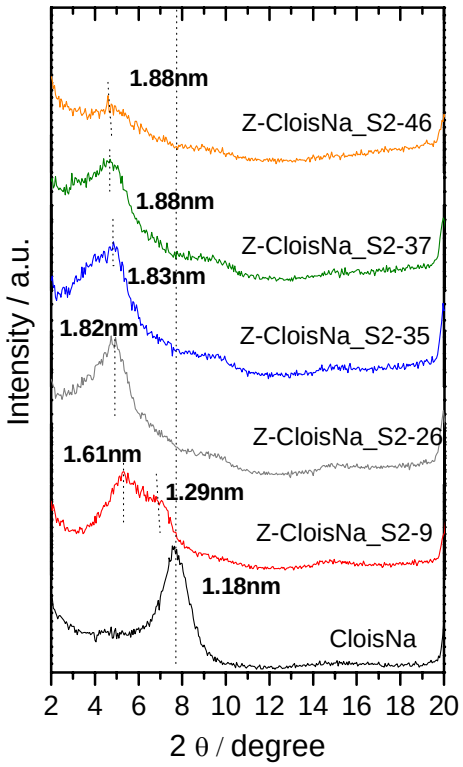

Figure 3.15 XRD patterns of Z-CloisNa_S2 bio-hybrids prepared from zein phases in pure ethanol mixed with CloisNa water suspension.

The infrared spectra of the pristine CloisNa, zein, and three Z-CloisNa_S2 bio-hybrids which contain 9.25, 26.2 and 46.6 g of protein per 100 g of CloisNa, respectively, are shown in Figure 3.16. Besides the vibrational bands at 3634, 1648 and 1045 cm^{-1} assigned to ν_{OH} of Al,Mg(OH), δ_{HOH} of water molecules in the clay and $\nu_{Si\text{-}O\text{-}Si}$ characteristic of the aluminosilicate, respectively (Figure 3.16 a), other bands that can be attributed to the intercalated protein are observed in the spectra of the bio-hybrids. The frequency of the band corresponding to (ν_{CO}) vibration mode of amide I that appears at 1658 cm^{-1} in the pristine zein (Figure 3.16 e) is shifted toward higher frequency values, reaching wavenumber values of 1664 cm^{-1} in the bio-hybrids (Figure 3.16 b, c and d). This shift may be a consequence of interactions between protonated amino groups in the protein and the negatively charged sites in the clay structure. Similar results involving changes in amide I band of zein by interaction with montmorillonite were reported by Ozcalik and Tihminlioglu (Ozcalik and

Tihminlioglu, 2013). The band ascribed to the NH stretching vibration mode of the amide A groups in zein also appears at higher wavenumber in the bio-hybrids, where the frequency depends on the amount of intercalated protein. This phenomenon suggests the existence of hydrogen bonding interactions between such groups of zein and the interlayer water molecules in the clay (Ruiz-Hitzky et al., 2004). The existence of interaction between the protein and the CloisNa clay is also confirmed by the displacement to lower wavenumber of the ν_{CN} amide II band of zein at 1538 cm^{-1}, appearing in the bio-hybrids at 1533 cm^{-1}.

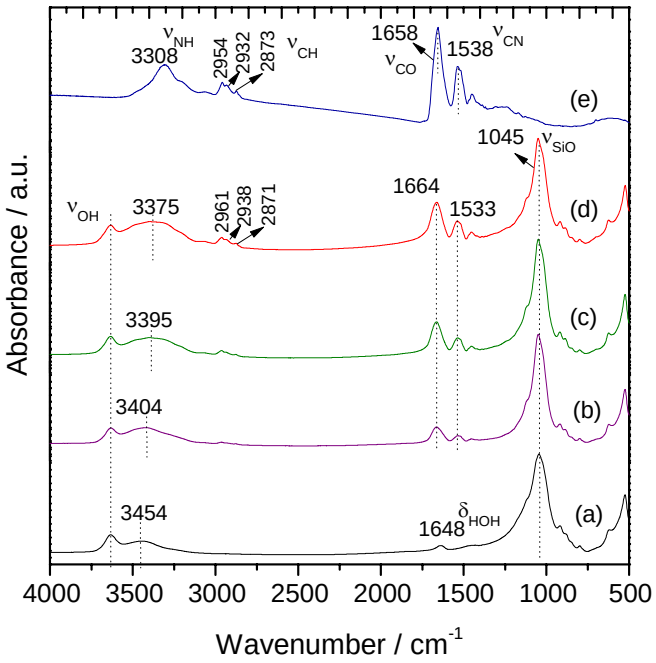

Figure 3.16 FTIR spectra in 4000-500 cm^{-1} region of (a) starting CloisNa, (b) Z-CloisNa_S2-9, (c) Z-CloisNa_S2-26 and (d) Z-CloisNa_S2-46 bio-hybrids materials, and (e) pristine zein.

The Z-CloisNa_S2-46 intercalation compound, with the highest content in zein, was chosen for characterization by TEM microscopy. In the images shown in Figure 3.17, the bright field represents the protein and the dark field stands for the layers of the montmorillonite. These TEM images show the presence of the characteristic platelets of montmorillonite tactoids, which confirm that the intercalation of zein does not affect the intrinsic organization of layered clay. By a calculation using an average of 8 sheets (measurement performed by the same microscope, Figure 3.17 b), it was found an increment basal average of 1.7 nm in this TEM image.

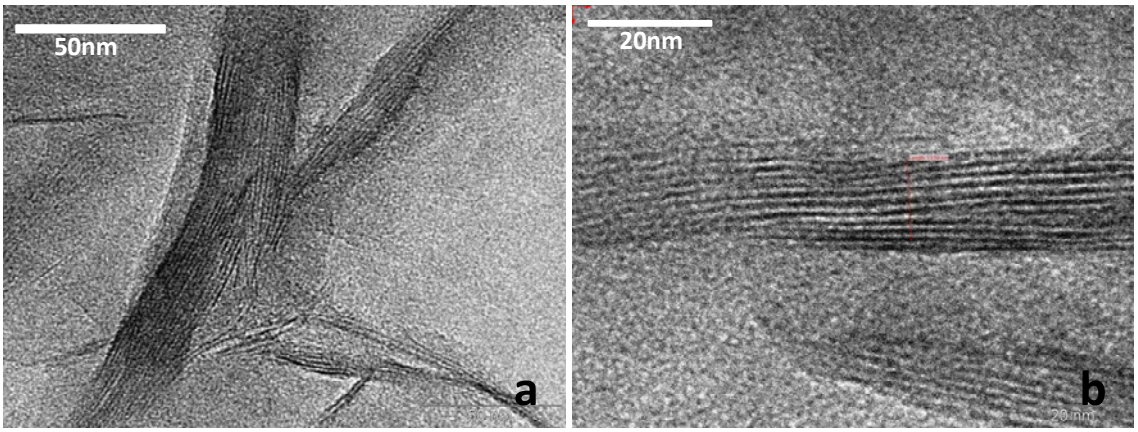

Figure 3.17 TEM images of Z-CloisNa_S2-35bio-hybrid sample.

- *Study of the intercalation mechanism of zein in CloisNa from absolute ethanol*

In order to understand the mechanism underlying this complex intercalation process, a systematic study of the individual steps followed to achieve zein intercalation in CloisNa were investigated. For this purpose, two stages were considered:

i) the formation of a first bio-hybrid based on the zein components present in the soluble fraction in pure ethanol; and

ii) the incorporation of the other zein molecules coming from PCT fraction after being solubilized in the ethanol/water mixture.

With the aim of reconstructing such steps, on the one hand, zein precipitate fraction (PCT) was separated and the extracted phase (EXT) was used to prepare bio-hybrids by addition of an aqueous clay suspension, resulting in a series of materials denoted as EXT-CloisNa bio-hybrids (Scheme 3.3a). On the other hand, bio-hybrids based only on the precipitate phase and CloisNa were prepared by direct mixture of the CloisNa aqueous suspension and the precipitate in pure ethanol, forming the so-called PCT-CloisNa bio-hybrids (Scheme 3.3b). In both cases, the series of bio-hybrids were formed in a final liquid phase of 80:20 (v/v) of ethanol:water final ratio.

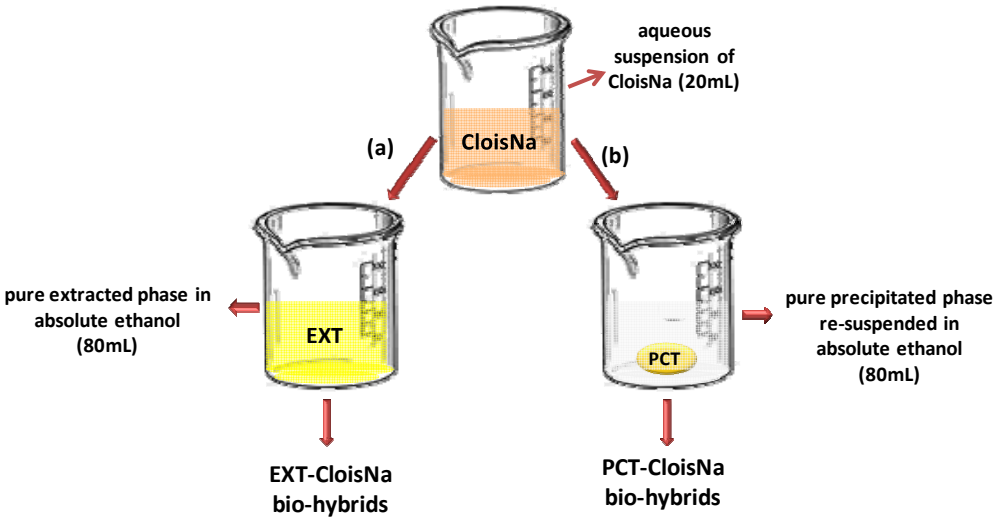

Scheme 3.3 Individual steps to achieve zein intercalation into CloisNa from (a) the extracted phase formed in pure ethanol and (b) the precipitate phase after re-suspension in absolute ethanol.

These EXT and PCT phases were obtained from three different initial amounts of zein dissolved in pure ethanol chosen to reach 20, 100 and 500g per 100g of CloisNa final ratio. As mentioned above, CloisNa aqueous suspensions are added to each one of these EXT and PCT fractions present in pure ethanol, obtaining their respective EXT-CloisNa and PCT-CloisNa bio-hybrids. The amount of protein adsorbed in CloisNa in each case was determined by CHNS chemical analysis (Table 3.4). From these values, it can be observed that the bio-hybrids based on the EXT phase show a low amount of adsorbed protein compared to those materials prepared from the PCT. This fact may be related to the adsorption of zein oligomers, shown in the SDS-PAGE results (Figure 3.9), which are present in the PCT fraction and become soluble in the aqueous ethanol solution formed with the water of the clay suspension. The adsorption of the extracted phase on CloisNa is also confirmed by UV-Vis spectroscopy of the supernatant separated after formation of the EXT-CloisNa bio-hybrids (Appendix A, Figure A.1), being clearly observed the decrease of the protein and carotenoid bands present in the EXT phase after the adsorption assay on the sodium montmorillonite.

Table 3.4 Estimation of protein content in EXT-CloisNa and PCT-CloisNa bio-hybrids.

Samples code	g of protein/100g of CloisNa*
EXT-CloisNa3	3.32
EXT-CloisNa10	10.2
EXT-CloisNa16	15.8
PCT-CloisNa18	18.0
PCT- CloisNA43	43.2
PCT-CloisNa65	65.5

*determined by CHNS chemical analysis

Figure 3.18 shows the XRD patterns of the EXT-CloisNa and PCT-CloisNa bio-hybrids prepared from the EXT and PCT phases, respectively. The diffractograms of the EXT-CloisNa samples (Figure 3.18 A) show a progressive increment in the interlayer distances as the adsorbed protein increases, reaching a basal spacing value of 1.66 nm for the EXT-CloisNa-15 sample. The basal spacing values, determined in the PCT-CloisNa bio-hybrids from the first *00l* reflection peak, range between 1.26 and 1.33 nm (Figure 3.18 B). These values seems to indicate that only a negligible intercalation took place in this case, being the protein adsorbed from the PCT phase located at the external surface of the layered clay.

The key to understand such adsorption behavior from one or the other zein phases can be associated with the nature of the protein fraction present before mixing them with the clay. Natural zein shows two reflections at approximately $2\theta = 9.3^{o}$ and 20.4^{o} in its XRD pattern, which are attributed to interhelix packing structure and zein α-helix backbone, respectively (Nedi et al., 2012). The zein extracted phase (EXT) shows only a reflection around 20.4° of 2θ (Figure 3.18 A), indicating the presence of zein α-helix structure, probably because the arrangement in molecular aggregates (interhelix packing) is not favored in pure ethanol. This is in agreement with the absence of zein aggregates in the extracted phase deduced from SDS-PAGE results (Figure 3.11A). Conversely, the diffractogram of the PCT phase (Figure 3.18B) resembles that of natural zein, showing the peak at 2θ = 9.3° ascribed to zein helical structure, together with a broad signal at $2\theta = 20\text{-}25^{o}$ that reveals the presence of interhelix packing domains (Nedi et al., 2012), being also corroborated by SDS-PAGE results (Figure 3.11). Such differences in the composition of each fraction have to be highly relevant in the

intercalation process. According to these premises, it is possible to assume that the intercalation of zein in CloisNa is favored by the absence of protein agglomerates and the presence of other components of the protein with lower molecular weight in the extracted phase. Meanwhile, the presence of aggregates seems to hinder the incorporation of zein molecules in the CloisNa layers.

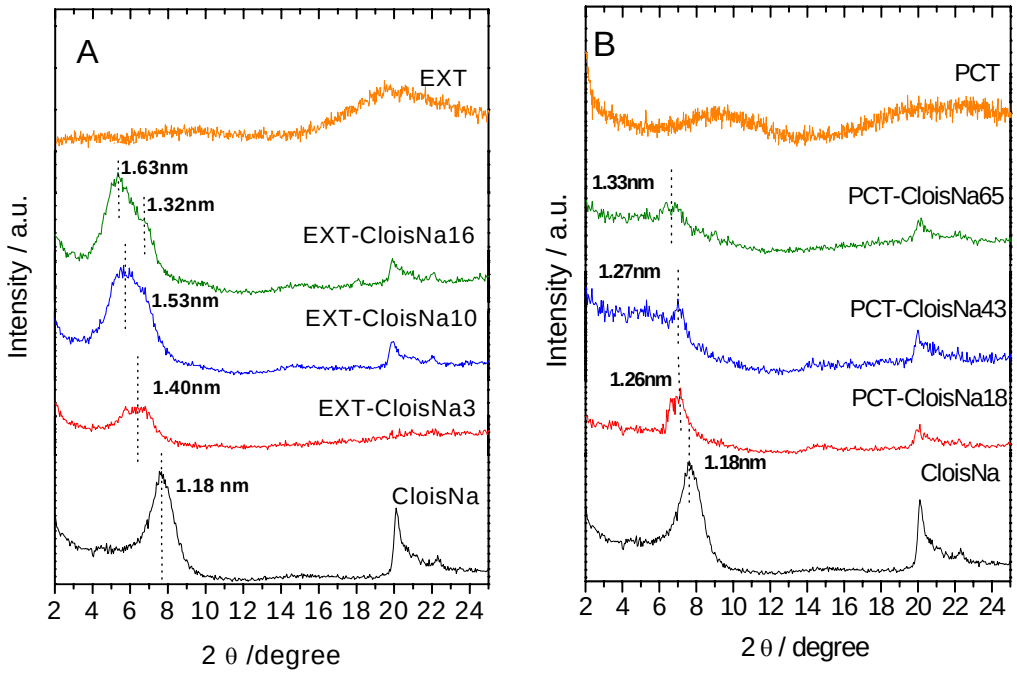

Figure 3.18 XRD patterns of the bio-hybrids prepared from (A) the extracted and (B) the precipitated fractions of zein at different concentrations.

The morphology of these dried bio-hybrids observed by FE-SEM (Figure 3.19) reveals a quite different texture in each type of material. From the images of the bio-hybrids based on the EXT phase (Figure 3.19 a and b), it is not possible to evidence the presence of aggregates, typically formed in pure EXT during the drying process (Figure 3.13 a and b), being EXT-CloisNa characterized by a homogeneous morphology. Thus, the interaction with the clay seems to impede the aggregation of the zein molecules. In contrast, PCT-CloisNa bio-hybrids (Figure 3.19 c and d) present a more compact texture, which somehow seems to remember the morphology of dried pure PCT (Figure 3.13 c and d).

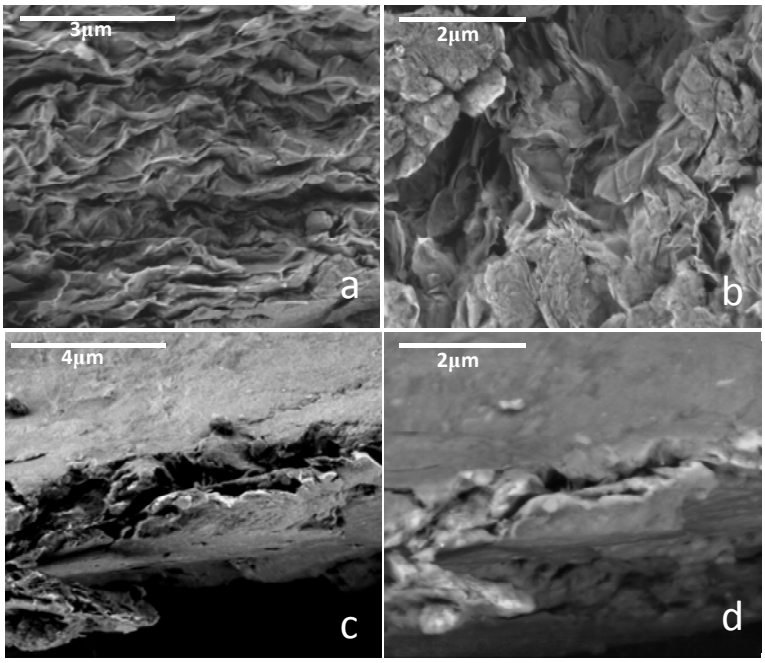

Figure 3.19 FE-SEM images of EXT-CloisNa-16 (a, b) and PCT-CloisNa-65 (c, d) bio-hybrids.

Considering that the EXT phase seems to play a significant role in the mechanisms of zein intercalation between the layers of montmorillonite, a series of bio-hybrids named as EXT-CloisNa/PCT was prepared, in which the EXT-CloisNa intercalation compound was employed as substrate for incorporation of the PCT phase. The main objective of this new set of experiments was to evaluate the importance of the EXT phase in the intercalation mechanism. Hence, EXT-CloisNa bio-hybrids were suspended in water and then mixed with the PCT phase suspended in pure ethanol, obtaining a 80:20 (v/v) ethanol:water final ratio (Scheme 3.4).

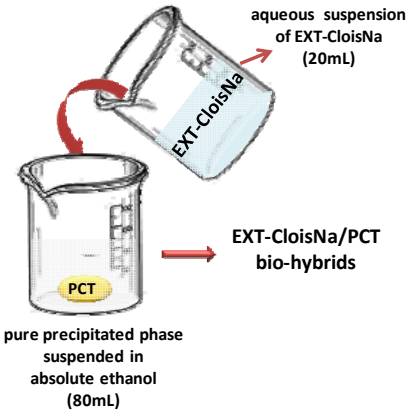

Scheme 3.4 Sequence of the steps followed to prepare EXT-CloisNa/PCT bio-hybrids from EXT-CloisNa mixed with PCT re-suspended in pure ethanol.

The XRD patterns of the EXT-CloisNa/PCT bio-hybrids are displayed in Figure 3.20. As can be observed, the characteristic *001* rational order peak in the starting EXT-CloisNa material (Figure 3.20 a) is displaced towards lower 2θ values in the EXT-CloisNa/PCT bio-hybrids (Figure 3.20 b - d). These basal spacing values slightly increase as the PCT content increases in the dispersion, reaching a maximum value of 1.88 nm (Figure 3.20 d). The basal spacing value estimated for this sample is quite similar to that of the Z-CloisNa_S2-46 bio-hybrid with the highest content in zein (1.88 nm, Figure 3.15). These results are in agreement with those reported by Weiss, in which it was observed that the intercalation of several proteins, such as salmin, serum and egg albumin *etc.*, generally never surpasses a basal spacing of about 1.8 nm, independently of the initial protein concentration (Weiss, 1969). These results suggest the reconstruction of the zein structure by incorporation of the PCT fraction into the interlayer region of the clay where the EXT phase of zein was previously intercalated.

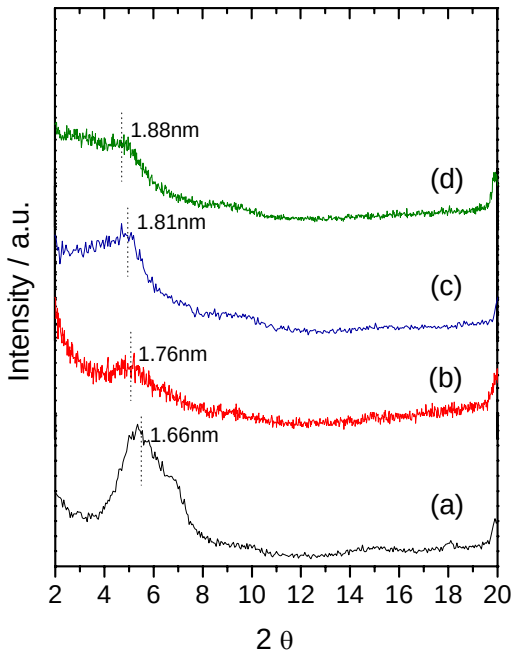

Figure 3.20 XRD patterns of (a) EXT-CloisNa16 bio-hybrid and the EXT-CloisNa/PCT bio-hybrids with different PCT phase from (b) 0.06, (c) 0.3 and (c) 1.5g of initial of zein in 80 mL of pure ethanol.

These evidences could indicate that the mechanism of zein intercalation in CloisNa from the zein phases separation in ethanol could be associated with two main stages:

i) the first one is associated with the formation of a bio-organoclay based on CloisNa and ethanol-soluble components of zein. According to previous characterization of the zein fractions obtained from pure ethanol described in this Thesis (Figure 3.11), the extracted phase only contains zein monomers and other protein components of low molecular weight. Since these smallest zein fractions are well dispersed in ethanol, they can be more easily incorporated into the water-swollen CloisNa, forming the EXT-CloisNa bio-hybrids.

ii) the second step is related to the possible cooperative role of adsorbed zein in the bio-hybrid that favors further adsorption of other zein molecules. Therefore, the interlayer region of this organically modified montmorillonite is assumed to be more compatible with the PCT protein, due to the presence of the protein particles. This fact will enhance the interactions between the zein fractions, and consequently will favor a mechanism of cooperative adsorption, facilitating the incorporation of the other zein fractions till "reconstruction" of the original protein.

In addition, these findings could explain the ability of this hydrophobic protein to penetrate into the interlayer region of sodium montmorillonite observed under the synthesis conditions used to prepare the Z-CloisNa_S2 bio-hybrid systems.

3.2.3 Zein-CloisiteNa bio-hybrids assembled from zein dissolved in alkaline medium

- *Characterization of the zein in alkaline medium*

Although the main solvent for zein is usually based on ethanol/water mixtures, solutions of alkali metal hydroxides (pH> 12) can be also dispersing agents of this protein. In alkaline medium, the solubility of zein is considerably increased due to the basic deamidation reaction that takes place in glutamine and asparagine amino acids (Shukla and Cheryan, 2001; Cabra et al., 2007). In other studies, the alkaline solubility of zein is attributed to the formation of alkali salts of phenolic-hydroxyl groups of tyrosine (Ofelt and Evans, 1949). Anyway, the important thing is that in such conditions it is possible to achieve the complete solubilization of zein in aqueous medium.

Figure 3.21 shows the SDS-PAGE gel analysis of zein dissolved in an alkaline medium (0.1 M NaOH), where it is clearly observed that this sample mainly contains the typical α-zein monomers (20 and 23 kDa), together with dimers (around 36 and 50kDa) in lower amount. According to Cabra et al. (Cabra et al., 2006), when the pH is above the isoelectric point (6.8), the protein structure is predominantly helical, suggesting that the α-helix structure (monomer) is favored in this conditions. In addition, the presence of smaller fractions of protein with molecular mass of about 10 and below 10 kDa, is also detected in this same electrophoretic pattern. These fractions may be formed by a protein hydrolysis involving glutamine transformation into glutamate at this alkaline pH value, which causes also a decrease of molecular weight, increases the charge sites and affects to the amino acids side chains reactivity (Zhang et al., 2011; Cabra et al., 2006).

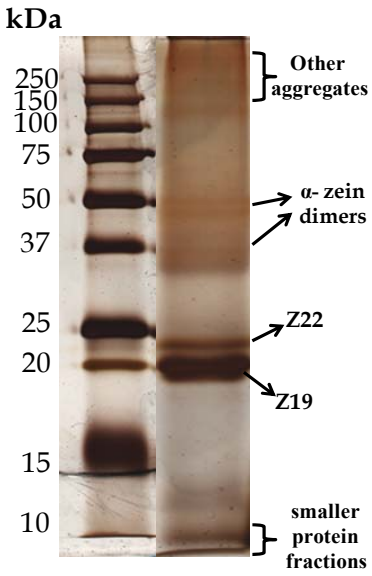

Figure 3.21 SDS-PAGE in 20% polyacrylamide of the alkaline-treated zein. The gel was silver stained.

FTIR and ^{13}C CP-MAS NMR spectra of the alkaline-treated zein and the untreated protein are shown in Figure 3.22. Comparing both FTIR spectra, a decrease in the absorbance in the amide I and II region (1600 to 1520 cm^{-1}) of the treated zein is clearly observed (Figure 3.22 A - b). This lower intensity of the bands can be related to changes in the secondary structure of the protein (α-helix), as it is directly associated with those amide groups. According to Zhang et al. (Zhang et al., 2001), a decrease in

the α-helix content implies the deamidation of glutamine units and the formation of a negatively charged glutamate residue, which produces weaker electrostatic balance in glutamine-rich loops, affecting the stability of the α-helix structure. In addition to these absorbance changes, it is also observed that the amide I and II bands are shifted toward higher and lower frequencies values, respectively, appearing in the alkaline-treated zein at 1663 and 1529 cm^{-1}. Another important change refers to the amide A band appearing at 3308 cm^{-1} in untreated zein (Figure 3.22 A - a), which is now transformed in a broad band centered at higher wavenumber values (3364 cm^{-1}) (Figure 3.22 A - b). All these observations clearly indicate that solubilization of zein in alkaline media provokes relevant changes in the zein structure. These findings are corroborated by ^{13}C NMR (Figure 3.12 B - b). The most interesting changes in the spectrum of zein dissolved in alkaline medium (Figure 3.22 B - b) are those related to the aromatic side chains and carbons from the amino acid aliphatic side chains, between the 129-124 ppm and 45-70 pmm ranges, respectively. Shifts in the signals assigned to the carbonyls from peptide groups between 173-175 ppm were also evidenced.

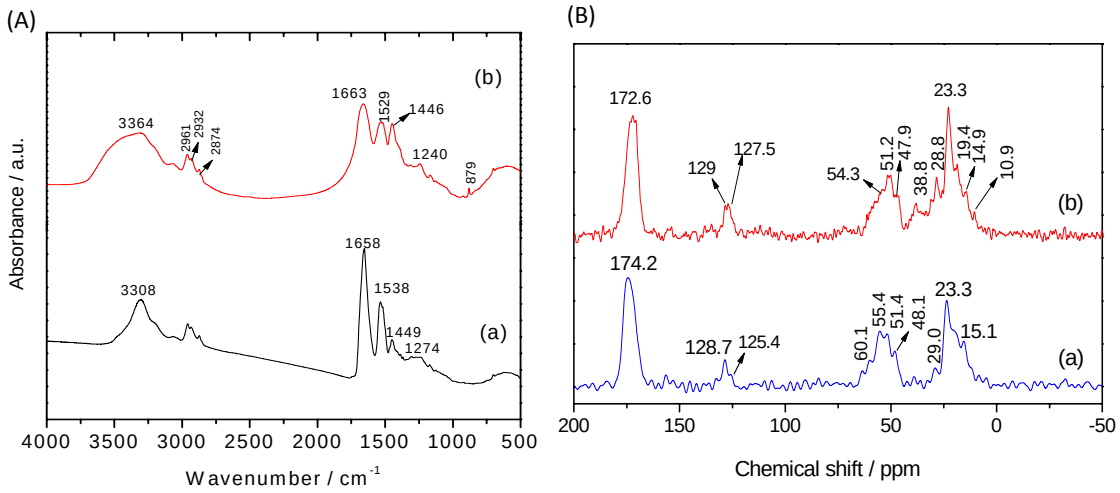

Figure 3.22 FTIR spectra in the 4000-500 cm^{-1} region and ^{13}C NMR spectra of (a) starting zein and (b) zein treated in alkaline medium (0.1 M NaOH)

FE-SEM images in Figure 3.23 display the morphology of the dried zein sample previously treated with 0.1 M NaOH. These images show the presence of zein as thick layers without evidence of the typical agglomerates of this protein. In this case, the

layered morphology may result from the negative charges on the zein surface as a consequence of the basic treatment, which could help to minimize the hydrophobic protein-protein interaction and promote the protein-water interaction.

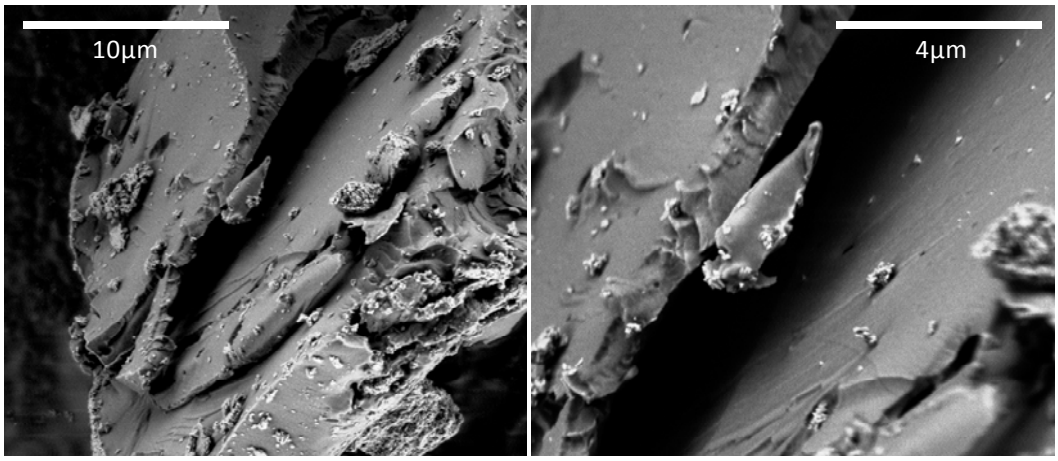

Figure 3.23 FE-SEM images of zein treated in alkaline medium (0.1 M NaOH).

- *Zein-CloisiteNa bio-hybrids assembled to zein dissolved in alkaline medium*

The third approach employed to prepare Z-CloisNa bio-hybrids consists in the use of zein dissolved in 0.1 M NaOH. For this purpose, CloisNa aqueous suspensions were mixed with the alkaline-treated zein at different concentration in protein (Scheme 3.5), leading to the Z-CloisNa_S3 bio-hybrids series after washing with distilled water till neutral pH.

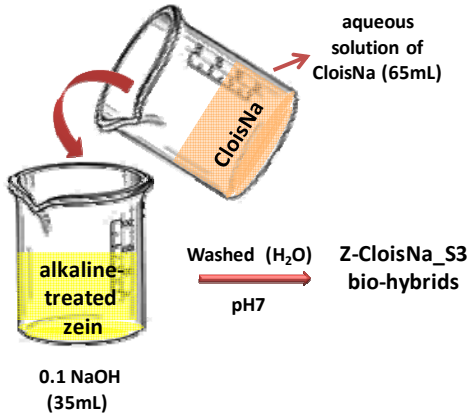

Scheme 3.5 Synthesis of Z-CloisNa_S3 bio-hybrids series prepared from zein dissolved in alkaline medium.

The adsorption isotherm of zein on sodium montmorillonite (Figure 3.24) fits well to the H-type isotherm of the Giles classification (Giles et al., 1960), which indicates the great affinity of the alkaline treated-protein towards this layered clay. Comparing the adsorption isotherms of zein on CloisNa using this third route (Figure 3.24) and the second one based on zein fractions obtained in pure ethanol (Figure 3.14), it is clear that larger amounts of zein are adsorbed from zein dissolved in 0.1 M NaOH. Table 3.5 summarizes the zein content in each bio-hybrid of the Z-CloisNa_S3 series and the codes assigned to these samples.

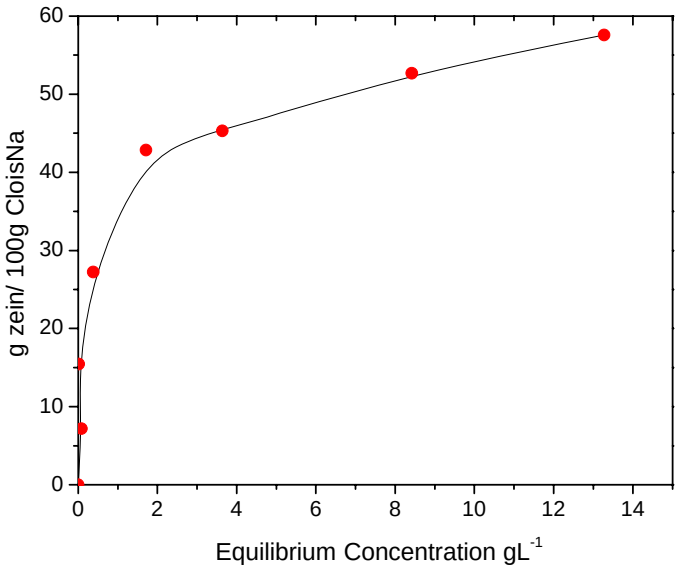

Figure 3.24 Adsorption isotherm at 23ºC of zein dissolved in 0.1 M NaOH on CloisNa. Adsorption amounts were deduced from CHNS chemical analyses.

Table 3.5 Zein-CloisiteNa bio-hybrids prepared by adsorption of different initial amounts of zein dissolved in 0.1 M NaOH.

Initial zein/clay ratio in solution (g zein /100 g clay)	Zein-cloisiteNa bio-hybrids Codes	adsorbed zein (g zein /100 g CloisNa)
10.0	Z-CloisNa_S3-7	7.18
20.0	Z-CloisNa_S3-15	15.4
40.0	Z-CloisNa_S3-27	27.2
100.0	Z-CloisNa_S3-42	42.8

166.0	Z-CloisNa_S3-45	45.3
333.3	Z-CloisNa_S3-52	52.6
500.0	Z-CloisNa_S3-57	57.6

The possible interaction of zein adsorbed on CloisNa was investigated by powder X-ray diffraction. Figure 3.25 - a shows the XRD patterns of the prepared Z-Clois_S3 bio-hybrids. In order to discard some effect of the strongly basic medium in which zein is dissolved, the diffractogram of CloisNa dispersed in a 0.1 M NaOH solution was also recorded. It is observed that the strong basic medium does not affect the structure of the clay, presenting the same XRD pattern with the *001* characteristic peak appearing at 1.18 nm. From the analysis of the *001* reflection in the patterns of the bio-hybrids (Figure 3.25 - a), a clear increase in the basal spacing is evidenced, which points out to intercalation of the protein into the CloisNa layers. From the *001* reflection, it is possible to estimate an interlayer distance increase up to 2.2 nm for the Z-CloisNa_S3-57 sample, which corresponds to the sample with the highest adsorbed zein content. The variation of the Δd_L with the amount of adsorbed zein is shown in Figure 3.25 - b. At low zein adsorption (approximately 45 g zein/100 g of clay), the Δd_L increases linearly with zein content suggesting a direct intercalation of the zein monomers. For higher zein contents, the bio-hybrids show interlayer distances up to 2.2 nm, which could be related to the intercalation of zein molecules as a bilayer.

At pH values above the isoelectric point of zein (approx. 6.2), both the protein and the CloisNa surface present the same negative charge. In these conditions, a repulsion force between the CloisNa layers and the alkaline-treated zein molecules would be expected. The fact that intercalation occurs clearly points out that the mechanism involved in the process is not due to electrostatic effects. The high intercalation degree evidenced for these Z-CloisNa_S3 systems could be associated with the fact that zein suffers deamidation and hydrolysis reactions during the treatment with 0.1 M NaOH, which generate smaller fractions of protein that could penetrate more easily in the clay lamellae favoring the progress of intercalation by organophilic interaction.

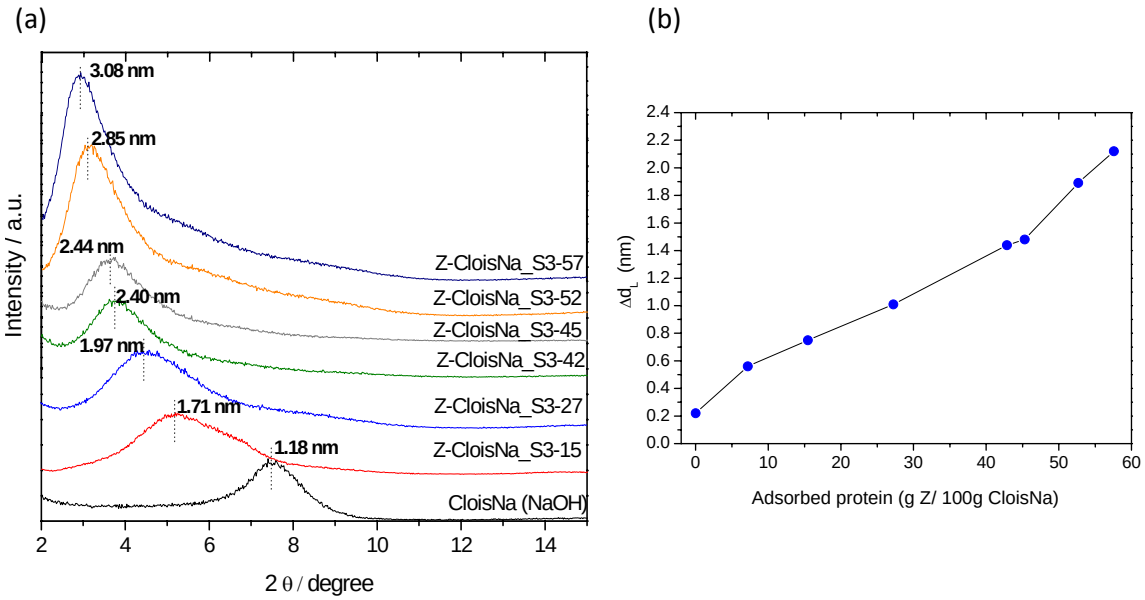

Figure 3.25 (a) XRD patterns of CloisNa after treatment with 0.1 M NaOH solution and Z-CloisNa_S3 bio-hybrids prepared from zein dissolved at different concentrations in 0.1 M NaOH. (b) Δd_L increasing of the Z-CloisNa_S3 bio-hybrids systems with zein content.

As it is curious that a protein with dissociated carboxyl groups (COO^-) resulting from the treatment in a strongly alkaline medium could participate in a cation exchange reaction with CloisNa, a semi-quantitative EDX analysis of sodium and silicon content (in at.%) was carried out in the bio-hybrids and CloisNa before and after treatment with 0.1 M NaOH. Pristine CloisNa showed a Na/Si ratio of 0.112 and 0.090 before and after treatment in alkaline medium, respectively. Interestingly, the Z-CloisNa_S3 samples show practically the same value of 0.090 for the Na/Si ratio than the NaOH treated CloisNa (Figure 3.26). These results suggest that the intercalation mechanism is not directed by a cation exchange reaction, and the presence of sodium cations can be due to their function as charge compensators of the negative charges in zein. Also a possible interaction with the amino groups with the water molecules accompanying Na ions in the clay interlayer region should not be discarded.

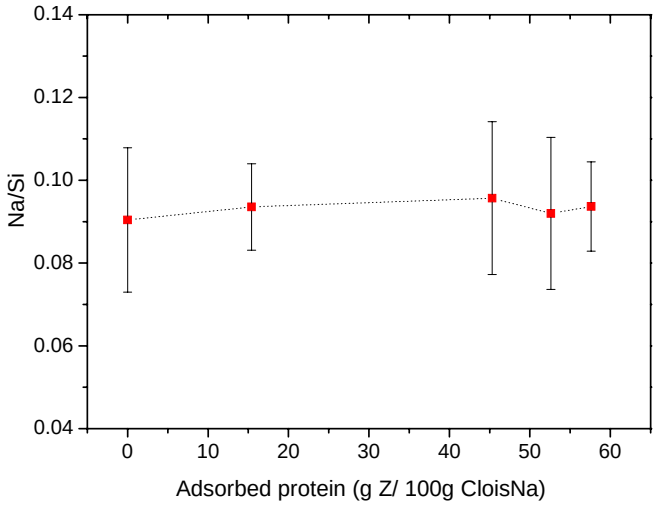

Figure 3.26 Sodium to silicon ratio (in at.%) as a function of zein content (g of zein/100g of CloisNa) in the bio-hybrids of the Z-CloisNa_S3 series. Data obtained from EDX-FE-SEM measurements where conditions were held constant in order to compare the results among the different of samples.

Thus, at the light of the above discussion, the intercalation mechanism of zein dissolved in alkaline medium into montmorillonite seems to be complex and may be driven by different types of factors: i) structural rearrangement of zein protein due to the deamidation and the hydrolysis reactions taking place under the basic conditions; and/or ii) interaction of amino acid units with hydrated interlayer cations present in the expanded clay. It should be noted that the use of a water solvent favors the swelling of the clay which can entrap the biopolymer in alkaline medium in a restacking process (Ruiz-Hitzky et al., 2009).

Characterization of Z-CloisNa_S3 bio-hybrids by IR spectroscopy (Figure 3.27) reveals, as in previous cases, perturbation of the amide I and amide II bands of zein which is possible due to interactions between this protein and the silicate. Thus, the amide I band at 1663 cm^{-1} in the zein treated in alkaline medium (Figure 3.27 d) is displaced to higher wavenumber values appearing in the Z-CloisNa_S3-42 (Figure 3.27 b) and Z-CloisNa_S3-57 (Figure 3.27 c) bio-hybrids at 1667 and 1669 cm^{-1}, respectively. Other important evidence is the shift up to 10 cm^{-1} in the frequency of the amide II band ($\nu_{C=O}$) in the Z-CloisNa_S3-42 bio-hybrid compared to that in the alkaline treated-zein. In addition to the changes in these bands, perturbation in the ν_{N-H} vibration mode of amide A in the protein is also evidenced, appearing in the bio-hybrids at higher

wavenumber. This shift is likely attributed to interactions of those groups with water molecules located in the interlayer region, which are reported as important adsorption sites on smectite clays (Ruiz-Hitzty et al., 2004). Unfortunately, a detailed analysis of the water band at 1643 cm^{-1}, ascribed to $\delta_{H\text{-}O\text{-}H}$ vibration of water molecules in the bio-hybrids, is very difficult, since this band appears completely overlapped with the amide I and II bands of the zein.

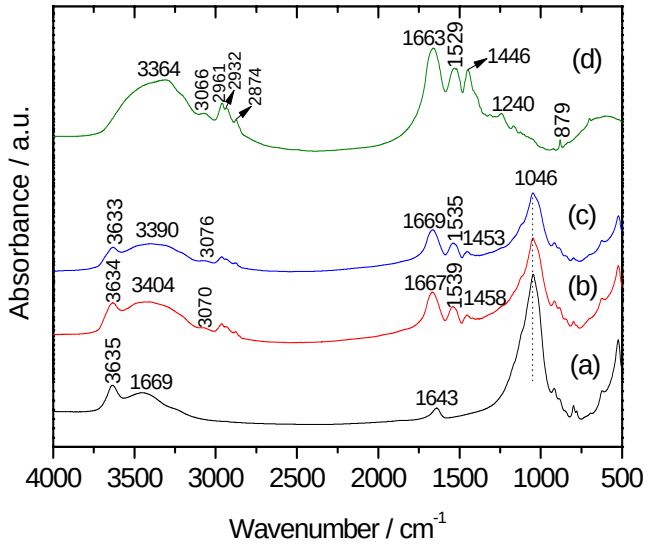

Figure 3.27 FTIR spectra in the 4000-500 cm^{-1} region of the (a) CloisNa treated with 0.1 M NaOH, (b) Z-CloisNa_S3-42, (c) Z-CloisNa_S3-57 and (d) zein recovered after treatment in 0.1 M NaOH.

^{13}C CP MAS NMR studies were also applied to characterize the Z-CloisNa_S3 bio-hybrid. Although the spectrum of the Z-CloisNa_S3-57 sample (Figure 3.28 b) shows very poor signal to noise ratio, it is possible to appreciate several peaks than are observed in the starting zein treated in alkaline medium (Figure 3.28 a.). In addition, it seems evident the presence of a new signal as a shoulder at 170.3 ppm in the bio-hybrid spectrum (Figure 3.28 b), which is assigned to the carbonyls groups, and suggests the existence of strong interaction of the alkaline-treated protein with the CloisNa.

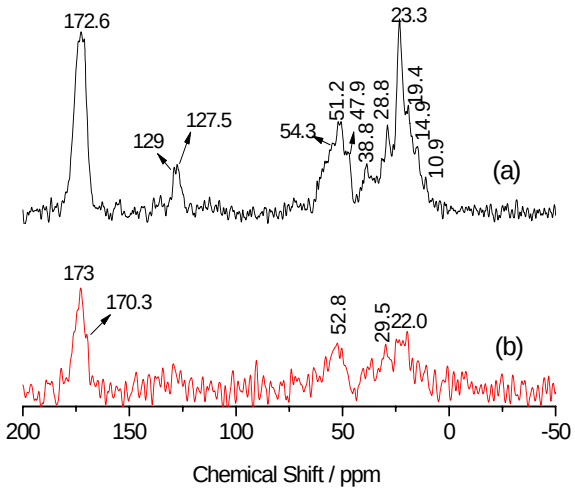

Figure 3.28 ^{13}C CP MAS NMR of the (a) zein after treatment in 0.1 M NaOH and (b) Z-CloisNa_S3-57 bio-hybrid.

FE-SEM images of Z-CloisNa_S3-42 (Figure 3.29 a, b) and Z-CloisNa_S2-57 (Figure 3.29 c, d) bio-hybrids reveal a very similar texture in both samples. As occurs in other bio-hybrids reported in this study, their morphology resembles to that of the layered clay. Zein is homogeneously incorporated in the bio-hybrid without formation of zein agglomerates, as can be seen with more detail in the inset in Figure 3.29 b. TEM images of the Z-CloisNa_S2-52 bio-hybrid (Figure 3.29 a, b), show an organized structure where the expanded lamellae of clay by the protein intercalation can be easily appreciated. The calculated value of the distance between two sheets, taking into account an average of six sheets measured by TEM, was 2.0 nm.

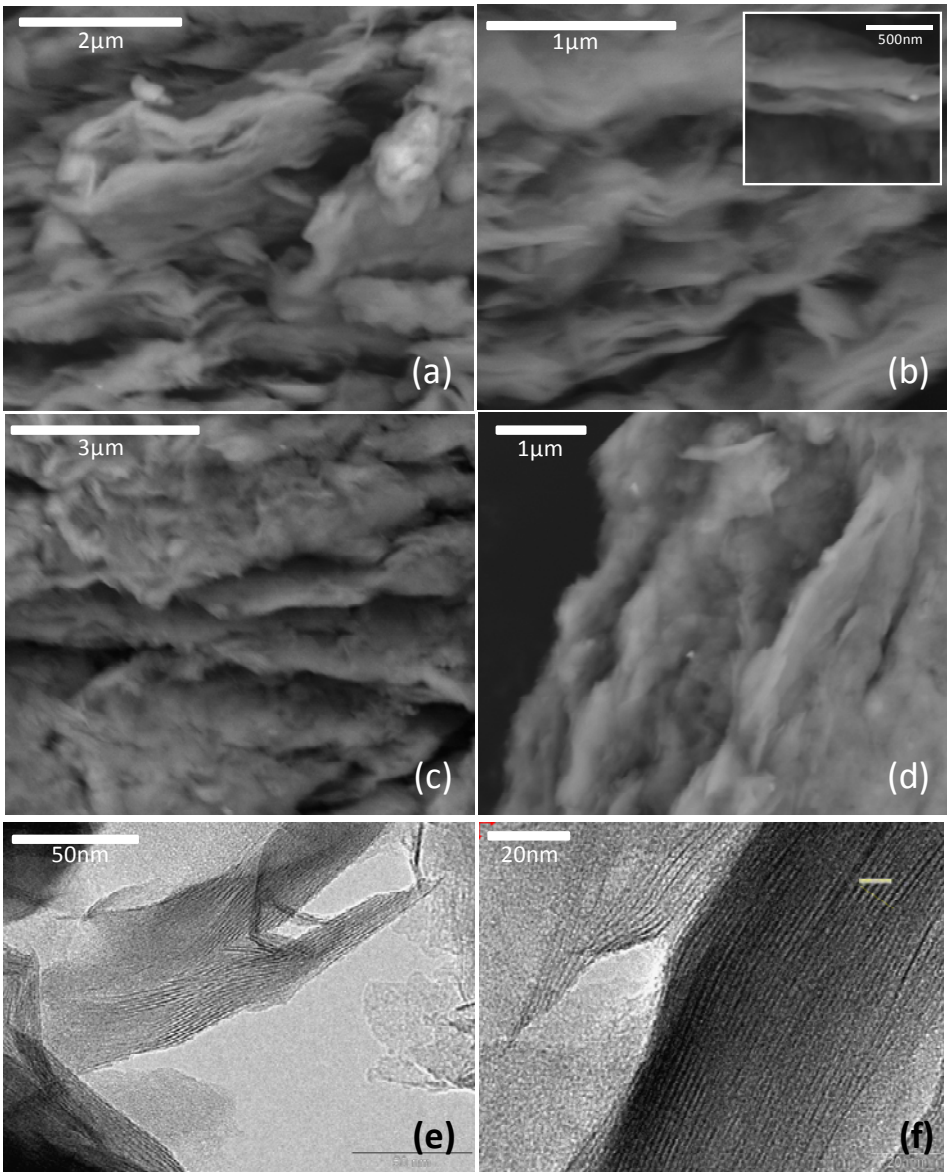

Figure 3.29 FE-SEM images of Z-CloisNa_S3-42 (a, b) and Z-CloisNa_S3-57 (c, d) bio-hybrids. TEM images of Z-CloisNa_S3-52 bio-hybrid (e, f).

3.3 ZEIN-LAYERED CLAYS AS NANOFILLERS IN BIOPOLYMER FILMS

Biopolymers are currently investigated as an alternative to petroleum-based polymers in diverse applications. It is well known that zein protein processed as films results in materials that show barrier properties, although their mechanical properties are inferior compared to those of films based on synthetic polymers such as polyvinyl alcohol (PVA) or polypyrrole, for instance (Nedi et al., 2012). As occurs in conventional polymers, the mechanical properties of biopolymers can be often improved by incorporation of inorganic nanoparticles, giving rise in this case to the so-called

bionanocomposites materials (Ruiz-Hitzky et al., 2010). However, many times it is difficult to achieve compatibility between the biopolymer matrix and the inorganic phase, being often required the addition of plasticizers (e.g. glycerol, sorbitol, olive oil), or other compatibilizing agents to obtain homogeneous systems (Sorrentino et al., 2007). In this sense, it has been reported that hydrophobic polymer matrices, such as zein, present low compatibility with hydrophilic clays, being necessary some previous organic modification of the clay or the addition of a compatibilizer during the synthesis process to achieve the formation of the desired bionanocomposites (Luecha et al., 2010; Nedi et al., 2012; Ozcalik and Tihminlioglu, 2013). However, the use of plasticizers very often results in more hydrophilic materials, with low resistance to moisture and decrease of barrier and mechanical properties. In the same way, the incorporation of organoclays that contains alkylammonium cations could be not convenient due to the toxicity of many of those cations.

Recently, it has been attempted the elaboration of organoclays with intercalated biomolecules, such as lipids, acting as biomodifier agents (Wicklein et al., 2010). The resulting bio-organoclay can be used in the preparation of bionanocomposites improving the compatibility between both components, while keeping the biocompatibility of the material. Besides, the reinforcement effect of these nanofillers may play an additional role incorporating barrier properties (Chivrac et al., 2010; Alcântara et al., 2012).

Taking into account this premises, it was explored the feasibility of zein-layered clays bio-hybrids as bio-organoclays in the preparation of bionanocomposites based on both zein and starch as polymer matrices. In this last case, it is especially relevant to evaluate the possible application of these bio-hybrids without using plasticizers, which may be of great interest for practical purposes. In this study, Z-CloisNa_S2-46 and Z-CloisNa_S3-45 bio-hybrids were tested, each one of quite similar composition, but prepared by different synthetic routes. In order to evaluate the effect of the bio-hybrid concentration in the polymer matrix, bionanocomposites with a loading of 1.25% (w/w) and 3.5% (w/w) in bio-organoclay were prepared following the methodology described in the experimental section (§ 2.3.1, (c)).

- *Appearance and transparency of the bionanocomposite films*

The transparency of the bionanocomposite films was studied in order to evaluate the compatibility of the Z-CloisNa bio-hybrids with zein (Z) and starch (STH) matrices (Figure 3.30). In those cases, zein-based (Z/Z-CloisNa) and starch-based (STH/Z-CloisNa) films were prepared without incorporation of any plasticizer in their composition. For comparison, zein and starch blank films containing only CloisNa clay, named as Z/CloisNa and STH/CloisNa, respectively, were also prepared and characterized (Figure 3.30).

Self-standing zein films that contain the unmodified CloisNa layered clay show great opacity and an inhomogeneous aspect, which points out to a poor compatibility between the clay and the zein matrix, being possible to clearly distinguish spots of the inorganic phase in the film (Figure 3.30 a). This behavior can be explained considering the hydrophilic nature of this clay, and the hydrophobic character of the biopolymer of the biopolymer matrix, which does not favor their mutual miscibility. In contrast, Z/Z-CloisNa_S2 and Z/Z-CloisNa_S3 bionanocomposite films incorporating Z-CloisNa_S2-46 and Z-CloisNa_S3-45 bio-hybrids, respectively, present a higher homogeneity and transparency, independently of the amount of bio-hybrid incorporated in the zein matrix (Figure 3.30 a). These results confirm a good dispersion and homogeneous distribution of the bio-hybrid phase within the zein matrix. The Z/Z-CloisNa_S3-45 bionanocomposite film, prepared with a 3.5% (w/w) loading in Z-CloisNa_S3 bio-hybrid, exhibits a lower transparency and the presence of wrinkles.

Interestingly, in the case of the bionanocomposite based on the starch polysaccharide, all the films appear very homogenous (Figure 3.30 b). Starch films loaded with neat CloisNa, STH/CloisNa, show homogeneity, but at same time they are very brittle, presenting clear fractures. This behaviour is likely due to the absence of plasticizer, which is commonly used in the preparation of starch films in order to increase the mobility of the polymer chains and consequently the flexibility of the resulting material. Conversely, starch films loaded with 1.25 (w/w) of Z-CloisNa_S2 or Z-CloisNa_S3 bio-hybrid materials do not present fractures, which indicates the good compatibility of the bio-hybrid and the polysaccharide matrix. These evidences suggest that Z-CloisNa bio-hybrids could act as bio-organoclays, enhancing the compatibility between the inorganic phase and the organic matrix without the necessity of adding any plasticizer or other compatibilizing agents.

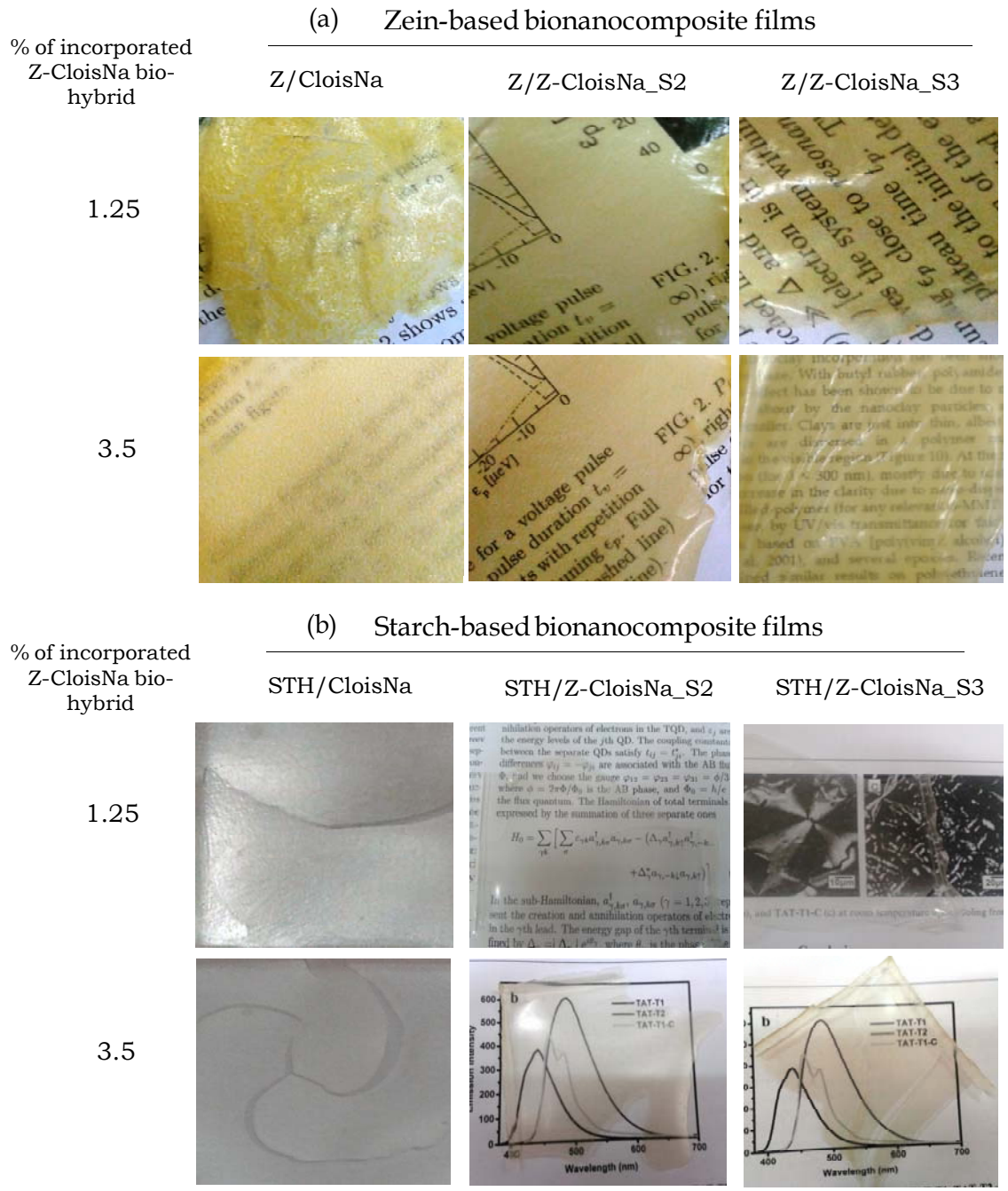

Figure 3.30 Photographs of (a) zein and (b) starch bionanocomposite films.

More insights on the compatibility of these zein bionanocomposite films were obtained from UV-Vis transmittance measurements in a wavelength range between 200 and 800 nm (Figure 3.31). All the films exhibited reduced light transmission in the visible region compared to the zein blank film. However, the transmittance values obtained for these bionanocomposite films were higher than those of zein films loaded with neat

CloisNa. This last material showed very low transmittance in the visible region, which is indicative of low transparency. This behavior is more accused in the case of the film loaded with 3.5% (w/w) of CloisNa in its composition, in which the transmittance reached only a value of around 1.7%, corroborating the opacity of this film (Figure 3.30 a). As previously signaled, this feature may be related to a poor compatibility of the CloisNa clay with the zein matrix, provoking a bad dispersion of the clay particles in the protein matrix. Transmittance values of the zein bionanocomposite films modified with Z-CloisNa_S2 and Z-CloisNa_S3 bio-hybrids decrease in comparison to the blank film as the percentage of the bio-hybrid in the zein matrix increases, presenting the Z/Z-CloisNa_S2 films higher values of transmittance than the Z/Z-CloisNa_S3 films at same concentration of bio-hybrid. Thus, the maximum values of transmittance are observed in films that contain 1.25% (w/w) of bio-hybrid, reaching 75% and 65% for Z/Z-CloisNa_S2-1.25% and Z/Z-CloisNa_S3-1.25% bionanocomposites, respectively. The lowest transmittance value was determined in the Z/Z-CloisNa_S3-3.5% bionanocomposite film, which was the sample with the highest bio-hybrid content (Figure 3.30 a). On the other hand, all starch bionanocomposite films show high transmittance values in the visible region (above 70%), indicating a high degree of transparency, and the lowest values of light transmission are observed for the bionanocomposite films loaded with 3.5% (w/w) of Z-CloisNa bio-hybrids. In contrast to that observed for the zein-based systems, the transparency of starch films loaded with neat CloisNa is quite similar to that of the blank film, indicating that in this case the clay is better dispersed within the starch matrix.

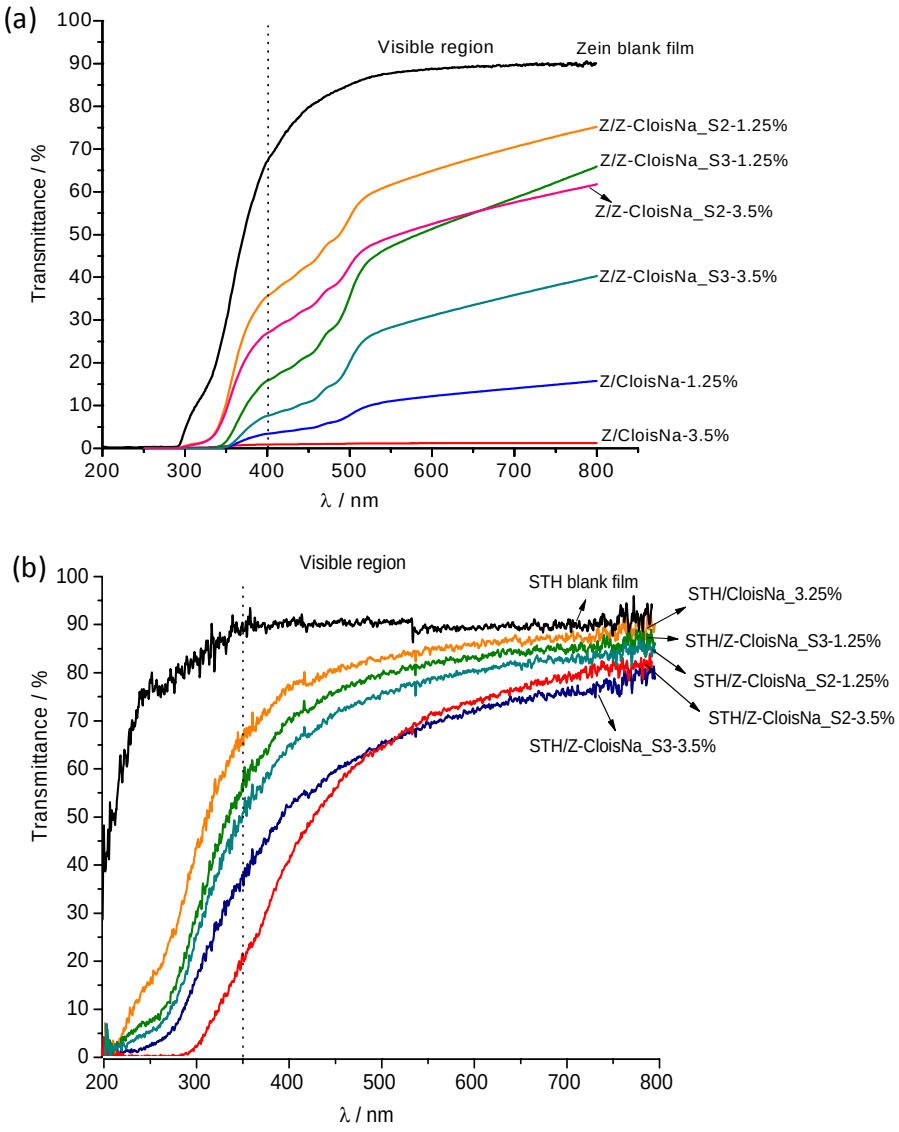

Figure 3.31 Transmittance measurements in the 200-800 nm of (a) and (b) zein bionanocomposite films loaded with 1.25 and 3.5% of CloisNa clay and with Z-CloisNa_S2 and Z-CloisNa_S2 bio-hybrids.

Comparing the FE-SEM images of zein and starch bionanocomposites loaded with 1.25% (w/w) of Z-CloisNa_S2 and Z-CloisNa_S3 bio-hybrids, clear differences can be observed in the morphology, depending on the bio-hybrid incorporated in the protein matrix (Figure 3.32). The Z/Z-CloisNa_S2 bionanocomposite film (Figure 3.32 a) displays a rough texture, with the presence of some pores. In contrast, the presence of the Z-CloisNa_S3 in the zein matrix (Figure 3.32 b), seems to favor a more uniform and compact texture. An analogous behavior was observed in the starch-based bionanocomposite film. In this case, FE-SEM images of STH/Z-CloisNa_S2 (Figure 3.32

c) reveal also a rough texture where the presence of pores can be indentified in the film surface. On the other hand, the STH/Z-CloisNa_S3 bionanocomposite films (Figure 3.32 d) show a homogeneous texture, where the Z-CloisNa_S3 filler seems to be well dispersed in the biopolymer matrix.

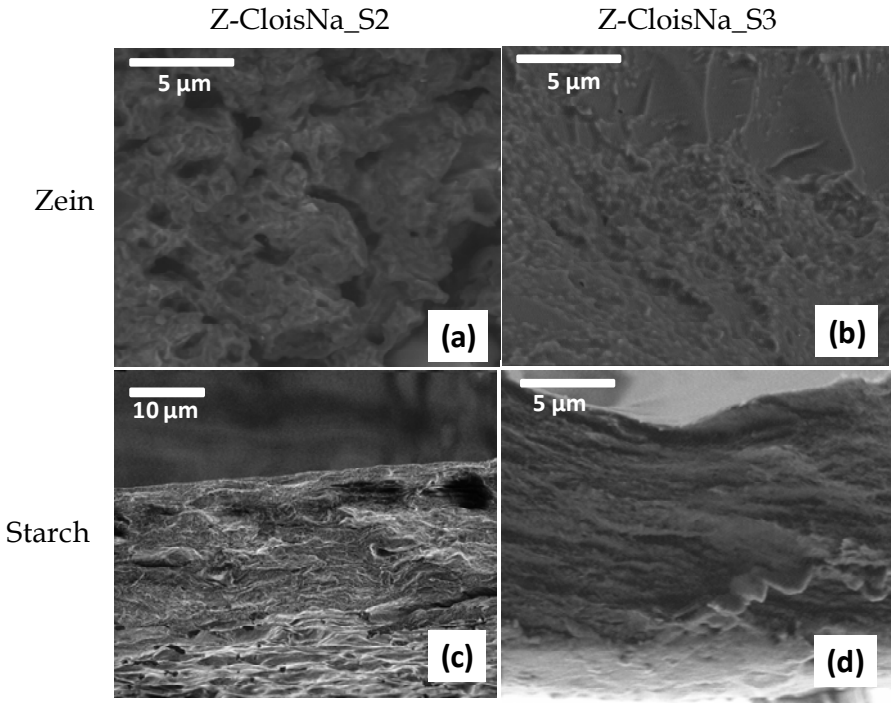

Figure 3.32 FE-SEM images of zein (a and b) and starch (c and d) bionanocomposites films loaded 1.25% (w/w) of Z-CloisNa_S2 and Z-CloisNa_S3 bio-hybrids.

- *Mechanical properties*

Tensile modulus and elongation at break have been used to describe the main mechanical properties of the prepared bionanocomposite films. Tensile modulus (E) indicates the stiffness of the material and is usually measured by a simple tensile test as the slope of the stress-strain curve (elongation curve), while elongation at break (ϵ_B) represents the film capacity for stretching, being easily obtained by equation 4.1 (Radebaugh et al, 1988):

$$\epsilon_B = \left(\frac{extension\ to\ break}{L_0}\right) \cdot 100 \qquad \text{(eq. 4.1)}$$

where L_0 is the original length of the sample between the grips.

Due to the high brittleness of zein and starch films loaded with neat CloisNa, it was not possible to measure the tensile properties of these materials. Although the bionanocomposite films loaded with the Z-CloisNa bio-hybrids show high homogeneity, the films containing 3.5% (w/w) of filler also exhibit great fragility, being not possible to obtain acceptable reproducibility in the traction measurements. Therefore, these bionanocomposites were also excluded from the study of mechanical properties. Similar behavior was observed for pure zein and starch films. These blank films showed high brittleness, which made not possible to measure such properties. However, although this was not exactly the blank of the bionanocomposite system, glycerol was added as plasticizer during the preparation of pure zein and starch films, in order to use them as reference in the mechanical properties studies.

The values of tensile modulus and elongation at break of bionanocomposites with 1.25% (w/w) loading in Z-CloisNa_S2 and Z-CloisNa_S3 are collected in Table 3.6, together with those measured for unloaded zein and starch films. All the bionanocomposite films here measured exhibit higher tensile moduli than those of the pristine biopolymer films, revealing the role of the bio-organoclay as filler increasing the material stiffness. In the case of zein-based bionanocomposite films, the measured modulus is very similar (around 1.2 GPa), independently of the bio-hybrid incorporated in the protein matrix. These Young´s modulus values increase about 2.5 times compared to those of the unmodified film of zein, being analogous to those reported by Nedi et al. (Nedi et al., 2012.) in thermoplastic zein films modified with 5wt% of CloisNa and using poly(ethylene glycol) as plasticizer (25 wt% to respect to polymer). These results clearly indicate that Z-CloisNa as bio-organoclay has a role as reinforcing additive in the zein bionanocomposite films, improving the mechanical properties even at low loading and without the addition of any plasticizer. These behaviors may be probably due to the good compatibility of the zein-CloisNa hybrid particles and the biopolymer matrix.

Similar results on the increase of the tensile modulus have been also observed in the case of starch bionanocomposite films, where the values observed were around twice those of the pristine starch film. According to the literature, these values are slightly higher than those reported by Chivrac and co-authors, in which a sodium

montmorillonite modified with cationic starch is used as filler of thermoplastic starch matrices (Chivrac et al., 2010). These high values here observed can be related to the use of only Z-CloisNa bio-organoclays, while in the work reported by Chivrac, diverse kind of plasticizers (glycerol, sorbitol and Polysorb®) that commonly decrease the Young´s modulus were also used. In contrast to the zein-based films, the positive effect of zein-based fillers on the starch biopolymer cannot be attributed to the compatibility between both systems, but it could be possibly due to their plasticizing effect.

Concerning the elongation at break values of the bionanocomposites, a decrease is observed with respect to the value measured for the neat zein and starch films, which are 3.10% and 10.70%, respectively. This result indicates a reduction in the plastic behavior of the bionanocomposite samples. This result was expected since in the biopolymer blank films here studied, glycerol was added as plasticizer to overcome the impossibility of prepare neat films due to their great brittleness, as above commented. Actually, it is well known the role of the plasticizer for improving plastic behavior, which results in increasing flexibility and stretchability of the biopolymer matrix, and subsequently in the elongation at break percentage. In the bionanocomposite films, the observed behavior can be attributed to the reduced mobility of the zein and starch chains after the incorporation of the bio-hybrids, as it has been also observed in other clay-reinforced polymer nanocomposites (Alexandre and Dubois2000).

Table 3.6 Tensile properties of the zein and starch bionanocomposite films loaded with 1.25% of Z-CloisNa_S2 and Z-CloisNa_S3 bio-hybrids. Zein and starch blank films were prepared from 80:20 (w/w) biopolymer:glycerol.

Film samples	E (GPa)	ϵ_B (%)
Zein film blank	0.47 ±0.11	3.10 ±0.73
Z/Z-CloisNa_S2	1.20 ±0.17	1.98 ±0.53
Z/Z-CloisNa_S3	1.26 ±0.09	2.01 ±0.26
Starch film blank	0.20 ±0.09	10.70 ±1.02
STH/Z-CloisNa_S2	0.49 ±0.15	1.98±0.04
STH /Z-CloisNa_S3	0.58 ±0.10	1.03±0.12

Despite this application of zein-based bio-hybrids is still in its beginnings, and some properties should be optimized, it was demonstrated that Z-CloisNa bio-hybrids reported in this Thesis can be used as nanofillers in the preparation of films, improving the compatibility, homogeneity and mechanical properties of films based on zein and starch biopolymers, here selected as examples, without the need of adding any compatibilizer or plasticizer.

3.4 Concluding remarks

This Chapter reported results on the intercalation of zein protein in layered clays, in the present case montmorillonite. In this study, montmorillonite containing Na ions or quaternary alkylammonium cations in the interlayer region was used. By different strategies of synthesis and the use of several techniques, it was possible to investigate the zein intercalation mechanism into montmorillonite, as well as the structure and properties of the resulting zein–montmorillonite bio-hybrids. It was deduced that the intercalation processes, as well as the cation located in the interlayer region of the clay, are strongly influenced by the solvent used for zein solubilization. The obtained bio-hybrids were evaluated as bio-organoclays for incorporation in zein and starch biopolymer films, avoiding the addition of compatibilizers or plasticizers. The resulting bionanocomposite films loaded with zein-based bio-hybrids exhibited good compatibility, homogeneity and mechanical properties. These introduced results point out that these new bio-hybrid materials prepared from different approaches could be associated with other polymers of different nature, being a promising ecological alternative to common organoclays based on alkyl ammonium cations, increasing the possibilities of research and applications in this innovative field.

CHAPTER 4

ZEIN-FIBROUS CLAYS BIO-HYBRIDS

This Chapter is devoted to the study of a new type of bio-hybrid materials based on the combination of fibrous clays (sepiolite or palygorskite) with zein, a hydrophobic protein extracted from corn. Several characterization techniques were used in order to discern the type of interaction between the protein and the clay fibers and to evaluate the reduced hydrophilic character of the novel bio-hybrids in comparison to the pristine clays. With the aim of showing that such property is relevant, zein-fibrous clay bio-hybrids were tested as additives (bio-organoclays) in the preparation of bionanocomposites for food packaging use, as an example of potential application, using alginate polysaccharide as a model polymer matrix. The mechanical and barrier properties of bionanocomposites films loaded with zein-clay bio-hybrids were investigated.

4.1 INITIAL CONSIDERATIONS

The possibility of modification of clay minerals with diverse organic compounds affords the preparation of a wide variety of hybrid materials provided with the desired properties (Ruiz-Hitzky et al., 2004; Ruiz-Hitzky et al., 2008; Ruiz-Hitzky et al., 2010). Amongst clay-based hybrids, the term organoclays has been mainly applied to those hybrids based on the incorporation of alkylammonium organic cations through ion-exchange reactions, which show hydrophobic behavior (Ruiz-Hitzky et al., 2010) Applications of such materials include uses as rheological additives in the manufacture of lubricating greases and paints, adsorption of low hydrophilic pollutants and more recently nanofillers in polymer-based nanocomposites. One of the major concerns for the use of this type of organoclays in certain applications, as for instance as fillers in plastics for food packaging, is related to the presence of alkylammonium surfactants that may show toxicity. Thus, preparation of bio-organoclays, in which the organophilic counterpart was of biological origin, is a new alternative for developing new clay hybrids for that and other applications. Recently, it has been reported that the association of phospholipids to layered (smectites) and fibrous (sepiolite) clay minerals gives rise to a family of bio-organoclays able to be employed in the removal of mycotoxins (Wickein et al., 2010) or the immobilization of certain enzymes (Wicklein, et al., 2011). In this way, the search of new clay-based bio-hybrids seems a promising line of research in view to replace common organoclays for certain of their present uses but also in the search of new applications.

Hence, analogously to organoclays based on layered silicates, clay minerals of fibrous morphology, such as sepiolite or palygorskite have been also employed to prepare organoclays for different applications (Ruiz-Hitzky et al., 2011). In this case, as these clays do not exhibit intercalation properties, macromolecules of biological origin, such as structural or functional proteins, interact directly with the external surface of the silicate (Olmo et al., 1987; Fernandes et al., 2009; Caballero et al., 2009; Fernandes, et al al., 2011), giving rise to bio-hybrid materials that could be used as bio-organoclays.

In this perspective, it is proposed in this Chapter the development of new bio-hybrid materials based on the assembly of the hydrophobic zein protein to sepiolite and palygorskite fibrous clays, in order to reduce the hydrophilic character of these clays. Since zein can act as barrier to moisture and oxygen due to its strong hydrophobicity (Takahashi et al., 1996.; Bai et al., 2003; Padua et al., 2004; Gáspár et al., 2005;

Ghanbarzadeh and Oromiehi, 2008), these interesting properties may be profited to reduce the hydrophilic character of pristine clays, as happens in the case of conventional organoclays based on long-chain alkylammonium cations. In order to evaluate the improved hydrophobic properties of zein-fibrous clay bio-organoclays, these bio-hybrids were employed as filler in biopolymer matrices, in which the polysaccharide alginate was chosen as polymer matrix. Thus, the first part of this Chapter is focused on the characterization of these bio-organoclays and afterwards, a detailed study about the properties of zein-fibrous clay bio-organoclay as filler in alginate matrix is discussed.

4.2 CHARACTERIZATION OF ZEIN-FIBROUS CLAYS BIO-HYBRIDS

Zein-clay bio-hybrid materials were prepared by direct adsorption of the protein on the sepiolite and palygorskite fibrous silicates, according to the procedure described in Chapter 2, section 2.3.2. The knowledge of the affinity between zein and clays is fundamental for the preparation of the bio-hybrid material and their use as bio-organoclays. Figure 4.1 shows the adsorption isotherms (23^{o}C) of zein in sepiolite and palygorskite from ethanol/aqueous solutions (80% v/v). In both cases, the adsorption isotherms show a sharp slope at low equilibrium concentration values fitting to a H-type isotherm, a special case of the L-type curve according to the Giles classification of isotherms (Giles et al., 1960). This behaviour is indicative of a high affinity between the sepiolite and palygorskite substrates and the zein adsorbate. Both curves reach a plateau corresponding to values of 25.0 g and 14.7 g of zein per 100 g of sepiolite and palygorskite, respectively. Taking into account that zein structure is a compact rectangular prism with dimensions of 16 x 4.6 x 1.2 nm^3 (Matsushima et al., 1997), it is expected that the adsorption process takes place only at the external surface of fibrous clays and not inside the nanosized tunnels of the fibres. Thus, the corresponding plateau values suggest a complete coverage of the silicate surface in both clays with by zein. It has been observed that for equilibrium concentrations higher than 3 g/L, the adsorbed zein amounts are greater than the values in the plateau. This behaviour may be related to the formation of molecular aggregates of zein in solution, as discussed in Chapter 3 (§ 3.2.1), which could be directly adsorbed on the silicate surface.

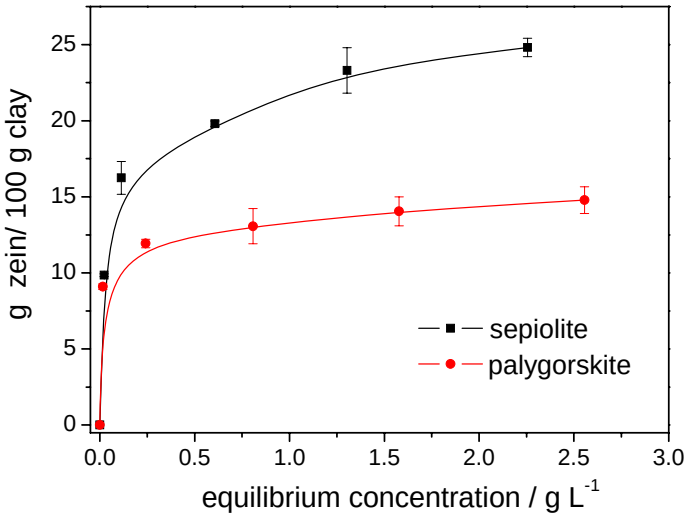

Figure 4.1 Adsorption isotherms at 23ºC of zein from ethanol/water (80% v/v) solution on sepiolite and palygorskite. Adsorption amounts were deduced from CHNS chemical analyses of the bio-hybrid solids.

Table 4.1 summarizes the zein-sepiolite and zein-palygorskite bio-hybrids prepared in this Thesis, including the initial amounts of zein employed in their synthesis as well as the respective amount of adsorbed protein on each one. The code number assigned to each sample indicates the approximate content of zein in grams per 100 grams of inorganic solid. Comparing the values in Table 4.1, it is clearly observed that at equal initial concentrations of zein, the amount of retained protein is greater when the substrate is sepiolite. This result can be explained by the higher specific surface area of this clay mineral compared with palygorskite, providing a larger specific area for the protein adsorption. Samples prepared from solutions with very high zein content result in bio-hybrid materials with adsorbed zein that may exceed 50.0 g and 28.0 g in sepiolite and palygorskite, respectively. These values are considerably higher than those corresponding to the plateau in the adsorption isotherms. This fact can be attributed not only to the coverage of the clays surface by several layers of protein, but also to the formation of molecular aggregates in solution at high concentrations of zein, which is a characteristic ability of this protein (Kim and Xu, 2008), that may be directly adsorbed on the silicate surface, or to the existence of more complex processes related to formation of zein microphases in ethanol-water media (Wang and Padua et al., 2010).

Table 4.1 Zein-sepiolite and zein-palygorskite bio-organoclays prepared in this work by adsorption of zein from ethanol/water (80% v/v) solutions containing different initial amounts of zein.

starting amounts (g zein /100 g clay)	zein-sepiolite bio-hybrids codes	zein content (g zein /100 g SEP)*	zein-palygorskite bio-hybrids codes	zein content (g of zein /100g PALY)*
10.0	Z-SEP10	9.85	Z-PALY9	9.30
20.0	Z-SEP16	16.31	Z-PALY12	11.93
40.0	Z-SEP20	19.74	Z- PALY13	13.07
66.6	Z-SEP24	23.53	Z- PALY14	14.05
100.0	Z-SEP25	25.02	Z- PALY15	14.78
166.0	Z-SEP29	29.21	Z- PALY18	17.80
333.3	Z-SEP54	53.59	Z- PALY21	20.80
500.0	Z-SEP48	47.88	Z- PALY28	28.40

* Data are the average value from n = 3 CHNS chemical microanalyses of the bio-hybrid solids.

Taking into account that a large part of the clay surface may be covered by the protein (according to the adsorption isotherms deduced from CHNS analysis), the N_2 adsorption-desorption technique was carried out in some bio-hybrids in order to determine their specific surface area (BET). The BET values of these zein-fibrous clays bio-hybrids materials are listed in the Table 4.2. The starting clays show a specific surface area of 340 and 186 m^2/g for sepiolite and palygorskite, respectively. However, a considerably reduction of the specific surface in the bio-hybrid materials is evidenced, most likely due to the protein adsorption, reaching values as low as 22 and 19 m^2g^{-1} for the bio-hybrids Z-SEP48 and Z-PALY28, respectively, which have the highest zein content. Given that both clays exhibit structural micropores whose dimensions are only accessible to small molecules (like the N_2 used in the specific surface area measurements), adsorption of the voluminous zein polypeptide chains inside the tunnels of these clays is not possible and so it could only take place on the external accessible surface of the clay (150 $m^2\ g^{-1}$ in sepiolite and 120 $m^2\ g^{-1}$ in palygorskite). Although they are not able to penetrate in the nanosized tunnels, the important decrease in specific surface area of the bio-hybrids with respect to that of the starting clay minerals confirms that the protein molecules are blocking the access of

nitrogen to the nanopores during the BET measurements, but without entering then. The decrease in the specific surface area values as zein content increases points out to the agglomeration of the particles by the action of this biopolymer.

Table 4.2 Specific surface area (BET) of the zein-sepiolite and zein-palygorskite bio-hybrids.

Samples		Specific surface area (m^2g^{-1})
Sepiolite		340
zein-sepiolite bio-hybrids	Z-SEP 16	147
	Z-SEP 24	47
	Z-SEP 48	22
palygorskite		186
zein-palygorskite bio-hybrids	Z-PALY 12	79
	Z-PALY 15	36
	Z-PALY 28	19

The infrared spectroscopy technique was a useful tool that provided information about the interactions between the zein with the silicates surface. The FTIR spectra of the starting components, zein, sepiolite and palygorskite, together with those of the corresponding bio-hybrids are included in Figure 4.2. The spectrum of zein in the 4000-250 cm^{-1} range (Appendix B – Figure B.1) presents the characteristic bands of proteins at 3308, 1658, 1538 cm^{-1}, which are assigned to the NH stretching vibration mode of the so-called amide A groups, the ν_{CO} vibrations of C=O of amide I and the ν_{CN} of C-N-H bond of amide II from the peptide groups, respectively. These bands are associated with the presence of zein predominantly in the α-helix structure (Forato et al., 2003). In the same spectrum, the stretching vibration bands in the 2950-2850 cm^{-1} range assigned to CH groups can be also distinguished. The spectra of the pristine sepiolite and palygorskite clays, also shown in the Appendix B – Figure B.1, present the characteristic bands of these silicates, including the broad band around 3600 cm^{-1} assigned to the stretching vibrations (ν_{OH}) of zeolitic water, and a group of bands around 1630 to 1615 cm^{-1} attributed to the bending vibrations (δ_{HOH}) of coordinated water molecules.

In the IR spectra of the zein-fibrous clays bio-hybrids (Figure 4.2), the amide I band of zein is observed at 1658 cm^{-1}, being more evident with the increasing of the amount of

zein adsorbed on clays. This band seems to be overlapped with the characteristic bands of the bending vibration modes of water in sepiolite and palygorskite from 1658 to 1615 cm^{-1}, making the interpretation of a possible interaction of amide groups of zein and hydroxyl groups in the clays very difficult. In addition, the band related to other characteristic group of the protein, is clearly defined in this spectra, such as the amide II band at approximately 1538 cm^{-1}. Special attention should be given to those bands that appearing at 3720 cm^{-1} and 3710 cm^{-1} in pristine sepiolite and palygorskite clays, respectively, which are assigned to the OH stretching vibrations of silanol groups (Si-OH) located at the external surface of the silicates (Figure 4.3 a). Perturbations in the OH stretching vibrations of silanol groups is often used to prove the existence of interactions between adsorbed organic or biological species and the sepiolite surface (Aranda et al., 2008; Wicklein et al., 2010). Thus, focusing in the 3750 – 3650 cm^{-1} wavenumber range (Figure 4.2 a), it is possible to observe in the IR spectra of oriented films of the Z-SEP14 and Z-SEP48 bio-hybrids a strong perturbation in the intensity of the band assigned to the OH stretching vibration of the silanol group ($\nu_{Si\text{-}OH}$), becoming this band practically unappreciable. A possible explanation for this observation is the strong interaction through hydrogen bonding between the freely accessible zein groups and the hydroxyl groups of the silicate surface producing a shift towards lower frequencies values (Ahlrichs et al., 1975; Darder et al., 2006). Similar results were observed for Z-PALY12 and Z-PALY14 bio-hybrids (Figure 4.3 a), where it is possible to appreciate the perturbation in the 3710 cm^{-1} band, assigned to the OH stretching vibration of the silanol groups in the natural palygorskite. On the other hand, in both bio-hybrids based on fibrous clays, the band characteristic of OH stretching vibrations of Mg-OH that appears at 3680 cm^{-1} in sepiolite and at 3698 cm^{-1} in palygorskite (Figure 4.3 a), remains unaltered even at high amounts of adsorbed zein. This behaviour is related to the presence of these groups located inside the talc-like structural blocks of both fibrous clays (Galán and Singer, 2011), thus becoming inaccessible to the adsorbed species. Once known that the principal interaction point between the protein and the fibrous clays takes place through of Si-OH groups located at the external surface of clays, it is possible to evaluate the degree of coverage of the silicate surface by zein with the decrease of the bands intensity at 3720 cm^{-1} and 3710 cm^{-1} in the sepiolite and palygorskite, respectively. These results can be better observed in Figure 4.3 b, which shows the variation of the relative intensity of these silanol bands with respect to those unaltered Mg-OH vibration band as a function of the amount of adsorbed protein. It is

possible to observe in Figure 4.3 b that the relative intensity of the two bands decreases as the coverage of the silicates surfaces with adsorbed zein increases, till the content of zein is approximately 23.5 g zein/100g sepiolite and 14.8 g of zein/100g palygorskite, respectively, which was the point where all the external surface is covered by zein in each silicate.

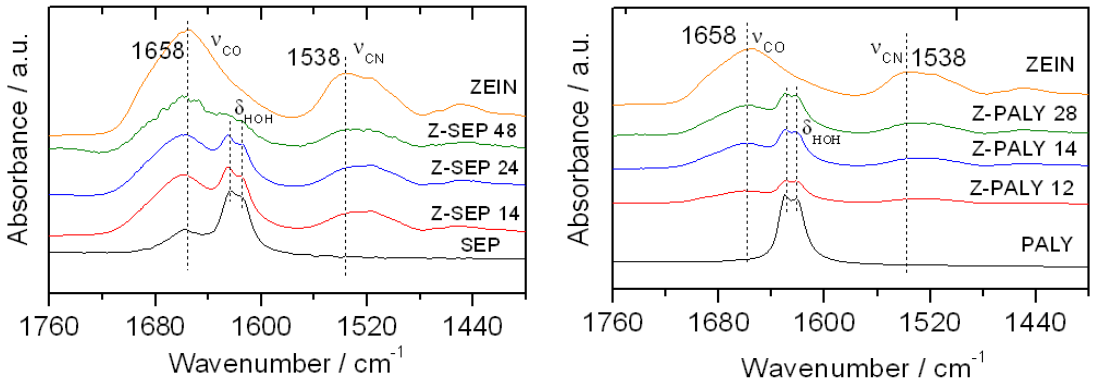

Figure 4.2 (a) IR spectra in the 1760-1400 cm^{-1} region of zein, pristine clays and various bio-hybrids.

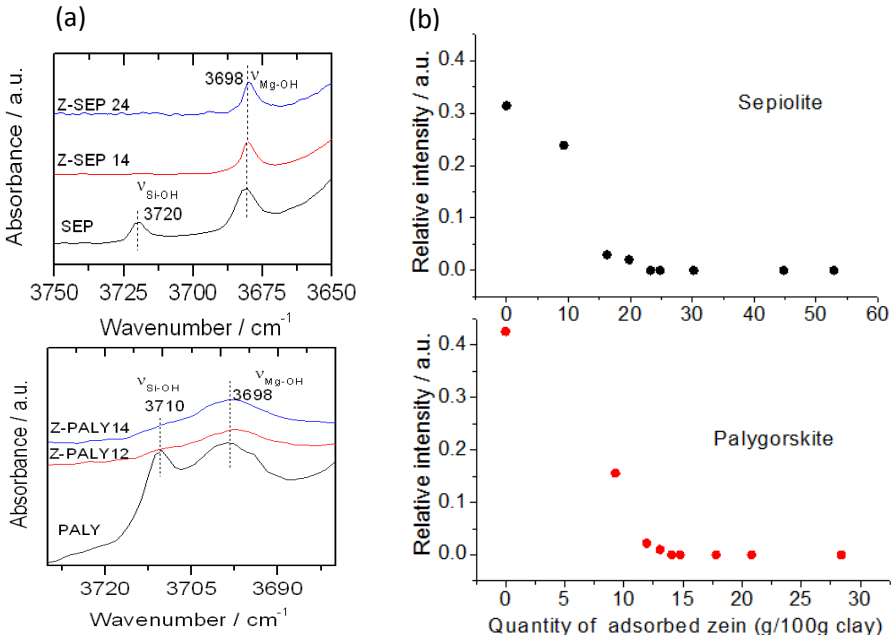

Figure 4.3 (a) IR spectra in the wavenumber range of the OH stretching vibration of the Si-OH and Mg-OH groups in the neat clays and two bio-hybrids based on each fibrous clay.
(b) Relative intensity of the OH stretching vibration bands attributed to Si-OH groups with respect to those of Mg-OH groups as a function of the quantity of adsorbed zein in bio-hybrids based on sepiolite and palygorskite.

High resolution solid–state NMR spectroscopy was applied in order to investigate the molecular interaction between the protein and the fibrous clays. The ^{13}C-NMR spectra of zein and selected samples of zein-sepiolite are presented in Figure 4.4. In the ^{13}C-NMR spectra of zein-sepiolite samples, the intensity of the characteristic signals of zein increase with the coverage of the silicate surface by protein. Thus, the spectra of the hybrid compounds Z-SEP16 and Z-SEP24 (Figure 4.4 a) still show a very poor signal to noise ratio on account of their carbon content, which is in accordance to the results of elemental chemical analysis of these compounds (7.4 and 9.9 % of C, respectively). Despite this difficulty, from the spectra of the bio-hybrids deconvoluted in Figure 3.3b, it is possible to evidence a small shift of the 174 ppm signal to lower ppm, suggesting the existence of interaction of zein with the silanols groups. This effect is more accused for the bio-hybrids with lower content in zein. In the spectrum of sample Z-SEP24 (Figure 4.4 a) a signal at 163 ppm is also observed, which can be also related to the presence of perturbed carbonyl groups. In contrast, the Z-SEP48 bio-hybrid sample with high content of adsorbed zein (Figure 4.4 a), presents a spectrum more similar that of the starting zein, indicating that a large part of the macromolecules are not interacting with the silicate surface. The deconvolution of its spectrum shows the presence of a shoulder in the 172 ppm signal (Figure 4.4 b) as well as of a new peak at 29 ppm (Figure 4.4 c). This latter evidence could to be associated with the existence of interactions between the protein and the silicate. A similar effect cannot be deduced for other samples due to the low resolution of their spectra in this region.

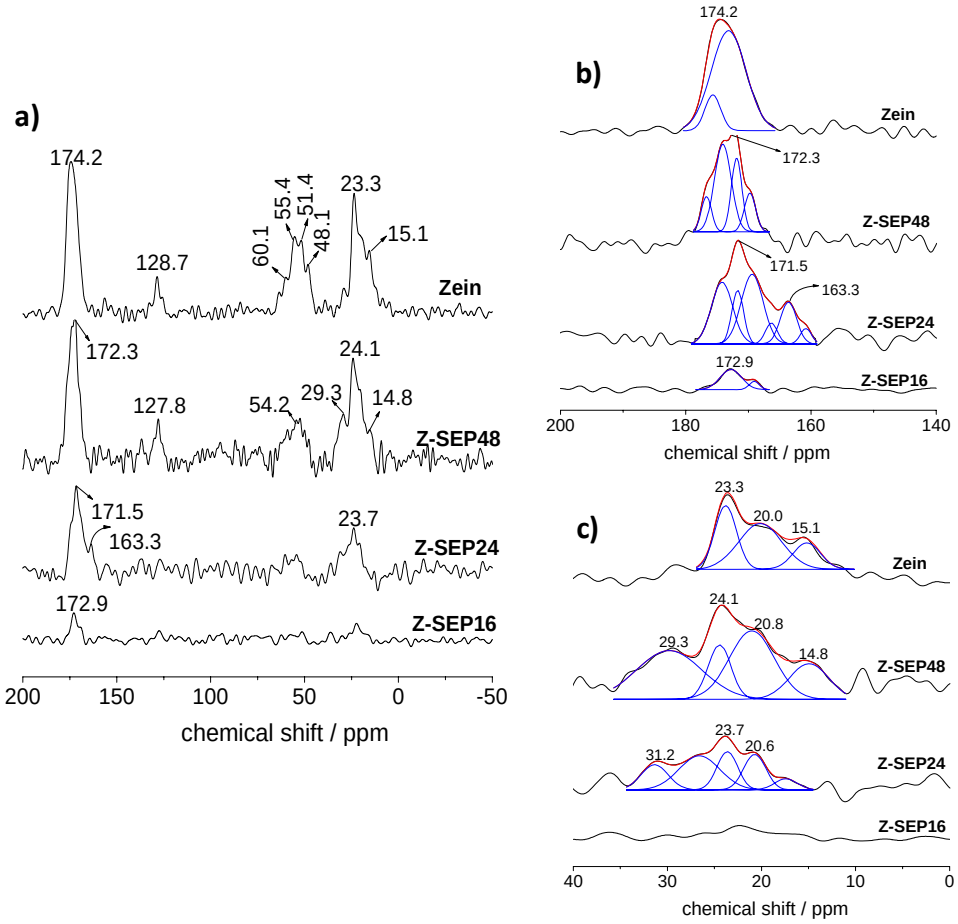

Figure 4.4 (a) ^{13}C CP/MAS NMR spectra of pure zein, Z-SEP48, Z-SEP24 and Z-SEP16. Deconvolution details of those ^{13}C NMR spectra in the (b) 200-140 and (c) 40-0 ppm range.

The morphology of prepared bio-hybrids was investigated by FE-SEM technique, which allowed to observe the textural differences in the bio-hybrids compared to the starting zein. This latter shows the presence of globular aggregates, which result from the strong zein-zein and zein-solvent interactions during the drying process, leading to the formation of those stable aggregates, already discussed in the Chapter 3, § 3.2.1.

In contrast, in the hybrid materials it is not possible to distinguish the presence of such type of protein agglomerates (Figures 4.5 a and b). In bio-hybrids based on both type of clays, the silicate fibers appear to be well integrated inside the structure of the zein, making difficult the protein-protein interaction which is the cause of formation of the aggregates. Therefore, this observation points out to the existence of a considerable interaction between the clay fibers and the protein, as already deduced by FTIR and NMR spectroscopic results. However, a careful analysis of the FE-SEM images of Z-SEP54 with the highest zein content (Figure 4.5 c and d), reveals the presence of small

spheres that could be attributed to the presence of segregated particles of this protein. This observation points out to the existence of zein-zein interaction that stabilizes increasing amounts of zein on clays, as 53.59 g zein/100g sepiolite, presented in Table 4.1. The TEM image of the same sample, presented as insert in the Figure 4.5 c, corroborates the presence of these small zein aggregates in the bio-hybrid that contain high amounts of the protein.

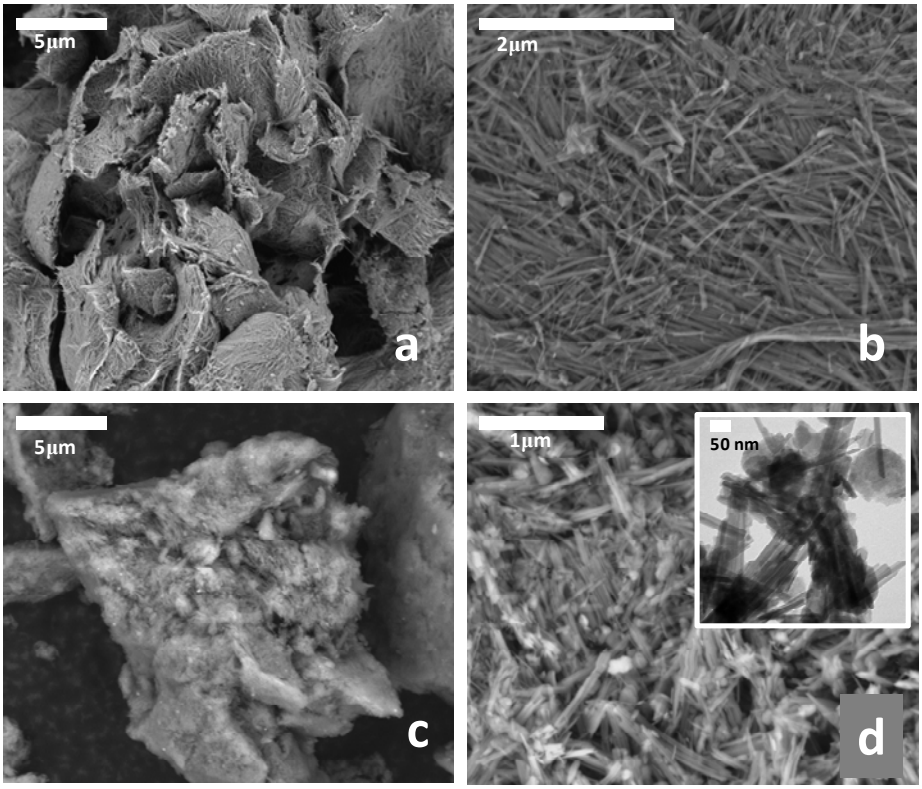

Figure 4.5 FE-SEM images of Z-PALY28 (a and b) and Z-SEP54 (c and d).bio-hybrids. Insert in the image (d) shows the TEM image of Z-SEP54.

The interactions occurring between zein and fibrous clays seem to have an important role in the thermal properties of the resulting bio-hybrid materials. Thermal properties of zein-clay hybrids were evaluated by TG-DTA and are presented in Figure 4.6. Zein shows the weight loss of about 6% below 90ºC, corresponding to physisorbed water molecules and is stable till ca. 500ºC (Appendix B – Figure B.2). When the protein is associated with clay fibers there are considerable changes in the TG and DTA curves. Analogous thermal profiles for all the bio-hybrid samples were evidenced independently of the inorganic substrate employed, showing a good stability up to 300 ºC, when polymer degradation starts (Figure 4.6 a-d). A tendency to develop

exothermic effects is more accused for the Z-SEP and Z-PALY bio-hybrid material with higher zein amounts adsorbed on the clay surface (Figure 4.6 c and d). Such differences may be attributed to the different aggregations of zein, which could result in the existence of the different steps for the thermal decomposition. The observed decrease in the thermal stability of zein in the bio-hybrids compared to the starting protein can be associated with the interactions between the zein and the fibrous clays that makes easier the oxidation of the protein. In the bio-hybrids based on sepiolite, a peak around 830ºC is observed, corresponding to the dehydroxilation of the silicate that changes into protoenstatite (Fernandes, et al., 2011).

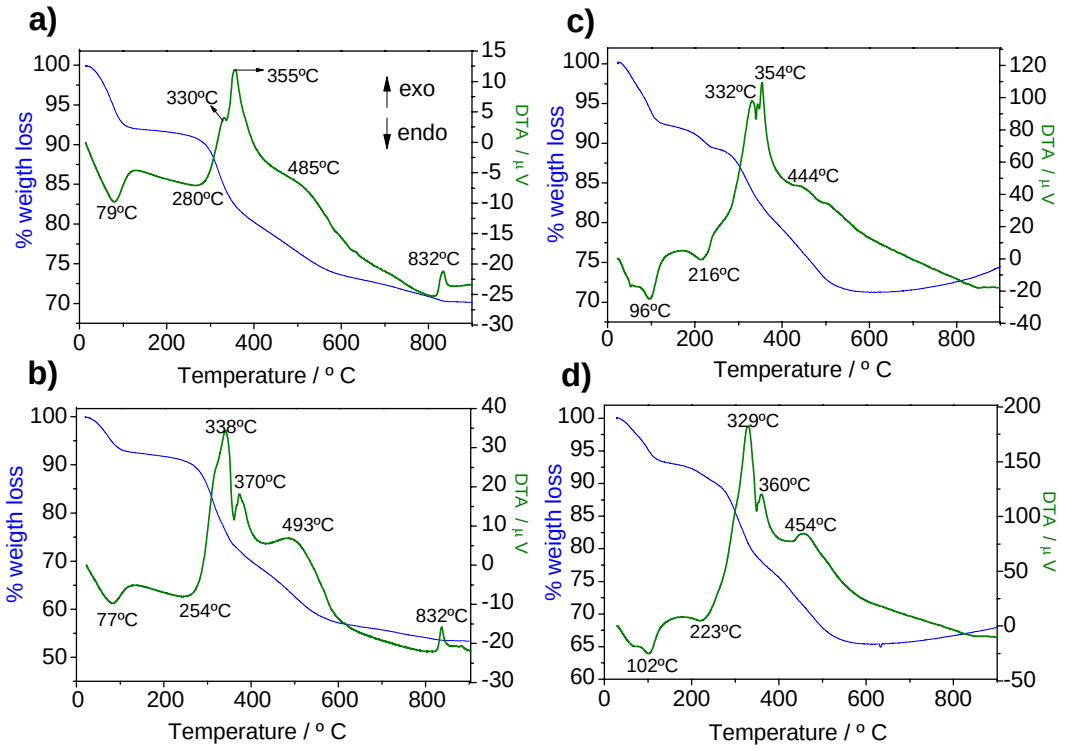

Figure 4.6 TG and DTA curves recorded in air flow conditions for Z-SEP24 (a), Z-SEP48 (b) zein-sepiolite bio-hybrids and Z-PALY14 (c) and Z-PALY28 (d) zein-palygorskite samples. Samples performed in air atmosphere.

Considering that zein is a hydrophobic protein, and that this feature may have some effect on the bio-hybrid, the water sorption properties of the resulting materials were investigated by means of an equipment which records the weight change in the sample with increasing relative humidity. In such measurements, it is remarkable that the assembly of zein to the pristine clay reduces the hydrophilic character of the silicates

(Figure 4.7), although in less extent as would be expected considering the significant hydrophobicity of this protein. The moisture sorption isotherms obtained at 25 ºC for the pure zein, pristine sepiolite and their respective bio-hybrids are classified in type II S-shaped or sigmoid isotherms (Bell and Labuza, (2000), which show three well-defined regions: the Langmuir sorption at low water activity (a_w), which reaches a plateau of concentration corresponding to the saturation of the specific sites of sorption; then, a linear increase of adsorbed water as a function of a_w according to Henry's law; and finally, an exponential increase corresponding to water aggregation or clustering at high a_w (Gouanvé et al., 2007).

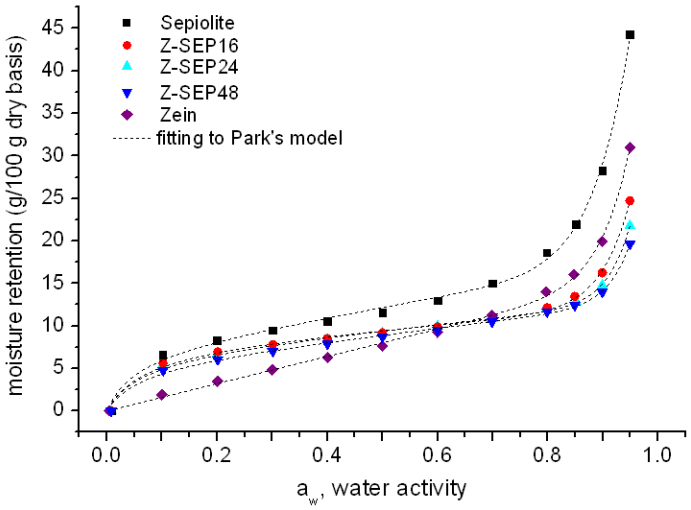

Figure 4.7 Moisture sorption isotherms obtained at 25ºC of pristine sepiolite, zein protein and different Z-SEP bio-hybrids showing the fitting of the experimental data to Park's model (dotted lines).

As shown in Figure 4.7, the experimental data for all the measured samples can be well fitted to the model of Park (eq. 5.1), which takes into account these coexisting sorption modes.

$$y = \left(\frac{A_L\ b_L\ x}{1+ b_L\ x}\right) + K_H\ x + K_a\ x^n \qquad \text{(eq. 5.1)}$$

where A_L is the Langmuir capacity constant, b_L the Langmuir affinity constant, K_H the Henry's solubility coefficient, K_a the equilibrium constant for the clustering reaction, and n the average number of water molecules per cluster (Bessadok et al, 2009). The fitting parameters are summarized in Table 4.3. Focusing on the Langmuir sorption

region, the decrease of A_L as the amount of associated zein increases in the bio-hybrids indicates a lower amount of adsorbed water with respect to pristine sepiolite due to the reduction of sites for water sorption. This fact is also supported by the analysis of the experimental kinetics data (Figure 4.8). The sorption kinetics in the bio-hybrids are slower in all the a_w range than those observed for pristine sepiolite, and closer to that of zein. Thus, it seems evident that the presence of zein in the bio-hybrids affects the water sorption, suggesting the less hydrophilic character of these samples in comparison to the pristine clays instead of a marked hydrophobic behaviour. It is known that zein aggregates formed in aqueous ethanol have the hydrophobic regions oriented towards the center of the aggregate, thus exposing the hydrophilic region (Yamada et al., 1995). This arrangement may be responsible for the reduced hydrophilic character of the bio-hybrids.

Table 4.3 Sorption parameters of water in zein-sepiolite bio-hybrids deduced from the fitting of the experimental data to Park's model:

Parameters	Sepiolite	Z-SEP16	Z-SEP24	Z-SEP48	Zein
A_L	7.41	7.67	6.94	5.88	4.94
b_L	18.93	14.97	15.49	15.90	0.060
K_H	10.90	5.29	6.45	7.31	15.75
K_a	57.08	32.42	30.24	23.74	39.57
N	14.50	18.23	22.85	22.92	17.71
χ^2	0.49	0.19	0.16	0.13	0.099
r^2	0.998	0.997	0.997	0.997	0.999

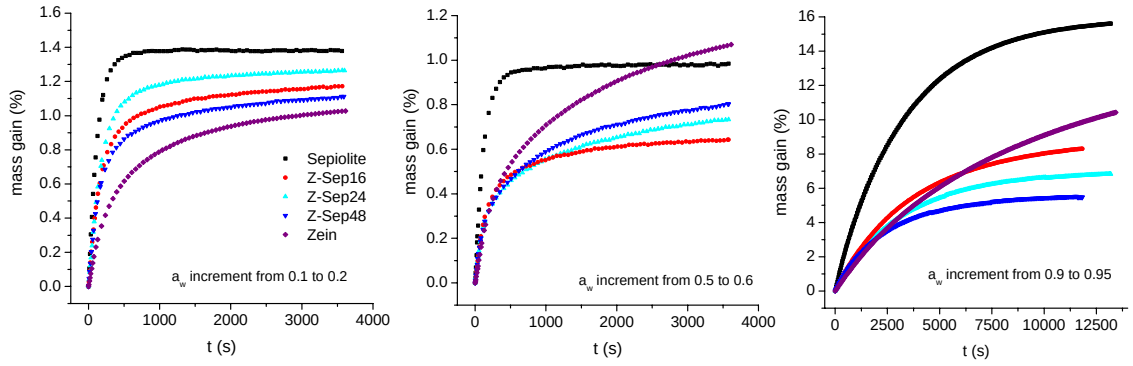

Figure 4.8 Water sorption kinetic curves obtained from water adsorption measurements at 25ºC for pristine sepiolite, zein protein and different Z-SEP bio-hybrids at different increments of water activity.

4.3 ZEIN- FIBROUS CLAYS BIO-HYBRIDS AS FILLER IN BIOPOLYMER MATRICES

Zein-fibrous clays bio-hybrids could be advantageous as an ecological alternative to alkylammonium-based organoclays for different applications, especially in the field of nanocomposites, i.e. acting as bio-organoclays. For this application, stability tests of these bio-hybrids were carried out. Washing tests in pure water of the Z-SEP48 bio-hybrid, chosen as example, provoked only a 2.6 % weight loss. This result indicates that zein-clay hybrids have a good stability in water, which could be also a proof of the strong interaction between both components.

Taking into account that zein-fibrous clay bio-hybrids show on the one side lower hydrophilicity than the unmodified clays, and on the other side organophilic properties, together with biocompatibity and biodegrability properties, this new class of materials could be good candidates as filler or additives of polymer matrices in the preparation of nanocomposites in general and bionanocomposites in particular. Those properties may help to improve the characteristics of polymers from biological origin such as polysaccharides or proteins, as their usually show high hydrophilicity and low stability in water. Thus, the polysaccharide alginate was chosen as a model biopolymer matrix to test the efficiency of zein-clay bio-organoclays as nanofillers in the development of bionanocomposites. This application has been chosen because natural polymers, such as polysaccharides and proteins, are receiving considerable attention for the development of green-plastics due to their availability, low cost, high biocompatibility and biodegradability, as well as good film-forming ability and flexibility in most cases (Tharanathan, 2003; Ruiz-Hitzky, 2010; Mittal, 2011).
However, much work is still needed to improve the mechanical and physical properties as well as the low water resistance of this type of biopolymer films (Zarate-Ramírez, 2011; Jerez, 2007, in order to allow their use in wet environmental conditions. In the present case, these novel bio-organoclays based on zein-fibrous clay systems may afford both the reinforcing role and the enhancement of water barrier properties due to the presence of zein.

In this way, bionanocomposite films were prepared by dispersion of the zein-sepiolite or zein-palygorskite bio-hybrid compounds within an alginate matrix. For the sake of

comparison, alginate bionanocomposites using neat sepiolite as filler as well as alginate films without incorporation of bio-hybrid particles have been also evaluated.

- *Mechanical properties and transparency of alginate-based bionanocomposites films*

Tensile properties (E) and the percentage of elongation at break (ϵ_B) of ALG/Z-SEP and ALG/Z-PALY bionanocomposite films were evaluated. Films of pure alginate and pure zein (2% w/v) have tensile modulus of approximately 3.9 and 0.5 GPa, respectively. The incorporation of neat zein in alginate diminishes both tensile modulus and elongation at break, presenting values of 1.12 GPa and 3.7%, respectively, in the case of an alginate film loaded with 25% of zein (w/w). Sepiolite alone acts a filler enhancing the modulus (*e.g.* 5.1 GPa in alginate films containing 50% sepiolite), but it diminishes the plastic behaviour of the system up to 3.3%.

Table 4.4 shows the nature of tensile modulus and elongation at break determined in alginate films with and without incorporation of the zein-clay bio-hybrids. In films of both ALG/Z-SEP and ALG/Z-PALY systems the increase of zein content in the alginate films, which is related to the incorporation of bio-organoclays with higher amount of zein, causes a slight decrease in the tensile modulus values, but at the same time, the values of elongation at break increase considerably. Similar results are observed when increasing zein content by increasing the mass ratio of a given bio-hybrid in the alginate film. This effect indicates that the addition of bio-hybrids increases the flexibility and stretchability of the biopolymer matrix, resulting in a plastic behaviour of the alginate-based bionanocomposite film. In this case zein may act as certain plasticizers that significantly affect the mechanical properties, simultaneously causing a slight decrease in the tensile modulus and a relevant increase in the plastic properties of the material. According to Wang et al. (Wang et al., 2006), this protein has a high affinity towards carboxylic groups, being the interactions between available functional groups of zein and carboxylic groups critical to reach zein plasticization. This fact has been also observed in beads prepared from a blend of zein and alginate in previous studies performed in our working group (Alcântara et al., 2010), although the current study, the interactions are established between the zein adsorbed on the clay surface and the carboxylic groups of the polysaccharide matrix. Therefore, these interactions between both biopolymers will account for the

plasticizing effect found in the final bionanocomposite materials. However, it is worthy to mention that the tensile modulus measured for ALG/Z-SEP and ALG/Z-PALY films may reach minimum values around 2 and 1.00 GPa, respectively, while other reinforced biopolymer materials such as starch (Muller et al., 2009) or cellulose (Dias et al., 2010), often present their best properties tensile modulus values below 1GPa.

Table 4.4 Mechanical properties of the alginate films loaded with zein-sepiolite and zein-palygorskite bio-organoclays. E = tensile modulus and ϵ_B = elongation at break.

Bio-hybrid filler	1:1[*]		1:2[*]		1:3[*]	
	E (GPa)	ϵ_B (%)	E (GPa)	ϵ_B (%)	E (GP)	ϵ_B (%)
Z-SEP16	3.79 ±0.95	8.84 ±2.03	3.02 ±0.98	9.62 ±2.03	2.58 ±1.04	9.24 ±1.44
Z-SEP24	2.76 ±0.87	15.43 ±1.01	2.33 ±0.84	15.21 ±1.89	2.06 ±0.95	14.94 ±1.77
Z-SEP48	2.40 ±0.89	20.09 ±1.11	2.00 ±1.04	19.30 ±2.44	1.95 ±0.97	19.90 ±2.02
Z-PALY12	1.86 ±0.24	5.78 ±1.58	1.47 ±0.98	6.90 ±1.56	1.33 ±1.00	6.06 ±1.52
Z- PALY14	1.62 ±0.75	10.39±2.04	1.35 ±1.02	10.06 ±2.14	1.22 ±0.78	10.36 ±2.66
Z- PALY28	1.48 ±1.00	12.98 ±1.53	1.25 ±0.99	12.59 ±2.12	1.00 ±0.83	12.98 ±0.09

[*] alginate/[zein-fibrous clay] ratio

The resulting self-standing films show considerable homogeneity and transparency, independently of the amount (Figure 4.9 a) and the type (Figure 4.9 b) of bio-hybrid incorporated in the alginate matrix. The small differences observed amongst bionanocomposite films can be associated with differences in their thickness. Light barrier properties of these bionanocomposite films were evaluated by measuring transmittance values in a wavelength range between 200 and 800 nm. From the data represented in Figure 4.10, it is clear that all the tested films exhibit reduced light transmission in the UV region, compared to the pure alginate films. It is observed that when the content in Z-SEP bio-hybrid in the alginate matrix increases, a decrease in the transmittance is produced. Transmittance in the UV region may decrease till around 10% of transmittance in alginate films incorporating the Z-SEP48 sample in a 1:3 alginate:bio-hybrid ratio, which is the sample with the highest content in bio-hybrid and so in zein. These results suggest a well dispersion of the bio-hybrid particles within the alginate matrix, acting as a good barrier to prevent the passage of UV light.

Thus, it can be concluded that zein-clay bio-hybrids can also play a role as additive of alginate films affording good transmittance in the visible region but inhibiting the passage of UV light, which can be of interest in view to a potential application in food protection, similarly to ginseng extract used as an antioxidant bio-additive that additionally impart light barrier properties to the alginate films (Norajit et al., 2010).

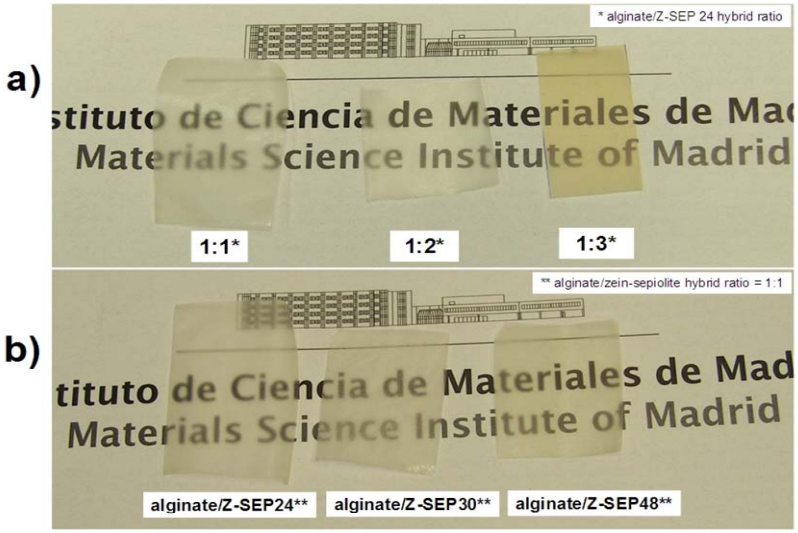

Figure 4.9 Macroscopic appearance of various bionanocomposites films based on ALG/Z-SEP24 biohybrid prepared with 1:1, 1:2 and 1:3 alginate:bio-hybrid ratios (a) and biocomposite films with a fixed 1:1 alginate:bio-hybrid ratio based on Z-SEP bio-hybrids of different zein content (b).

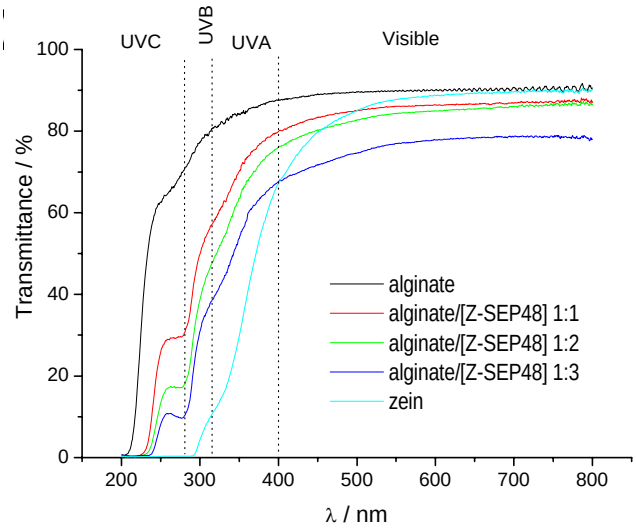

Figure 4.10 Transmittance measurements in the 200-800 nm wavelength range of films of pure alginate, pure zein and ALG/Z-SEP48 bionanocomposites with different alginate:bio-hybrid ratio.

- *Contact angle measurements*

Measurements of contact angle constitute a useful tool to determine the hydrophobic or hydrophilic characteristics of a surface. Table 4.5 shows contact angle (θ) values determined in alginate-based bionanocomposite films. A quantitative definition of the relative terms hydrophobic and hydrophilic surfaces has been done for surfaces exhibiting water contact angles higher than 65º and lower than 65º, respectively, (Vagler, 1998). Pure alginate film shows a value around 90º, which may be related to the slow diffusion of the water from the outside to inside of the film due to their crystallinity. In the case of the alginate-based bionanocomposites, all the films here analyzed showed hydrophobic surfaces with very close values. Films of alginate loaded with neat sepiolite shows a decrease in the contact angle to a value close to 67º in comparison to the film of pure alginate. The bionanocomposites incorporating Z-SEP bio-hybrids show contact angles between 81º and 88º (Table 4.5). This significant increase in the contact angle in comparison to the alginate-sepiolite film may be related to the reduced hydrophilicity showed by sepiolite fibers once assembled to zein protein, as observed in moisture sorption isotherms (Figure 4.7), making these alginate-bio-hybrid films have a higher hydrophobic surface than the alginate films loaded only with pristine sepiolite.

Table 4.7 Contact angles of water on alginate films loaded in a 1:1 alginate:bio-hybrid ratio with sepiolite and Z-SEP bio-hybrid in the ratio alginate:bio-filler of 1:1.

Sample	Contac angle / degree
Alginate	90.4 ± 20.08
Alginate/Sep	67.1 ± 15.33
Alginate/Z-SEP10	88.2 ± 4.95
Alginate/Z-SEP29	81.3 ± 2.17
Alginate/Z-SEP47	84.3 ± 5.13

- *Water uptake studies*

Given that one of the major drawbacks in the use of hydrophilic polymers as bioplastics, is their higher tendency towards water absorption, any improvement in water resistance is highly important for its practical application. In this way, it is expected that the reduced hydrophilicity of zein-clay bio-organoclay (Figure 4.7) may contribute to decrease the water uptake of alginate films. Figure 4.11 shows the swelling indices, expressed as weight of water incorporated per weight of dry sample, determined for films of pure alginate and various bionanocomposites incorporating Z-SEP and Z- PALY bio-hybrids, as a function of the time of contact with bi-distilled water (pH 5.5). For all the tested films, the amount of adsorbed water remains practically constant after around 1-2 h of immersion in water. Although the pure alginate films show a high contact angle degree, this later reach a maximum water uptake of around 1.2 g of water per g of film after 3 h, but then they start to disintegrate, making impossible subsequent measurements. This result is mainly related to the effect of the many hydroxyl groups present in the alginate chain (Chapter 2, §2.2, Figure 2.1) that facilitate the swelling of the film by incorporation of water molecules, which therefore provoke the increase of intermolecular distances between the polymer chains, driving to disintegration of the membrane. On the one side, water uptake properties of alginate films are clearly influenced by the content of zein in the Z-SEP (Figure 4.11 a) or Z-PALY (Figure 4.11 b) bio-hybrids, used as fillers. In both systems, water uptake decreases when the zein content in the bio-hybrid increases, reaching values of 0.54 and 0.80 g/g for films prepared in 1:1 ratio with alginate containing Z-SEP48 and Z-PALY28 bio-hybrids, respectively. On the other side, it is observed that the amount of bio-hybrid incorporated in the alginate film also plays an important role in the water uptake properties. Thus, for instance, it is observed that water uptake value decreases when the content in bio-hybrid increases reaching a value around 0.75, 0.64 and 0.47 g of water per gram of film for the alginate/[ZSEP24] samples, prepared in the proportion of 1:1, 1:2 and 1:3 alginate:bio-hybrid, respectively (Figure 4.12). This observed behavior may be clearly related to the presence of zein because as its content increases either, because there is more bio-hybrid or because its zein content is higher, the interaction between the alginate matrix and available functional groups of the zein increases. The interaction of the zein adsorbed on the surface of the silicates with the hydroxyl groups in the polysaccharide represents a

limitation to the uptake of water by alginate and, so, it difficults the passage of water through the film interfaces.

It must be indicated that the water uptake index of the bionanocomposites based on the palygorskite bio-hybrids are higher than those of films based on sepiolite. As above discussed, this behavior may be associated with the amount of zein adsorbed on sepiolite which is higher than palygorskite, causing a hydrophobic effect more pronounced in these materials.

The use of neat sepiolite as filler leads to water uptake values close to those of samples with the lowest zein content (ca. 0.9 g/g film), which again prove the effect of zein on the observed behavior. Similar results were reported for studies on the incorporation of zein protein in starch films, which resulted in more water resistant materials due the hydrophobic character of this protein (Gáspár et al., 2005). All these results suggest a significant compatibility between the bio-hybrids and the alginate matrix as the films become more stable and water resistant than pure alginate and alginate-sepiolite films, being so a promising alternative as bioplastic for applications in food packaging.

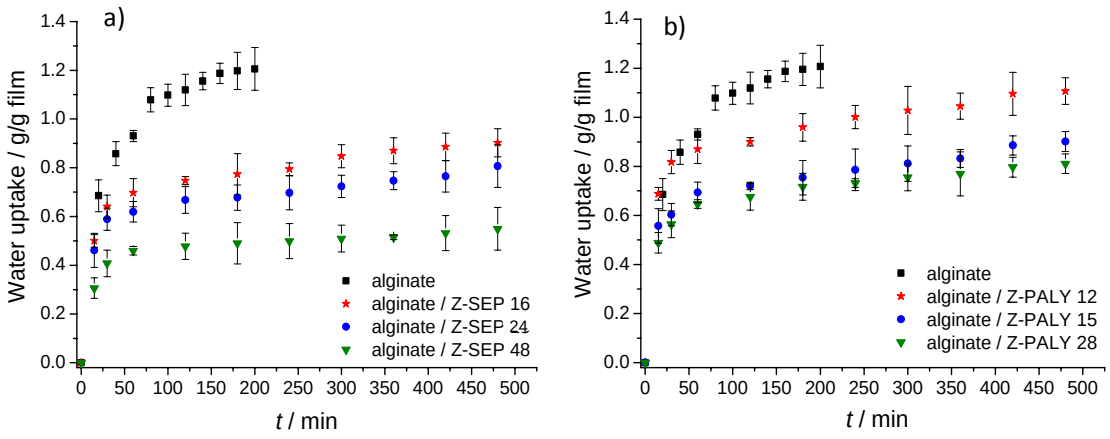

Figure 4.11 Effect of (a) zein-sepiolite and (b) zein-palygorskite bio-organoclays on the water uptake of alginate films with a 1:1 content of nanofiller exposed to deionized water (pH 5.5).

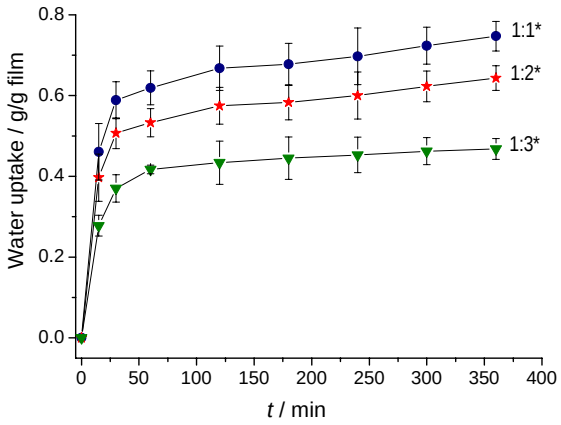

Figure 4.12 Water uptake of ALG/Z-SEP24 bionanocomposites films prepared in different ratio of alginate:bio-hybrid. (*alginate:bio-hybrid ratio)

- *Water vapour barrier properties of the bionanocomposites films*

In view to the potential use of zein-fibrous clay bio-hybrids as filler in hydrophilic polymer matrices of application in the food sector, their influence in the improvement of the gas barrier properties in these type of matrices was analyzed. Since the main function of food packaging is often to avoid or at least to decrease moisture transfer from the surrounding atmosphere to the food, another property explored in this chapter has been the water vapour barrier effect of these bio-hybrid films, which was calculated through the water vapour transmission rate according to the E 96-80 ASTM norm, following the protocol previously described (Chapter 2, Experimental Section, § 2.4.2.). Water vapour transmission rate (WVTR) properties of pure alginate and diverse bionanocomposite films are shown in Figure 4.13. As observed, the passage of water vapour through alginate films is altered by the presence of the bio-hybrid used as filler. The WVTR of the bionanocomposite films changed significantly depending on both type and concentration of zein in the incorporated bio-hybrid. In all cases, WVTR values are lower for bionanocomposites than for the unloaded alginate film. Alginate loaded with neat sepiolite show WVTR values of ca. 0.95 mg $h^{-1}cm^{-2}$, which are close to those of films with the same loading of bio-hybrids with the lowest content in zein. The decrease of WVTR as the zein content increases suggests that the protein afforded by the bio-hybrid to the bionanocomposite film is responsible for the barrier properties, playing the major role in the reduction of water vapour passage. The increase in water

vapour barrier properties of alginate/zein-clay bionanocomposite films can be not only attributed to the tortuous path for water vapour diffusion due to homogenous distribution of the bio-hybrid particles within the biopolymer matrix, consequently increasing the effective diffusion path length, but also to the hydrophobicity afforded by zein. This protein can exert a barrier at the interface and the medium of the film, making the incorporation of water molecules difficult, as previously described in drug delivery beads prepared by combination of alginate and zein (Alcântara et al., 2010). These properties corroborate that zein-based bio-organoclays can be effective additives for increasing barrier and water resistance properties of hydrophilic matrices. Moreover, the choice of bio-hybrids with a wide variety of zein content may allow the development of bionanocomposites in which these properties could be tuned as a function of the desired requirements.

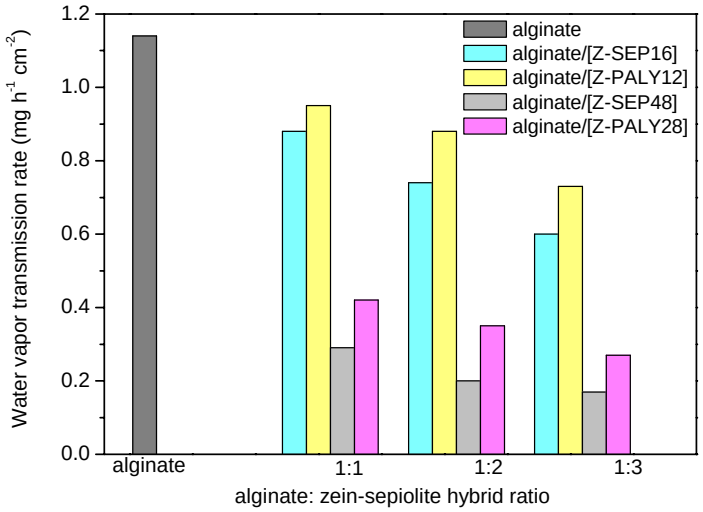

Figure 4.13 Water vapor transmission rate of alginate based bionanocomposite films incorporating zein-sepiolite and zein-palygorskite bio-organoclays at different loadings.

- *Gas permeation studies in bionanocomposite films*

Similarly to other hydrophilic polymeric membranes, alginate films show low gas permeation property in dry state, but in wet conditions its permeabilities increase substantially (Park and Lee, 2001), being a disadvantageous feature for some applications, such as in the food packaging sector. Therefore, gas barrier properties of alginate films reinforced with zein-fibrous clays nanofiller were also evaluated in wet

conditions. This study specially focused on alginate films loaded with zein-sepiolite bio-hybrids, because they were the bio-hybrids with the highest amount of adsorbed protein, showing the best water resistance properties. For this purpose, films previously cross-linked with Ca^{2+} ions, were swollen in water overnight and then permeabilities of pure gases through these wet membranes were evaluated (Chapter 2, Experimental section, § 2.4.4). Table 4.6 shows the water uptake properties of these cross-linked membranes. It is observed that, all the membranes become more stable after the cross-linking process, especially those based on pure alginate that now are stable even after 24h. However, the cross-linking with Ca^{2+} ions seems to be less effective in the bionanocomposite membranes compared to the pure alginate, since the water uptake values found for these films are quite similar to those of uncross-linked membranes (Table 4.6). This behavior of crosslinking in the bionanocomposite films can be attributed to the fact that many of the carboxylic groups of the alginate available for the cross-linking process with calcium cations are already blocked interacting with zein, as discussed above. Here again, it is observed a decrease in water absorption with the increase of the zein in the sepiolite bio-hybrid and with the bio-hybrid content in the polysaccharide matrix, which is in accordance with the hydrophobic efficiency introduced by the zein present in the bio-hybrid decreasing the water adsorption and increasing the barrier properties.

Table 4.6 Water uptake of membranes based on pure alginate and on alginate loaded with Z-SEP16 and Z-SEP24 bio-hybrids, in both cases before and after the cross-linking process.

	Water uptake (g H_2O/g membrane	
Sample	Uncross-linked membranes	Cross-linked membranes with Ca^{2+}
alginate	-	2.75 ± 0.33
alginate/[Z-SEP 16] (1:1)*	0.90± 0.19	0.84± 0.15
alginate/[Z-SEP 16] (1:2)*	0.82± 0.12	0.70± 0.12
alginate/[Z-SEP 24] (1:1)*	0.75± 0.11	0.68± 0.17
alginate/[Z-SEP 24] (1:2)*	0.64± 0.09	0.52± 0.09

* The values correspond to the alginate:bio-hybrid ratio

In polymeric membranes, the permeability of a given gas depends on several factors such as the ratio between the crystalline and amorphous zones, polymeric chain mobility and specific interactions between the functional groups of the polymers and the gases in the amorphous zones (Kim et al., 1992; Filho and Bueno, 1992). In bionanocomposite membranes, the factors involved in the permeation of a gas can be still more complex, since other components, such as fillers, can play a significant role in the gas permeation properties, increasing the selectivity toward a determinate gas or improving the barrier properties of the membrane as a whole. However, in high humidity conditions, the permeation properties can undergo drastic changes, being therefore important to verify the permeability properties in such conditions. In this sense, the permeability values of wetted membranes of pure alginate and alginate loaded with Z-SEP16 and ZSEP24 bio-hybrids in a 1:1 and 1:2 alginate:bio-hybrid ratio towards CO_2, O_2, He and N_2 are presented in the Figure 4.14. In general, all the membranes show a pronounced permeability towards CO_2 compared to the other tested gases.

Pure alginate film (Figure 4.14 a) shows an increase in the CO_2 permeability when the gas pressure increases, while permeabilities slight decrease with pressure in the case of He, O_2 and N_2. Similar trends towards carbon dioxide permeation in water swollen membranes were observed in other studies reported in the literature, although the permeability values found here for alginate membranes are considerably higher compared to those found on diverse hydrogel membranes based on alginic acid or chitosan (Nakabayashi et al., 1995; Park and Lee, 2001; Zou and Ho, 2006). This behavior can be explained considering the high solubility of acid gases, such as CO_2 in water, which may facilitate the passage of this type of gas by the wetted membranes by increasing its concentration inside the membrane (Nakabayashi et al., 1995). In contrast, solubility of He, O_2 and N_2 in water is lower than CO_2, because they have weaker interactions with water molecules and therefore the effect result in a lower permeability of these gases when pressure increases (Lannung, 1930; Weast, 1972). According to various studies reported in the literature, which have qualitatively analyzed the state of water in cellulose-type membrane, it was concluded that these polysaccharide-based membranes have a certain degree of molecular order which controls the water entering to the membrane affecting to other gases permeability (Taylor et al., 1959; Wu and Yuan, et al., 2002).

In the same way than WVTR measurements, the permeabilities towards the same gases in the bionanocomposites membranes decrease significantly and depend on the incorporated type and the amount of the bio-hybrid, being in all cases lower than the ones measured for the membranes based on pure alginate (Figure 4.14 b -4.14 e). The decrease in the permeability values is more marked when the membrane incorporates higher amounts of bio-hybrid. Therefore, a decrease in the CO_2 permeability is observed because, as explained above, the involved membrane presents a lower content in water. The increase in the content of carbon dioxide in the membranes by raising the gas pressure leads to a higher permeability in the membrane with Z-SEP16 (Figure 4.14 b and 4.14c) compared to the membrane loaded with Z-SEP24 (Figure 4.14 d and 4.14 e), which can be related to the higher water content in the first one. In contrast to that observed in membranes of pure alginate, the wetted membranes based on alginate/ZSEP show a slight increase in the permeability of He, O_2 and N_2 gases as the gas pressure increases. It is also remarkable that the coefficients of permeability of He, O_2 and N_2, in Z-SEP-loaded membranes are lower than those found for the alginate membrane, indicating the gas barrier effect of the bio-hybrids in these bionanocomposite films. In addition, these results reveal that the lower permeability in wetted bionanocomposite membranes towards these gases, does not seem to be only associated with their water content, but also with the amount and type of bio-hybrid incorporated in the polymer matrix, that make the passage of the gases more difficult. The increase in the barrier properties of alginate/Z-SEP bionanocomposite material can be attributed to the tortuous path for gas diffusion due to the bio-hybrid particles distributed in the polysaccharide matrix, consequently increasing the effective diffusion path length. Furthermore, the good dispersion of the bio-hybrid within the biopolymer matrix may result in a lower free volume between polymer chains and filler, improving therefore the barrier properties under humid conditions.

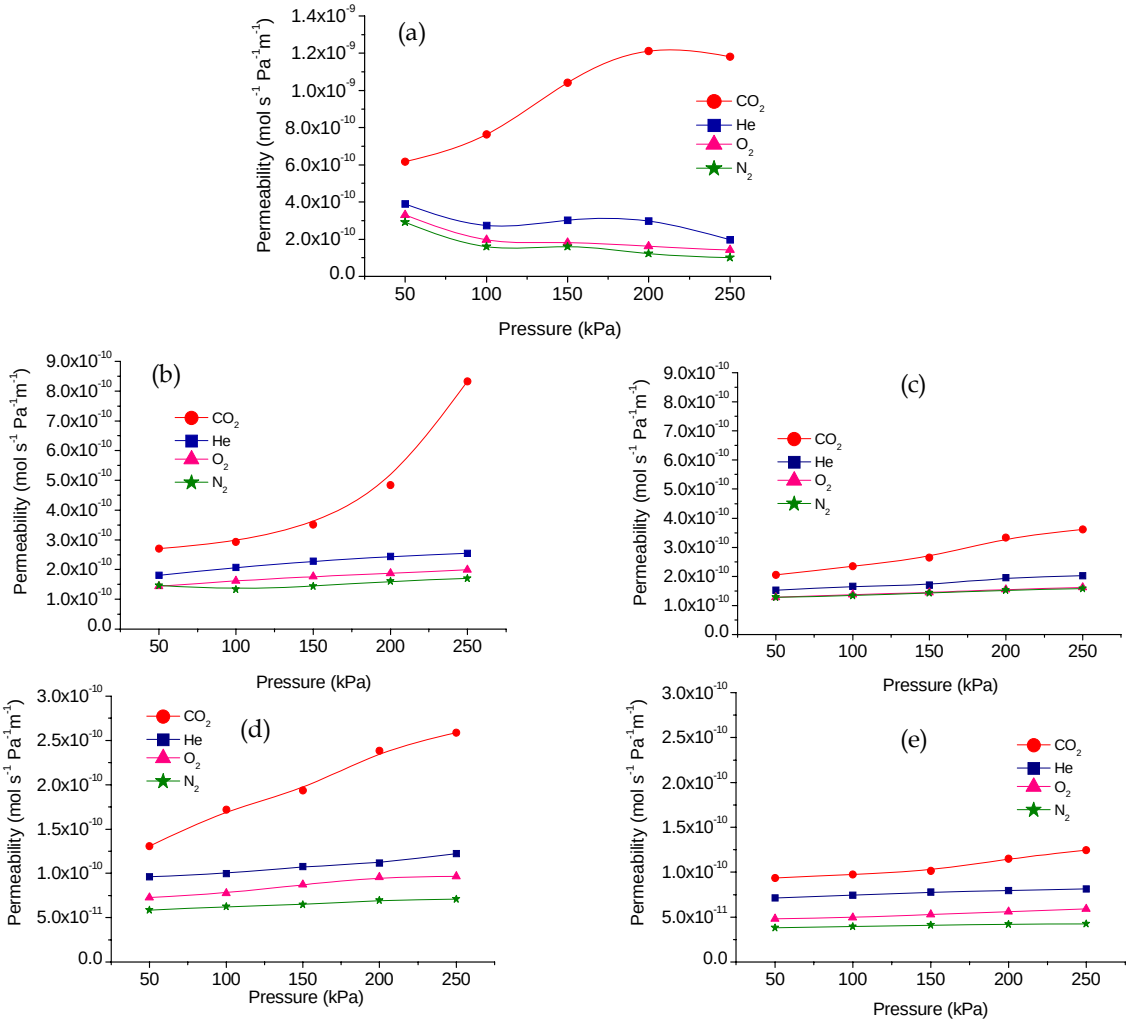

Figure 4.14 Gas permeation properties of wetted membranes cross-linked with Ca^{2+} ions, based on in pure alginate (a), as well as alginate/[Z-SEP16] (b and c) and alginate/[Z-SEP 24] (d and e) bionanocomposite in a 1:1 and 1:2 alginate:bio-hybrid ratio, respectively.

In view of a potential application in food packaging, special attention was given to the oxygen permeabilities of the bionanocomposite films (Figure 4.15). As commented above, the O_2 permeability increases with the pressure, and at same time it decreases depending on the type (Z-SEP16 or Z-SEP24) and amount of the incorporated bio-hybrid (Figure 4.15 a). Thus, the film loaded with Z-SEP16 bio-hybrid in the 1:1 alginate:bio-hybrid ratio mass shows higher O_2 permeability values than the alginate films with ZSEP24 in the same proportion.

In both systems, a decrease in the permeability values is measured when the amount of bio-hybrid is increased to a 1:2 alginate:bio-hybrid mass ratio. In this sense, an marked

barrier effect was demonstrated for the alginate/[Z-SEP24] film in the 1:2 ratio, which presentS a O_2 permeability almost constant with increasing pressure, reaching values below to 5.0x10^{-11} mol s^{-1}Pa^{-1}m^{-1}. From these results, it is clear the contribution of zein to the observed behavior towards the passage of gases in bionanocomposite membrane. This effect is better observed in the Figure 4.15 b, which shows the variation of the O_2 permeability and water uptake of the film with respect to the percentage of zein present in the bionanocomposite material. In this Figure it is possible to observe that although the protein limits the indiscriminate entry of water molecules, this behavior does not strongly affect the oxygen permeabilities until 10% of total zein fraction in the film. However, for a higher content of zein the permeability toward O_2 is significantly reduced. These results suggest that bionanocomposite films based on Z-SEP bio-hybrid can be effective against oxygen even in high humidity conditions, which is an advantageous feature that would allow the application of these materials in the food packaging sector.

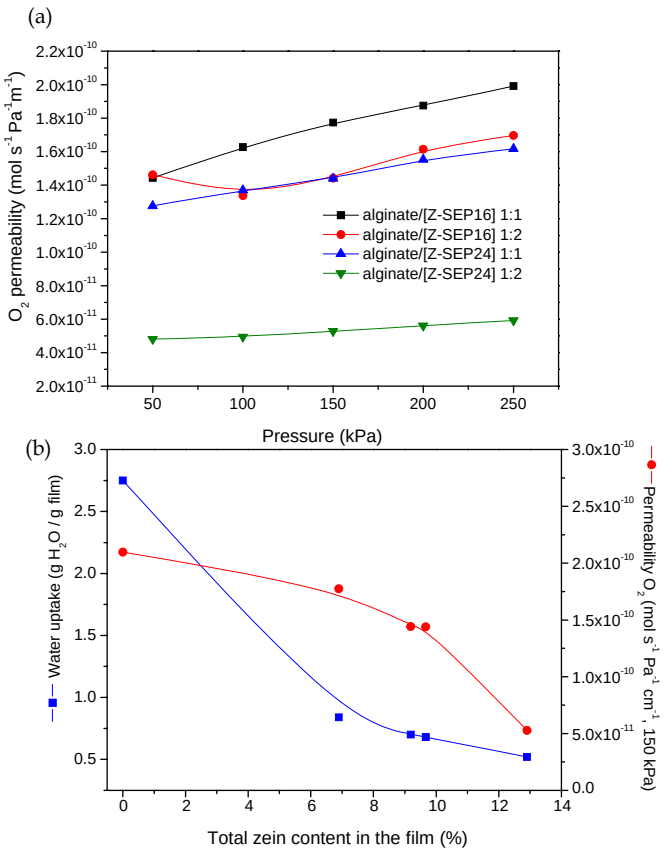

Figure 4.15 Oxygen permeation of the bionanocomposite wetted membranes (a) and evolution of water uptake values and O_2 permeability with zein content in alginate-ZSEP bionanocomposites membranes (b).

To corroborate the potential of those membranes based on alginate/Z-SEP bionanocomposite in food packaging application, several of them have been evaluated for protection of apple slices against oxidation. Figure 4.16 shows the aspect of the apple slices after being coated with alginate/Z-SEP films with different content of the Z-SEP24 bio-hybrid, i.e., different zein content, at various periods of time. In accordance to the results discussed above, the protective role of the bionanocomposite films can be clearly evidenced with the simple experiment shown in Figure 4.16. The membrane with highest content in zein (i.e., 3:1 proportion) shows the best barrier properties to the passage of oxygen, preventing the oxidation of the fruit slice even after 3 days. This result yields a preliminary verification of the good barrier properties of the alginate/zein-clay bionanocomposites towards the passage of water vapor and oxygen, being so promising materials for packaging applications in the food area.

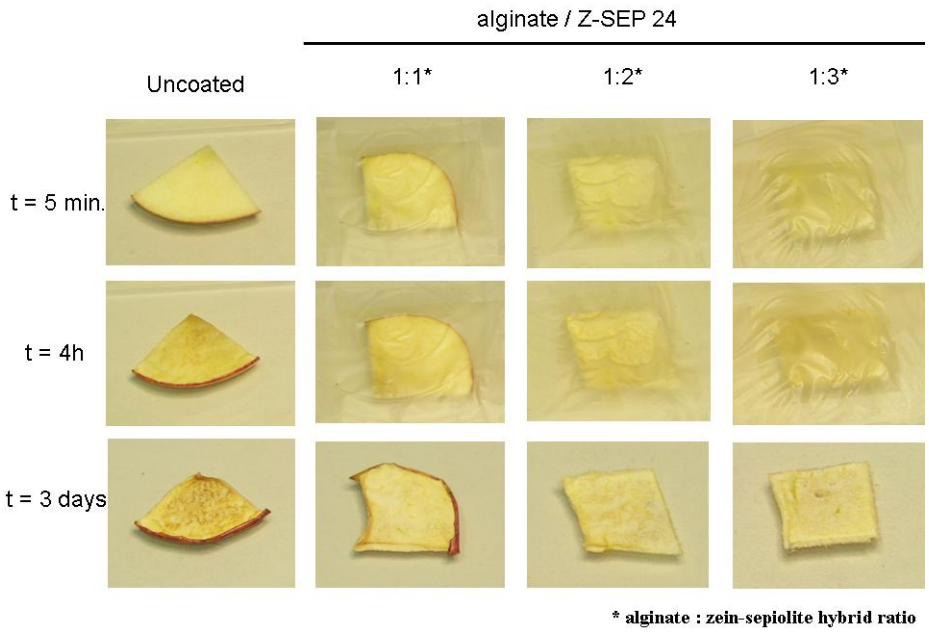

Figure 4.16 Evaluation of the protective role of various alginate/[Z-SEP24] bionanocomposite films against oxidation of apple slices.

4.4 CONCLUDING REMARKS

The present Chapter introduces a new type of bio-organoclay material based on the combination of sepiolite or palygorskite fibrous clays with zein. The assembling of these components reduces the hydrophilic character of the pristine clays, conferring new properties to the resulting bio-hybrids, which can be applied as fillers in the preparation of bionanocomposites.

A first approach of this application is the preparation of alginate-based bionanocomposites for potential use in food packaging. These alginate/zein-clay systems are able to form self-supporting films that show a marked resistance to the passage of water molecules in comparison to pristine alginate films. Mechanical properties, water uptake, contact angle measurements, water vapor transmission rate (WVTR), and gas permeation properties were evaluated in the alginate-based bionanocomposite films with zein-clay bio-hybrid as filler. The results reveal that the proportion of each of the bio-hybrid employed in the formulation of alginate bionanocomposite films has a crucial role in the water vapour barrier and gas permeation properties. It is observed a significant decrease in the water uptake with the increase of the zein content adsorbed on the clays, as well as with the proportion of zein-clay bio-hybrid incorporated in the alginate matrix. This behaviour was extremely important in the permeability of gases through the bionanocomposite films in high humidity conditions, which showed a prominent permeability toward CO_2, while the barrier properties toward O_2 were not strongly affected by the degree of plasticization occasioned by the water molecules in the bionanocomposite membranes. Indeed, the bionanocomposite films prepared here, present homogeneity, transparency, as well as improved barrier properties, being therefore promising as new ecofriendly materials with potential applications in food packaging.

CHAPTER 5

ZEIN-SEPIOLITE BIONANOCOMPOSITE FOAMS

The main purpose of this Chapter focus on the preparation of cellular structures based on zein foams reinforced with sepiolite fibres. The novel zein bionanocomposite foams were prepared by a new, easy and ecofriendly foaming method. The resulting porous materials can be provided with magnetic properties by assembling a sepiolite modified with magnetic nanoparticles to the zein matrix. The structure and properties of the resulting bionanocomposite foams were studied in relation between the kinds of filler. Zein-based bionanocomposite foams were designed in order to show good water stability as well as magnetic and mechanical properties, which could be profited for applications in environmental remediation, such pollutants retention in aqueous media.

5.1 INITIAL CONSIDERATIONS

It is well known that polymer-clay based bionanocomposites are a versatile class of materials that can be conformed by different types of processing, resulting in varied structural and multifunctional properties. In this sense, bionanocomposites processed as foams result of interest for a variety of applications, including tissue engineering (scaffolds), packaging, building insulation, adsorbents and absorbents, or weight-bearing structures, among others. Foams are defined as materials containing gaseous voids surrounded by a polymer denser matrix (Lee et al., 2005). Depending on the cell morphology and the physical properties, these materials can be classified as closed or open cells and rigid or flexible foams, respectively.

Although there are several methodologies in order to obtain bionanocomposite foams, such as gas foaming, particulate leaching or the ice segregation-induced self-assembly (ISISA), (Darder et al., 2011), one of the most employed methods is still the conventional freezing with subsequent drying. In this procedure, the porous structure is imposed by the growth of ice crystals during the freezing step and their further elimination by sublimation under vacuum. The main reason for this selection is that the majority of the polymer matrices in bionanocomposite foams are based on hydrophilic polysaccharides or proteins, where water is used as the main solvent (Darder, et al., 2007; Ruiz-Hitzky et al., 2010; Darder et al., 2011). In general, this kind of matrix may show some inconveniences, such as high hydrophilicity, which may limit the stability properties in aqueous media of the resulting material. Conversely, materials based only on hydrophobic biopolymers, such as the zein protein, can offer high stability in water, but at the same time, its high hydrophobicity becomes a drawback in the foaming preparation, in the freeze-drying step due to the need of ethanol as solvent. To overcome this difficulty, it is necessary to appeal to other strategies and experimental methodologies in order to facilitate the foaming process, that include the use of supercritical CO_2 and the modification of zein chains with hydrophilic biopolymers (Salerno et al., 2007; Salerno et al., 2012).

The incorporation of inorganic solids as fillers in the biopolymer matrix may help the foaming process, acting as nucleation sites that control the cell density, and at the same time affording enhanced mechanical and physical properties (Lee et al., 2005; Darder et al., 2011). In this context, it has been reported in the literature the use of several fillers in biopolymer foams from smectite clays (Ohta and Nakazawa, 1995) to cellulose

whiskers (Svagan et al., 2010). Recently, sepiolite was used as filler in PVA foams with potential application as scaffolds for bone tissue engineering and bioreactors. These foams are characterized by the presence of a reinforced interconnected structure and porosities ranging from 89.5% to 95%, depending on the clay content incorporated in the PVA matrix (Killeen et al., 2012; Wickein et al., 2013). In addition to the structural properties associated with the presence of the sepiolite, the incorporation of other additives assembled to the filler can provide additional functional properties to the bionanocomposite foam. For instance, the assembly of an enzyme to the sepiolite fibers used as filler in a PVA foam gave rise to a bioactive cellular material useful for bioreactor and biosensing applications (Wickein et al., 2013). Similarly, nanoparticles assembled to the sepiolite could result in different foam structures showing also the properties associated with these nanoparticles. According to a recently patented procedure (Ruiz-Hitzky et al., 2011.), it is possible to obtain a modified sepiolite by assembling superparamagnetic nanoparticles from a ferrofluid constituted by oleic acid-modified magnetite nanoparticles, which are anchored to the sepiolite surface mainly by interaction with the silicate hydroxyl groups (González-Alfaro et al., 2011).

Taking into account these premises, this Chapter is addressed to the synthesis and characterization of new bionanocomposite foams based on zein and the microfibrous sepiolite clay. As previously discussed (Chapter 3, §3.2.2.), it is possible to attain the separation of zein phases in absolute ethanol media. Based on this observation and on the very poor solubility of zein in pure water, a new method of preparation of zein foams is here proposed. Thus, neat sepiolite was used as filler in the preparation of such bionanocomposite foams. Moreover, considering that the incorporation of the magnetic nanoparticles in the zein-sepiolite porous foam allows to provide the material with magnetic properties, sepiolite modified with magnetite nanoparticles (SepNp) was also employed as nanofiller in the preparation of superparamagnetic zein bionanocomposite foams. As it will be proven, these zein-sepiolite superparamagnetic bionanocomposite foams can be considered a very interesting material for diverse applications, such as environment remediation, where their magnetic properties could facilitate the recovery of the porous adsorbent material from the aqueous media using an external magnetic field (magnet).

The final goal of the research introduced in this Chapter was the development of novel zein bionanocomposite foams based on a natural fibrous silicate and presenting cellular structure by using a new, easy and ecofriendly foaming method. These

materials were designed in order to show good water stability and mechanical and magnetic properties, which can make them interesting as adsorbents for pollutants retention in aqueous media. To show their potential applicability, bionanocomposites foams were evaluated in herbicide retention from aqueous solutions.

5.2 SYNTHESIS AND CHARACTERIZATION OF ZEIN-SEPIOLITE BIONANOCOMPOSITE FOAMS

Zein-sepiolite bionanocomposite foams were prepared by a mechanical mixing of zein with 0, 3.5 and 7% (w/w) of pure sepiolite (Sep) or sepiolite modified with magnetic nanoparticles (SepNp). As commented previously in the Experimental section (see Chapter 2, § 2.3.3, Figure 2.2), a mechanical mixture of both components was conformed as pellets, and then the soluble fractions of protein were extracted in absolute ethanol. The alcohol-treated pellet was then immersed in pure water to swell the material for subsequent freezing and lyophilization, giving rise to the zein bionanocomposite foam. Given that the strategy employed in the preparation of these zein foams is new, a study of each individual step of the foaming process was carried out, being presented at the beginning of this section. The study of the relationship between the structure and the properties of the resulting foams was also addressed in this section, as well as the possibility to provide the foam with superparamagnetic properties by using a magnetite-modified sepiolite instead of neat sepiolite.

- *Study of the foaming process in the preparation of zein foams*

Zein bionanocomposite foams were prepared considering the solubility of zein in pure ethanol and pure water. In this context, the foaming process of zein was investigated in detail. In the study of this process, two steps have been considered: i) the immersion of the zein-based pellet in absolute ethanol; ii) the posterior immersion of this alcohol-treated pellet in pure water, followed by the consolidation of the obtained structure by means of freeze-drying technique. In order to have a comprehensive understanding of the phenomena that take place during the foam formation, a careful study of the process was carried out in pellets made of neat zein.

i) *Immersion of the pellet of absolute ethanol*

A weighted amount of zein was conformed as a pellet and immersed in absolute ethanol (Figure 5.1 a), where the alcohol provokes the extraction of soluble components in a process described in Chapter 3, § 3.2.2. Figure 5.1 b shows the cross-section of the zein pellet, in which it is clearly evidenced the aspect change to a rubbery and sticky material, like a resin, whose handling became extremely complicated. Actually, it seems that the zein particles are agglutinated by the alcohol penetration that induces partial solubilization of zein and agglomeration of non-soluble fractions, being an important step for the stabilization of the pellet conformation. The morphology of this material observed by FE-SEM microscopy once frozen in liquid N_2, and dried by lyophilization is shown in Figure 5.1 c. This image reveals a homogeneous and compact structure in resulting material, far away from the searched porous structure.

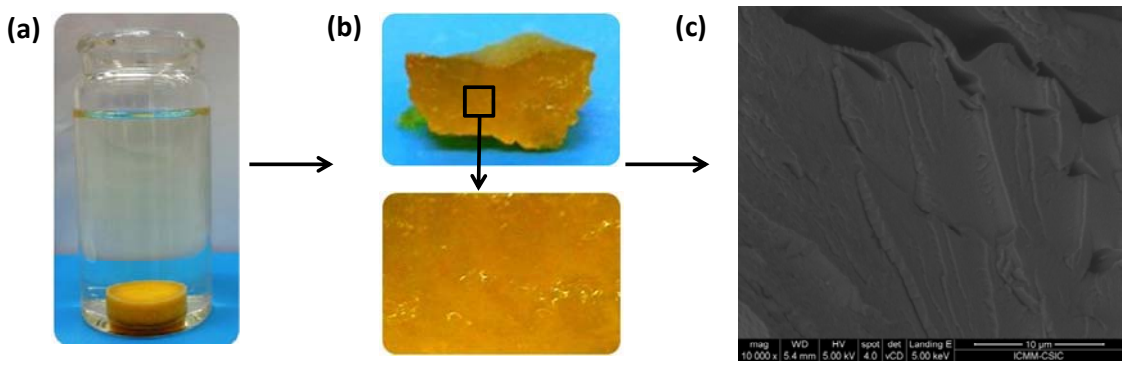

Figure 5.1 Photographs of (a) pure zein pellet when immersed in absolute ethanol and (b) cross-section of the resulting alcohol-treated pellet. (c) FE-SEM image of the material once frozen in liquid N_2 and dried by lyophilization.

ii) *Immersion of the alcohol-treated zein pellet in pure water*

The second stage in the zein foam synthesis is based on the immersion of the alcohol-treated zein pellet in pure water. It was observed that its gelatinous and yellow appearance took a whitish color with a spongy appearance once submerged in water (Figure 5.2 a). In addition, the abrupt swelling of the pellet was also observed in this step, increasing almost three times its initial size. The presence of new pores at the surface began to be visible, as well as inside the pellet, as shown in the cross-section of

the material (Figure 5.2 a and b). The new texture observed in the material resulting after this step can be associated with absorption of water by the zein residue, which can promote the formation of cellular structures after drying. These results suggest the possibility of formation of porous in zein bionanocomposite foams by this procedure, i.e. using water as a porogen.

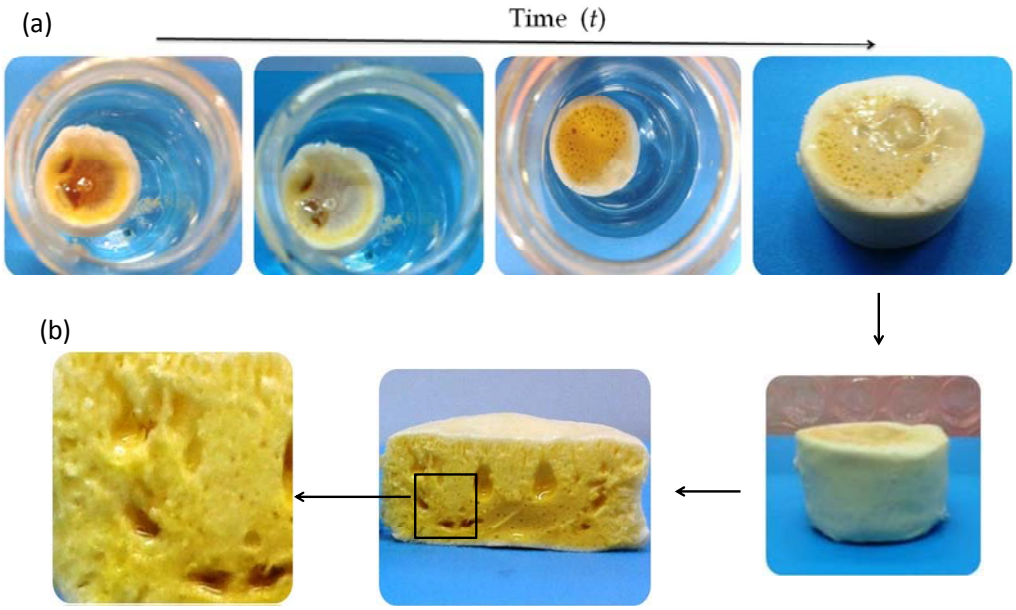

Figure 5.2 Photographs of samples at different stages of the second step of the foaming process, in which the alcohol-treated pellet is immersed in pure water, and (b) cross-section of the resulting pellets once removed from water.

Considering that in foams processing the freezing conditions (rate and temperature) may have influence in the structural arrangement, the structuration process of the water-swollen zein pellet was investigated under two different freezing conditions: i) by direct immersion of the swollen material in liquid nitrogen at –195.8 ºC and ii) by conventional freezing at -20ºC. The frozen materials were dried by lyophilization and the morphology of the resulting solids was observed by FE-SEM (Figure 5.3). Images of the cross–section of both types of foam samples, frozen by liquid N_2 (Figure 5.6 a and b) and in a conventional freezer (Figure 5.6 c and d), showed a cellular structure consisting of open cells, composed by well-defined pores of rounded shape, and a compact cell wall. Basically, the main dissimilarity between the two types of frozen systems is related to the pore size, which evidenced the presence of larger pores in the material obtained by conventional freeze-drying than in the sample frozen in liquid N_2.

Both methodologies gave rise to materials with similar pore size, although with slightly larger pores in those produced by conventional freezing, which was then selected for the preparation of the diverse zein bionanocomposite foams here studied. These results indicate that in our case the obtained porous framework is not strongly influenced by the ice growth, which suggest that the porous arrangement in zein foams is achieved in the immersion of alcohol-treated pellet in water during the process. Therefore, the freezing and subsequent lyophilization steps do not have a crucial role in the further growth of the pores during the consolidation of the foam. These results are quite different to those reported for other types of biopolymers, such as polyvinyl alcohol (PVA), whose final structure was strongly influenced by the freezing conditions (Gutiérrez et al., 2007). Indeed, these results show also that the foaming methodology employed here is efficient to achieve the formation of foams based on pure zein, without requiring the addition of CO_2 or other components commonly employed as porogens in order to attain the porous network formation (Salerno et al., 2007; Qu et al., 2008; Salerno et al., 2010; Salerno et al., 2012).

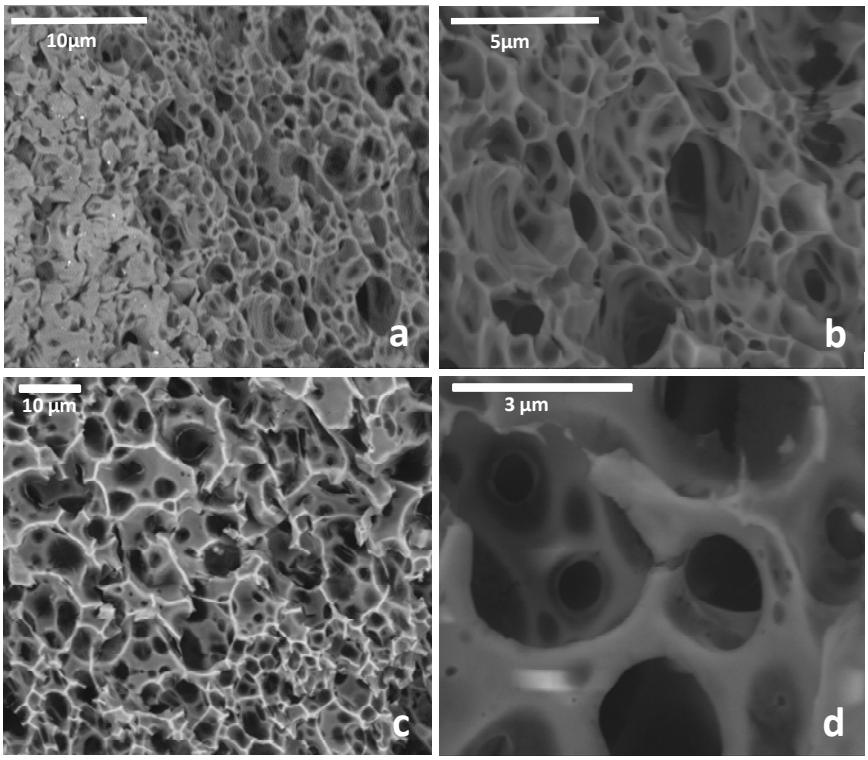

Figure 5.3 FE-SEM images of the cross-sections of zein samples resulting after swelling the alcohol-treated pellets in water, followed by freezing in (a and b) liquid nitrogen and (c and d) conventional freezer, and finally lyophilized.

Figure 5.4 shows the actual aspect of a foam of pure zein before (Figure 5.4 a) and after (Figure 6.4b) the foaming process. The initial zein pellet (Figure 5.4 a), presents a more compact structure, being evident the presence of some empty spaces probably due to an incomplete packing of the zein particles in the pressing process. In contrast, after the water swelling and freeze-drying processes (Figure 5.4 b), it is clearly observed an increase in the size of the pellet once formed the foam, being evident the presence of a porous structure. As discussed previously, the origin of these cellular structures at the micrometer scale is provoked by the immersion of the alcohol-treated pellet in water, and the incorporation of water molecules that replace the ethanol inside the pellet an then act as a template for generation of the porous network once frozen.

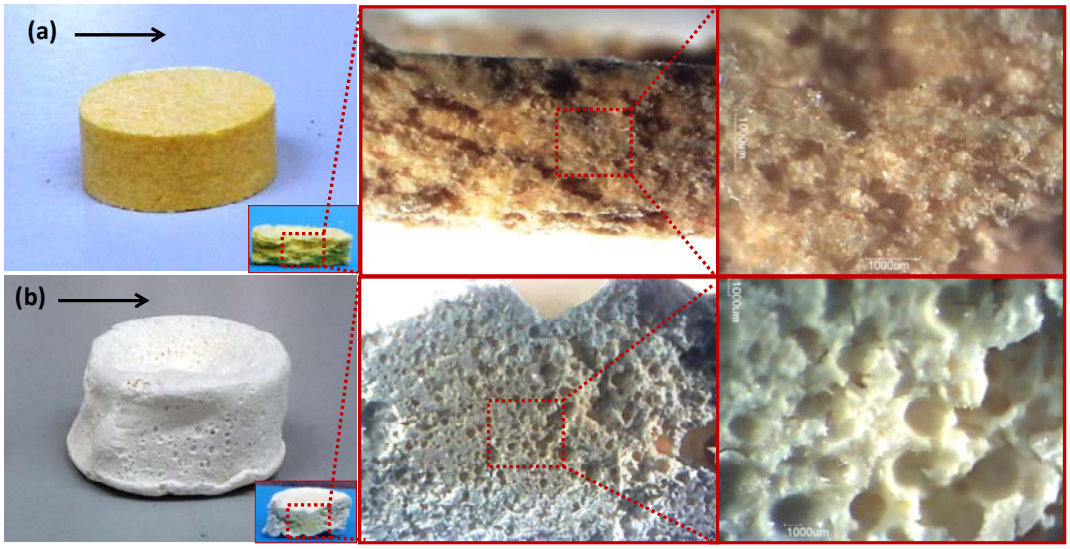

Figure 5.4. Photographs and optical images of zein pellets: (a) before and (b) after the foaming process.

- *Zein-based bionanocomposites foams*

Following the above-mentioned foaming process, various zein-sepiolite bionanocomposite foams were prepared. In order to incorporate superparamagnetic properties to the foam, a first approach was to immerse previously formed Z and Z-Sep foams in a ferrofluid containing magnetite nanoparticles. However, this approximation resulted in a non-uniform impregnation of the foam, and therefore,

alternatives have been explored, such as the direct incorporation of pure magnetite-oleic acid Np alone or incorporated to sepiolite fibers were also used as nanofiller in zein-based bionanocomposites foams. Both Np and SepNp were prepared according to the method reported by González-Alfaro et al. (González-Alfaro et al., 2011). In the case of zein bionanocomposite pellets based on Sep, SepNp or Np, it is observed that, before being processed as foams, there is an increase of the apparent density (ρ^*) with the increase in the percentage of filler in the zein material with respect to the unmodified zein material (Table 5.1 A). It was also observed a slightly increase in the true or skeletal density (ρ_s), determined by means of a He pycnometer. A similar trend with increasing of apparent and true density values with Sep or SepNp content is observed in the resulting bionanocomposite foams (Table 5.1 B). The increase is more accused in the bionanocomposite materials that incorporate 7% of filler in its composition.

Comparing the characteristics of the systems before (Table 5.1 A) and after (Table 5.1 B) the foaming process, it is clearly observed that the apparent density decreases about twice after the foaming process. These results suggest that the swelling and freeze-drying steps have a direct effect in the consolidation of the structure in these bionanocomposite materials. Relative density is considered as a relevant feature in cellular solids, and it can be calculated by the ratio of the density of the cellular material (ρ^*) and the skeletal density (ρ_s). In the present case, bionanocomposite materials before the foaming process show relative density values of around 0.3 (Table 5.1 A), which resemble to typical values of solids containing isolated pores (Gibson, and Ashby, 2001). Conversely, this parameter decreased drastically in the bionanocomposite materials after the foaming process, reaching values of around 0.1, typical of foam materials. Other important characteristic of the bionanocomposite foams is the percentage of porosity, which is calculated from the relative density. These values are comparable amongst samples before the foaming processing, being around 75-79%. In the bionanocomposite foams, they are clearly higher reaching values of approximately 91%, which confirms the creation of a highly porous network. It is noteworthy that the relative density values are quite similar amongst foams independently of the nature of the filler and its content in the bionanocomposite (Table 5.1A and Table 5.1B). This fact may be related to the small amount of the inorganic counterpart incorporated in the zein matrix, which does not provoke an important

variation of these parameters, analogously to that reported by Wicklein et al. in studies on PVA-sepiolite nanocomposite foams (Wickein et al., 2013).

Table 5.1 Apparent (ρ*) and true density (ρ_s) values determined by He picnometry of bionanocomposite samples (A) before and (B) after processing as foams.

Pellets #	**(A)** starting bionanocomposite pellets			
	ρ* (g/cc)	ρ_s (g/cc)	Relative density	% Porosity
Z	0.289± 0.005	1.37 ± 0.09	0.210	79.0
ZNp3.5	0.311± 0.002	1.39± 0.03	0.223	77.6
ZNp7	0.345± 0.001	1.40 ± 0.05	0.246	75.3
Z-Sep3.5	0.313± 0.003	1.39 ± 0.06	0.225	77.5
Z-Sep7	0.345± 0.003	1.41 ± 0.07	0.244	75.5
Z-SepNp3.5	0.336± 0.003	1.39 ± 0.06	0.241	75.9
Z-SepNp7	0.333± 0.019	1.43 ± 0.11	0.233	76.7
Foams#	**(B)** bionanocomposite foams			
	ρ* (g/cc)	ρ_s (g/cc)#	Relative density	% Porosity
Z	0.125± 0.011	1.30 ± 0.03	0.096	90.0
ZNp3.5	0.116± 0.004	1.27± 0.11	0.091	90.8
ZNp7	0.130± 0.001	1.39± 0.04	0.093	90.6
Z-Sep3.5	0.115± 0.009	1.26± 0.03	0.091	90.8
Z-Sep7	0.125± 0.010	1.40 ± 0.05	0.092	90.7
Z-SepNp3.5	0.117± 0.001	1.25± 0.11	0.093	90.6
Z-SepNp7	0.122± 0.012	1.32 ± 0.06	0.092	90.7

#the numbers in the code samples indicate the percentage of filler in the final composition of the foam.

In spite of the porosity of foams is very similar amongst bionanocomposites, the size of pores may significantly change depending on the kind of filler incorporated in the zein matrix. In this sense, mercury intrusion porosimetry was employed in order to investigate the porous distribution in the bionanocomposite foams containing 7% of filler (Figure 5.5). Indeed, all the studied samples showed the presence of macropores, but different pore distribution profiles were observed in foams containing different type of filler incorporated in the zein. The foams based on pure protein exhibit a macroporous structure with a wide distribution of pores, showing a maximum at 1.43 μm. However, when zein is loaded with Sep, the corresponding Z-Sep foam shows a macroporous structure characterized by the presence of three principal populations of

pores with mean diameters centred at 150.0, 6.0 and 2.4 μm. A multi-modal distribution of pore diameters was also observed in foams incorporating magnetite-oleic acid Np, appearing three major mean pore diameters at around 100.0, 8.8 and 1.4 μm, although the total pore volume was similar to that of Z-Sep foams. Interestingly, foams based on Z-SepNp bionanocomposite show a very different profile of the porous size distribution in the 0.1-60 μm range, with a majority of pores diameters centred at 9.0 and 2.5 μm. Such distribution, indicative of a greater homogeneity of this foam, could be attributed to the fact that nanoparticles in this case are well dispersed as they are supported on the sepiolite fibers. The total pore volume in Z-SepNp foam materials is higher than in the zein bionanocomposite foams filled with pure Sep or Np, and it can be associated with a highly connected porosity that could facilitate the accessibility of mercury. Another remarkable effect of the microstructure in zein bionanocomposite foams afforded by the presence of the filler is associated with the increase of mesopores in the 8 to 3 nm range. The increasing of mesoporosity when the filler is present was also observed by other authors, and it could indicate that in our case, the presence of Np, Sep or SepNp avoids the collapse of the microcellular texture when the zein foam is formed. This feature could be a relevant characteristic in the resulting materials for certain applications, as for instance pollutants uptake, since as the presence of mesopores affords a high internal reactive surface area, while the facile molecular transport through broad "highways" the porous network is facilitated by the interconnected macropores (Darder et al., 2011; Wicklein, et al., 2013).

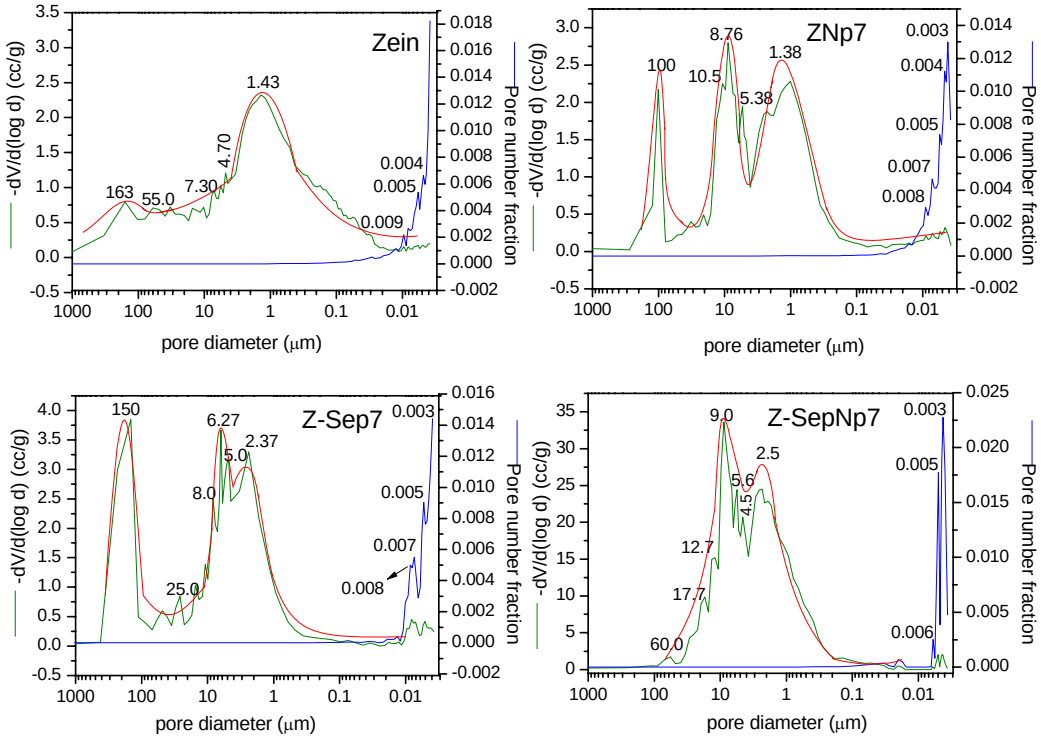

Figure 5.5 Pore size distributions determined from Hg intrusion in (a) pure zein, (b) Z-Np, (c) Z-Sep and (d) Z-SepNp bionanocomposite foams.

Specific surface area (S_{BET}) deduced from BET N_2 adsorption isotherms were determined in the prepared bionanocomposite foams and are summarized in Table 5.2. The specific surface area determined for the pure zein foam was 5.8 m^2/g, while bionanocomposite foams based on Np and SepNp yielded higher S_{BET} values of 10 and 11 m^2/g, respectively. However, a slight decrease in the specific surface area is determined in the Z-Sep7 foam (5.33 m^2/g). In fact, this value is lower than the theoretical value calculated for a simple physical mixture of sepiolite and zein, where the contribution of 7% w/w of the Sep filler would be 27 m^2/g. This result points out to the existence of interaction between both counterparts in the foam, possibly involving the ionic groups from the protein and the silanol groups located at the external surface of the silicate, as discussed in the Chapter 4 of this Thesis. The fact that the materials based on magnetic nanoparticles (Np and SepNp) show a higher surface available for interaction with other compounds may be beneficial in view to the retention properties of these foams. The average size of mesopores determined from the BJH (Barrett-

Joyner-Halenda) isotherms was in the range of 15-3 nm for these samples, which agrees with the results deduced from the Hg porosimetry measurements.

Table 5.2 Specific surface area (S_{BET}) of foams based on pure zein and zein bionanocomposite foams loaded with 7% of Np, Sep and SepNp fillers.

Foams	Specific surface area (m^2g^{-1})
Pure zein	5.87
Z-Np7	10.0
Z-Sep7	5.33
Z-SepNp7	11.0

In all cases, the FE-SEM images of zein bionanocomposite foams (Figure 5.6) displayed a distinctive multi-modal distribution of pores composed of very large pores around 100 μm and many other pores of few microns, in agreement with the porous size distribution determined by Hg porosimetry. As discussed above, it is presumed that these pores can be preferentially generated in the foaming process when the alcohol-treat pellet is immersed in water to provoke its swelling. Similar morphologies with the coexistence of pores of different sizes have been reported in the literature in foams prepared from varied polymer-solvent systems (Gutiérrez et al., 2007; Wicklein, et al., 2013). However, it should be indicated that, here, each zein bionanocomposite foam shows also a particular morphology depending on the kind of filler incorporated into the zein matrix. Thus, Z-Np bionanocomposite foams (Figure 5.6 a - c) show a non-homogeneous texture, where it is possible to distinguish the presence of Np filler domains, as indicated by the white arrows in Figure 5.6 a and b. In addition, the resulting microcellular structure of the bionanocomposite loaded with 7% of Np seems to be very similar to that of the foam prepared with pure zein, which would suggest a poor dispersion of the Np in the protein matrix. These observations could also explain the observed similarity in the pore distribution and the specific surface area of foams based on pure zein and on Z-Np bionanocomposites. In contrast, bionanocomposite foams containing sepiolite (Sep) or sepiolite assembled to magnetite nanoparticles (SepNp) show important differences in the cell microstructure compared to the pure zein foam. Z-Sep bionanocomposite foams show a more uniform porous texture, with pore sizes ranging from several micrometers to hundred of nanometers (Figures 5.6 d -

f). In contrast to the pure zein foam, the Z-Sep foams show a porous cell wall where it is possible to distinguish the presence of the microfibrils of clay homogeneously dispersed within the zein matrix (Figure 5.6 f). Z-SepNp bionanocomposites foams show also a good dispersion of the SepNp filler into zein, being not possible to observe segregation of the filler (Figures 5.6 e - h). This fact can be associated with the fact that the magnetite-oleic acid Np was previously assembled to the sepiolite fibers, improving so their compatibility with zein, as occurs in Z-Sep foams samples. In addition, a homogeneous and uniform distribution of macropores is also observed in Z-SepNP foams, with most of the pores below 10 μm, in accordance to the Hg porosimetry measurements. Furthermore, it is also possible to appreciate the presence of the SepNp filler intergraded in the foam matrix, confirming a good compatibility between this filler and zein (Figure 5.6 i).

The results discussed above seem to indicate that the incorporation of inorganic nanoparticles of different nature within the zein biopolymer matrix affect somehow the foaming process, resulting in the development of inhomogenous porous architectures in the final bionanocomposites foams. Indeed, the higher affinity between zein and sepiolite allows a more uniform distribution of this filler as well as its magnetic derivatives within the zein matrix. It should be remarked that the homogeneity as well as the differences in the interconnected porous structure of these bionanocomposite foams have to be considered as relevant in view to explain differences in the structural and functional properties of these materials.

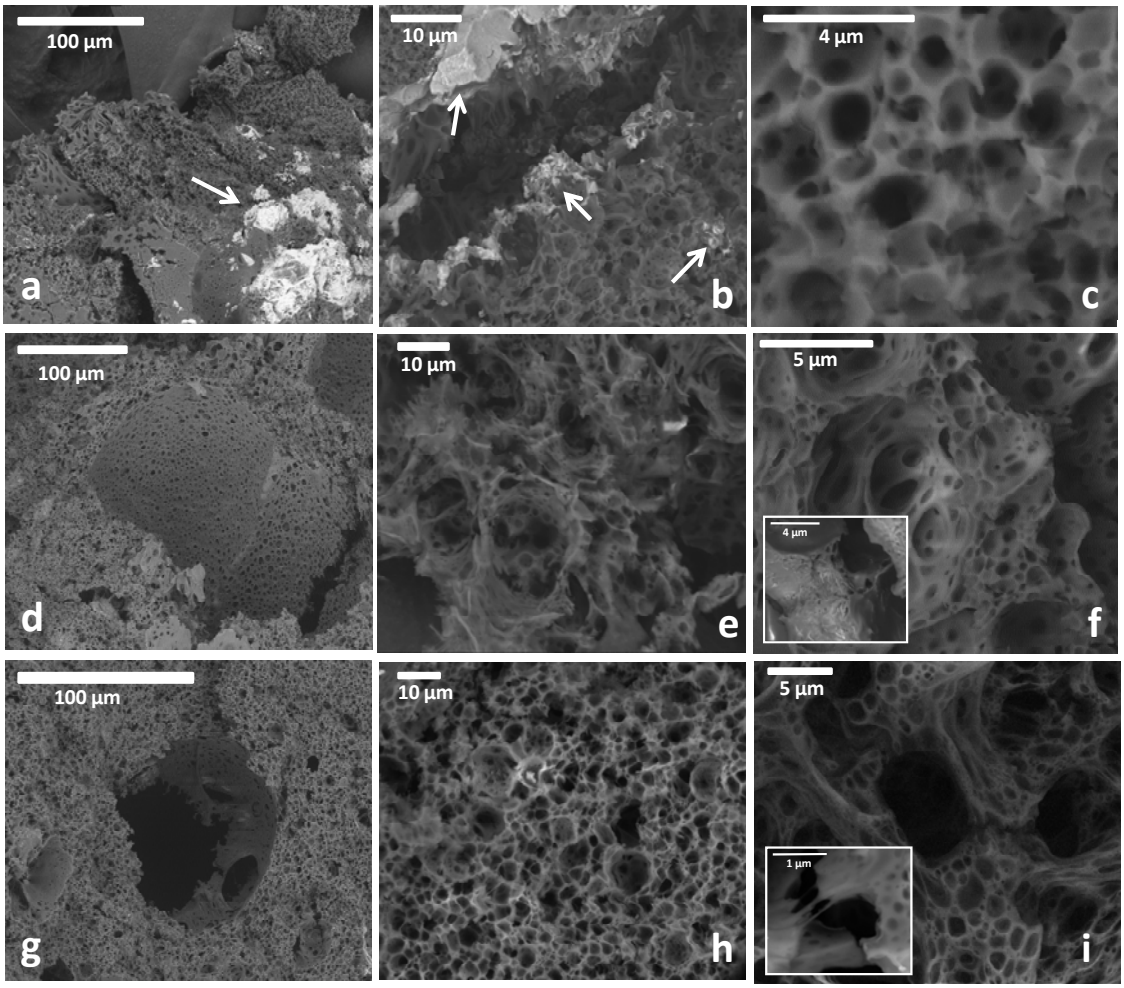

Figure 5.6 FE-SEM images of (a–c) Z-Np, (d–f) Z-Sep and (g-i) Z-SepNp bionanocomposite foams containing 7% of filler. Arrows in a and b images indicate segregated Np material. Insets in f and i images show part of the foams at higher magnification.

The mechanical properties of the bionanocomposite foams were evaluated by measuring the compressive strength of various foams with different amount and type of filler incorporated in the zein matrix. The compressive modulus (E) indicates the capacity of a material or structure to withstand axially directed pushing forces. Figure 5.7 shows the compressive modulus of the zein foams loaded with 0, 3.5 and 7% of Np, Sep and SepNp as nanofillers. The foam based on pure zein shows a compressive modulus of approximately 15 MPa. This modulus is slightly lower in foams based on Z-Np bionanocomposites, reaching values of around 13.5 and 12.0 MPa for bionanocomposites incorporating 3.5 and 7% of magnetite-oleic acid nanoparticles, respectively. This behavior is likely due to two main reasons. The first one is related to

the low homogeneity of these foams as evidenced in the FE-SEM pictures (Figure 5.7 a - c), which could provoke tension points in the foam porous network, weakening the material. The other key point can be associated with the presence of oleic acid assembled to these magnetic nanoparticles, which may act as a plasticizer in the bionanocomposite, affecting the mechanical properties of the foams and provoking a small decrease in their compressive modulus. The role of oleic acid as plasticizer in zein was already reported by Padua and co-authors, proving the existence of strong interactions between both components (Lai and Padua, 1997; Wang et al., 2005).

Conversely, a reinforcement effect of sepiolite is clearly observed in foams based on the Z-Sep bionanocomposite, with increasing values as the amount of sepiolite increases. Thus, clay loadings of 3.5 and 7% lead to compressive values of 16 and 19 MPa, respectively. The improved Young`s modulus in Z-Sep foams was expected, since these foams showed a good dispersion of the fibrous clay in the cell walls. In addition, in the present case, the influence of porosity in the mechanical properties appears to be practically null, since porosity is very similar amongst all the studied systems, which supports the idea that the reinforcement effect could be mainly attributed to the presence of sepiolite fibers in the bionanocomposite foam. The compressive moduli of foams prepared from Z-SepNp bionanocomposites show lower values compared to the Z-Sep based foams. This decrease is probably related to the presence of oleic acid in the nanofiller, as discussed above. In spite of this, these foams show a reinforcement effect due to the sepiolite, and the bionanocomposite foam that contains 7% of SepNp filler shows a Young´s modulus very close to that of the bionanocomposite foam comprising 3.5% of Sep (around 16 Mpa). This behavior can be attributed to a real contribution of the clay present in the SepNp filler, which in fact is composed of approximately 50% of sepiolite and 50% magnetite-oleic acid Np, which represents a sepiolite content of 3.5% in the bionanocomposite containing 7% of SepNp nanofiller. The role of sepiolite in this reinforcement effect can be related to the existence of interactions between the silanols of the sepiolite surface and the protonated amino groups from the protein, as discussed previously in the Chapter 4 of this Thesis and reported elsewhere (Alcântara et al., 2012).

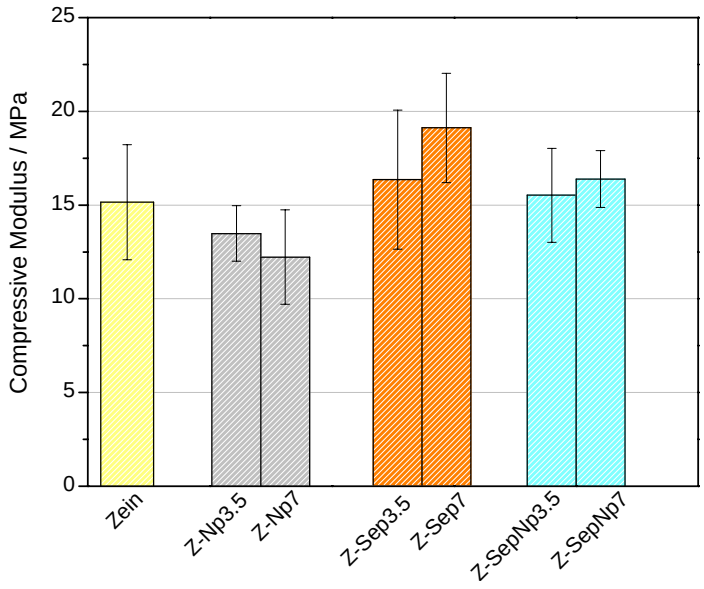

Figure 5.7 Compression moduli of foams based on pure zein and zein bionanocomposites loaded with 3.5 and 7% of magnetite-oleic acid Np, Sep and SepNp.

The thermal stability of foams based on zein bionanocomposites loaded with 7% of filler were investigated from TG/DTA curves recorded in the 25 – 700ºC range, under air flow conditions (Figure 5.8). In all cases, the TG profiles are very similar, presenting in the range between 25 and 200ºC a weight loss associated with the removal of water molecules physically adsorbed. Heating at temperatures higher than 200ºC produces some mass loss events in the foams based on zein and zein loaded with magnetic nanoparticles, which are related to different exothermic processes as evidenced in the corresponding DTA curves. The weight loss between 200 and 350ºC is related to the partial decomposition of the biopolymer in the case of the Z-Np and Z-SepNp foams, together with the elimination of oleic acid assembled to the magnetite nanoparticles. In contrast, foams based on the bionanocomposites loaded with pure sepiolite (Z-Sep) shows only an exothermic peak around 344ºC in the range of 200-350ºC, which indicate an increase in the thermal stability of these materials compared to those based only on zein or zein loaded with Np. The exothermic processes at temperatures above 400ºC observed in all the samples can be attributed to the final decomposition of the biopolymer (Alcântara et al., 2010).

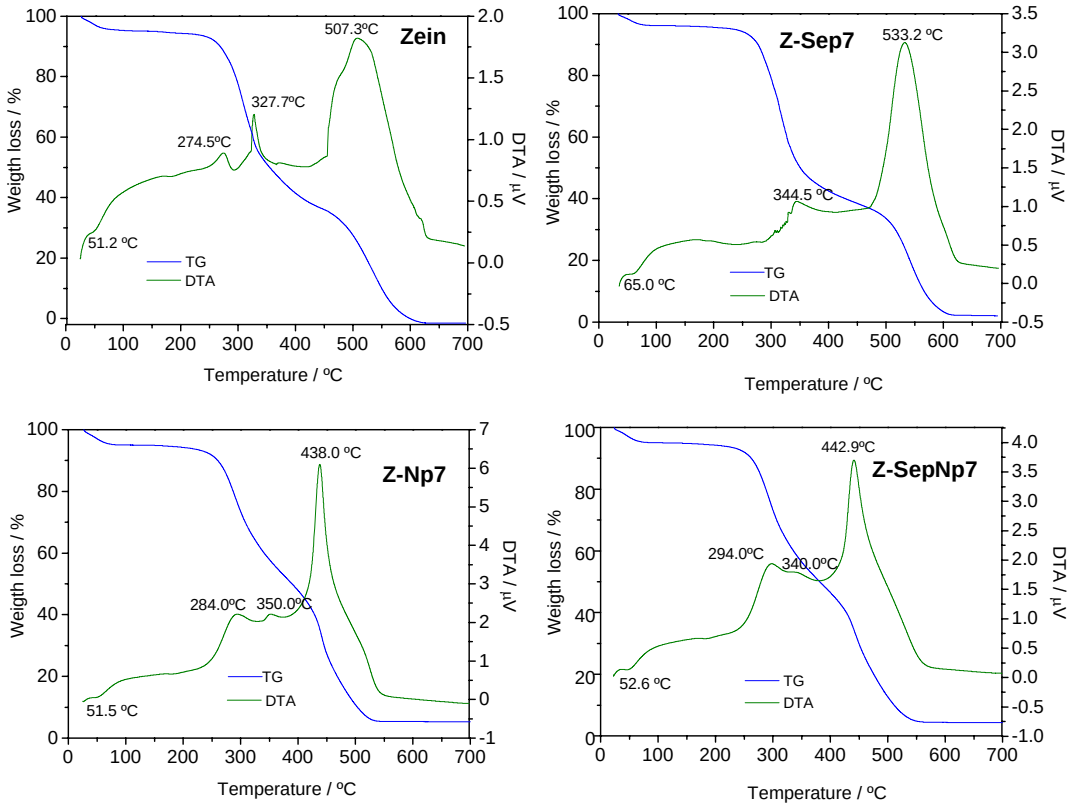

Figure 5.8 TG and DTA curves (under air flow) of foams based on pure zein and zein bionanocomposite loaded with 7% of Np, Sep and SepNp.

The magnetic properties of the bionanocomposite foams prepared with 7% of Np and SepNp filler were characterized using vibrating sample magnetometry (VSM) at room temperature, and the corresponding curves are presented in Figure 5.9 a. It is observed that both Z-Np and Z-SepNp based foams show hysteresis loops typical of a superparamagnetic response, similar to the starting magnetic particles (González-Alfaro et al., 2012) incorporated in the bionanocomposite, which indicates that Np and SepNp remain non-agglomerated once incorporated in the zein matrix, thus keeping the superparamagnetic properties. Anyway, taking into account that the magnetization value is represented by emu per gram of total material in Figure 5.9 a, and that in these systems the magnetic response is ascribed only to the magnetite nanoparticles, the observed decrease of the magnetization saturation in the Z-SepNp7 and Z-Np7 foams is clearly due to the low content in magnetic material in the foams. However, the decrease is slightly lower to that expected for a 7% of Np or SepNp content. In fact, the magnetic response of Np and SepNp was estimated about 6.8 and 4.1, respectively, in previous studies (González-Alfaro et al., 2011). However, in this case the values are 4.4

and 3.1, respectively (Figure 5.9 a). These discrepancies may be related to their partial oxidation of the magnetite Np to form maghemita Fe_2O_3 (Zheng et al., 2005) during the foam formation, perhaps facilitated by a partial removal of oleic acid from shell. The picture of Z-SepNp7 (Figure 5.9 b) shows the magnetic attraction of this bionanocomposite foam by a magnet.

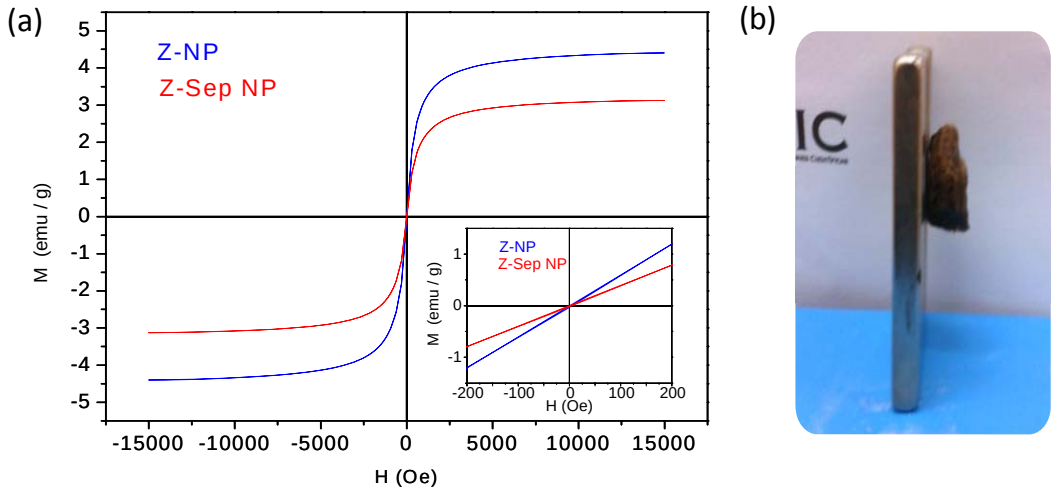

Figure 5.9 (a) Magnetization curves at room temperature of foams based on Z-Np and Z-SepNp bionanocomposites loaded with 7% of Np and SepNp, respectively; (b) Picture showing the Z-SepNp7 foam attracted by a magnet.

5.2 ZEIN-SEPIOLITE BIONANOCOMPOSITE FOAMS AS ADSORBENTS FOR HERBICIDE REMOVAL

The widespread use of pesticides in agriculture and other activities increases the presence of these chemical substances in soils and groundwater, becoming a serious environmental problem. Pesticides are generally applied in higher doses than those required for the control of pests and the excess reaches soils and groundwater due to transport processes such as leaching, runoff, etc. (De Wilde et al., 2007). Several adverse effects of pesticides on human health/animal were reported in the literature, which include teratogenesis, oncogenesis, mutagenesis, hemotoxic and neurotoxic effects, endocrine disorders, among other unwanted reactions (Maroni, M and Fait, A. 1993; Cardoso et al., 2006; Undabeytia et al., 2008). In this sense, adsorption processes are generally known to be one of the most effective techniques for removal of these

environmentally hazardous pollutants. On the other hand, biosorption processes using cheap and biodegradable materials, are currently considered as a desirable technological and ecological alternative in water treatments. In this area, bionanocomposite foams become an attractive material for the removal of pollutants or harmful compounds. A recent example of this use of macroporous bionanocomposite foams based on locust bean gum (LBG) and a layered silicate in the removal of dyes from water (Instituto de Ciencia de Materiales de Madrid (ICMM). http://www.icmm.csic.es/divulgacion/posters/ARQUITMateriales%20Hibridos.pdf, accessed May, 2013; Padilla-Ortega et al., 2012).

In the present study, the porosity of the prepared zein-based foams was profited, together with the biodegradability and the functionalities afforded by the protein, for application as biosorbents. Besides being environmentally friendly, these porous materials provided with magnetic properties result in a new type of the so-called magnetosorbents (Machado et al., 2010), which show the advantage of a rapid recovery from the aqueous medium with the help of an external magnetic field. Considering these premises, the zein-based foams here developed were evaluated in the removal of an herbicide present in aqueous medium. For this study, the above prepared and characterized foams based on zein bionanocomposites loaded with 7% w/w of Np, Sep and SepNp were selected for retention of (4-chloro-2-methylphenoxy)acetic acid (MCPA) herbicide (Figure 5.10). This herbicide was chosen as model due to its organophilic character and its widespread use.

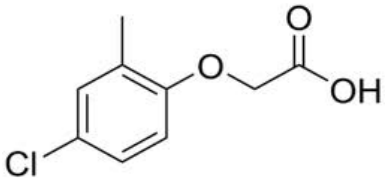

Figure 5.10 Chemical structure of the MCPA herbicide.

- *Stability of foams based on zein bionanocomposite in water*

As the zein foams have to be used in aqueous media, the first study was the evaluation of the stability of the different foams in water. In this way, the foams were immersed during 1 month in water, and then dried and weighted. The weight loss of each foam after this treatment (Figure 5.11) was analyzed considering the foam

composition. In general, it is observed that the stability of the foam in water increases with the content in nanofiller. Thus, the foam based on pure zein shows a mass loss around 8.5%. A slight improve of the water stability is observed in foams based on zein incorporating magnetic-oleic acid Np. However, the increase in stability in water is still more accused by when the bionanocomposite incorporated sepiolite, with weight losses below 5% in both Z-Sep and Z-SepNp foam systems. This behavior can be associated with the existence of interactions between both components and with the good distribution of the nanofiller, as commented previously (Chapter 4). The increase in the water stability of bionanocomposites containing sepiolite was also recently reported in the case of PVA-sepiolite foams (Wickein, et al., 2013) and polysaccharide-fibrous clays films (Alcântara et al., *submitted*). It is worth to mention that the mass loss values determined in the foams prepared in the present work are considerably smaller when compared to those of systems based on chitosan or PVA, probably because these last polymer matrices contain more hydrophilic chains which are very sensitive to water, being possible to reach their total solubilization in contact with water. Therefore, porous systems based on zein may be advantageous for the intended use of removal of pollutants in water since this is a hydrophobic protein highly stable in water.

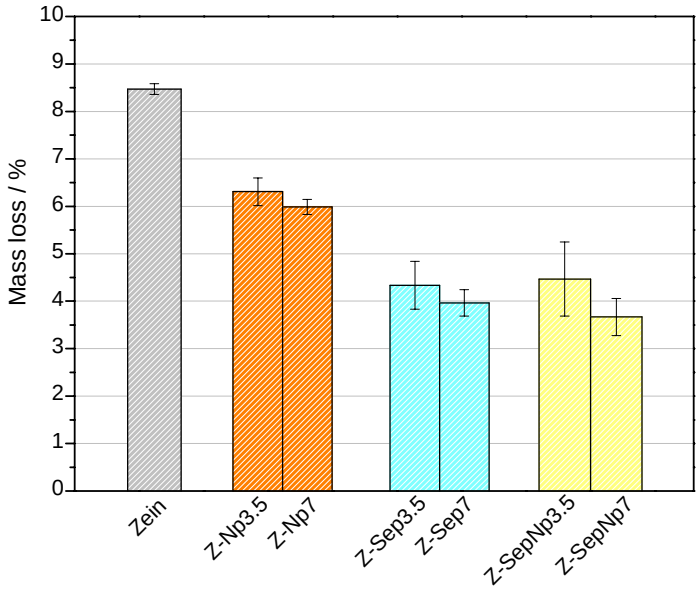

Figure 5.11 Variation of the mass of foams based on zein bionanocomposites after one month of immersion in pure water (pH 5.5).

Evolution of water as a function of time of immersion of the zein bionanocomposite foams incorporating 7% w/w of nanofiller is displayed in Figure 5.12. It is clear that the water absorption properties of the foams are clearly influenced by the type of filler present in the bionanocomposite, although in all cases water content increases with the time of immersion to the water till reaching a plateau. Foams loaded with Np and SepNp show a similar water absorption than the neat zein foam, being observed a slight reduction in the water uptake values at the plateau for the foam based on Z-SepNp. Conversely, foams based on the Z-Sep bionanocomposite present water uptake value approximately twice higher that of neat zein at the plateau region. These different behaviors can be likely associated with the intrinsic hydrophilic/hydrophobic nature of the involved bionanocomposite, and probably also with the degree of dispersion of the nanofiller within the protein matrix. However, it cannot be discarded that the presence of oleic acid molecules associated with the magnetite Np may provide the foam with extra hydrophobicity.

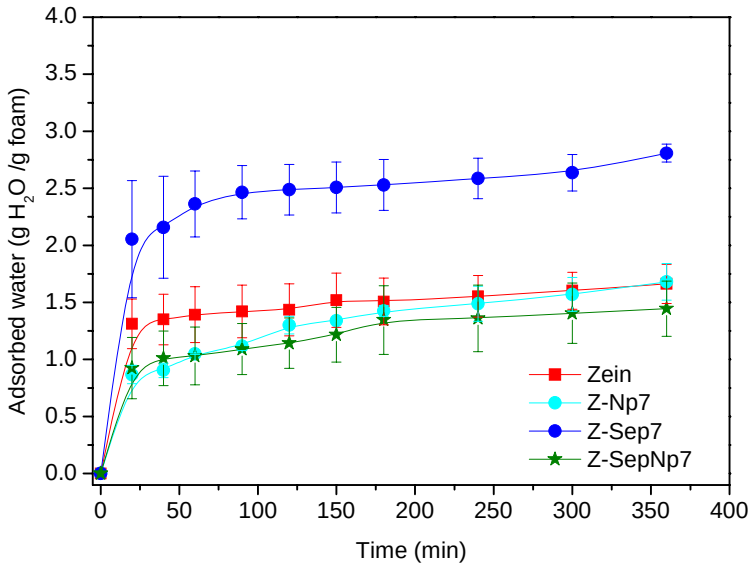

Figure 5.12 Water absorption of the zein bionanocomposite foams loaded with 7% w/w of Np, Sep and SepNp.

- *Herbicide uptake by zein bionanocomposite foams in aqueous media*

Foams based on zein bionanocomposites with 7% w/w in Np, Sep and SepNp as filler were selected to evaluate their ability in the retention of the MCPA herbicide in aqueous solution. Prior to the systematic absorption studies, a kinetic experiment was conducted in order to determine the optimal conditions regarding the contact time for adsorption of MCPA on the selected foams. The kinetic study (Figure 5.13) was performed using four different initial concentrations of herbicide (0.005, 0.1, 0.5 and 1 mmolL^{-1}). At low initial concentrations of MCPA (Figure 5.13 a and b), the foams show a tendency to reach the adsorption equilibrium state more rapidly (around 24 h) than when higher initial MCPA concentrations are used. The kinetic curves show that for the highest concentrations (0.5 and 1 mmol L^{-1}) the foams reach the equilibrium only after a contact time of approximately 48-72 h (Figure 5.13 c and d), with no significant changes in the adsorbed amount at longer times. To be sure that the equilibrium was reached, a contact time of 72 h was used in the adsorption study.

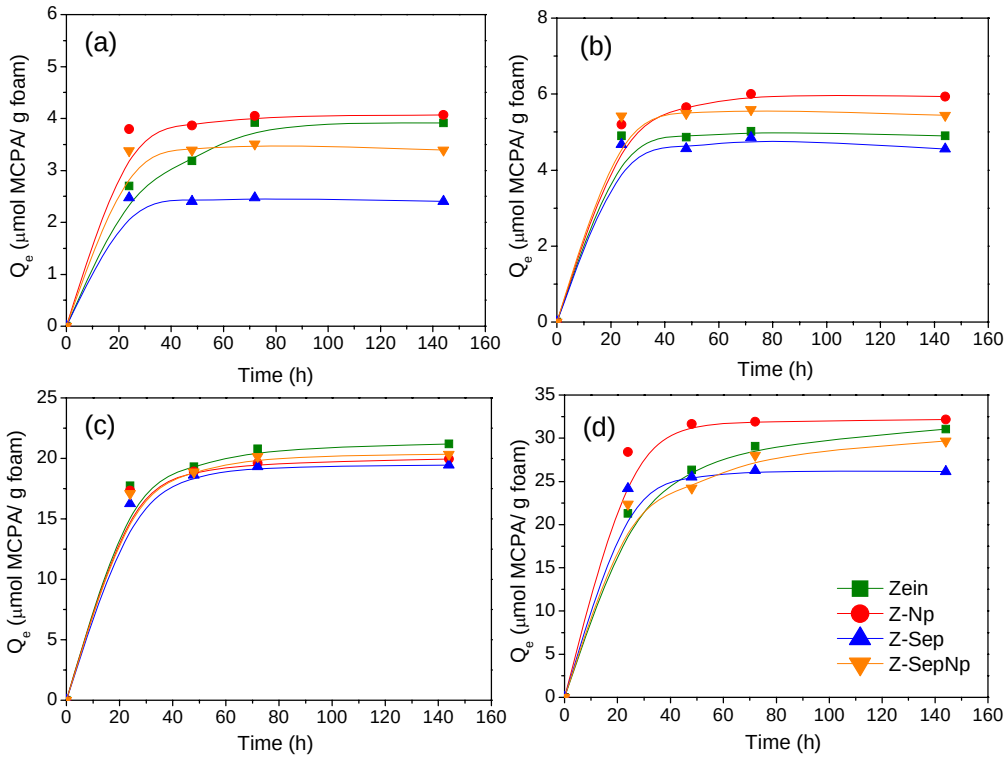

Figure 5.13 Kinetic study of MCPA adsorption of various foams from initial herbicide concentrations of (a) 0.05, (b) 0.1, (c) 0.5 and (d) 1 mmol/L. Experiment performed using 20 mL of MCPA solution and 50 mg of foam.

Adsorption isotherms of MCPA on the zein based foams are displayed in Figure 5.14. From these isotherms, it is clear that zein bionanocomposite foams show good adsorbent properties for this herbicide. For the sake of comparison, pristine Np, Sep and SepNp fillers were also tested as adsorbents, but the obtained retention values were negligible. In a general way, the adsorption isotherms resemble to a Langmuir isotherm (Giles et al., 1960), where the adsorption herbicide profile seems very similar amongst the bionanocomposites foams. From the inset in Figure 5.14, it is observed that at lower equilibrium concentrations (below 0.1 mmol L^{-1}), practically a complete adsorption of the herbicide takes place in the foams based on Z-Sep and Z-SepNp bionanocomposites.

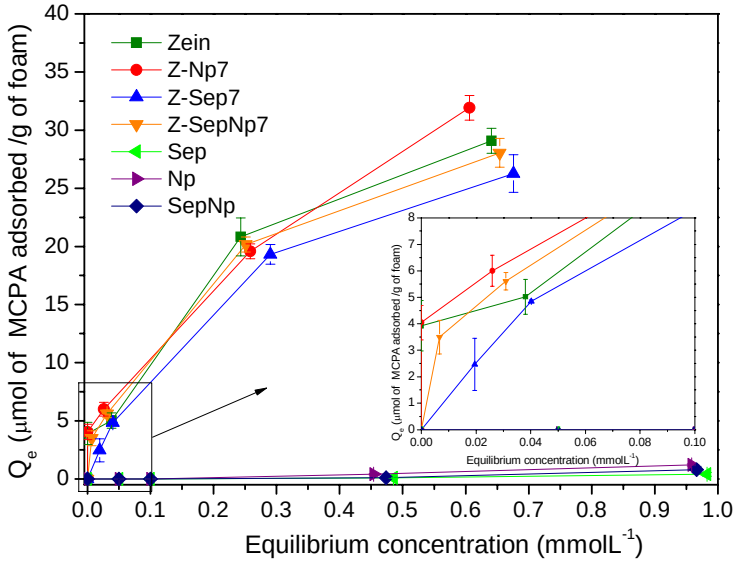

Figure 5.14 Adsorption isotherms of MCPA on zein-based bionanocomposite foams and neat Sep, magnetite-oleic acid Np, and SepNp.

Comparing the performance in herbicide retention, the different foams show close values of adsorbed MCPA ranging between 25 and 33 µmol g^{-1}. This behavior indicates that the MCPA adsorption is mainly ascribed to its affinity towards zein, and the small differences among the foams could be related to their different textural properties and the presence of the fillers. It is noteworthy that the small content of filler incorporated in the foam matrix affords other interesting features, like improved water resistance and magnetic properties in some cases, but it does not cause drastic changes in the adsorption capacity of zein.

The adsorption data on different foams (isotherms in Figure 5.14) were analyzed according to the Langmuir equation (eqn. 5.1):

$$\Gamma = \frac{b x_m C_s}{1 + b\, C_s} \qquad \text{eqn. 5.1}$$

where Γ is the adsorbed amount of MCPA, b the affinity constant between the herbicide and the foam material, x_m the maximum adsorbed amount, and C_s the equilibrium MCPA concentration. The parameters calculated from the fitting of the experimental values to this equation are reported in Table 5.3.

Table 5.3 Parameters calculated from the fitting of experimental data of MCPA adsorption on zein based on bionanocomposite foams to the Langmuir isotherm model.

Samples foams	x_m (μmol g^{-1})	b (L $mmol^{-1}$)	r^2
Zein	40	4.30	0.9746
Z-Np7	52	2.63	0.9636
Z-Sep7	36	3.87	0.9999
Z-SepNp7	35	5.97	0.9907

The affinity of zein for MCPA could be mainly attributed to the hydrophobic character of the zein and the presence of aromatic groups in some of its aminoacid residues, but the availability of amino functional groups in zein to interact with the MCPA molecule trough its carbonyl groups (Figure 5.10) should be also taken into account.One of the possible reasons for the small differences in the maximum adsorbed values of MCPA could be related to the influence of sepiolite in the Z-Sep and Z-SepNp bionanocomposite foams on the S_{BET} (Table 5.2), due to interactions between the clay and the biopolymer that may decrease the number of sites available for MCPA adsorption. On the other hand, the presence of oleic-acid associated with the magnetite nanoparticles present in foams of the Np and SepNp bionanocomposites, could also contribute as binding sites for the herbicide adsorption. Thus, these could be the reasons of the slight increase in the retention capacity of foams incorporating magnetite-oleic acid Np, showing a maximum adsorption value of 52 μmol g^{-1}, and the

decrease in those foams containing sepiolite, which yielded adsorption values of 35 or 36 μmol g^{-1}.

When comparing the results obtained in this study with those reported for other bionanocomposite and bio-hybrid systems, they can be considered satisfactory and quite similar in relation to the retention of herbicides. For instance, chitosan-montmorillonite and montmorillonite modified with thioflavin-T (TFT) materials have been used for clopyralid (Celis et al., 2012) and norflurazon (Undabeytia et al., 2010) herbicide adsorption, respectively, reaching in some cases a efficiency of around 38 - 90 μmol g^{-1} for different compositions and 7 μmolg^{-1}, respectively, which allows to envisage application of the here reported zein-based bionanocomposite foams as biosorbents for environmental remediation.

Desorption experiments were conducted in order to check the possibility of reuse the foams in new adsorption experiments. The study of MCPA desorption from the zein foams was carried out with those samples resulting from the adsorption of MCPA at an initial concentration of 0.1 mmol L^{-1}. Thus, the supernatant solution was replaced by pure water or 70/30 (v/v) water/acetone solution, according to the procedure described in the experimental section (Chapter 2, § 2.35). The respective leaching media were selected considering the stability of the zein materials in these solvents. Figure 5.15 shows the desorption curves of MCPA from the foams as a function of time in contact with water or 70/30 (v/v) water/acetone. A different behavior is evident depending on the solvent employed in the desorption process. In all cases, the MCPA release in water is very slowly, reaching low percentages of desorption (<15%) even after 70 hours (Figure 5.15 a). This behavior is even more accused in the case of the Z-Np foam, where the maximum desorption value is around 7%. This fact can be related to the highly hydrophobic nature of this foam, which limits the entry of water hindering the desorption of MCPA in this medium. Conversely, the use of water/acetone solutions improves the MCPA desorption (Figure 5.15 b), making possible to reach a maximum desorption of around 50% and 75% for the foams based on Z-Np and Z-Sep bionanocomposites, respectively, after 70 hours. The MCPA desorption seems to be favored by the presence of the acetone, most likely due to the improved solubility of the herbicide in this solvent. Thus, it would be interesting the use of other solvents, which could provoke a higher herbicide release allowing the foam available for reuse in a new adsorption cycle.

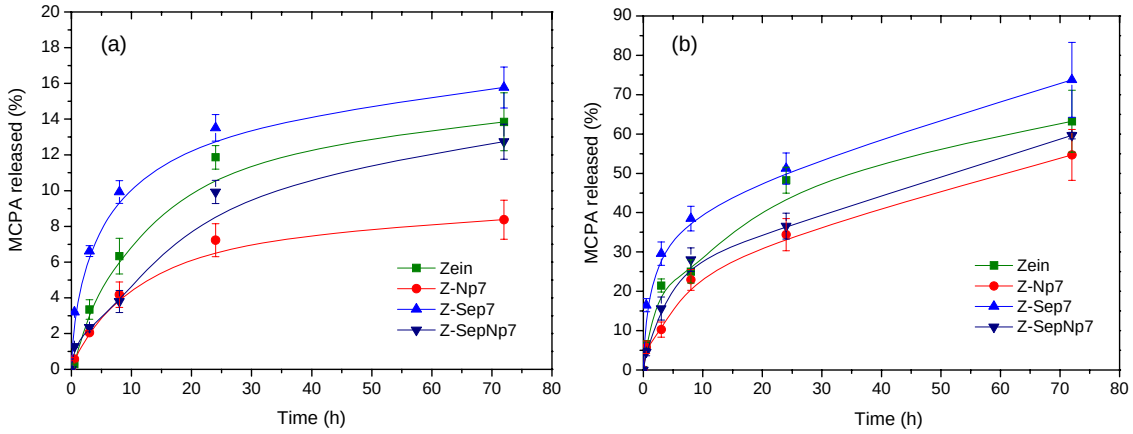

Figure 5.15 Curves of the evolution of the MCPA desorption from zein bionanocomposite using (a) pure water (pH 5.5) and (b) of a 70/30 (v/v) water/acetone solution.

It is also worth mentioning that in the case of foams based on Np and SepNp bionanocomposites the superparamagnetic properties can be profited for their easy separation from the aqueous medium. As shown in the Figure 5.16, when a magnet is placed near the foam this is attracted and can be than easily removed from the solution. The present properties make these bionanocomposites very attractive as bio-magnetosorbent porous materials for application in environmental remediation, considering also the good mechanical properties and the improved resistance in water achieved by these bionanocomposite foams based on low cost materials.

Figure 5.16 Picture showing the superparamagnetic properties based on Z-SeNp7 bionanocomposite from the aqueous media by applying an external magnetic field (a Nd magnet, in this case).

5.4 CONCLUDING REMARKS

The systematic study carried out shows the possibility to prepare zein-based bionanocomposite foams, reinforced with natural sepiolite fibrous clay, by a new, easy and ecofriendly foaming method. The novel porous materials can be provided with magnetic properties by using a sepiolite modified with magnetic nanoparticles instead of the neat sepiolite or by incorporating magnetite nanoparticles into the zein matrix. The existence of strong affinity between zein and the sepiolite-based fillers results in materials with good mechanical properties and improved water resistance, and in certain cases, the use of magnetite-based fillers introduces interesting superparamagnetic properties in the bionanocomposite foams. These materials offer interesting results for the retention of MCPA, tested as a model herbicide, which supports the potential use of these biocompatible and biodegradable functional bionanocomposites in environmental remediation.

CHAPTER 6

ZEIN-LAYERED HYDROXIDES

This Chapter constitutes a first exploration on the development of bio-hybrids based on zein and layered solids provided with positively charged layers, as it is the case of layered hydroxides. For this purpose, MgAl layered double hydroxide and the $Co_2(OH)_3$ layered simple hydroxide were chosen as hosts, and various approaches of synthesis were explored to attain the formation of the zein-layered hydroxide bio-hybrids. Both the synthesis procedure and the anion located in the interlayer region of the inorganic host material have a strong influence on the final features of the resulting bio-hybrids. The interest of the new resulting bio-hybrids based on zein-MgAl layered double hydroxide may be addressed to biomedicine, while those based on $Co_2(OH)_3$ layered single hydroxide could have potential application in magnetic and optical devices.

6.1 INITIAL CONSIDERATIONS

To the current date, the majority of publications in bio-hybrid materials employ clays, with preference on the montmorillonite aluminosilicate as inorganic counterpart. However, the use of other layered solids, such as layered metal hydroxides of the type of layered *double* hydroxides (LDH) and layered *single* hydroxide (LSH), is becoming more and more attractive due to their low cost, versatility and prominent applications in diverse field of interest (Rives, 2006). The possibilities to be prepared easily and by various synthetic approaches is an additional advantage for certain applications e.g. biomedicine. In this sense, diverse methods of synthesis, including direct anion-exchange and coprecipitation or "co-organized assembly", are usually employed in the preparation of the bio-hybrid materials based on LDH (O´Hare, 2002; Darder et al., 2005; De Roy et al., 2006). LDH show the special feature that they can be heated at moderated temperatures (300-500°C) to yield the corresponding mixed oxides, which may then recover their original structure after treatment with aqueous solutions containing anionic species (Rives, 2002). This property of layered double oxides (LDO) is very useful to incorporate organic species within the LDH structure. In this sense, several biopolymers, such as polysaccharides and other biomolecules, intercalated in LDH through the reconstruction method have been reported in the literature (Choy et al., 2004; Forano and Prevot, (2013).

In the case of protein molecules, the studies reported in the literature have been almost exclusively focused on the intercalation of certain amino acids (Aisawa et al., 2001; Nakayama et al., 2004) and short length peptides within the interlayer of LDH or LSH (Si et al., 2012). The synthesis of new bio-hybrid materials based on zein and layered hydroxides can be explored, taking advantage from the possibility of having negatively charged groups in zein when the pH of the solution is raised above its isoelectric point, as for instance by treatment in alkaline medium. Thus, the present chapter introduces the formation of bio-hybrids resulting from the combination of zein and a 2:1 MgAl-LDH and a $Co_2(OH)_3$ LSH, as well as the main results of the synthesis and physico-chemical characterization of these new zein-layered hydroxides. The resulting zein-based bio-hybrids could show potential interest, for instance in Biomedicine and Materials Science.

6.2 SYNTHESIS AND CHARACTERIZATION OF ZEIN-LAYERED DOUBLE HYDROXIDE BIO-HYBRIDS

Preparation of zein-layered hydroxide bio-hybrid materials has been addressed by different routes of synthesis in order to achieve zein intercalated in the LDH. In this way, a MgAl LDH containing different type of interlayer anions and zein protein solubilized in alkaline solution under different experimental conditions (submitted to magnetic stirring or ultrasonication) were tested with the aim to reach fully zein intercalated LDH solids.

- *Characterization of the zein solubilized in alkaline medium under ultrasonication*

As previously discussed, zein can be solubilized in alcohol solutions (Chapter 3, § 3.2.1) or in strong alkaline media (e.g. 0.1 M aqueous NaOH) (Chapter 3, § 3.2.3). In this last case, the treatment results in a deamidation reaction of the glutamine amino acid together with the possible formation of alkali salts of the phenolic-hydroxyl groups in tyrosine (Ofelt and Evans, 1949; Shukla and Cheryan, 2001; Cabra et al., 2007). Considering that alkaline media treatments ensure the presence of negative charges in the protein structure, this medium was selected for the solubilization of zein, and it is also favorable for the synthesis of many layered hydroxides (Auerbach et al., 2004). According to the electrophoresis results reported in Chapter 3 (§ 3.2.3, Figure 3.18), the treatment of zein in a basic medium breaks the protein in smaller fractions of protein size between 14 and 10 kDa, although the presence of Z19 and Z22 monomers and α-zein dimers was also evidenced. With the aim of promoting a greater number of smaller fractions of zein that can enter more easily in the interlayer region of the LDH, zein solved in 0.1 M NaOH was submitted to ultrasonication (US) treatment, applying an energy of 10, 30 and 60 kJ/0.5 g of zein with the help of an ultrasound tip.
Figure 6.1 shows the analysis of SDS-PAGE of the resulting alkaline-treated zein after being homogenized under different US energies. It is observed that the alkaline-treated zein samples disaggregated under energies of 10 and 30 kJ (Figure 6.1 a and b, respectively), show a very similar distribution of protein fractions, being also analogous to the one of alkaline-treated zein without using US (Chapter, § 3.2.3, Figure 3.18). The patterns show evidence of the typical bands ascribed to Z19 and Z22 as well

as to their respective dimers of around 37 and 50 kDa. Conversely, zein treated in alkaline medium but ultrasonicated at higher energies seems to suffer major changes. Thus, SDS-PAGE of the zein solubilized in 0.1 M NaOH and submitted to US treatment with 60 kJ of energy (Figure 6.1 c), shows the presence of the characteristic bands at 22 kDa and 20 kDa corresponding to the α-helix structure, as well as other bands between 15 and 10 kDa ascribed to the presence of smaller fractions of protein. In addition to the hydrolysis provoked under basic conditions (Zhang et al., 2011), the presence of small fractions of the protein may be also related to breakdown of protein aggregates by the high US energy employed in the solubilization process. Considering that the alkaline-treated zein under US using 10 and 30kJ of energy shows a very similar molecular mass distribution than zein treated in NaOH without US, this latter approach was chosen in the synthesis of zein-LDH bio-hybrids. In addition, the treatment in alkaline medium and applied US energy of 60 kJ was also selected for comparison, as this method provided the smaller zein fractions.

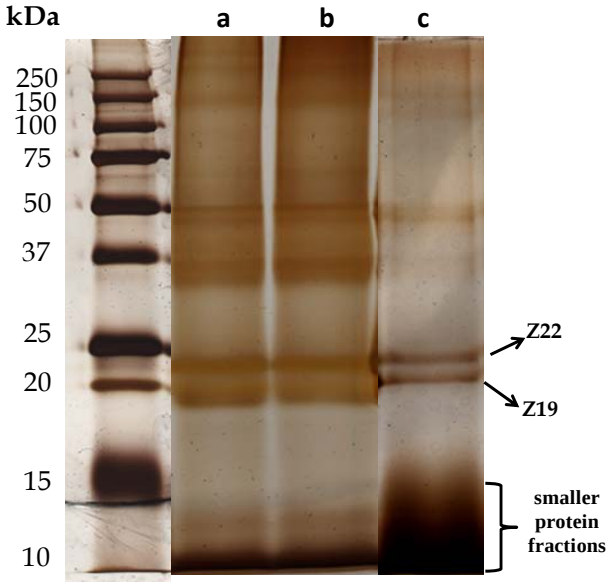

Figure 6.1 SDS-PAGE profiles in 20%acrylamide of zein after being dissolved in 0.1 M NaOH under US applying energy of (a) 10, (b) 30 and (c) 60 kJ/0.5 g of zein. The gel was silver stained.

FTIR spectra of the alkaline-treated zein with and without applying 60 kJ US are shown in Figure 6.2. Comparing both spectra, it can be observed that the band at 1663 cm^{-1} ascribed to the amide I is preserved in the zein treated under US (Figure 6.2 b), which indicates that the secondary structure of protein (α-helix) remains unaltered after the

US treatment, and corroborates so the SDS-PAGE results (Figure 6.1). In the spectrum of zein treated by magnetic stirring (Figure 6.2 a), the bands at 1529 cm^{-1} and 1446 cm^{-1} are assigned to amide II and amide III, respectively. However, they are slightly splitted in the spectrum of the zein treated under US (Figure 6.2 b), appearing new bands at 1580, 1538, 1441 and 1408 cm^{-1}. Thus, this behavior may be related to the effect of the high energy applied during ultrasonication. The ^{13}C NMR spectrum of this sample treated under US (Figure 6.3 b), shows the typical signals at 172.5 ppm assigned to carbonyl carbons, indicating that the presence of the α-helix structure is preserved, as pointed out in the FTIR results (Figure 6.2b). However, it can be easily observed the presence of a shoulder at 180 ppm, which evidences the changes in the zein structure when submitted to the US treatment.

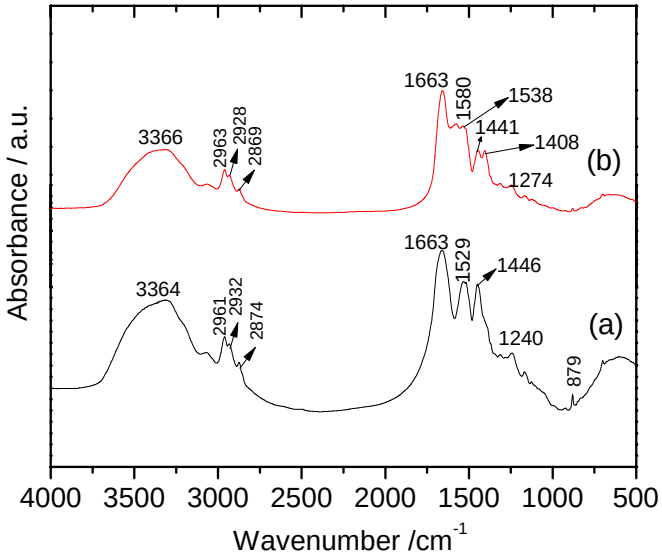

Figure 6.2 FTIR spectra (4000-500 cm^{-1} region) of the zein dissolved in 0.1 M NaOH by (a) magnetic stirring and (b) treated with US (60 kJ/0.5 g of zein).

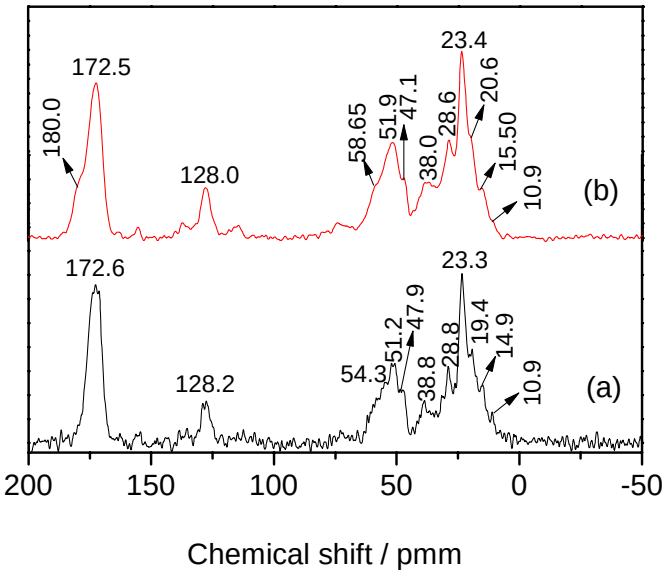

Figure 6.3 ^{13}C NMR spectra of zein dissolved in 0.1 M NaOH by (a) under magnetic stirring and (b) treated with US (60 kJ/0.5 g of zein).

Figure 6.4 shows FE-SEM images of the zein sample treated with 0.1 M NaOH under US. The images reveal a morphology quite analogous to the one of zein without US treatment (Chapter 3, Figure 3.20), being evident the presence of zein as layers. As discussed above, this morphology may be associated with the negative charges on the zein surface and the breakage in smaller fractions, which would favor the protein-water interaction, avoiding the presence of the typical agglomerates of this protein.

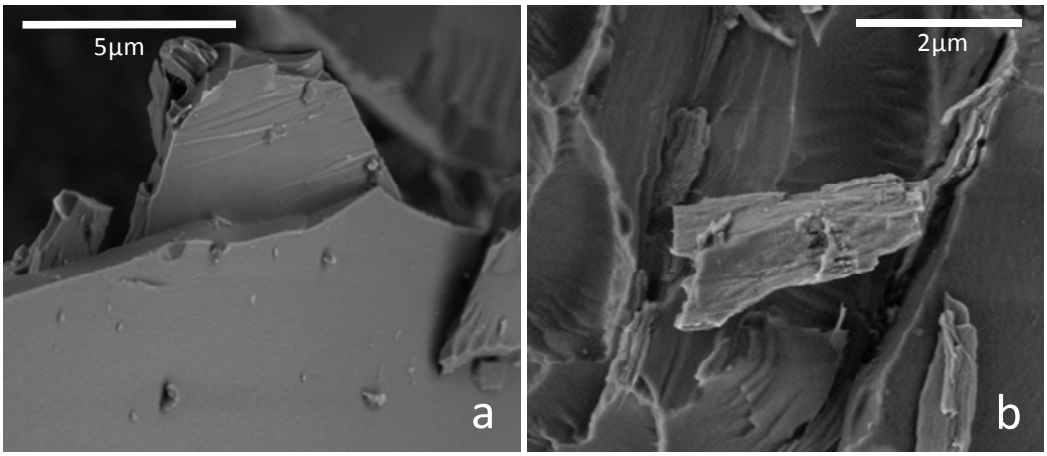

Figure 6.4 FE-SEM images of zein dissolved in 0.1 M NaOH by US (60 kJ/0.5 g of zein).

- *Zein-layered double hydroxides bio-hybrids*

A LDH based on Mg and Al metals in a 2:1 MgAl ratio containing chloride, nitrate or carbonate as interlayer anions were chosen, as they are probably the most studied LDH materials. Three different routes of synthesis were explored in view to prepare the corresponding zein-layered double hydroxide bio-hybrids (Z-LDH):

i) ion-exchange: this method attempted to achieve the replacement of the interlamellar anion from the LDH (Cl^- or NO_3^-) by zein in its anionic form.

ii) co-precipitation: in this case, the LDH was formed in the presence of the alkaline-treated zein by addition of aqueous solution of Mg^{2+} and Al^{3+}, maintaining the pH constant at 11 in view to achieve the co-precipitation of the LDH with the protein intercalated in its anionic form.

iii) reconstruction: the LDH was formed from the corresponding layered double hydroxide (LDO) mixed oxide obtained by calcination of MgAl-LDH, containing carbonate ions in the interlayer region, by addition of a solution containing zein in its anionic form.

6.2.1 Ion exchange method

In order to favor the incorporation of an anion by ion-exchange reaction, the new anion must stabilize better the solid, or it has to be in a very higher concentration to shift the equilibrium for replacing the anion in the precursor material. The major limitation of this method is the efficiency in the exchange, since when it is low, it may lead to the formation of co-intercalated materials or mixed phases (Cavani et al, 1991; De Roy, et al., 2006). In a first step, two Mg-Al LDH were synthesized with Cl^- or NO_3^- interlayer anion, MgAl-Cl and MgAl-Nit, respectively (Chapter 2, § 2.3.4). The MgAl-Cl and MgAl-Nit synthesized with a 2:1 Mg:Al ratio have as theoretical formula $[Mg_{0.67}Al_{0.33}(OH)_2]Cl_{0.33}\cdot nH_2O$ and $[Mg_{0.67}Al_{0.33}(OH)_2]_2(NO_3)_{0.33}\cdot nH_2O$, respectively. In both samples, the content of Mg and Al was analyzed by EDX in several areas of the solids and found that the Mg:Al ratio corresponds to that expected in the two compounds. Figure 6.5 shows the diffractograms of the starting LDH samples. The basal distances calculated by the Bragg's equation for MgAl-Cl (Figure 6.5 a) and MgAl-Nit LDHs (Figure 6.5 b) coincide with the values reported in the literature for the MgAl-LDH materials containing chloride and nitrate anions (De Roy et al., 2006). In

these same XRD patterns, it is possible to verify the purity of the obtained phases. The (*hkl*) Miller's indices in these samples can be assigned considering a hexagonal symmetry (Vaccari, 1998). The values of the crystallographic parameters were assigned considering this symmetry, being the *c* axis three times the distance between two adjacent layers (i.e. d_{003}), and the *a* axis the distance between two adjacent metal centers in a layer (two times the value of d_{110}). The *c* parameter determined for MgAl-Cl and MgAl-Nit is 2.3 and 2.4 nm, respectively, which implies that this solid is a three layers polytype (3R) corresponding to the rhombohedral symmetry with hexagonal unit cell (Vaccari, 1998). The polytypism occurs when compounds with the same chemical composition are organized identically in two dimensions, but differently in the third. In the case of LDH, this happens when the brucite-like layers can stack in different sequences generating structures that differ in the *c* crystallographic parameter (Vaccari, 1998). In the here prepared materials, the basal distances deduced from the interlayer distance of the (*003*) reflection are 0.77 and 0.82 for MgAl-Cl and MgAl-Nit, respectively.

The XRD patterns of the bio-hybrids prepared by ion-exchange reaction of Cl^- or NO_3^- by zein treated with 0.1 M NaOH under stirring and by US (Figure 6.5 a and b) show the characteristic (*012*), (*018*), (*110*) y (*113*) reflections, indicating the preservation of the LDH structure. Very similar XRD patterns are observed in the bio-hybrids, suggesting that the ion-exchange reaction does not take place, independently of the method used to dissolve zein or the kind of anion present in the interlayer. Considering that the thickness of a brucite-type is approximately 0.48 nm (Miyata, 1980), the increment of the interlayer distance for the Z-LDH based on MgAl-Cl and MgAl-Nit corresponds to 0.29 nm and 0.33 nm, respectively. These values are consistent with the size of the respective Cl^- and NO_3^- ions (Kielland, 1937), and, therefore, this fact suggests that in both cases zein is not located in the interlayer of the LDH structure. According to these results, it can be assumed that, in both bio-hybrids, assembled zein (12.2 g and 11.3g /100 g Z-LDH-Cl_ie and Z-LDH-Nit_ ie, respectively) has to be located at the external surface of the LDH. These results are similar to those reported for diverse peptides, which pointed out the difficulty to achieve the intercalation of these biomolecules into LDH by this method (Yasutake et al., 2008). However, a careful analysis of the XRD pattern of the bio-hybrid derived from MgAl-Nit and zein treated under US (60kJ), Z-LDH-NO_ie-US, evidences a slight shoulder at 2θ of 4.4º, i.e. approximately 2.0 nm,

(arrow in Figure 6.5 b). This indicates the presence of intercalated phase in the sample. Elemental analysis of this bio-hybrid revealed a zein content of 13.6 g of zein/100 g of MgAl-LDH. All these results indicate that intercalation of zein in LDH by ion exchange process is very difficult, requiring perhaps long reaction times or to carry out the process into several steps. Since the intercalation of zein by these conditions was not achieved, this method was discarded for further studies.

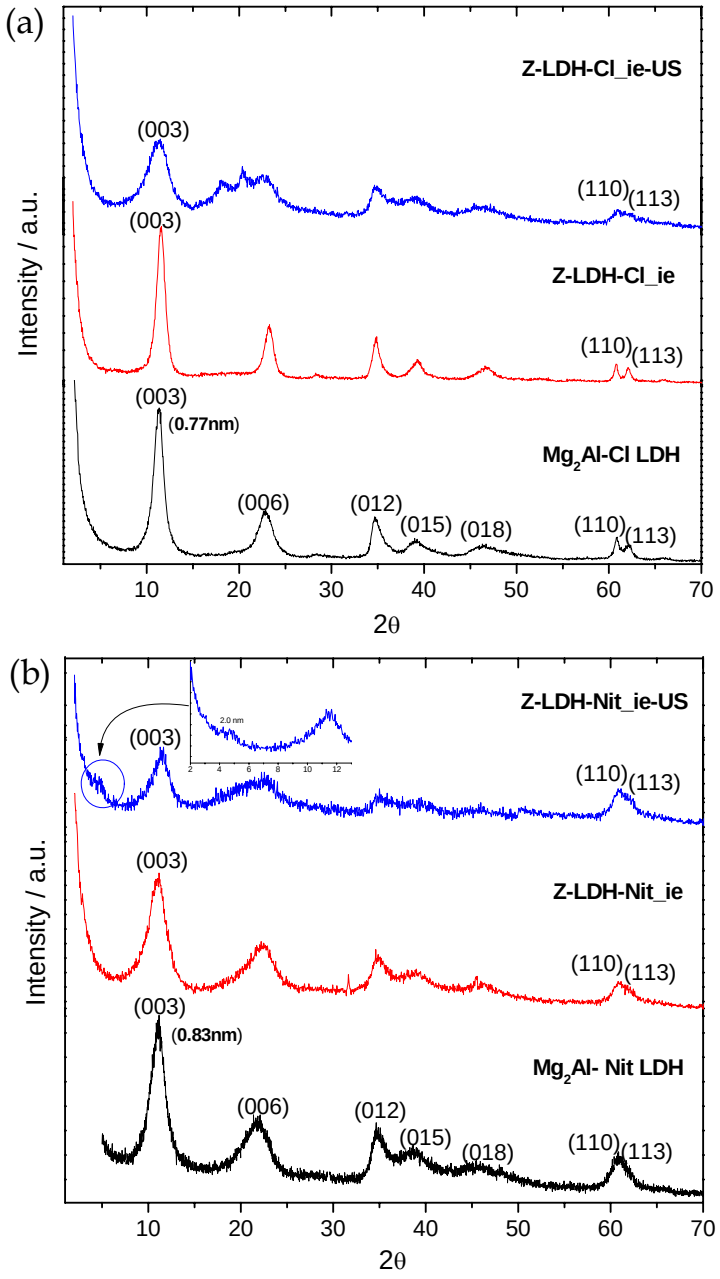

Figure 6.5 XRD diffractograms of pristine (a) MgAl-Cl and (b) MgAl-NO LDH and their respective Z-LDH bio-hybrids prepared by the ion-exchange method from zein treated in 0.1 M NaOH with and without use of US (60kJ).

6.2.2 Co-precipitation method

The co-precipitation of the LDH at constant pH in the presence of zein treated with 0.1 M NaOH was the second approach used in this work to achieve bio-hybrids based on zein intercalated in LDH. This method consists in the slow addition of the aqueous solution containing the divalent and trivalent cations to an aqueous solution of the protein treated with 0.1 M NaOH, with the simultaneous addition of 1 M NaOH to keep a pH of 11, under constant stirring. This simultaneous addition of reagents keeping the pH constant favors the co-precipitation of the LDH and the anion of interest located in the interlayer region (Cavani et al., 1991; De Roy et al., 2006).

The preparation of the zein bio-hybrids by this approach involved the use of Mg and Al solutions prepared from chloride and nitrate salts. Figure 6.6 shows the XRD patterns of Z-LDH systems prepared from both types of solution and zein dissolved in 0.1 M NaOH under magnetic stirring and US irradiation of 60 kJ. There are no significant differences between the XRD of the Z-LDH-Cl bio-hybrid with prepared without US and that of the pristine MgAl-Cl (Figure 6.6a). This result indicates again that the protein could be assembled outside the interlayer region of the MgAl LDH structure. Conversely, the XRD pattern of the material prepared from zein prepared under US is quite similar to that of the pristine LDH, but the presence of a new XRD peak at 1.86 nm can be indentified (Z-LDH-Cl_cppt-US, Figure 6.6a). This new peak at lower 2θ values than the *003* reflection of MgAl LDH can be ascribed to a phase of intercalated zein. The XRD patterns of Z-LDH bio-hybrids synthesized from solutions of Mg and Al nitrate salts solution (Figure 6.6b) show also the presence of two peaks at lower 2θ values than the *003* reflection ascribed to MgAl–LDH. The material prepared from zein solubilized in 0.1 M NaOH by magnetic stirring, Z-LDH-NO_cppt, shows a phase in which the basal space of the new peak is 2.15 nm (Figure 6.6b). This basal space is larger in the bio-hybrids synthesized from zein dissolved in 0.1 M NaOH under US (Z-LDH-NO_cppt-US), with a value of about 2.67 nm considering the two first XRD diffraction peaks in the corresponding pattern shown in Figure 6.6 b. Taking into account a thickness of 0.48 nm for the brucite layer, the basal space increase of the different intercalated phases the Z-LDH-Cl_cppt-US, Z-LDH-NO_cppt and Z-LDH-NO_cppt-US bio-hybrids can be calculated as 1.38 nm, 1.84 nm and 2.19 nm, respectively. These values are quite similar to those observed in Zein-CloisNa bio-hybrids prepared from the zein solubilized in alkaline media (Chapter 3, § 4.2.3). In

spite of the presence of intercalated phases in three of the four Z-LDH bio-hybrid systems, in all cases the more intense peak still corresponds to the *003* reflection of non-intercalated MgAl-LDH, indicating that they are composed by intercalated and non-intercalated phases, with a higher content in the last one. According to studies of bio-hybrids based on phenylalanine (Phe), a control of pH in the 8-10 range is required to attain the precipitation of the searched intercalated phases (Aisawa et al., 2001). Therefore, the formation of mixed phases could be a result of pH variation during the synthesis.

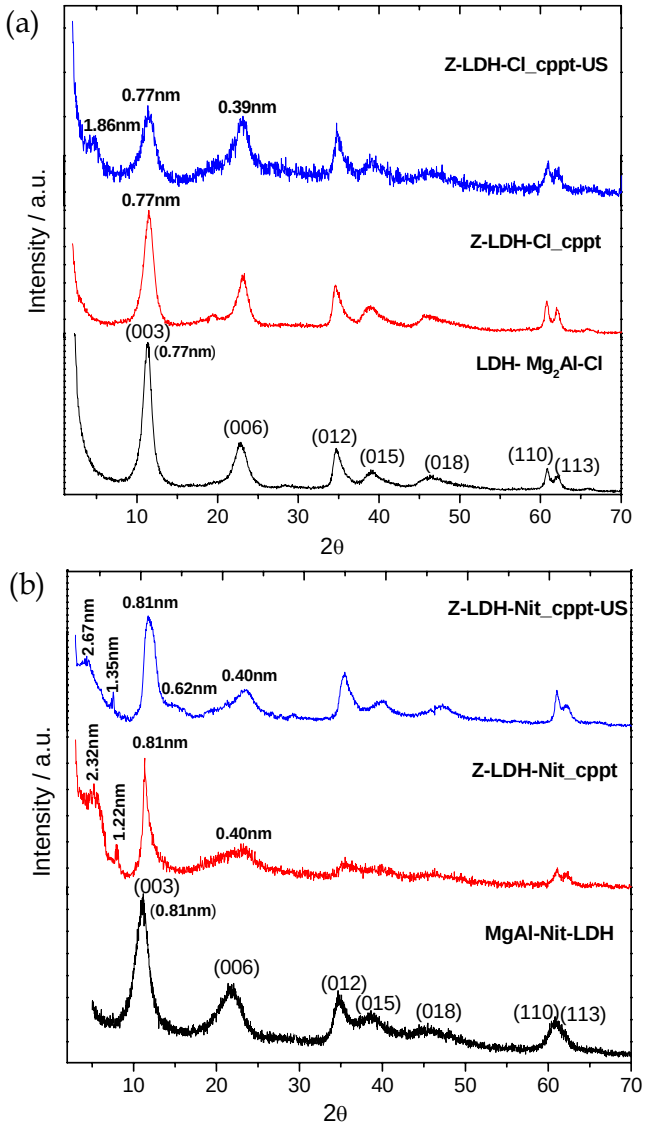

Figure 6.6 XRD pattern of LDH and Z-LDH bio-hybrids prepared by co-precipitation from zein treated with 0.1 M NaOH under magnetic stirring, and from Mg and Al chlorides (a) and nitrate (b) salts.

The amount of zein in the Z-LDH-Cl_cppt-US, Z-LDH-NO_cppt and Z-LDH-NO_cppt-US bio-hybrids was calculated from the CHNS chemical analysis (Tabla 6.2). The protein content is higher in the Z-LDH-NO_cppt-US bio-hybrid. The fact the treatment of zein in 0.1 M NaOH under US favors a high degree of disaggregation in zein and higher content of small zein fractions, as observed in SDS-PAGE results (Figure 6.1), could indicate that in Z-LDH-Cl_cppt-US and Z-LDH-Nit_cppt-US a portion of total zein can be intercalated. As nitrate ions show lower stability as interlayer anion compared to chloride anions, it may also facilitate the intercalation of zein in the case of Z-LDH-Nit_cppt and Z-LDH-Nit_cppt-US bio-hybrids. However, the co-precipitation method seems to be partially efficient for achieving bio-hybrids with complete intercalation of the protein into the LDH.

Table 6.2 Zein content in Z-LDH bio-hybrids prepared by co-precipitation method.

Z-LDH bio-hybrid samples	% of C	Zein content (g Z/100 g of LDH)
Z-LDH-Cl_cppt-US	15.2	40.0
Z-LDH-NO_cppt	16.1	43.23
Z-LDH-NO_cppt-US	21.3	57.55

The interaction between zein and MgAl LDH in these bio-hybrids was investigated by FTIR spectroscopy. Figure 6.7 shows the vibrational spectra of the Z-LDH bio-hybrids prepared from zein dissolved in 0.1 M NaOH under US (60 kJ), and those of zein and the MgAl LDH with chloride and nitrate interlayer anions. In the spectra of both bio-hybrids (Figure 6.7 a and b), the presence of the typical absorption bands between 600-400 cm^{-1} is observed, being ascribed to the deformation vibration modes of metal-oxygen bonds in the LDH layers (Cavani et al., 1991; Velu et al., 1999). In the spectrum of MgAl-Cl, a band at 1370 cm^{-1} is also observed, likely due to the v_3 vibrational mode of carbonate anions, which could be incorporated during the LDH synthesis and from atmospheric CO_2 (Camacho et al., 2009). In Z-LDH-Cl_cppt-US bio-hybrid (Figure 6.7a), the band at 1659 cm^{-1} is assigned to the amide I, being shifted towards lower wavenumber compared to that observed for Z-NaOH-US. Conversely, this band is

displaced towards higher wavenumber values in Z-LDH-NO_cppt-US bio-hybrid, appearing at 1672 cm^{-1} (Figure 6.7b). Interesting differences are also observed in the frequency of the amide II characteristic vibration band, which appears as a single band at around 1545 cm^{-1} in the Z-LDH bio-hybrids. All these shifts may be related to the existence of interactions between the negatively charged glutamate groups of the alkaline-treated zein and the LDH host. In the spectrum of the Z-LDH-NO_cppt-US bio-hybrid, a band at 1379 cm^{-1} is also evidenced, being attributed to nitrate ions of the non-intercalated LDH-phase (Miller and Wilkins, 1952).

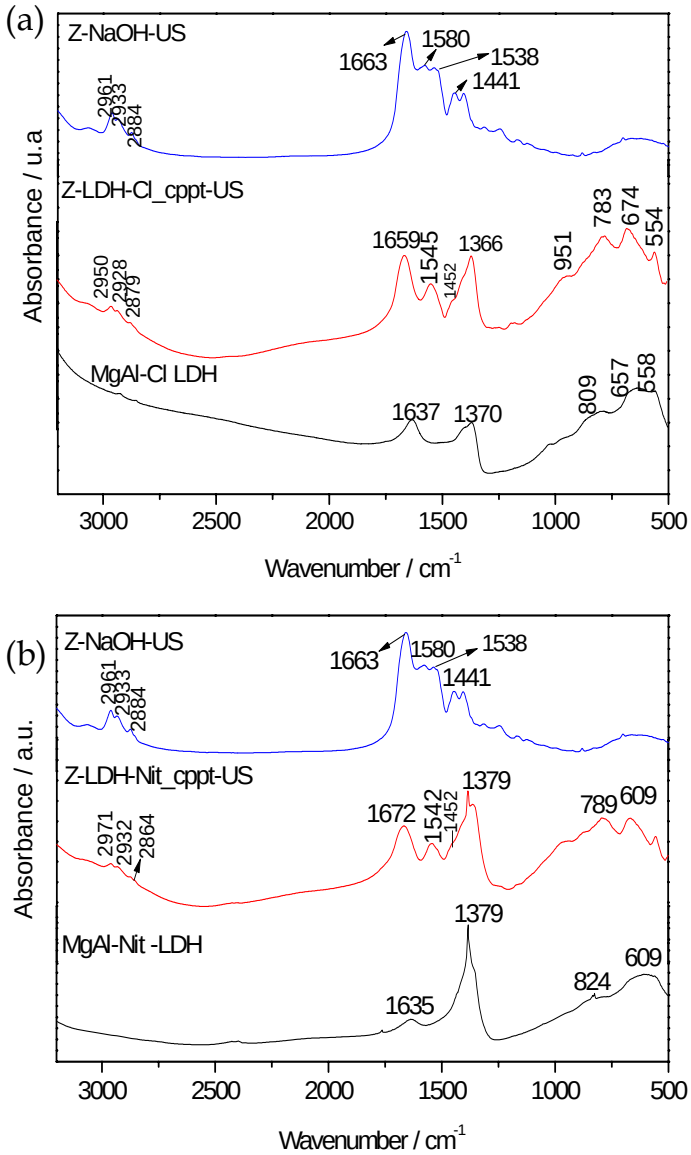

Figure 6.7 Spectra in the FTIR 3200-500 cm^{-1} region of LDH and Z-LDH bio-hybrids prepared by co-precipitation of zein dissolved in 0.1 M NaOH under US from Mg and Al chloride (a) and nitrate (b) salts.

Solid state ^{13}C NMR spectra of Z-NaOH-US and Z-LDH-Cl_cppt-US bio-hybrid are shown in Figure 6.8. Both spectra are very similar, being the main differences related to the signal of the carbonyl carbons. In the starting zein, this signal appears at 172.5 ppm showing a shoulder at 180 ppm, but both are shifted toward lower magnetic fields in the bio-hybrids, appearing in Z-LDH-Cl_cppt-US at 170 ppm and 173 ppm, respectively. The small shift of both signals reflects a weaker interaction between the negatively charged groups present in biopolymer and the positive counterions when these are the charged LDH layers, which is in agreement with the above discussed results obtained from FTIR.

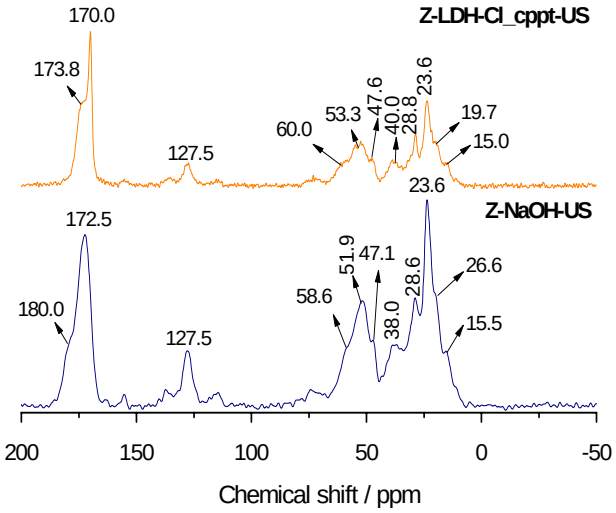

Figure 6.8 Solid state ^{13}C NMR spectra of Z-NaOH-US and the Z-LDH-Cl_cppt-US bio-hybrid.

Figure 6.9 shows TG and DTA curves of Z-NaOH-US and the Z-LDH-Cl_cppt-US and Z-LDH-NO_cppt-US bio-hybrids in the range of 25-100°C temperature, obtained under air flow. Several steps of decomposition are observed in the case of Z-NaOH-US, which could correspond to pyrolysis events at temperatures below 430°C and to the decomposition and combustion of the protein at temperatures higher than 500°C. The thermal behavior of the Z-LDH-Cl_cppt-US and Z-LDH-NO_cppt-US bio-hybrids is very different (Figure 6.9). In both cases, the thermal stability of zein is increased up to temperatures around 400 °C. From the TG/DTA curves of Z-LDH-Cl_cppt-US and Z-

LDH-NO_cppt-US bio-hybrids, weight losses up to 200 ºC are determined, being 10 and 12% respectively, , which are related to the elimination of water molecules. Above 200 °C both bio-hybrids undergo thermal decomposition in two main stages: i) between 200 ºC and 450 ºC, where a partial elimination of zein occurs, being associated which the exothermic peaks at 388 and 355 ºC, for Z-LDH-Cl_cppt-US and Z-LDH-NO_cppt-US, respectively; and ii) between 450 ºC and 600 ºC, where the combustion of the organic matter associated with the exothermic processes is completed. In this temperature range, the dehydroxylation of the LDH and the elimination of residual chloride or nitrate anions also occur (Constantino and Pinnavaia, 1995), as deduced from the comparison with the TGA/DTA curves of MgAl-LDH (Appendix C, Figure C.1)

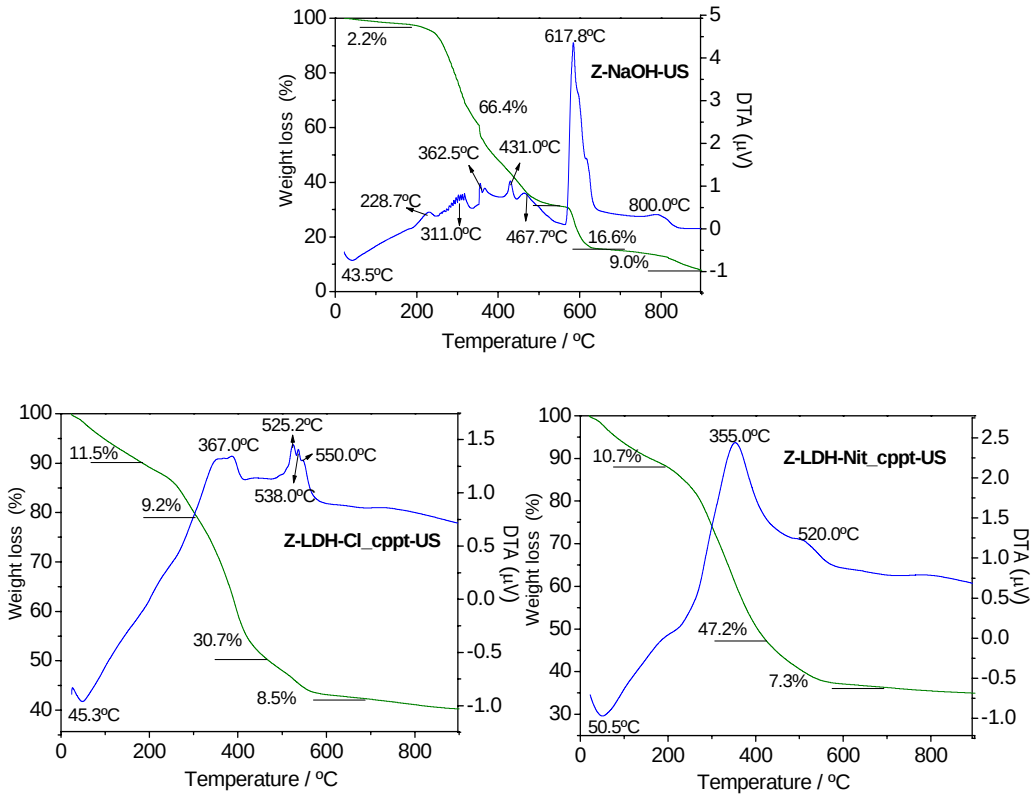

Figure 6.9 TG and DTA curves obtained in air flow of Z-NaOH-US, and the Z-LDH-Cl_cppt-US and Z-LDH-NO_cppt-US bio-hybrids.

Bio-hybrids prepared by co-precipitation from zein solubilized in 0.1 M NaOH under US (60 kJ) as well as MgAl-Cl and MgAl-NO LDH hosts were observed by FE-SEM (Figure 6.10). Both LDH (Figure 6.10 a and b) show the typical "sand-rose"

morphology of many LDH materials (Leroux et al., 2004). The aspect of Z-LDH bio-hybrids is quite different (Figure 6.10 c and d). The presence of zein in the synthesis medium seems to lead to the aggregation of the formed LDH particles, providing compactness to the resulting materials. Similar morphologies has been evidenced in other hybrid systems prepared also from co-precipitation of the LDH in presence of biomolecules, for instance alginate (Leroux et al., 2004) and ι-carrageenan (Darder et al., 2005) polysaccharides.

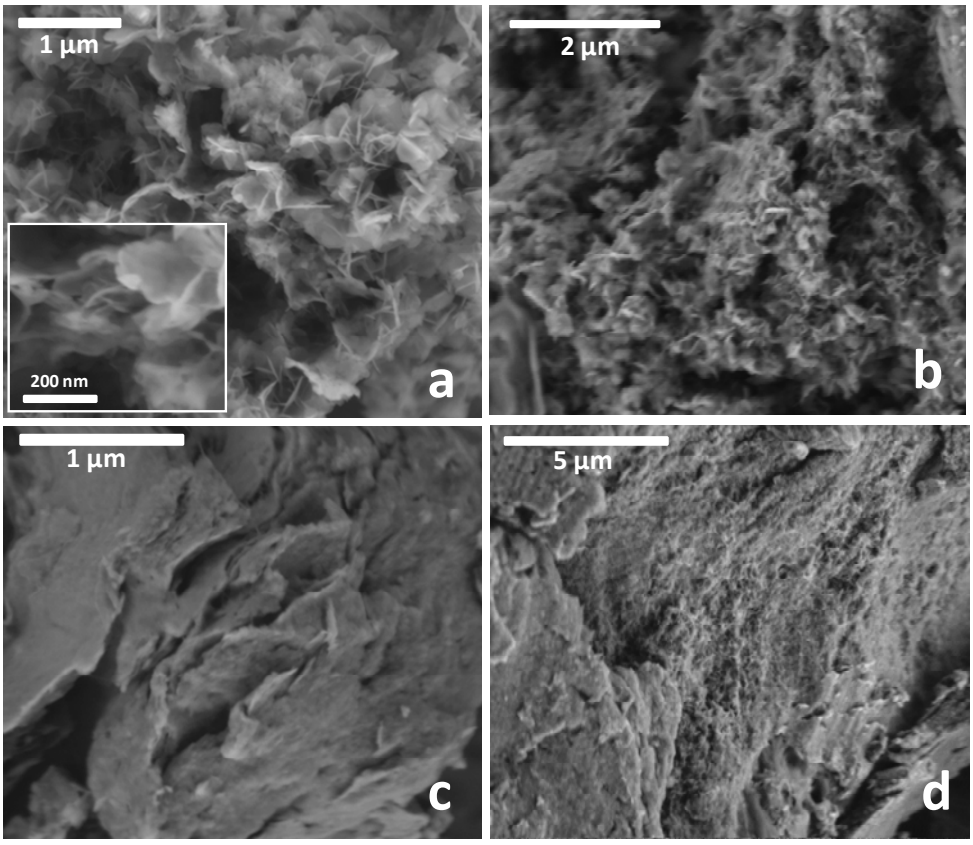

Figure 6.10 FE-SEM images of (a) MgAl-Cl and (b) MgAl-NO LDH, as well as the (c) Z-LDH-Cl_cppt-US and (d) Z-LDH-NO_cppt-US materials.

6.2.3 Reconstruction method

The third attempt in preparation of Z-LDH bio-hybrids was the reconstruction method. In this way, a MgAl LDH containing carbonate ions in the interlayer region (MgAl-Carb) was firstly synthesized. This MgAl-Carb was calcined at 350 ^{o}C, giving rise to the corresponding Mg Al layered double oxides (LDO). The reconstruction of the LDH

structure by LDO hydration is carried out using a solution containing the anion of interest.

Figure 6.11 shows the XRD patterns of the MgAl-Carb LDH before and after the thermal treatment for 3h at 350ºC to produce MgAl-LDO, and those of the bio-hybrids prepared from the LDO and zein dissolved in 0.1 M NaOH under magnetic stirring (Z-LDH_rec) and under US 60 kJ (Z-LDH_rec-US). The pristine MgAl-Carb LDH presents the characteristic reflections of LDH, where the highest intensity peak corresponds to the (*003*) plane, from which it is possible to determine a basal distance of 0.76 nm, which is in agreement with the values reported in the literature for this LDH containing carbonate anions (Rives, 2002; De Roy et al., 2006). In the pattern of the MgAl-LDO resulting from calcination of the MgAl-Carb LDH, it is not possible to detect any of the typical peaks of the LDH, but rather those assignable to amorphous MgO (periclase) (Leroux and Besse, 2001.; Rives, 2002). Reconstruction of the LDH structure using a solution of zein in 0.1 M NaOH under magnetic agitation (Z-LDH_rec) is confirmed by the presence of the (*110*) and (*113*) reflections, at the same typical angles observed in the MgAl LDH structure. The (*003*) reflection peak appears at slightly lower 2θ angles than in the pristine MgAl-Carb LDH, indicating that zein was not intercalated between the LDH layers. Taking into account that the reconstruction is carried out in CO_2-free water, the LDH layer charge was probably compensated by OH^- anions, resulting in a phase known as meixnerite (Miyata, 1980). In the case of the Z-LDH_rec-US bio-hybrid, the XRD pattern is poorly defined, showing the presence of scatter between 20-30º in 2θ, which could be related to the presence of amorphous zein. In this diffractogram, it is possible to appreciate the (*110*) and (*113*) characteristic reflections of the LDH structure and the presence of new peaks at 1.54 nm, 0.75 nm and 0.50 nm, which could be assigned to (*003*), (*006*) and (*009*) reflections, respectively. From those values, it is possible to calculate a basal spacing of 1.51 nm, which points out to the presence of zein intercalated into the reconstructed LDH. Bearing in mind that a bucite layer thickness is 0.48 nm, the increment in the interlayer spacing in the Z-LDH_rec-US bio-hybrid is 1.03 nm. Elemental analysis of this bio-hybrid reveals a zein content of 36 g per 100g of LDH, which is lower than in other zein-LDH bio-hybrids. It is also clear that zein dissolved in 0.1 M NaOH under US is sufficiently disaggregated to facilitate its intercalation within the inorganic layers.

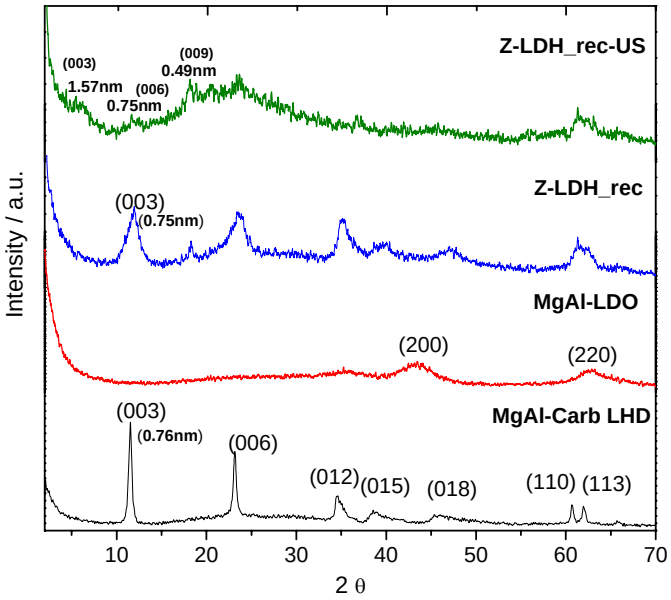

Figure 6.11 XRD patterns of pristine MgAl-Carb LDH, the MgAl-LDO resulting after its calcination at 350ºC, and the Z-LDH bio-hybrids prepared by reconstruction of this LDO material in the presence of zein dissolved in 0.1 M NaOH under magnetic stirring (Z-LDH_rec) and US (60 kJ) (Z-LDH_rec-US).

FTIR spectra of the Z-LDH_rec-US bio-hybrid, Z-NaOH-US, the starting MgAl-CO LDH and the MgAl-LDO material are displayed in Figure 6.12. Comparing these spectra, it is observed that the band at 1663 cm^{-1} in Z-NaOH-US assigned to ν_{CO} vibrations of C=O of amide I is shifted toward a lower wavenumber in Z-LDH_rec-US bio-hybrid, appearing at 1658 cm^{-1}, which indicates the existence of possible interactions of the negatively charged groups with the positively charged LDH sheets. In the spectrum of the bio-hybrid, the presence of the band ascribe to the $\nu_{3\ asym\ C-O}$ stretching mode of the carbonate anion at 1363 cm^{-1} can be also distinguished. The vibrational bands between 2915 and 2848 cm^{-1} are attributed to ν_{C-H} vibration of CH_2 groups from the protein and the bands in the 800-400 cm^{-1} region are ascribed to the host inorganic lattice vibrations of the reconstructed LDH structure.

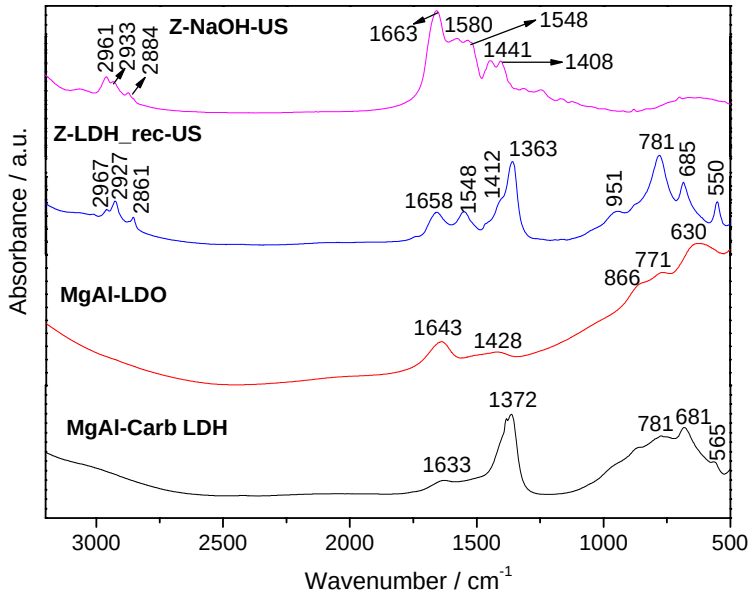

Figure 6.12 FTIR spectra in the 3200-500 cm^{-1} region of pristine MgAl-Carb LDH, the MgAl-LDO resulting after calcination at 350°C, the Z-LDH_rec-US bio-hybrid and Z-NaOH-US used in the reconstruction.

Figure 6.13 shows FE-SEM images of the Z-LDH_rec-US bio-hybrid and pristine MgAl-Carb LDH. As in the case of LDH containing Cl^- and NO_3^- ions, MgAl-Carb LDH shows the particular "sandy-rose" morphology (Figure 6.13 a and b). However, the reconstructed Z-LDH_rec-US bio-hybrid presents a more compact aspect (Figure 6.13 a and b), formed by agglomerates of lamellar particles probably cemented by the presence of zein.

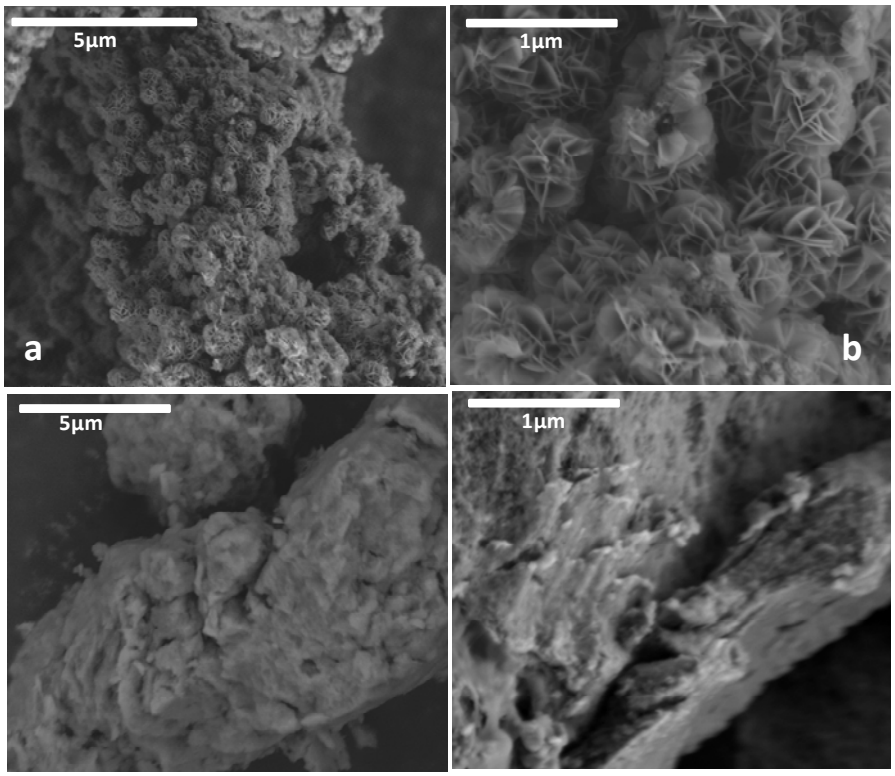

Figure 6.13 FE-SEM images of pristine MgAl-Carb LDH (a and b) and Z-LDH_rec-US (c and d).

6.3 SYNTHESIS AND CHARACTERIZATION OF ZEIN-LAYERED SINGLE HYDROXIDE BIO-HYBRIDS

Besides LDH, the preparation of zein-based bio-hybrids by intercalation into layered simple hydroxides (LSH) has been also explored. The LSH materials, such as $Co_2(OH)_3$ (Co-LSH), present quite similarities to LDH, only that in LSH the inorganic layers are composed of only one type of metal cation (Newman and Jones1999). In the present case, the preparation of zein-layered simple hydroxide (Z-LSH) bio-hybrid was done by co-precipitation and ion-exchange methods of a Co-LSH. For this purpose, the $Co_2(OH)_3(CH_3COO)\cdot H_2O$ LSH was used, with acetate anions in the interlayer region. The choice of this LSH is based on the fact that small peptides have been already intercalated in it (Si et al., 2012). Based on the previous results on zein intercalation in LDH, zein was previously solubilized in 0.1 M NaOH under US (60 kJ) (Z-NaOH-US) could be more easily intercalated, this solution was chosen in the preparation of Z-LSH bio-hybrids. However, inspired in the work of Si and co-authors, a solution of 60%

(v/v) ethanol/water was added to previous ultrasonicated zein solution. The bio-hybrids based on zein and LSH were prepared by co-precipitation and ion-exchange procedures.

Figure 6.14 shows the XRD patterns of pristine Co-LSH and the Z-LSH bio-hybrids prepared by co-precipitation (Z-LSH_cppt) and ion-exchange (Z-LSH_ie) methods. It is observed in the diffractogram of pristine LSH that the peak at 6.0º in 2θ, which is related to the *003* reflection, appears in the same position than in the bio-hybrid prepared by the co-precipitation procedure, showing both materials a similar basal spacing of 1.27 nm. Considering that the thickness for hydroxide layer of the cobalt triple deck layers is ~0.6 nm (Dujardin and Mann, 2002), a basal increment of 0.67 nm is deduced, corresponding to the presence of acetate anions (Kielland, 1937). The XRD pattern of the Z-LSH_ie bio-hybrid prepared by ion-exchange does not show any reflection in the 2 to 10º range in 2θ. However, a new peak at approximately 12.2º in 2θ is clearly evidenced, corresponding to a basal spacing of 0.73 nm. According to Laget et al. (Laget et al., 1999) and Si et al. (Si et al., 2012), when the OH/exchanged anion ratio deviates from 3, the exchange reaction is not topotactic, and a dissolution–recrystallization processes may take place. Thus, a possible exfoliation of the structure could also take place in the Z-LSH_ie material. In order to corroborate this finding a mechanical mixture of the Z-NaOH and LSH was prepared employing the same amounts of each component used in the ion exchange reaction. In the XRD pattern of this mechanical mixture (Figure 6.15) the peak of the starting LSH is still evidenced. This result discards a possible dilution effect and suggests that the observed changes in the XRD pattern of Z-LSH_ie (Figure 6.15) could be associated with the exfoliation of the LSH sheets due the incorporation of the protein. The zein content in this sample is 11.4 g of zein/100 g of Co-LSH determined by elemental chemical analysis. The cobalt-based layered hydroxide seems to be more susceptible to exfoliation according to various studies, as for instance those about hybrids prepared by ion-exchange reactions of Co-Ni LDH with formamide (Liang et al., 2010) or through assembling of Co-Al LDH with carbon nanotube *via* electrostatic forces (Liu et al., 2006).

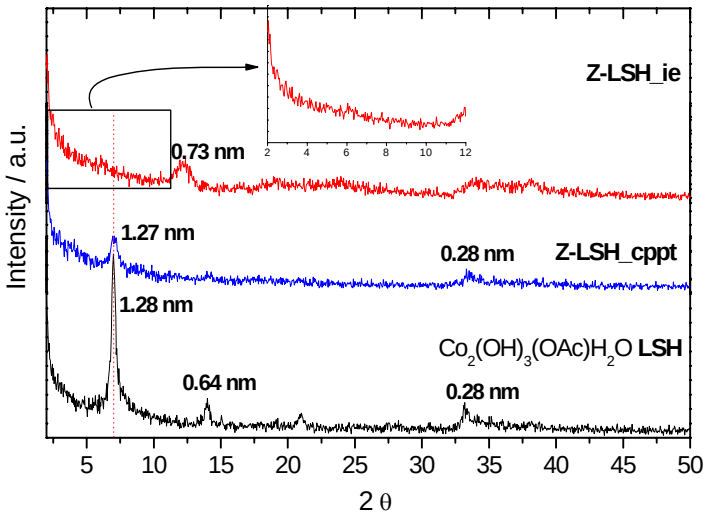

Figure 6.14 XRD patterns of pristine Co-LSH, and Z-LSH_cppt and Z-LSH_ie bio-hybrids prepared by co-precipitation and ion-exchange methods, respectively.

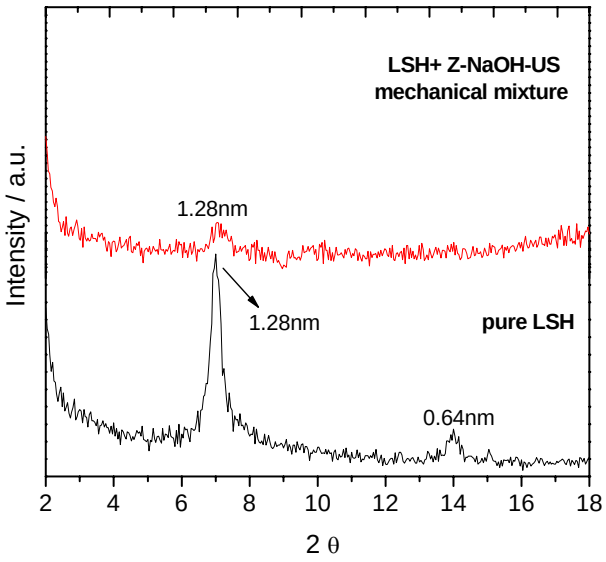

Figure 6.15 XRD patterns of pristine Co-LSH containing acetate anions and the mechanical mixture based on Co-LSH and Z-NaOH-US.

The interaction between the zein and the Co-LSH substrate in the Z-LSH_ie bio-hybrid was investigated by IR spectroscopy (Figure 6.16). Besides the bands below 800 cm^{-1} assigned to the metal-oxygen vibrations of the Co-LSH framework, also observed in the pristine LSH (Figure 6.16 a), the spectrum of the Z-LSH_ie shows specific bands between 2961-2859 cm^{-1} associated with ν_{C-H} vibration mode of the biopolymer (Figure

6.16 b). In this last spectrum, it is possible to detect differences in the bands at 1650 and 1534 cm^{-1} ascribed to the C=O and C-N vibration modes in comparison to those of the Z-NaOH-US (Figure 6.16 c). These differences could be indicative of interactions between the biomacromolecule and the LSH, as explained in the case of Z-LDH bio-hybrids. In addition, it is also observed that the asymmetric and symmetric stretching vibration modes of COO^- groups, appearing at 1577 and 1404 cm^{-1}, respectively in the pristine LSH (Figure 6.16 a), disappear in the bio-hybrid material, indicating that the removal of the acetate anion from the LSH.

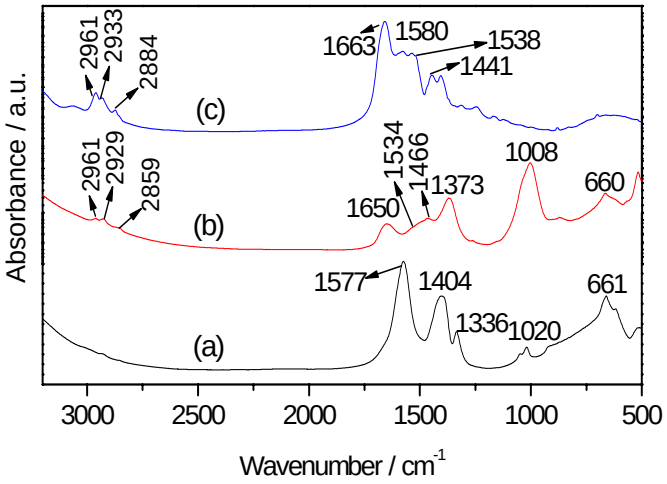

Figure 6.16 FTIR spectra in the 3200-500 cm^{-1} region of pristine (a) $Co_2(OH)_3(CH_3COO)$-LSH, the (b)Z-LSH_ie bio-hybrid and the (c) Z-NaOH-US.

Figure 6.17 shows the TG and DTA curves of the Co-LSH and the Z-LSH bio-hybrids obtained under air flow. In all cases, weight loss in the 25 -200 ^oC and 900-1000 ^oC range are observed, which are related to the elimination of water molecules physically adsorbed and the condensation of the structural hydroxyl groups of the LSH layers, respectively. Pristine Co-LSH and Z-LSH_cppt bio-hybrid show a quite similar thermal behavior, showing a strong exothermic event in temperatures between 200 and 370 ^oC, which is attributed to the elimination of the interlayer acetate anions, corroborating that zein was not intercalated in the bio-hybrid. The Z-LSH_ie bio-hybrid presents quite different TG and DTA profiles to those of the LSH and the Z-LSH_cppt bio-hybrid. Various mass losses are observed above 200 ^oC, which are accompanied by events in the DTA curves. The weight loss between 200 and 400 ^oC is attributed to the

partial decomposition of the biopolymer and elimination of remaining acetate anions. The total weight loss associated with processes at temperatures between 350 and 900 ºC may be associated with the final decomposition of the zein associated with the layered solid in different ways.

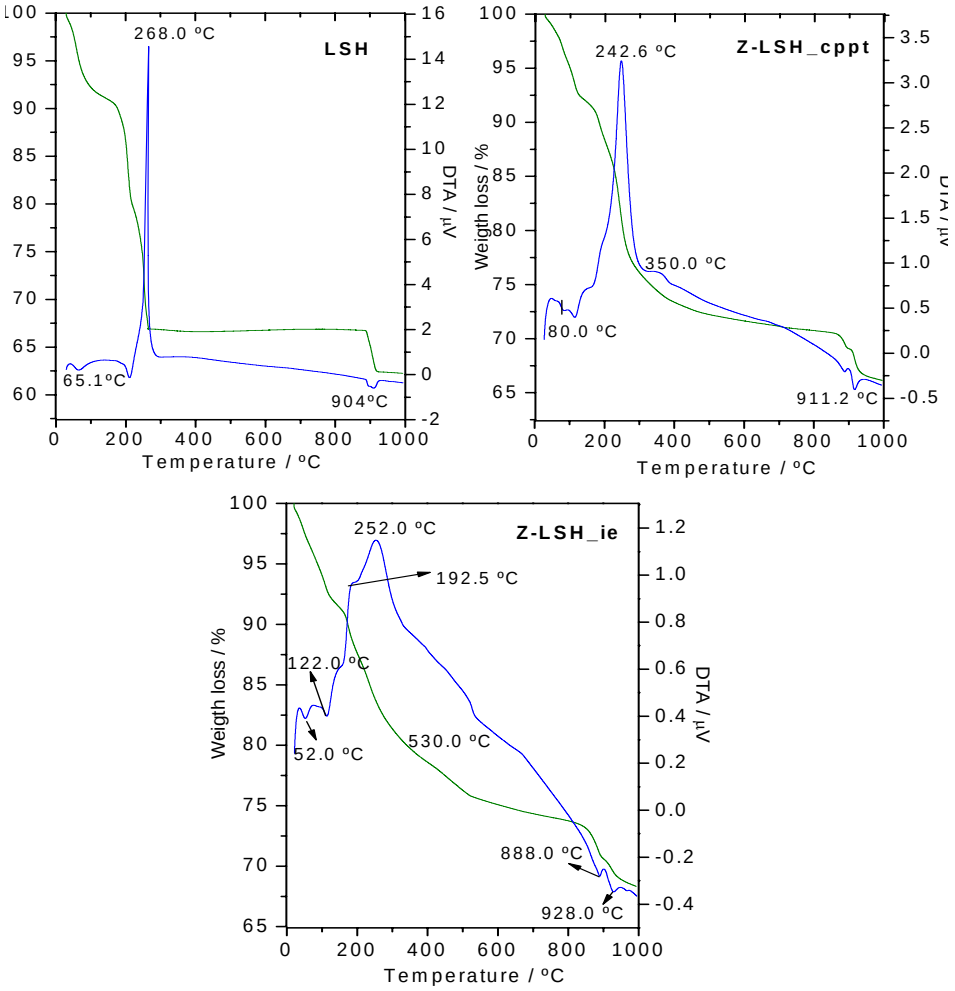

Figure 6.17 TG and DTA curves carried out under air flow of Co-LSH and Z-LSH_cppt and Z-LSH_ie bio-hybrids.

FE-SEM images Co-LSH (Figure 6.18 and b) and the Z-LSH_cppt bio-hybrid (Figure 6.18 c) shows similar morphologies, consisting of thin platelet–shaped microcrystals, related to the LSH material. Conversely, the Z-LSH_ie bio-hybrid presents a more compact morphology, resembling to related materials based on the assembly of peptides to Co-LSH (Si et al., 2012). This sample was analyzed with more detail by

TEM, where it can be clearly appreciated the presence of highly exfoliated Co-LSH and some intercalated phases in the Z-LSH_ie bio-hybrid, corroborating the XRD results.

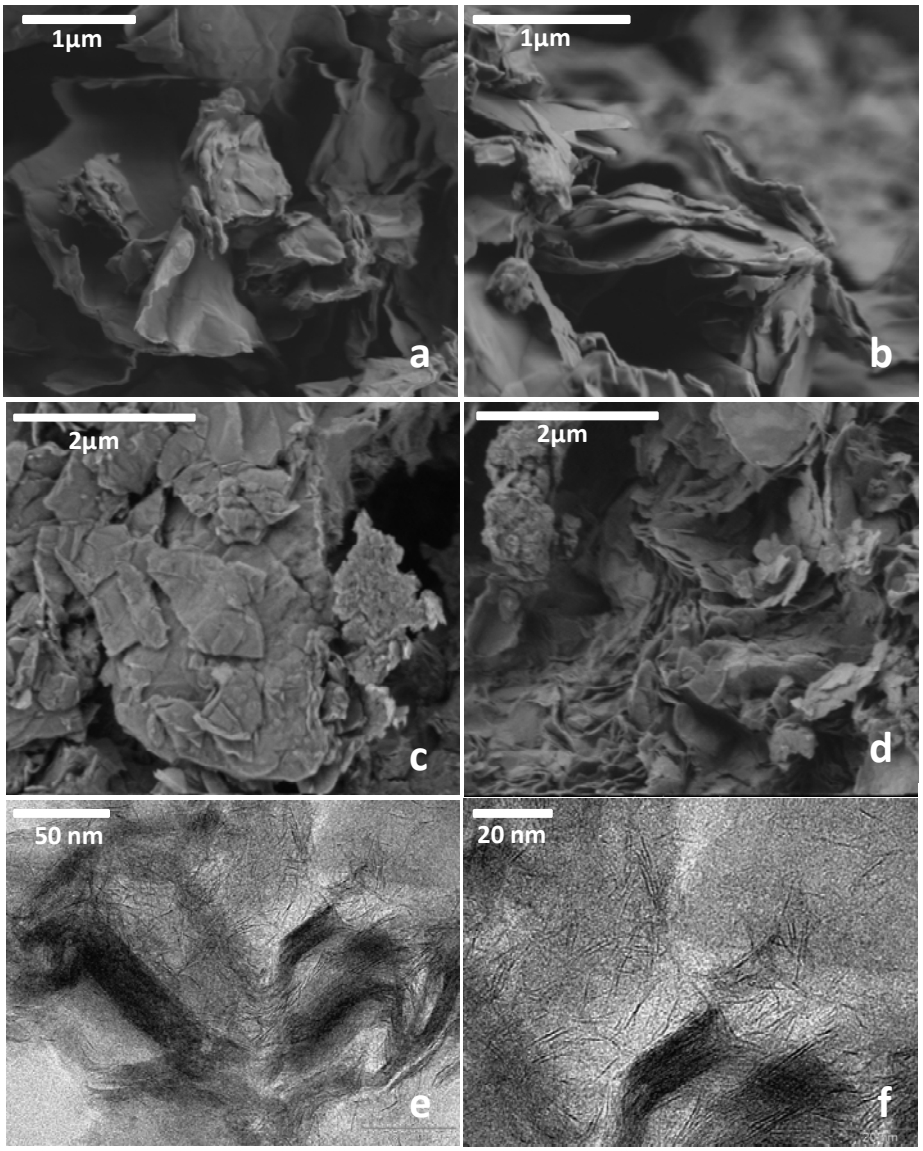

Figure 6.18 FE-SEM images of pristine Co-LSH (a and b), Z-LSH_ cppt (c) and Z-LSH_ie (d) bio-hybrids. TEM images of Z-LSH_ie bio-hybrid (e and f).

4.4 CONCLUDING REMARKS

A first exploration on the development of bio-hybrids based on zein and MgAl layered double and $Co_2(OH)_3$ simple hydroxide as inorganic host materials was carried out

employing various synthetic approaches. Although the intercalation in layered hydroxides is usually more difficult than in montmorillonite, the results shown in this Chapter show that zein can be intercalated in LDH and LSH host solids. Different interlayer anions in LDH can have strong influence on the assembly to zein, resulting in different bio-hybrid structures. The solubilization of zein in 0.1 M NaOH, is some cases performed under US irradiation, seems to favor the incorporation between the LDH layers. In this sense, mixed phases with partial intercalation were observed in the case of bio-hybrids prepared by co-precipitation method, while the reconstruction method allowed to prepare a single intercalated phase, but with low crystallinity. Highly exfoliated intercalated phase was evidenced for the bio-hybrid based on Co-LSH prepared by the ion-exchange method. Thus, this preliminary study has shown the possibility to prepare zein-layered hydroxides bio-hybrids, which could have interest in applications in biomedicine, biosensing or as materials for electronic devices. However, a depth study of the properties should be carried out in the near future, in view of the possible applications of these bio-hybrids.

CHAPTER 7

CONCLUSIONS

The work reported in this Dissertation allows drawing some general conclusions regarding the development of new bio-hybrids and bionanocomposites based on the combination of the corn protein zein and various inorganic solids. It permits as well to establish specific conclusions that highlight the findings reported in each chapter of this Thesis.

- Besides the known solvents for solubilization of zein, such as 80%(v/v) ethanol/water mixtures or 0.1 M NaOH, it has been found in this work that absolute ethanol allows the separation of zein in two fractions: a soluble one containing zein monomers and protein components of low molecular weight, and a non-soluble fraction comprising zein monomers and dimers together with other high molecular weight aggregates. Thus, zein presents different characteristics depending on the solubilization conditions, which can give rise to different assemblies with the inorganic solids, being of crucial importance in the preparation of the most diverse bio-hybrids.

- The formation of bio-hybrids based on zein assembled to layered clays was studied following different routes of synthesis, using pure alcohol or aqueous solutions of 80%(v/v) ethanol/water and 0.1 M NaOH. It has been deduced that zein adsorption processes are strongly influenced by the kind of interlayer cation and the solvent used for the dispersion of the protein. Intercalation from zein in 80%(v/v) ethanol/water medium is favored when the interlayer cations of the montmorillonite are quaternary alkylammonium ions (Clois30B). In the same medium, no intercalation was produced when sodium was the interlayer cation (CloisNa), being the bio-hybrids formed with most of the protein molecules situated

at the external surface of the clay. However, the intercalation of zein in sodium montmorillonite was achieved by the controlled addition of clay swollen in water to the zein fractions in absolute ethanol. The proposed intercalation mechanism was the formation of a bio-organoclay based on incorporation of the ethanol-soluble components of zein, which favors the adsorption of the other fractions of zein by a possible cooperative process. The intercalation of zein in sodium montmorillonite was also achieved by solubilization of zein in 0.1 M NaOH. In this case, it was suggested that the intercalation mechanism is not directed by a cation exchange reaction, since the presence of sodium cations is maintained in the bio-hybrids, most probably acting as charge compensators of the negative charges in zein or due to interaction with amino groups of the protein, with the polarized water molecules accompanying sodium ions in the clay interlayer space.

- Bio-hybrids based on the combination of sepiolite or palygorskite fibrous clays with zein were prepared in 80%(v/v) ethanol/water. In this case, the amount of retained protein was greater on sepiolite due to the higher specific surface area of this clay mineral compared to palygorskite. Zein adsorption on fibrous-clays took place on the external surface of the silicates, where a physico-chemical characterization revealed that the fundamental interaction mechanism in both clays was associated with hydrogen bonding between the freely accessible zein groups and the hydroxyl groups of the silicate surface. The assembling of these components reduced the hydrophilic character of the pristine clays, conferring new properties to the resulting bio-hybrids.

- Zein-sepiolite mixtures were processed as bionanocomposite foams, through a new method of synthesis based on the hydrophobic feature of zein and the different solubility of zein components in absolute ethanol. The subsequent removal of ethanol in water, followed by a freeze-drying process gave rise to low-density materials with cellular structure. These macroporous materials were also provided with superparamagnetic properties by the incorporation of magnetite nanoparticles or sepiolite modified with magnetic nanoparticles.

- New bio-hybrids based on zein and layered hydroxides have been synthesized by different methods using a MgAl layered double hydroxide (LDH) and $Co_2(OH)_3$

layered simple hydroxide (LSH). The intercalation of zein in both layered hydroxides was favored by the use of ultrasonication during zein solubilization in 0.1 M NaOH. It was found that zein intercalation in LDH was strongly influenced by the method of synthesis (ion-exchange, co-precipitation or reconstruction), as well as by the kind of interlayer anion in the layered hydroxide. Thus, no intercalation took place by ion-exchange reaction, the co-precipitation method gave rise to mixed intercalated phases, and the reconstruction method allowed the formation of an intercalated structure, although the presence of adsorbed zein outside of the host material could not be discarded. Concerning the assembly of zein with $Co_2(OH)_3$ LSH, the co-precipitation method did not result in an intercalated phase, while a highly exfoliated intercalated phase was evidenced when using the ion-exchange reaction method. In both types of bio-hybrid systems, the main interaction between the components is related to weaker interaction between the negatively charged groups present in the protein and the positive charges of the layered host material.

- The zein-clay bio-hybrids can be considered as bio-organoclays and were successfully used as fillers in biopolymer matrices, without requiring the addition of any compatibilizer or plasticizer. Zein-fibrous clays as filler in hydrophilic polymer matrices (e.g. alginate, starch) are able to form homogeneous and transparent self-supporting bionanocomposite films. These bionanocomposites showed improved resistance to the passage of water and better light and gas barrier properties that the neat biopolymers. The permeability tests conducted at high humidity conditions revealed that these bionanocomposite films showed a prominent permeability toward CO_2, while the barrier properties toward O_2 were enhanced. Such features are associated with the content in adsorbed zein on the fibrous clays, as well as the proportion of zein-clay bio-hybrid incorporated in the hydrophilic matrix. These materials show potential interest for application in the food sector, e.g. as bioplastics.

- Finally, zein-sepiolite processed as bionanocomposite foams showed good mechanical properties and improved water resistance. The use of sepiolite modified with magnetic nanoparticles instead of neat sepiolite introduced interesting superparamagnetic properties in the bionanocomposite foams. These materials

revealed interesting results for the retention of MCPA herbicide, which supports the potential use of these biocompatible and biodegradable functional bionanocomposites in environmental remediation. Additionally, these porous materials were easily removed from the aqueous medium with the help of an external magnetic field, thanks to their superparamagnetic properties, being very attractive as bio-magnetosorbent materials.

APPENDIX A

ZEIN-LAYERED CLAYS BIO-HYBRIDS

A.1 Characterization of zein-layered clays bio-hybrids

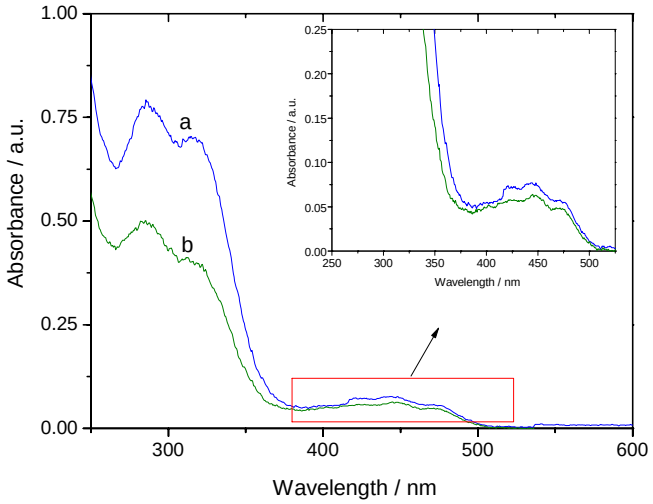

Figure A1. UV-Vis (250-600 cm^{-1} region) of (a) extracted phase from zein in pure ethanol and the supernatant of EXT-ClosiNa bio-hybrid.

APPENDIX B

ZEIN-FIBROUS CLAYS BIO-HYBRIDS

B.1 Characterization of zein-fibrous clays bio-hybrids

- *FTIR studies*

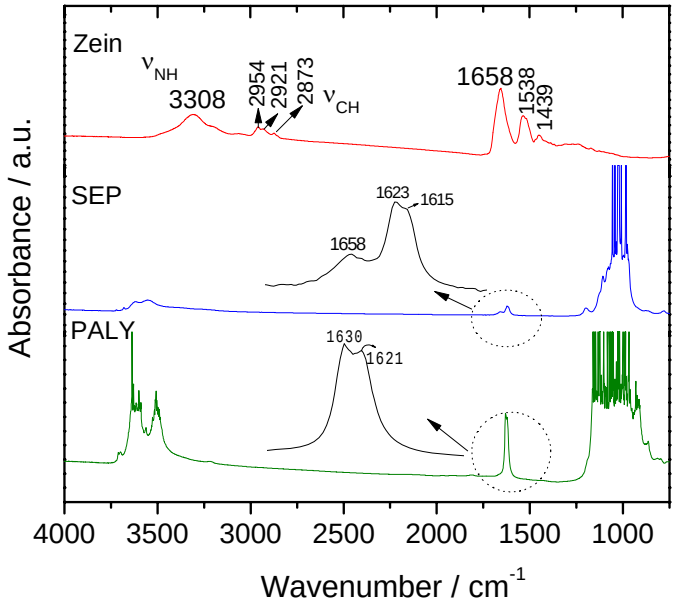

Figure B.1 FTIR spectra in the 4000-500 cm^{-1} region of starting zein, sepiolite (SEP) and palygorskite (PALY).

- *Thermal analysis*

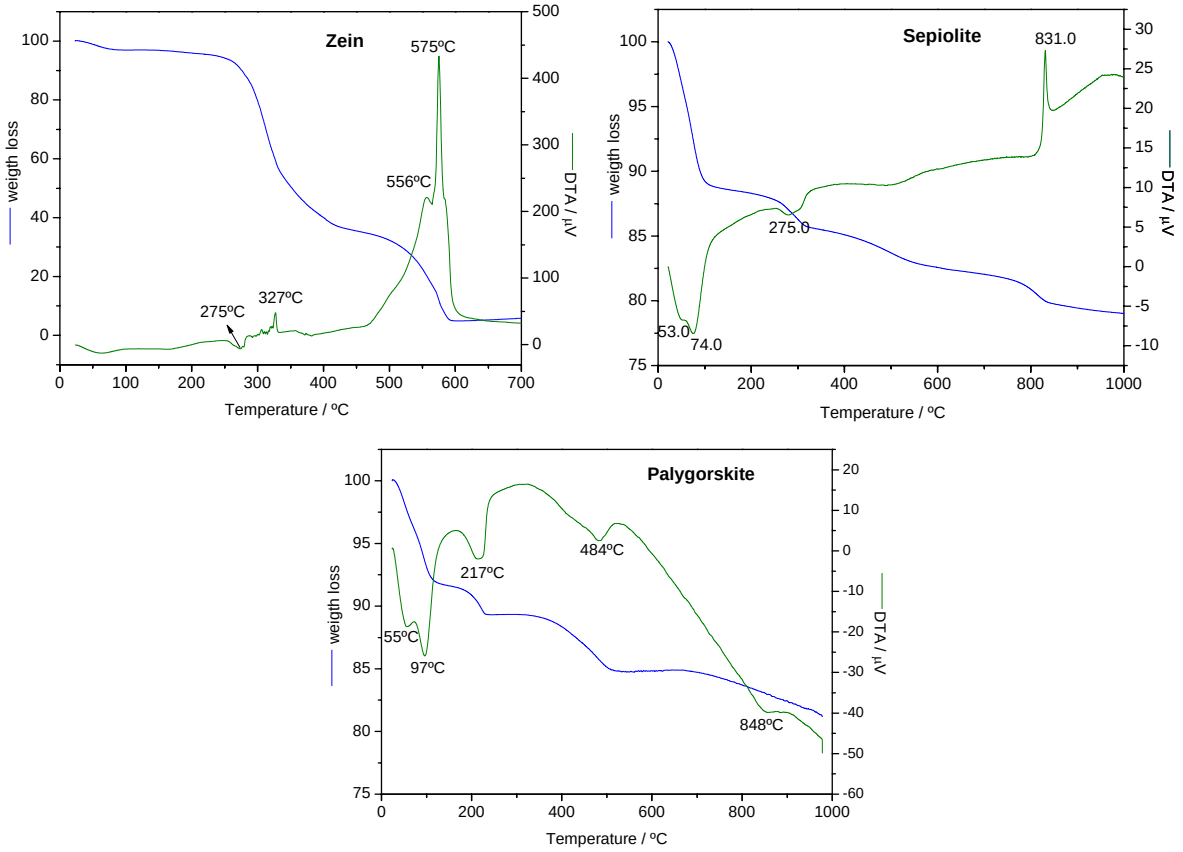

Figure B.2 TG and DTA curves (air) for starting zein protein and sepiolite and palygorskite clays.

APPENDIX C

ZEIN-LAYERED HYDROXIDES BIO-HYBRIDS

C.1 Characterization of zein-layered double hydroxide bio-hybrids

Pure MgAl LDH containing chloride or nitrate ions display a TG/DTA typical of LDHs, where water molecules adsorbed on the surface and located on the interlayer water are eliminated to 300ºC, followed endothermic phenomena related to the dehydroxylation of the brucite type octahedral layers and release of interlayer anions (between 300 and 450ºC) and at temperatures above 500°C are associated with a complete dehydroxylation of the material to form the spinel ($MgAlO_4$) and magnesium oxide (MgO) (Constantino and Pinnavaia, 1995).

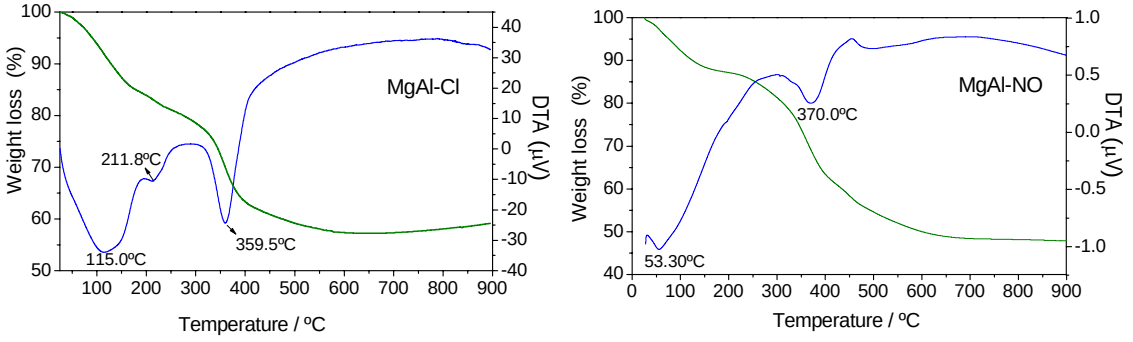

Figure C1. TG and DTA curves recorded in air flow for MgAl-Cl and MgAl-NO LDHs.

BIBLIOGRAPHY

Ahlrichs, J.L., Serna, C. and Serratosa, J.M. (1975). Folding in sepiolite crystals. *Clays and Clay Minerals* 23: 119-124.

Aisawa, S., Kudo, H., Hoshi, T., Takahashi, S., Hirahara, H., Umetsu, Y., and Narita, E. (2004). Intercalation behavior of amino acids into Zn–Al-layered double hydroxide by calcination–rehydration reaction. *Journal of Solid State Chemistry*, 177:3987–3994.

Aisawa, S., Takahashi, S., Ogasawara, W., Umetsu, Y., and Narita, E. (2001). Direct Intercalation of Amino Acids into Layered Double Hydroxides by Coprecipitation. *Journal of Solid State Chemistry*, 162: 52-62.

Alcântara, A. C. S., Darder, M., Aranda, P., and Ruiz-Hitzky, E. (2012). Zein-fibrous-clays biohybrids materials. *European Journal Inorganic Chemistry*, 2012: 5216–5224.

Alcântara, A.C.S., Darder, M., Aranda, P. and Ruiz-Hitzky, E. Polysaccharide-fibrous clay bionanocomposites. *Applied Clay Science*, submitted.

Alcântara, A.C.S., Darder, M., Aranda, P., and Ruiz-Hitzky, E. (2008). Interacciones de zeína con minerales de la arcilla. *Macla*, 9:25-6;

Alcântara, A.C.S., Darder, M., Aranda, P., and Ruiz-Hitzky, E. (2011). Zein-clay biohybrids as nanofillers of alginate based bionanocomposites. *Abstracts of Papers of the American Chemical Society*, 241:114-115.

Alcântara, AC.S., Aranda, P., Darder, M., and Ruiz-Hitzky, E. (2010). Bionanocomposites based on alginate-zein/layered double hydroxides materials as drug delivery systems. *Journal of Materials Chemistry*, 20: 9495-9504

Alexandre, M., and Dubois, P. (2000) Polymer-layered silicate nanocomposites: preparation, properties and uses of a new class of materials. *Materials Science and Engineering: R: Reports*, 28: 1-63

Alvarez, A., Santarén, J., Esteban-Cubillo, A., and Aparicio, P. (2011). Current Industrial Applications of Palygorskite and Sepiolite In: Galán, E., Singer., A, editors. *Developments in palygorskite-sepiolite research: A new outlook on these nanomaterials*. Oxford, UK: Elsevier B.V. pp. 281-298.

Anderson, T. J., and Lamsal, B. P. (2011). Zein Extraction from Corn, Corn Products, and Coproducts and Modifications for Various Applications: A Review. *Cereal Chemistry*, 88:159-173.

Angellier-Coussy, H., and Gastaldi, E. (2012). Protein-Clay Nano-Biocomposites. In Averous, L., and Pollet, E. editors, *Environmental Nano-Biocomposites*, chapter 12, pages 323-344. Springer, London, 1 edition.

Aranda, P. and Ruiz-Hitzky, E. (1999). Polyethylene (oxide)/NH -smectite nanocomposites. *Applied Clay Science*, 15: 119–135.

Aranda, P., Kun, R., Martín-Luengo, M.A., Letaïef, S., Dékány I., and Ruiz-Hitzky, E. (2008). Titania-sepiolite nanocomposites prepared by a surfactant templating colloidal route. *Chemistry of Materials*, 20: 84-89

Argos, P., Pedersen, K., Marks, D. M., & Larkins, B. A. (1982). A structural model for maize zein proteins. *Journal of Biological Chemistry*, 257: 9984-9990.

ASTM E96/E96M–12 - *Standard test methods for water vapor transmission of materials*

Auerbach, S.M., Carrado, K. A., and Dutra, P., editors. (2004) *Handbook of Layered Materials*, Marcel Dekker: New York.

Averous, L., and Pollet, E. (2012). Green Nano-Biocomposites. In Averous, L., and Pollet, E. editors, *Environmental Nano-Biocomposites*, chapter 1, pages 1–12. Springer, London, 1 edition.

Avnir, D., Coradin, T., Lev, O., and Livage, J. (2006). Recent bio-applications of sol–gel materials. *Journal of Materials Chemistry*, 16:1013–1030.

Bai, J., Alleyne, V., Hagenmaier, R. D., Mattheis, J. P., and Baldwin, E. A. *Postharvest Biology and Technology*, 2003, 28, 259-268.

Bell, L.N., Labuza, T.P. (2000). *Moisture sorption. Practical aspects of isotherm measurement and use.* American Association of Cereal Chemists, Inc., St. Paul, MN.

Belver, C., Aranda, P., Martín-Luengo, M.A., Ruiz-Hitzky. E. (2012). New silica/alumina–clay heterostructures: Properties as acid catalysts. *Microporous and Mesoporous Materials,* 147:157–166.

Bergaya, F., Jaber, M., and Lambert, L-F. (2012). Clays and Clay minerals as Layered nanofillers for (bio)polymers. In Averous, L., and Pollet, E. editors, *Environmental Nano-Biocomposites*, chapter 3, pages 41–75. Springer, London, 1 edition.

Bergaya, F., Theng, B. K. G., and Lagaly, G., editors, *Handbook of Clay Science*, chapter 10. Elsevier Science Ltd.: Amsterdam.

Bessadok, A., Langevin, D., Gouanvé, F., Chappey, C., Roudesli, S. and Marais, S. (2009). Study of water sorption on modified Agave fibres. *Carbohydrate Polymers*, 76: 74–85.

Bicudo, R.C., Bicudo, T.C., Forato, L.A., Colnago, L.A., Lanças,F.M. (2006). Análise de zeínas α do milho por LC ESI Q/TOF, *Comunicado Técnico - Embrapa*, 77:1-3

Bicudo, T.C., Forato, L.A., Batista, L.A.R. and Colnago, L.A. (2005). Study of the conformation of Y-zeins in purifield maize protein bodies by FTIR and NMR spectroscopy. *Analytical and Bioanalytical Chemistry* , 383: 291-296.

Brigatti, M. F., Galán, E., and Theng, B. K. G. (2006). Structures and mineralogy of clay minerals. In Bergaya, F., Theng, B. K. G., and Lagaly, G., editors, *Handbook of Clay Science*, chapter 2. Elsevier Science Ltd.: Amsterdam.

Bugs, M. R., Forato, L. A., Bortoleto-Bugs, R. K., Fischer, H., Mascarenhas, Y. P., Ward, R. J., and Colnago, L. A. (2004). Spectroscopic characterization and structural modeling of prolamin from maize and pearl millet. *European Biophysics Journal*, 33:335-343

Cabra, V., Arregin, R., Vazquez-Duhalt, R., and Farres, A. (2006). Effect of temperature and pH on the secondary structure and processes of oligomerization of 19 kDa alpha-zein. *Biochimica et Biophysica Acta*, 17645:1110-1118.

Cabra, V., Arregin, R., Vazquez-Duhalt, R., and Farres, A. (2007). Effect of alkaline deamidation on the structure, surface hydrophobicity, and emulsifying properties of Z19 alpha-zein. *Journal of Agricultural and Food Chemistry*, 55:439-455

Cabra,V., Arreguin, R., Galvez, A., Quirasco, M., Vazques-Duhalt , R., and Farres, A. (2005). Characterization of 19 kDa α-zein of high purity. *Journal of Agricultural and Food Chemistry*, 53:725-729.

Camacho, D. I., Morales, R., Arizaga, G. G. C., Wypych, F., and Krieger, N. (2009). Immobilization of laccase on hybrid layered double hydroxide. *Química Nova*, 32:1495–1499.

Cardoso, L.P., Celis, R., Cornejo, J., and Valim, J.B. (2006). Layered double hydroxides as supports for the slow release of acid herbicides. *Journal of Agricultural and Food Chemistry*, 54: 5968-75

Cavani, F., Trifito, F. and Vaccari, A., (1991). Hydrotalcite-type anionic clays: Preparation, properties and applications, Catalysis Today, 11: 173-301

Celis, R., Adelino, M. A., Hermosín, M. C., and Cornejo, J. (2012). Montmorillonite-chitosan bionanocomposites as adsorbents of the herbicide clopyralid in aqueous solution and soil/water suspensions, *Journal of Hazardous Materials,* 209-210:67-76.

Centi G., and Perathoner, S. (2008). Catalysis by layered materials: A review, *Microporous and Mesoporous Materials*, 107:3–15.

Cervantes-Uc, J.M., Cauich-Rodriquez, J.V., Vazques- Torres, H., Garfias-Mesias, L.F., and Paul, D.R. (2007) Thermal degradation of commercially available organoclays studied by TGA-DTA. *Thermochimica Acta*, 457:92-102.

Charradi, K., Forano, C., Prevot, V., Madern, D., Amara, A. B. H., and Mousty, C. (2010). Characterization of hemoglobin immobilized in MgAl-layered double hydroxides by the coprecipitation method. *Langmuir*, 26:9997–10004.

Chen, B., and Evans, J. R.G. (2005). Thermoplastic starch–clay nanocomposites and their characteristics, *Carbohydrate Polymers*, 61: 455-463.

Chen, P., and Zhang, L. (2006). Interaction and Properties of Highly Exfoliated Soy Protein/Montmorillonite Nanocomposites. *Biomacromolecules*, 7:1700–1706

Chivrac, F., Pollet, E., Dole, P., and Avérous, L. (2010). Starch-based nano-biocomposites: Plasticizer impact on the montmorillonite exfoliation process. *Carbohydrate polymers*, 79:941-947.

Choy, J. H., Jung, J.S., Oh, J.M., Park, J. S., Jeong Y. J., Kang, Y. K, Han, O.J. (2004) Layered double hydroxide as an efficient drug reservoir for folate derivatives. *Biomaterials*, 25: 3059-3064.

Choy, J. H., Kwak, S. Y., Jeong, Y. J., and Park, J. S. (2000). Inorganic layered double hydroxides as nonviral vectors. *Angewandte Chemie-International Edition*, 39:4042–4045.

Choy, J. H., Kwak, S. Y., Park, J. S., Jeong, Y. J., and Portier, J. (1999). Intercalative nanohybrids of nucleoside monophosphates and DNA in layered metal hydroxide. *Journal of the American Chemical Society*, 121:1399–1400.

Cong, H., Radosz, M., Towler, B. F., Shen. Y. (2007). Polymer–inorganic nanocomposite membranes for gas separation. *Separation and Purification Technology.* 55: 281–291

Constantino, V.R.L., and Pinnavaia, T.J. (1995). Basic properties of $Mg^{2+1-x}Al^{3+x}$ layered double hydroxides intercalated by carbonate, hydroxide, chloride, and sulfate anions, *Inorganic Chemistry*, 34:883-892

Cornejo, J., and Hermosin, M.C. (1988). Structural alteration of sepiolite by dry grinding. *Clay Minerals.* 23:391-398.

Darder, M., Aranda, P., and Ruiz-Hitzky, E. (2007). Bionanocomposites: A new concept of ecological, bioinspired, and functional hybrid materials. *Advanced Materials*, 19:1309–1319.

Darder, M., Aranda, P., Ferrer, M.L., Gutiérrez, M.C., Del Monte, F., and Ruiz-Hitzky, E. (2011). Progress in bionanocomposite and bioinspired foams. *Advanced Materials*, 23:5262-5267

Darder, M., Colilla, M., and Ruiz-Hitzky, E. (2003). Biopolymer-clay nanocomposites based on chitosan intercalated in montmorillonite. *Chemistry of Materials*, 15:3774–3780.

Darder, M., Colilla, M., and Ruiz-Hitzky, E. (2005). Chitosan–clay nanocomposites: application as electrochemical sensors. *Applied Clay Science*, 28: 199–208

Darder, M., Lopez-Blanco, M., Aranda, P ; Leroux F., Ruiz-Hitzky, E. (2005). Bio-nanocomposites based on layered double hydroxides. *Chemistry of Materials*, 17:1969–1977.

Darder, M., Lopez-Blanco, M., Aranda, P., Aznar, A.J., Bravo. J., and Ruiz-Hitzky, E. (2006). Microfibrous chitosan-sepiolite nanocomposites. *Chemistry of Materials*, 18:1602-1610;

De Cristofaro, A., and Violante, A. (2001). Effect of hydroxyl-aluminium species on the sorption and interlayering of albumin and montmorillonite. *Applied Clay Science*, 19:59–67;

De Roy, A., Forano, C., and Besse, J.B. (2006). Layered Double Hydroxides: synthesis and post-synthesis modifications. In: Rives, V. editor, *Layered Double Hydroxides – Present and Future*, chapter 1, pages 1–39. Nova Science Publishers, Inc., 1 edition

De Wilde, T.; Spanoghe, P.; Debaer, C.; Ryckeboer, J.; Springael, D.; Jaeken, P. (2007). Overview of on-farm bioremediation systems to reduce the occurrence of point source contamination. *Pest Management Science*, 63, 111–128

Delahaye, E. Eyele-Mezui, S., Diop, M., Leuvrey, C., Rabu, P., and Rogez, G. (2010). Rational synthesis of chiral layered magnets by functionalization of metal simple hydroxides with chiral and non-chiral Ni(II) Schiff base complexes. *Dalton Transactions*, 39:10577–10580.

Deng, L., Kim, T.J., and Hägg, M. B. (2009). Facilitated transport of CO_2 in novel PVAm/PVA blend membrane. *Journal of Membrane Science*. 340: 154-163

Dias, A. B., Muller, C.M.O., Larotonda, F.D.S. and Laurindo, J.B. (2010). Mechanical and barrier properties of composite films based on rice flour and cellulose fibers. *LWT - Food Science and Technology* 44: 535-542

Dujardin, E. and Mann, S., (2002). Bio-inspired Materials Chemistry. *Advanced Materials*, 14:775–788

Dunlop, J. W. C. and Fratzl, P. (2010). Biological Composites. *Annual Review of Materials Research* 40:1-24.

Esen, A. (1987). A proposed nomenclature for the alcohol-soluble proteins (zeins) of maize (Zea mays L.*). Journal of Cereal Science*, 5:117-128.

Esen, A. (1990). An immunodominant site of gamma-zein1 is in the region of tandem hexapeptide repeats. *Journal of Protein Chemistry*, 9:453-460

Fernandes, F. M., Ruiz, A. I., Darder, M., Aranda, P. and Ruiz-Hitzky, E. (2009). Gelatin-clay bio-nanocomposites: structural and functional properties as advanced materials. *Journal of Nanoscience and Nanotechnology*, 9:221-229.

Fernandes, F.M., Darder, M., Ruiz, A. I., Aranda P. and Ruiz-Hitzky, E. in *Nanocomposites with Degradable Properties: Synthesis, Properties and Future Perspectives*, V. Mittal, ed. Oxford University Press, New York, 2011, pp. 209-226.

Fernandes, F.M., Manjubala, I., Ruiz-Hitzky, E. (2011). Gelatin renaturation and the interfacial role of fillers in bionanocomposites, *Physical Chemistry and Chemistry Physical,* 13:4901-4910.

Filho, G.R., Bueno, W.A. (1992). Water state of Cuprophan (hemodialysis membrane). *Journal of Membrane Science,* 74: 19-27

Forano, C., Prevot, V. (2007). Enzyme-based Bioinorganic Materials. In: Ruiz-Hitzky, E., Ariga, K., and Lvov, Y. M., editors, *Bio-inorganic Hybrid Nanomaterials - Strategies, Syntheses, Characterization and Application*, chapter 15, pages 443–484. Wiley-VCH, Weinheim, 1 edition.

Forato, L.A., Bicudo, T. C., Colnago, L.A. (2003). Conformation of α-zein in solid state by Fourier transform IR. *Biopolymers (Bioespectroscopy)*, 72:421-426

Forato, L.A., Colnago, L. A., Garratt, R.C., Lopes, M.A. (2000). Identification of free acids in maize protein bodies and purified α-zein by ^{13}C and ^{1}H nuclear magnetic resonance. *Biochimica at Biophisica Acta*, 1543:106-114.

Forster, P. M, Tafoya, M. M., and Cheetham, A. K. (2004). Synthesis and characterization of $Co_7(OH)_{12}(C_2H_4S_2O_6)(H_2O)_2$—a single crystal structural study of a ferrimagnetic layered cobalt hydroxide. *Journal of Physics and Chemistry of Solids*, 65: 11-16

Galán, E. (1996). Properties and applications of palygorskite-sepiolite clays, *Clay Minerals,* 31:443-453

Galán, E., Singer., A, editors. *Developments in palygorskite-sepiolite research A new outlook on these nanomaterials*. Oxford, UK: Elsevier B.V

García-Romero, E., Suárez, M. (2010). On the chemical composition of sepiolite and palygorskite. *Clays Clay Minerals,* 58, 1-20

Gáspár, M. Benkó, Z. Dogossy, G. Réczey K. and Czigány T. (2005). Reducing water absorption in compostable starch-based plastics. *Polymer Degradation and Stability*, 90:563-569.

Ghanbarzadeh B. and Oromiehi A.R. (2008). Biodegradable biocomposite films based on whey protein and zein: Barrier, mechanical properties and AFM analysis *International Journal of Biological Macromolecules*, 43:209-213.

Gibson, J.G., and Ashby, M.F., editors (2001). *Cellular Solids. Structure and Properties*, chapter 1, pages 1–14. Cambridge University, Edinburgh, 2 edition

Gieseking, J. E. (1939). The Mechanism of Cation Exchange in the Montmorillonite-Beidellite-Nontronite Type of Clay Minerals. *Soil Science*. 47:1-14

Giles, C.H., MacEwan, T.H., Nakhwa, S.N., and Smith, D. (1960) Studies in adsorption. A system of classification of solutions adsorption isotherms, and its use in diagnosis of adsorption mechanisms and in measurement of specific surface areas of solids. *Journal of the Chemistry Society*, 111: 3973-3993

Gómez-Romero, P. and Sanchez, C., editors, *Functional Hybrid Materials*, chapter 2. Wiley-VCH: Weinheim; Sanchez, C., Belleville, P., Popall, M., and Nicole, L. (2011). Applications of advanced hybrid organic–inorganic nanomaterials: from laboratory to market. *Chemical Society Reviews*, 40: 696-753

González-Alfaro, Y., Aranda, P., Fernandes, F. M., Wicklein, B., Darder, M., and Ruiz-Hitzky, E. (2011). Multifunctional porous materials through Ferrofluids. *Advanced Materials*, 23, 5224–5228.

Gouanvé, F., Marais, S., Bessadok, A., Langevin, D. and Métayer, M. (2007). Kinetics of water sorption in flax and PET fibers. *European Polymer Journal*, 43: 586–598

Gougeon, R. D., Soulard, M., Reinholdt M., Miehé-Brendlé, J., Chézeau, J. M., LeDred, R., Marchal, R., and Jeandet, P. (2003). Polypeptide Adsorption on a Synthetic Montmorillonite: A Combined Solid-State NMR Spectroscopy, X-ray Diffraction, Thermal Analysis and N2 Adsorption Study. *European Journal of Inorganic Chemistry*, 1366-1372

Gutiérrez, M. C., García-Carvajal, Z. Y., Jobbágy, M., Rubio, F., Yuste, L., Rojo, F., Ferrer, M. L. and Del Monte, F. (2007). Poly(vinyl alcohol) scaffolds with tailored morphologies for drug delivery and controlled release. *Advanced Functional Material,* 17:3505–3513

Hendricks, S. B. (1941). Base exchange of the clay mineral montmorillonite for organic cations and its dependence upon adsorption due to van der Waals forces. *Journal of Physical Chemistry*, 45:65-81

Herrero, M., Labajos, F. M., and Rives V. (2009). Size control and optimisation of intercalated layered double hydroxides, *Applied Clay Science*, 42: 510–518.

http://www.gpo.gov/fdsys/pkg/CFR-2011-title21-vol3/pdf/CFR-2011-title21-vol3-art184.pdf. Accessed on May 11, 2013

http://www.quantachrome.com/pdf_brochures/07128.pdf, Accessed June, 10st, 2013

Hussein, M. Z., Rahman, N. S. S. A., Sarijo, S. H., and Zaina, Z. (2012). Herbicide-intercalated zinc layered hydroxide nanohybrid for a dual-guest controlled release formulation, *International Journal of Molecular Sciences*, 13:7328–7342

Jerez, A. Partal, P. Martinez, I. Gallegos C. and Guerrero, A. (2007). Protein-based bioplastics: effect of thermo-mechanical processing. *Rheological Acta*, 46: 711-720.

Jiang, Q., Reddy, N., and Yang Y. (2010). Cytocompatible cross-linking of electrospun zein fibers for the development of water-stable tissue engineering scaffolds, *Acta Biomaterialia,* 6: 4042-4051.

Kale, A., and Cheryan, M. (2009). Size exclusion chromatography of zein and xanthophylls: optimization of operating parameters. *Process Biochemistry*, 44: 481–485

Karbowiak, T., Debeaufort, F., Champion, D., Voilley, A. (2006). Wetting properties at the surface of iota-carrageenan-based edible films. *Journal of Colloid and Interface Science,* 294: 400

Kielland, J. (1937). Individual Activity Coefficients of Ions in Aqueous Solutions. *Journal of American Chemistry Society,* 59:1675-78

Killeen, D., Frydrych, M. and, Chen, B. (2012). Porous poly(vinyl alcohol)/sepiolite bone scaffolds: Preparation, structure and mechanical properties. *Materials Science and Engineering C*, 32: 749–757

Kim, M-J., Park, Y-I., Youm, K-H and Lee, K-H. (1992). Gas permeation through water-swollen polysaccharide/poly (vinyl alcohol) membranes. *Journal of Applied Polymer Science*, 91 3225-3232

Kim, S. and Xu, J. Giles. (2008) Aggregate formation of zein and its structural inversion in aqueous ethanol. *Journal of Cereal Science,* 47: 1–5.

Kong, X., Rao, X., Han, J., Wei, M., and Duan, X. (2010). Layer-by-layer assembly of bi-protein/layered double hydroxide ultrathin film and its electrocatalytic behavior for catechol, *Biosensors and Bioelectronics*, 26:549–554.

Kumar, P., Sandeep, K.P., Alavi, S., Truong, V.D., and Gorga, R.E. (2010).Preparation and characterization of bio-nanocomposite films based on soy protein isolate and montmorillonite using melt extrusion*, Journal of Food Engineering*, 100: 480-489

Kumar, P., Sandeep, K.P., Alavi, S., Truong, V.D., and Gorga, R.E. (2010). Effect of Type and Content of Modified Montmorillonite on the Structure and Properties of Bio-Nanocomposite Films Based on Soy Protein Isolate and Montmorillonite, *Journal of Food Science*, 75:N46–N56

Laget, V., Hornick, C., Rabu, P., and Drillon, M. (1999). Hybrid organic-inorganic layered compounds prepared by anion exchange reaction: correlation between structure and magnetic properties. *Journal of Materials Chemistry*, 9:169–174

Lai, H.-M., and Padua, G. W. (1997). Properties and microstructure of plasticized zein films, *Cereal Chemistry*, 74: 771-775

Lannung, A. (1930). The solubilities of helium, neon and argon in water and some organic solvents. *Journal of American Chemistry Society*, 52: 68–80.

Lawton, J. W. (2002). Zein: A History of Processing and Use. *Cereal Chemistry*, 79: 1-18.

Lee, L.J., Zeng, C., Cao, X., Han, X., Shen, J., and Xu, G. (2005). Polymer nanocomposite foams. *Composites Science and Technology*, 65:2344-2363

Leroux F. and Taviot-Gueho, C. (2005). Fine tuning between organic and inorganic host structure: new trends in layered double hydroxide hybrid assemblies, *Journal of Materials Chemistry,* 15: 3628–3642

Leroux, F. and Besse, J.P. (2001). Polymer Interleaved Layered Double Hydroxide: A New Emerging Class of Nanocomposites. *Chemisty of Materials*, 13: 3507-3515.

Leroux, F., editor (2012). *Recent Patents on Nanotechnology. Special issue in Layered Double Hydroxide.* 6, number 3

Leroux, F., Gachon, J., and Besse, J.P., (2004). Biopolymer immobilization during the crystalline growth of layered double hydroxide. *Journal of Solid State Chemistry*, 177:245-250.

Li, Y., Li, J. Xia, Q., Zhang,B., Wang,Q. and Huang,Q. (2012). Understanding the Dissolution of α‑Zein in Aqueous Ethanol and Acetic Acid Solutions, *Journal of Physical and Chemistry B*, 116:12057−12064

Liang, J., Ma, R., Iyi, N., Ebina, Y., Takada, K., and Sasaki, T. (2010) Topochemical Synthesis, Anion Exchange, and Exfoliation of Co-Ni Layered Double Hydroxides: A Route to Positively Charged Co-Ni Hydroxide Nanosheets with Tunable Composition. *Chemisty of Materials*, 22: 371-378

Lin, J J., Wei, J-C., Juang, T-Y., and Tsai, W-C. (2007). Preparation of protein-silicate hybrids from polyamine intercalation of layered montmorillonite. *Langmuir*, 23:1995-1999

Liu, Z., Ma, R., Osada, M., Iyi, N., Y., Ebina, Y., Takada, K., and Sasaki, T. (2006). Synthesis, Anion Exchange, and Delamination of Co-Al Layered Double Hydroxide: Assembly of the ExfoliatedNanosheet/Polyanion Composite Films and Magneto-Optical Studies. *Journal of American Chemistry Society*, 128:4872-4880

Luecha, J., Hsiao, A., Brodsky, S., Liu, G.L., and Kokini, J.L. (2011). Green microfluidic devices made of corn proteins, *Lab on a Chip*, 11:3419-3425.

Luecha, J., Sozer, N., and Kokini, J. L. (2010). Synthesis and properties of corn zein/montmorillonite nanocomposite films. *Journal of Materials Science*, 45:3529–3537

Machado, L.C.R., Lima, F.W.J., Paniago, R., Ardisson, J.D. Sapag, K., and Lago, R.M. (2010). Polymer coated vermiculite–iron composites: Novel floatable magnetic adsorbents for water spilled contaminants. *Applied Clay Science*, 31:207– 215

Manley, R. H., and Evans, C. D. (1943). Binary Solvents for Zein. *Industrial and Engineering Chemistry*, 35:661-665

Maroni, M and Fait, A. (1993) Health effects in man from long-term exposure to pesticides. A review of the 1975-1991 literature. *Toxicology* 78:1-180.

Matsushima, N.; Danno, G. I.; Takezawa, H.; Izumi, Y. (1997). Three-dimensional structure of maize α-zein proteins studied by small-angle X-ray scattering, *Biochimica et Biophysica Acta (BBA)-Protein Structure and Molecular Enzymology*, 1339:14-22

McArdle, B. (1998). Herbicidal and insecticidal protein-polysaccharide delivery compositions and methods for controlling plant and insect populations, *US Patent*, 5,474,146

Miller, F.A., and Wilkins, C. H. (1952). Infrared spectra and characteristic frequencies of inorganic ions their use in qualitative analysis, *Analytical Chemistry*, 24:1253-1294

Mittal, V., editor. (2011). *Nanocomposites with Biodegradable Polymers. Synthesis Properties, and Future Perspectives*, Oxford University Press, New York.;

Miyata, S. (1980). Physico-Chemical properties of synthetic hydrotalcites in relation to composition. *Clays and Clay Minerals*, 28: 50-56

Mohammad, K. B., and Esen, A. (1990). Zein Degradation in the Endosperm of Maize Seeds During Germination. *American Journal of Botany*, 77:973-980.199.

Momany, F.A., Sessa, D.J., Lawton, J.W., Selling, G.W., Hamaker, S.A., and Willett, J.L. (2006). Structural characterization of alpha-zein. *Journal of Agricultural of Food Chemistry*. 54:543-547.

Muller, C.M.O., Laurindo J. B., and Yamashita, F. (2009). Effect of cellulose fibers addition on the mechanical properties and water vapor barrier of starch-based films. *Food Hydrocolloids* 23: 1328-1333

Nakabayashi, M., Okabe, K., Fujisawa, E., Hirayama, Y., Kazama, S., Matsumiya, N., Takagi, K., Mano, H., Haraya, K. and Kamizawa, C. (1995). Carbon dioxide separation through water-swollen-gel membrane. *Energy Conversion and Management* 36: 419-422.

Nakayama, H.; Wada, N., Tsuhako, M. (2004).Intercalation of amino acids and peptides into Mg–Al layered double hydroxide by reconstruction method. *International Journal of Pharmaceutics*, 269:469–478

Nakayama, H.; Wada, N., Tsuhako, M. (2004).Intercalation of amino acids and peptides into Mg–Al layered double hydroxide by reconstruction method. In*ternational Journal of Pharmaceutics*, 269:469–478

Nalawde, P.m Awave, B., Kada,. V.J., and Hirlekar, R.S. (2009). Layered double hydroxide: A review, *Journal of Scientific & Industrial Research*, 68:267-272

Nedi, I., Maio, E.D, and Iannace, S. (2012). The role of protein– platicizer-clay interactions on processing and properties of thermoplastic zein bionanocomposites. *Journal of Applied Polymer Science*, 125:314-323

Nedi, I., Maio, E.D, and Iannace, S. (2012). The role of protein–platicizer-clay interactions on processing and properties of thermoplastic zein bionanocomposites. *Journal of Applied Polymer Science*, 125:314-323

Nelson, D.L., Lehninger, A. L., and Cox, M.M. (2008). *Principles of biochemistry*, W.H. Freeman, New York, 5 edition

Newman, S.P., and Jones, W. (1999). Comparative study of some layered hydroxide salts containing exchangeable interlayer anions. *Journal of Solid State Chemistry*, 148:26–40

Norajit, K., Kim K. M. and Ryu, G. H. (2010). Comparative studies on the characterization and antioxidant properties of biodegradable alginate films containing ginseng extract. *Journal of Food Engineering,* 98: 377-384

O`Hare, D. M. (2002) Drug delivery system comprising a drug intercalated between a layered double hydroxide, *Patent* WO 0247729.

O`Hare, D., and Wang, Q. (2012). Recent Advances in the Synthesis and Application of Layered Double Hydroxide (LDH) Nanosheets. *Chemical Reviews*, 112:4124–4155

Ofelt, C. W., and Evans, C. B. (1949). Aqueous zein dispersion. *Industrial and Engineering Chemistry*, 41:830-833.

Ohta, S and Nakazawa, H (1995). Porous clay-organic composites: Potential substitutes for polystyrene foam, *Applied Clay Science*, 9:425-431.

Olmo, N., Lizarbe, M. A., and Gavilanes, J. G. (1987). Biocompatibility and degradability of sepiolite-collagen complex, *Biomaterials*, 8: 67–69.

Olmo, N., Turnay, J., Herrera, J. I., Gavilanes, J. G., and Lizarbe, M. A. (1996). Kinetics of in vivo degradation of sepiolite-collagen complexes: effect of glutaraldehyde treatment. *Journal of Biomedical Materials Research*, 30: 77–84.

Ozcalik, O. and Tihminlioglu, F. (2013). Barrier properties of corn zein nanocomposite coated polypropylene films for food packaging applications. *Journal of Food Engineering*, 114:505-513.

Padilla-Ortega, E., Darder, M., Aranda, P., Leyva-Ramos, R. and Ruiz-Hitzky, E. (2012). Bionanocomposites quitosano-vermiculita: propiedades de adsorción de cadmio *Macla*, 16: 110-111.

Padua, G. W., Rakotonirainy A. M. and Ha, T. T. *US Pat. 0056388A1*, 2004.

Padua, G.W., and Wang, Q. (2002). Formation and properties of corn zein films and coatings. In Gennadios, A. editor, *Protein-based films and coatings*, chapter 2, pages 43-67. CRC press, USA, 1 edition

Park, J. H., Park, S. M., Kim, Y. H., Oh, W., Lee, G. W., Karim, M. R., Park, J. H., and Yeum, J. H. (2012). Effect of montmorillonite on wettability and microstructure properties of zein/montmorillonite nanocomposite nanofiber mats. *Journal of Composite Materials*, 47:251-257

Park, Y-I., Lee, K-H. (2001). Preparation of water-swollen hydrogel membranes for gas separation. *Journal of Applied Polymer Science,* 80: 1785-1791.

Pomes, A. F. (1971). Zein. In Mark, H. F., Gaylord N. G., and Bikales, N. M. editors, *Encyclopedia of Polymer Science and Technology: plastics, resins, rubbers, fibers,* pages 125-132. *Interscience Publishers*, New York, vol. 15.

Qu, Z. H., Wang, H. J., Tang, T.T., Zhang, X. L., Wang, J. Y., and Dai, K. R. (2008). Evaluation of the zein/inorganics composite on biocompatibility and osteoblastic differentiation, *Acta Biomaterialia,* 4:1360–1368

Radebaugh, G. W., Murtha, J. L., Julian, T. N. and Bondi, J. N. (1988). Methods for evaluating the puncture and shear properties of pharmaceutical polymeric films. *International Journal of Pharmaceutics*, 45: 39-46

Rives, V. (2002). Characterisation of layered double hydroxides and their decomposition products. *Materials Chemistry and Physics*, 75:19-25

Rives, V. (2002). Characterisation of layered double hydroxides and their decomposition products. *Materials Chemistry and Physics*, 75:19-25

Rives, V., and Ulibarri, M.A. (1999). Layered double hydroxides (LDH) intercalated with metal coordination compounds and oxometalates, *Coordination Chemistry Reviews,* 181: 61-120

Rives, V., editor. (2006). *Layered Double Hydroxides – Present and Future*, Nova Science Publishers, Inc., 1 edition.

Rogez, G., Massobrio, C., Rabu, P. and Drillon, M. (2011). Layered hydroxide hybrid nanostructures: a route to multifunctionality. *Chemical Society Reviews,* 40: 1031–1058.

Ruiz Hitzky, E., Aranda, P., Darder, M., and Alcântara, A.C.S. (2010). Materiales composites basados en biohíbridos zeína-arcilla, su procedimiento de obtención y usos de estos materiales. ES Patent, 2353100 and PCT/ES2010/070404.

Ruiz-Hitzky E, Aranda P, Darder M. (2009). Polymer- and biopolymer layered solid nanocomposites: organic-inorganic assembling in two-dimensional hybrid systems. In: Ariga K, Nalwa HS, editors. *Bottom-up nanofabrication: supramolecules, self-assemblies, and organized films*. Stevenson Ranch, CA: American Scientific 1693 Publisher; 39–76.

Ruiz-Hitzky, E. (2001). Molecular access to intracrystalline tunnels of sepiolite. *Journal of Materials Chemistry*, 11:86–91.

Ruiz-Hitzky, E. (2004). Organic-inorganic materials: From intercalation chemistry to devices. In Gómez-Romero, P. and Sanchez, C., editors, *Functional Hybrid Materials*, chapter 2. Wiley-VCH: Weinheim.

Ruiz-Hitzky, E. and Van Meerbeeck, A. (2006). Clay mineral and organoclay-polymer nanocomposites. In Bergaya, F., Theng, B. K. G., and Lagaly, G., editors, *Handbook of Clay Science*, chapter 10. Elsevier Science Ltd.: Amsterdam.

Ruiz-Hitzky, E., Aranda, P., Darder, M., and Rytwo, G. (2010). Hybrid materials based on clays for environmental and biomedical applications. *Journal of Materials Chemistry*, 20, 9306–9321.

Ruiz-Hitzky, E., Aranda, P., Alvarez, A., Santarén, J., and Esteban-Cubillo, A. (2011). Advanced materials and new applications of sepiolite and palygorskite. In: Galán, E., Singer., A, editors. *Developments in palygorskite-sepiolite research: A new outlook on these nanomaterials*. Oxford, UK: Elsevier B.V. pp. 393-452.

Ruiz-Hitzky, E., Aranda, P., and González-Alfaro, Y. Spanish Patent, 201030333, 2010 and PCT ES2011/070145, 2011.

Ruiz-Hitzky, E., Aranda, P., and Darder, M. (2008). Bionanocomposites. In *Kirk-Othmer Encyclopedia of Chemical Technology*, pages 1–28. John Wiley Sons, Inc., Hoboken, NJ.

Ruiz-Hitzky, E., Aranda, P., Darder, M., Fernandes, F.M., Matos, C.R.S. (2010). Espumas rígidas de tipo composite basadas en biopolímeros combinados con arcillas fibrosas y su método de preparación. ES Patent, 2342871 and PCT/ES2009/07052.

Ruiz-Hitzky, E., Ariga, K., and Lvov, Y. M., editors, *Bio-inorganic Hybrid Nanomaterials - Strategies, Syntheses, Characterization and Application*, chapter 2, pages 1–40. Wiley-VCH, Weinheim, 1 edition.

Ruiz-Hitzky, E., Darder, M. and Aranda, P. in *Bio-Inorganic Hybrid Materials: Strategies, Syntheses, Characterization and Applications* E. Ruiz-Hitzky, K. Ariga and Y. Lvov, ed. Wiley-VCH, Weinheim, 2008, ch. 1, pp. 1-40.

Ruiz-Hitzky, E., Darder, M. and Aranda, P. in *Annual Review of Nanoresearch*. G. Cao, Q. Zhang and C. J. Brinker, ed. World Scientific Publishing, Singapore, 2010; vol. 3, pp. 149-189.

Ruiz-Hitzky, E., Darder, M., and Aranda, A. (2005). Functional biopolymer nanocomposites based on layered solids. *Journal of Materials Chemistry*, 5:3650-3662.

Ruiz-Hitzky, E., Darder, M., and Aranda, P. (2005). Functional biopolymer nanocomposites based on layered solids. *Journal of Materials Chemistry*, 15:3650–3662.

Ruiz-Hitzky, E., Darder, M., and Aranda, P. (2008). An introduction to bio-nanohybrid materials. In Ruiz-Hitzky, E., Ariga, K., and Lvov, Y. M., editors, *Bio-inorganic Hybrid Nanomaterials - Strategies, Syntheses, Characterization and Application*, chapter 2, pages 1–40. Wiley-VCH, Weinheim, 1 edition.

Ruiz-Hitzky, E., Darder, M., and Aranda, P. (2010). Progress in bionanocomposite materials. In *Annual Review of Nanoresearch*, Cao, G., Zhang, Q., Brinker, C. J., Eds. World Scientific Publishing: Singapore; vol. 3. 149-189.

Ruiz-Hitzky, E., Darder, M., Aranda, P., and Ariga, K. (2010). Advances in biomimetic and nanostructured biohybrid materials. *Advanced Materials*, 22:323–336.

Ruiz-Hitzky, E., Darder, M., Aranda, P., and Ogawa, M. (2011). Hybrid and biohybrid silicate based materials: molecular vs. block-assembling bottom–up processes. *Chemical Society Reviews*, 40:801-828.

Ruiz-Hitzky, E., Darder, M., Aranda, P., del Burgo, M. A. M., and del Real, G. (2009). Bionanocomposites as new carriers for influenza vaccines. *Advanced Materials*, 21:4167–4171.

Ruiz-Hitzky, E., Darder, M., Fernandes, F.M., Wicklein, B., Alcântara, A.C.S., and Aranda, P. (2013). Fibrous clays based bionanocomposites. *Progress in Polymer Science*, in press. dx.doi.org/10.1016/j.progpolymsci.2013.05.004

Ruiz-Hitzty, E., Aranda, P., and Serratosa, J.M. (2004). Clay-organic interactions: Organoclay complexes and polymer-clay nanocomposites. In Auerbach, S.M., Carrado, K. A., and Dutra, P., editors, *Handbook of Layered Materials*, chapter 3, 91-54, Marcel Dekker: New York.

Salerno, A., Oliviero, M., Di Maio, E., and Iannace, S. (2007). Thermoplastic foams from zein and gelatin. *International Polymer Processing*, 22:480-488.

Salerno, A., Zeppetelli, S., Di Maio, E., Iannace, S., and Netti, P.A. (2012). Architecture and properties of bi-modal porous scaffolds for bone regeneration prepared via supercritical CO_2 foaming and porogen leaching combined process. *Journal of supercritical fluids*, 67:114-122.

Salerno, A., Zeppetelli, S., Di Maio, E., Iannace, S., and Netti, P.A. (2010). Novel 3D porous multi-phase composite scaffolds based on PCL, thermoplastic zein and ha prepared via supercritical CO_2 foaming for bone regeneration. *Composites Science and Technology*, 70:1838–1846

Sanchez, C., Arribart, H., and Guille, M. M. G. (2005). Biomimetism and bioinspiration as tools for the design of innovative materials and systems. *Nature Materials*, 4:277–288

Sanchez, C., Belleville, P., Popall, M., and Nicole, L. (2011). Applications of advanced hybrid organic–inorganic nanomaterials: from laboratory to market. *Chemical Society Reviews*, 40: 696-753

Sessa, D.J., Eller, F. J., Palmquist, D.E., and Lawton, J.W. (2003). Improved methods for decolorizing corn zein. *Industrial Crops and Products*, 18:55–65

Shewry, P.R., and Tatham, N.G. (1990). Cereal seed storage proteins: structures, properties and role in grain utilization, *Journal of Experimental Botany*, 53: 947-958

Shukla, R., and Cheryan, M. (2001). Zein: the industrial protein from corn. *Industrial Crops and Products*, 13:171-192.

Si, S., Taubert, A., Mantion, A., Rogeza, G. and Rabu, P. (2012). Peptide-intercalated layered metal hydroxides: effect of peptide chain length and side chain functionality on structural, optical and magnetic properties, *Chemical Science*, 3:1945-1957

Sorrentino, A., Gorrasi, G., and Vittoria, V. (2007). Potential perspectives of bio-nanocomposites for food packaging applications. *Trends in Food Science and Technology*, 18:84e-95

Sothornvit, R., Hong, S.-I., An, D. J., Rhim, J.W. (2010). Effect of clay content on the physical and antimicrobial properties of whey protein isolate/organo-clay composite films protein-based on bionanocomposites, *LWT - Food Science and Technology*, 43:279-284

Svagan, A.J., Jensen, P., Dvinskikh, S.V., Furó, I., and Berglund, L.A. (2010). Towards tailored hierarchical structures in cellulose nanocomposite biofoams prepared by freezing/freeze-drying. *Journal of Materials Chemistry*, 20:6646-6654

Swiegers, G., editor. (2013). *Bioinspiration and Biomimicry in Chemistry: Reverse-Engineering Nature*, Lehn, J-M., Benyus, J. (Forewords), John Wiley Sons, Inc., Hoboken, NJ

Takahashi, H., Yamada K., and Yanai, N. (1996).*US Pat. 5,585,060*,

Talibudeen. O. (1950). Interlamellar adsorption of protein monolayers on pure montmorillonoid clays. *Nature*, 166: 236

Tang, Z., Kotov, N. A., Magonov, S., and Ozturk, B. (2003). Nanostructured artificial nacre, *Nature Materials*, 2:413-418.

Taylor, F.W, Zobel, H. F., Hellman, N. N. and Senti, F. R. (1959). Effect of Structure and Crystallinity on Water Sorption of Dextran. *Journal of Physical Chemistry B*, 63: 599-603

Tharanathan, R.N. (2003). Biodegradable films and edible coatings: Past, present and future. *Trends in Food Science and Technology*, 14:71-78.

Tran, A.T.T., and James, B. J. (2012). A study the interaction forces between the bovine serum albumin protein and montmorillonite surface. *Colloids and Surfaces A: Physicochemical and Engineering Aspects*, 414:104– 114.

Trujillano, R., Holgado, M. J., and Rives V. (2002) Alternative synthetic routes for NiAl layered double hydroxides with alkyl and alkylbenzene, sulfonates . S*tudies in Surface Science and Catalysis*, 142:1387-1394.

Undabeytia, T., Nir, S., and Rubin, B. (2010). Organo-clay formulations of the hydrophobic herbicide norflurazon yield reduced leaching, *Journal of Agricultural and Food Chemistry, 48*: 4767-4773.

Undabeytia, T., Nir, S., Sánchez-Verdejo, T., Villaverde, J., Maqueda C., and Morillo., E. (2008). A clay–vesicle system for water purification from organic pollutants, *Water Research, 42*: 1211-1219.

V. Caballero, F. M. Bautista, J. M. Campelo, D. Luna, J. M. Marinas, A. A. Romero, J. M. Hidalgo, R. Luque, A. Macario and G. Giordano, *Proc. Biochem.,* 2009, 44, 334-342.

Vaccari, A. (1998). Preparation and catalytic properties of cationic and anionic clays. *Catalysis Today*, 41: 53-71.

Velu, S., Suzuki, K., Okaki, T., Tomura, S., Ohashi, F. (1999) Synthesis of new Sn-incorporated layered double hydroxides and their thermal evolution to mixed oxides. *Chemisty of Materials,* 11: 2163-2172

Villaverde, J., Kah, M. and Brown, C.D. (2008). Adsorption and degradation of four acidic herbicides in soils from southern Spain. *Pest Management Science*, 64:703–710.

Wang, H. J., Lin, Z. X., Liu, X. M., Sheng, S. Y., Wang, J. Y. (2005) Heparin-loaded zein microsphere film and hemocompatibility, *Journal of Controlled Release*, 105:120-131.

Wang, Q, Wang, Q, Wang, X. and Padua, G. W. (2006). Zein dynamic adsorption to carboxylic and alkyl coated surfaces. *Journal of Agricultural and Food Chemistry*, 54: 517-522

Wang, Q., Crofts, A. R., and Padua, G. W. (2003). Protein-Lipid Interactions in Zein Films Investigated by Surface Plasmon Resonance. *Journal of Agricultural and Food Chemistry,* 51:7439-7444

Wang, Q., Wang, J-F., Geil, P. H., and Padua, G.W. (2004). Zein Adsorption to Hydrophilic and Hydrophobic Surfaces Investigated by Surface Plasmon Resonance, *Biomacromolecules,* 5:1356–1361

Wang, Y. and Padua, G. W. (2010) Formation of zein micro phases in ethanol-water. *Journal of Cereal Science,* 26: 12897–12901.

Wang, Y. and Padua, G. W. (2010). Formation of zein microphases in ethanol-water. *Langmuir,* 26: 12897-12901.

Wang, Y., Filho, F. L., Geil, P., and Padua, G. W. (2005). Effects of processing on the structure of zein/oleic acid films investigated by X-ray diffraction, *Macromolecular Bioscience*, 5: 1200–1208.

Wasa, T. and Takahsahi, J. (1998) Coating agent for food excelent in workability in coating. *US Patent*, WO 98/14076

Weast, R.C. (Ed.), CRC Handbook of Chemistry and Physics Online, 52th ed., CRC Press, 1971-1972.

Weiss, A. (1969) in *Organic Geochemistry*, Eglinton G. and Murphy, M. T. J. (editors), Springer Verlag, Berlin, 737–781;

Wickein, B., Aranda, P., Ruiz-Hitzky, E, and Darder, M. (2013). Nanostructured bioactive foams based on polyvinyl alcohol-sepiolite nanocomposites, *Journal of Materials Chemistry B*., 1:2911-2920

Wicklein, B., Darder, M., Aranda, P., Ruiz-Hitzky, E. (2010). Bio-organoclays based on phospholipids as immobilization hosts for biological species. *Langmuir*, 26:5217-5225.

Wicklein, B., Darder, M., Aranda, P., Ruiz-Hitzky, E. (2011). Phospholipid–sepiolite biomimetic interfaces for the immobilization of enzymes. *ACS Applied Materials and Interfaces*, 3:4339-4348

Wu, J. and Yuan, Q. (2002). Gas permeability of a novel cellulose membrane. *Journal of Membrane Science*, 204: 185-194

Y. González-Alfaro, P. Aranda, F. M. Fernandes, B. Wicklein, M. Darder, and E. Ruiz-Hitzky. (2011). Multifunctional porous materials through ferrofluids. *Advanced Materials*. 23: 5224–5228.;

Yamada, K., Takahashi, H. and Noguchi, A. (1995). Improved water resistance in edible zein films and composites for biodegradable food packaging. *International Journal of Food Science and Technology*, 30: 599-608.

Yang, J.-M., Zha, L.-S., Yu, D.-G. and Liu, J. (2013). Coaxial electrospinning with acetic acid for preparing ferulic acid/zein composite fibers with improved drug release profiles, *Colloids and Surfaces B: Biointerfaces,* 102: 737-743.

Yao, H.-B., Tan, Z.-H., Fang, H.-Y., and Yu, S.-H. (2010). Artificial nacre-like bionanocomposite films from the self-assembly of chitosan/montmorillonite hybrid building blocks. *Angewandte Chemie International Edition*, 49:10127–10131

Yasutake, A., Aisawa, S., Takahashi ,S., Hirahara, H., and Narita, E. (2008). Synthesis of biopolymer intercalated inorganic-layered materials: Intercalation of collagen peptide and soybean peptide into Zn–Al layered double hydroxide and layered zinc hydroxide. *Journal of Physics and Chemisty of Solids*, 69:1542-1546

Yuan, Q., Lu, W., and Pan, Y. (2010). Structure and properties of biodegradable wheat gluten/attapulgite nanocomposite sheets. *Polymer Degradation and Stability* 95:1581-1587

Zarate-Ramírez, L. S., Martínez, I., Romero, A., Partal P., and Guerrero A. (2011). Wheat gluten-based materials plasticised with glycerol and water by thermoplastic mixing and thermomoulding.*Journal Science and Food Agricultural,* 91, 625-633.

Zhang, B., Luo, Y., and Wang, Q. (2001). Effect of acid and base treatments on structural, rheological, and antioxidant properties of α-zein. *Food Chemistry*, 124:210–220

Zheng , W., Gao , F., and Gu , H. (2005). Magnetic polymer nanospheres with high and uniform magnetite content, *Journal of Magnetism and Magnetic Materials*, 288: 403-410

Zou, J and HO, W.S.W. (2006). CO_2 – selective polymeric membranes containing amines in crosslinked poly (vinyl alcohol). *Journal of Membrane Science*, 286: 310-321